AD-A117 463

RIA-80-U450

EN

TECHNICAL LIBRARY

AD-A117 463

USADACS Technical Library

5 0712 01004163 9

AMMRC TR 80-15

CHARACTERIZATION OF TURBINE CERAMICS AFTER LONG-TERM ENVIRONMENTAL EXPOSURE

GEORGE D. QUINN

Date Published - April 1980

Prepared under
Interagency Agreement EC-76-A-1017

by
ARMY MATERIALS AND MECHANICS RESEARCH CENTER
WATERTOWN, MASSACHUSETTS 02172

for

U. S. DEPARTMENT OF ENERGY

Division of Transportation Energy Conservation

DOE/CS/54102-H02

The findings in this report are not to be construed as an official Department of the Army position, unless so designated by other authorized documents.

Mention of any trade names or manufacturers in this report shall not be construed as advertising nor as an official indorsement or approval of such products or companies by the United States Government.

DISPOSITION INSTRUCTIONS

Destroy this report when it is no longer needed.
Do not return it to the originator.

UNCLASSIFIED

SECURITY CLASSIFICATION OF THIS PAGE *(When Data Entered)*

REPORT DOCUMENTATION PAGE		READ INSTRUCTIONS BEFORE COMPLETING FORM
1. REPORT NUMBER AMMRC TR 80-15	2. GOVT ACCESSION NO.	3. RECIPIENT'S CATALOG NUMBER
4. TITLE *(and Subtitle)* CHARACTERIZATION OF TURBINE CERAMICS AFTER LONG-TERM ENVIRONMENTAL EXPOSURE		5. TYPE OF REPORT & PERIOD COVERED Final Report 6. PERFORMING ORG. REPORT NUMBER
7. AUTHOR(s) George D. Quinn		8. CONTRACT OR GRANT NUMBER(s)
9. PERFORMING ORGANIZATION NAME AND ADDRESS Army Materials and Mechanics Research Center Watertown, Massachusetts 02172 DRXMR-EO		10. PROGRAM ELEMENT, PROJECT, TASK AREA & WORK UNIT NUMBERS Interagency Agreement EC-76-A-1017
11. CONTROLLING OFFICE NAME AND ADDRESS U.S. Department of Energy Office of Transportation Washington, D.C. 20545		12. REPORT DATE April 1980 13. NUMBER OF PAGES 100
14. MONITORING AGENCY NAME & ADDRESS*(if different from Controlling Office)*		15. SECURITY CLASS. *(of this report)* Unclassified 15a. DECLASSIFICATION/DOWNGRADING SCHEDULE
16. DISTRIBUTION STATEMENT *(of this Report)* Approved for public release; distribution unlimited.		
17. DISTRIBUTION STATEMENT *(of the abstract entered in Block 20, if different from Report)*		
18. SUPPLEMENTARY NOTES		
19. KEY WORDS *(Continue on reverse side if necessary and identify by block number)* Silicon nitride Silicon carbide Static fatigue Mechanical properties Fractography		
20. ABSTRACT *(Continue on reverse side if necessary and identify by block number)* (SEE REVERSE SIDE)		

DD FORM 1 JAN 73 1473 EDITION OF 1 NOV 65 IS OBSOLETE

UNCLASSIFIED

SECURITY CLASSIFICATION OF THIS PAGE *(When Data Entered)*

Block No. 20

ABSTRACT

An experimental program was conducted to investigate the possible degradation in mechanical properties of silicon-based ceramics exposed to high temperature oxidizing environments. Thirteen materials were studied, all with potential for use in energy conversion devices such as the gas turbine. The materials ranged from some of the better known silicon nitrides and carbides to experimental grades. Testing included flexural stress rupture at 1200 C and stepped temperature stress rupture (STSR) experiments. The latter test was devised for this study and is a variation of the stress rupture test in which a range of temperatures is employed. The purpose of the STSR test is to explore the potential stress/temperature regimes of static fatigue failure. In addition, a combined cycle durability sequence was applied to selected materials. This procedure is a simple service simulation involving static heat soaks and rapid thermal cycling on bend bars. In nearly all cases, material degradation and/or time-dependent failure was observed. Extensive fractography was conducted to identify mechanisms of failure.

FOREWORD

This is the final technical report under Task III of ERDA-TEC (now Department of Energy Office of Transportation)/ AMMRC Interagency Agreement EC-76-A-1017. The work carried out under Task III was to obtain preliminary mechanical property data on ceramic turbine materials after high temperature exposure in air for hundreds of hours, with and without thermal cycling. The NASA Technical Monitor of this program was Mr. C. P. Blankenship and the DOE Technical Monitor was Mr. R. Schulz. The Principal Investigator was Mr. G. D. Quinn of AMMRC. Additional AMMRC staff who participated in the program were: Dr. R. N. Katz, Mr. G. E. Gazza, Dr. E. M. Lenoe, Dr. D. R. Messier, Mr. V. Ociepka, Mr. R. Cicerone, and Mr. M. Slavin.

CONTENTS

Page

FOREWORD iii

I. INTRODUCTION. 1

II. EXPERIMENTAL PROCEDURE. 2

A. Specimen Preparation 2

B. Room Temperature Flexural Strength 3

C. Flexural Stress Rupture. 3

D. Stepped Temperature Stress Rupture. 5

E. Combined Thermal Exposure-Thermal Cycling. 5

F. Fractography 7

III. MATERIAL CHARACTERIZATION 7

A. Norton NC 132 Hot-Pressed Silicon Nitride. 8

B. Norton NC 136 Hot-Pressed Silicon Nitride. 8

C. Norton NCX 34 Hot-Pressed Silicon Nitride. 9

D. Norton NC 350 Reaction-Bonded Silicon Nitride. 9

E. Kawecki Berylco Industries Reaction-Bonded Silicon Nitride. . 10

F. Ford 2.7 Reaction-Bonded Silicon Nitride. 11

G. Norton NC 203 Hot-Pressed Silicon Carbides 12

H. Carborundum 1977 Alpha Silicon Carbide. 12

I. Carborundum 1978 Alpha Silicon Carbide. 12

J. Norton NC 433 Siliconized Silicon Carbide. 13

K. Norton NC 435 Siliconized Silicon Carbide. 13

L. General Electric Silcomp CRC Siliconized Silicon Carbide. . . . 14

M. General Electric Silcomp CC Siliconized Silicon Carbide. . . . 15

Page

IV. RESULTS AND DISCUSSION

A. Norton NC 132 Hot-Pressed Silicon Nitride. 16

B. Norton NC 136 Hot-Pressed Silicon Nitride. 28

C. Norton NCX 34 Hot-Pressed Silicon Nitride. 32

D. Norton NC 350 Reaction-Bonded Silicon Nitride. 37

E. Kawecki Berylco Industries Reaction-Bonded Silicon Nitride. . 44

F. Ford 2.7 Reaction-Bonded Silicon Nitride. 50

G. Norton NC 203 Hot-Pressed Silicon Carbide. 56

H. Carborundum 1977 Alpha Silicon Carbide. 61

I. Carborundum 1978 Alpha Silicon Carbide. 65

J. Norton NC 433 Siliconized Silicon Carbide. 72

K. Norton NC 435 Siliconized Silicon Carbide. 74

L. General Electric Silcomp CRC Siliconized Silicon Carbide. . . . 78

M. General Electric Silcomp CC Siliconized Silicon Carbide. . . . 83

V. CONCLUSIONS 87

VI. ACKNOWLEDGMENTS 89

APPENDIX. TABULATED SUMMARY OF DATA. . . . 90

LITERATURE CITED. 95

I. INTRODUCTION

Silicon-based ceramics have considerable potential for use in structural applications at high temperature and promise to play an important role in energy conversion devices. A severe impediment to the use of ceramics is the lack of mechanical property data after long-term exposure to oxidizing environments, particularly with temperature cycling. For example, data on materials such as hot-pressed silicon nitride indicate that strength could degrade by as much as fifty percent after a few hundred hours exposure at 1371 C.[1] Due to the lack of property data after exposure, many ceramic components for gas turbines have been designed using mechanical properties of virgin material.

In the few cases where an attempt has been made to account for the time-dependent degradation of the material, only one mechanism of failure has been assumed. This is slow crack growth which can be analytically described by a power law relation between crack velocity and stress intensity with an Arrhenius temperature dependence. To date, the veracity of this analytical relationship has not been confirmed for any of the silicon-based ceramics, including hot-pressed silicon nitride. Although some data exists regarding crack velocity in macroscopic fracture mechanics specimens, it has not yet been demonstrated that such data accurately pertains to the growth of real flaws in the material.* Considerable evidence indicates an alternate but prominent mechanism of strength reduction in hot-pressed silicon nitride is the formation of deep surface pits due to oxidation attack. These pits develop with no applied stress. Thus a model of failure based only upon slow crack growth from preexisting flaws (virgin defects) may predict a sample able to endure hundreds of hours, yet the sample may fail on loading due to the prior formation of pits from high temperature exposure under zero stress.

A program of research was undertaken to address these durability-related issues. Static fatigue testing was conducted to identify mechanical property degradation under the influence of stress in an oxidizing environment. High temperature testing in furnaces was employed. Recognizing that the static environment in a test furnace may not adequately represent actual service conditions, an alternate procedure was employed as well. Unstressed samples were exposed to a crude simulated service environment and subsequent property degradation was measured.

In the instances where material failure or degradation occurred, our investigation was directed at identifying the mechanism involved. Extensive fractography was employed to this end. Insufficient time or resources were available, however, to conduct a definitive investigation on each material. It is our intention that where problem areas are identified other investigators will pursue these matters more fully.

Thirteen materials were chosen for evaluation:

Silicon Nitride

Hot-pressed - Norton NC 132
Norton NC 136
Norton NCX 34

Reaction-bonded - Norton NC 350
Kawecki Berylco Industries
Ford 2.7

Silicon Carbide

Hot-pressed - Norton NC 203

Siliconized - Norton NC 433
Norton NC 435
General Electric Silcomp CC
General Electric Silcomp CRC

Sintered alpha - Carborundum 1977
Carborundum 1978

These materials are representative of the spectrum of materials currently available in the Si_3N_4 and SiC families of ceramics. While it is tempting to draw comparisons between the materials on the basis of the data presented in this report, it is inappropriate to do so for two reasons. First, each material is at a different stage of development or maturity. For example, NC 132 may be the most mature hot-pressed silicon nitride, whereas NCX 34 is still an experimental grade. In a few years, some of these materials may no longer be available, having been made obsolete by successive generations of refinements. (As of this printing, several are already not available.) In each of the thirteen cases, the date of material fabrication (or at least vendor delivery) will be identified. A few observations regarding material designations are in order here. Manufacturers should be encouraged to apply specific designations to their material grades so as to avoid confusion regarding the successive generations of a given material. These designations should be updated (such as the change from HS 130 to NC 132) or subscripted (for example, with calender notations) to make valid comparison of data bases and observations regarding material refinements. Some confusion in the technical community already exists due to the ambiguous references to "old" and "new" vintages of some of the above listed materials.

*A program of research is now underway by G. Quinn and E. Lenoe at AMMRC to investigate this issue.

1. MILLER, D. et al. *Brittle Materials Design, High Temperature Gas Turbine Materials Technology.* Westinghouse Corporation, Contract DAAG46-71-C-0162, Final Report, AMMRC CTR 76-32, Volume IV, December 1976.

A second reason for not drawing direct comparisons in the data presented below is that each material represents a different balance between materials properties and fabricability. For example, there are applications where the high strength performance of hot-pressed silicon nitride may be required and other applications where the lower strength-more creep resistant reaction-sintered forms may be more appropriate. It is probable that many of these materials will have one or more unique roles for which it is the best overall engineering choice.

II. EXPERIMENTAL PROCEDURE

At least three testing procedures were conducted for each material in the program. Samples were allotted approximately equally to each procedure although some flexibility was exercised. The minimum number of samples per material was the 32 tested for NCX 34 and the maximum was 105 for the NC 132. An attempt to use a common bend bar size of 0.216 × 0.280 × 5.08 cm or 0.203 × 0.280 × 5.08 cm was made.

The first procedure was to establish a reference strength level by breaking a control group of samples in four-point bending at room temperature. These will hereafter be referred to as the "control" strengths. In addition to mean strength, standard deviation, high and low strength values, a two-parameter Weibull modulus is reported. The modulus value is calculated by two methods as will be discussed below. Fractography was directed at identifying the origins of failure, particularly in cases where multimodal flaw distributions were evident.

High temperature flexural stress rupture tests were conducted at 1200 C as the second major experimental procedure. This temperature is representative of working temperatures to be expected in certain gas turbine applications and other energy conversion devices. A bank of furnaces constructed for this purpose permitted experiments to run for several hundred hours. Trials were usually terminated at 300 hours if samples were still intact, although in some cases trials of much longer duration were conducted. Sufficient samples were tested to discern any trend toward diminishing load-carrying capacity with time. In the cases where static fatigue failures were confined to narrow stress ranges (samples fail on loading or survive intact) only enough samples were used to establish an approximate critical stress level.

Static fatigue failures over a broader range of temperatures were investigated via a stepped temperature stress rupture (STSR) procedure specifically devised for this program.[2] The STSR procedure is very similar to the common flexural stress rupture test except that a range of temperatures is employed with each sample. This test, to be described in detail below, was conducted over the range of 1000 C to 1400 C (1300 C for the siliconized materials) and is intended to detect the temperature and stress ranges where time-dependent failure can occur. The test is useful in detecting temperature regimes where material instabilities may exist. The choice of the range of temperatures (and their sequence) is arbitrary but represents temperatures that structural ceramics will be exposed to in service.

For several of the materials of special interest, and where sufficient samples were available, a fourth procedure was applied. A combined cycle exposure pattern was performed wherein a group of samples was alternately heat treated in an oxidizing environment (a furnace in air) and then thermally cycled in a flame heating-compressed air quench apparatus. The specific sequence will be discussed below, but a cumulative exposure of 360 hours and 500 thermal shock cycles was accumulated on each of twelve samples. While not intended to match any specific application, the purpose of this procedure is to impart a more abusive treatment to the samples than that generated by a static oxidation treatment.

Finally, in several cases where results indicated further testing to be appropriate and where samples were available, additional stress rupture tests at different temperatures were conducted.

A. Specimen Preparation

Unless otherwise indicated, the bend bar samples for this study were cut from billets in a direction perpendicular to the pressed direction (that is, the sample long dimension was perpendicular to the plate thickness). Specimens were usually 0.216 × 0.280 × 5.08 cm long and were carefully ground by a surface grinder such that surface striations ran parallel to the long axis.* All four long faces were machined with either a 220 or 280 grit diamond wheel with a final finish removal rate of about 1.5×10^{-4} cm (0.00005 inch) per pass. In this manner about 0.008 cm (0.003 inch) of material was removed from each face in the final finishing phase. A wheel speed of 1500 surface meters per minute was used (5000 feet/minute). All four long edges were chamfered approximately 40° to a depth of about 0.015 cm. Again, specifications called for striation markings to be parallel to the long axis. In the case of the hot-pressed materials, the surface finish achieved was better than 5 microinches RMS as measured by a profilometer along the long axis.

*Several groups of specimens were machined to 0.203 x 0.280 x 5.08 cm. These are noted in the text.

2. QUINN, G. D., and KATZ, R. N. *Stepped Temperature Stress-Rupture Testing of Silicon Based Ceramics.* Am. Cer. Soc. Bull., v. 51, no. 11, 1978, p. 1057.

B. Room Temperature Flexural Strength

Flexural strength of the control samples, the combined cycle sample, and the survivor stress rupture samples were measured on a universal testing machine.* The four-point bending fixtures had an outer span of 3.04 cm and an inner span of 1.52 cm. Crosshead speed was 5×10^{-3} cm/minute. The stress rupture survivors were mounted so that the most highly stressed zone during the high temperature test was again loaded in a tensile manner within the inner load pins of the room temperature fixture. The control samples, being 5.08 cm long, occasionally permitted two breaks per sample. In such cases, care was taken to insure the previously stressed portion of the sample was not reinserted into the inner gage length.

Stress at failure was calculated from the elastic beam equation for the maximum outer fiber stress. No adjustments were made for subsurface flaws or for curvature in the case of samples that survived high temperature testing which were subsequently broken to measure retained strength. The Weibull parameters were determined for a two-parameter function with the cumulative failure probability P for a given point calculated as $P = i/(N+1)$ where i is the ranked number of the data point and N is the number of data points. The Weibull modulus is the slope of a least-squares fitted line through a ln ln $(1/(1-P))$ versus ln (stress) plot. A goodness of fit percentage (coefficient of determination) is reported for each such plot. A percentage of 100 corresponds to an excellent fit to the data. In addition, the Weibull two-parameter modulus and characteristic value were recalculated with an unbiased maximum likelihood estimation scheme.† This alternate method may be a more statistically valid method and also provides confidence limits on the estimates. These latter results are presented in tabular form in Section V.

C. Flexural Stress Rupture

A small and inexpensive mechanical test furnace was designed and constructed to perform the flexural stress rupture tests (Figure 1). The furnace is made with refractory firebrick and utilizes silicon carbide heating elements to attain temperatures up to 1500 C in air with less than 20 amps at 120 Vac. Four-point bend fixtures were machined from hot-pressed silicon carbide (Norton NC 203 grade) and have spans of 3.81 and 1.91 cm (Figure 2). Loading is effected by a deadweight lever arm mechanism on the top of the furnace which transmits a load to the fixtures. A dial gage monitors load train deflection. A timer connected to a microswitch on the load beam detects failure. The microswitch also shuts furnace power off immediately so as to minimize oxidation of the fracture surfaces of the samples. Thirteen such furnaces have been built at a cost of less than $500 per unit (excluding bend fixtures, controller, and labor). Complete details of the design, construction, and operation of this furnace as well as the fixtures are in Reference 3.

Temperatures are measured with a platinum thermocouple that is located approximately 5 mm from the sample midspan. An automatic controller maintains the furnace within one or two degrees

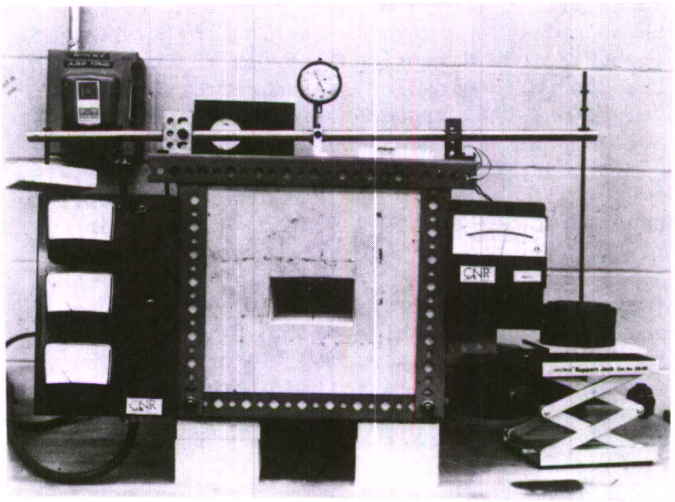

Figure 1. One of the thirteen mechanical test furnaces used for flexural stress rupture testing. The door is removed to show the size of the test chamber and the fixtures inside.

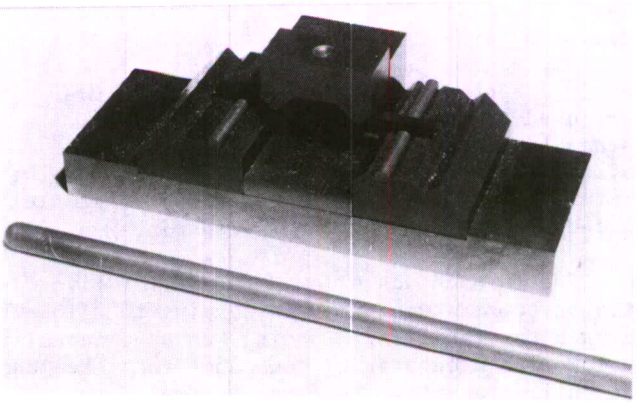

Figure 2. Silicon carbide four-point bend fixtures with a sample in place. The base is large so as to evenly distribute the load onto the firebrick below. A 15-cm-long loading rod with rounded tip (foreground) brings the load through the top of the furnace onto the recess in the upper loading block.

*Instron Corp., Canton, Mass.

†D. Neal and D. Mason, AMMRC, "Determination of Failure Probabilities of Slip Cast Fused Silica," to be published.

3. QUINN, G. D. *Guide to the Construction of a Simple 1500 C Test Furnace.* Army Materials and Mechanics Research Center, AMMRC TN 77-4, August 1977.

Centigrade. In practice a tolerance of 2 C was attempted. All furnaces were monitored by a single multipoint recorder; all thermocouples were identically located, and all thermocouples were from the same lot of platinum wire. An experiment was conducted with all thermocouples simultaneously measuring the same spot within a furnace and readouts agreed to within 1 C. Such temperature control and precautions are necessary to minimize errors in the time to failure experiments. As will be shown in the NC 132 results of this report, a 5 C error at 1200 C can result in a 22 percent change in the time to failure.

An error analysis calculation[4] was conducted to determine the error in stress that results from the cumulative errors in the loading system. These include dimensional errors in the fixtures, the deadweight loading system, errors in the weight and the furnace-to-furnace variations. All samples were measured at their midpoint for dimensions. There was no guarantee the sample would fail at this point and a worst possible taper of 0.001 cm was assumed. An error in fixture alignment (lateral offset of inner load pins) of 0.012 cm was assumed for a worst case. These errors and errors in the loading mechanism and the weights combine to cause a total error in stress of a few percent. No provision was made for lack of parallelism of the load pins, as this error was extremely small relative to the sample dimensions since the fixtures were precision machined. A slight recess in the upper loading block (visible in Figure 2) ensured an even load application. If the load rod was not exactly centered in the recess, the error would still be small relative to the inner load pin span which was 1.91 cm. The maximum stress on the sample was calculated from the standard elastic solution for outer fiber stress for a beam in bending. No corrections were employed for samples that subsequently bowed due to excessive creep. No corrections to the stress were used to account for subsurface flaws. Rather surprisingly, all but a few samples failed from within the inner gage length of the fixtures. A very small fraction of the samples failed from beneath an inner load pin.

The furnace was allowed to sit for five minutes at temperature prior to loading to allow the furnace to stabilize. Loading was done manually by lowering a laboratory jack such that the load pan on it transmits its force to the overhead loading beam. This process takes about 5 seconds and is done in a smooth manner. Elapsed times are measured from the instant the full load is applied to the loading beam. Stress rupture data representation in this report is on a log time axis that begins at 0.01 hour (36 seconds). Shorter times to failure are treated as failures on loading since they may be influenced by the exact manner of loading. The counterbalance on the load beam was designed so that during heatup (load pan resting on lab jack and not on the loading beam) a slight preload was applied to the samples. This preload, which serves to keep the fixtures aligned and prevent toppling, initially caused a stress of the order of 5 MPa on the samples but was reduced to 0.03 MPa later in the program.

Creep strains of intact specimens were estimated by photographing the samples at 5X and measuring midspan deflection relative to the *inner* loading pins. Maximum creep strain (ε_t) was calculated from the formula:

$$\varepsilon_t = 4tv/L^2$$

where t = the specimen thickness

v = the midspan deflection relative to the inner spans

L = the inner span length.

This formulation assumes only that the creep strain is constant within the inner gage length and that the creep strain is a linear function of distance through the thickness. The minimum value of outer fiber strain that could be estimated in this fashion was 0.1 percent. The values reported in this report are least accurate (±50%) for such small strains, but increase in accuracy with increasing curvature (practical considerations apply). Attempts to correlate creep deformations to load train deflections via a dial gage failed because of furnace expansion. Several hours at temperature were required before the entire furnace stabilized. Creep strains less than 0.05 percent will be deemed 'insignificant' or nonmeasureable in this report.

The experimental procedure was verified by determining the stress rupture behavior of HS 130 grade of silicon nitride* and then comparing results with published data. Good agreement was obtained between previously published data and results achieved with the above experimental technique.[5]

*Norton Company, Worcester, Mass.

4. SCHENCK, H., Jr. *Theories of Engineering Experimentation.* McGraw Hill Company, New York, 1968.

5. QUINN, G. D., KATZ, R. N., and LENOE, E. M. *Thermal Cycling Effects, Stress Rupture and Tensile Creep in Hot-Pressed Silicon Nitride.* Proceedings of the DARPA/NAVSEA Ceramic Gas Turbine Demonstration Engine Program Review, Castine, Maine, MCIC 78-36, August 1977, p. 715-737.

D. Stepped Temperature Stress Rupture

Most conventional stress rupture testing was conducted at 1200 C in this study. Alternately, to gain insight into materials stability over a wider range of temperatures, a stepped temperature stress rupture (STSR) test was devised.[2] This test is useful in screening materials for stability over portions of the temperature range which may be missed in the more conventional stress rupture testing. The STSR test allows one to quickly focus on temperature and stresses where a material may exhibit time-dependent failure.

The STSR test is an extension of the common flexural stress rupture test to include a range of temperatures. The temperature cycle chosen for our requirements (and which conveniently fits into the usual laboratory work week) is illustrated in Figure 3. A flexural specimen is loaded into the standard furnace with four-point bend fixture and the furnace is heated to 1000 C in air with no load applied to the sample. At 1000 C a deadweight load is applied. Should the sample survive 24 hours at that temperature, the furnace is then heated (approximately 1/2 hour) to 1100 C and again allowed to soak for 24 hours. This cycle is repeated for 1200 C, 1300 C, and 1400 C, but in the last case, the soak is maintained for 60 hours. This cycle sequence was arbitrarily chosen, but the range encompasses temperatures that critically stressed ceramic components such as nozzles and blades will experience in vehicular gas turbines with turbine inlet temperatures of up to 1400 C. Throughout the test, the same sample is subjected to a constant deadweight load. In the event a sample breaks, the furnace is immediately cooled and the time of failure is denoted by an arrow on the STSR plot. The arrow is labelled with the stress that was applied to the sample. A series of trials are executed with differing loads corresponding to stress levels calculated from the elastic beam formula.

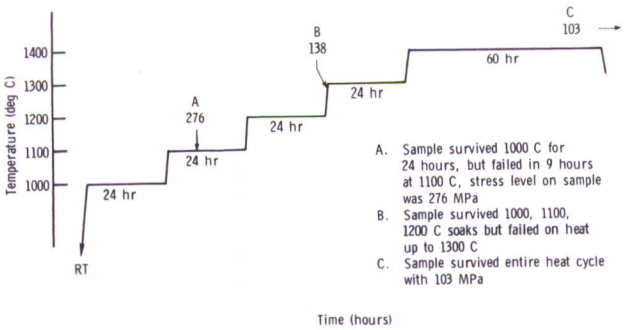

Figure 3. The stepped temperature stress rupture schedule. Load is applied at 1000 C.

E. Combined Thermal Exposure-Thermal Cycling

The combined thermal exposure-thermal cycling tests consist of five repetitions of: 24-hour soaks at 1000 C, 1200 C, and 1371 C with a subsequent 100 thermal shocks from room temperature (RT) up to 1371 C and then down to room temperature. In this manner twelve samples each accumulate 360 hours exposure and 500 thermal shock cycles as shown in Figure 4. The materials with substantial free silicon content have a 1300 C step substituted for the 1371 C step, and a peak thermal shock temperature of 1300 C. The thermal soaks are carried out in air in a furnace (similar to the stress rupture model) equipped with a specially constructed Si_3N_4 muffle to protect samples from the possibility of contamination with the furnace refractories. Thermal cycling was accomplished in the AMMRC thermal fatigue rig, shown in Figures 5 and 6, which is modeled after the one initially described by Johnson and Hartsock.[6]

The thermal fatigue apparatus cycles specimens between a heating and cooling station. The heating station consists of an oxyacetylene torch which uses oxygen and MAPP* gas. MAPP gas is a stabilized acetylene and can be stored in liquid form. It is cleaner and safer to use than acetylene and generates flame temperatures nearly as high. MAPP was used to provide sufficiently fast heatup times on the specimens. Standard acetylene welding equipment was used with the addition of extra pressure regulators to insure constant gas flows. A heating tip with twelve small apertures is used. The oxy-fuel gas ratio was set so that the flame was nearly neutral, that is, not oxidizing or carburizing in welding terminology. The turntable is set to rotate at 20 seconds per sample which is sufficient to allow the sample to reach steady state conditions. The sample is then indexed into a compressed air quench station. The air nozzle is located 1 cm below the sample and is directed at the hottest portion of the sample.

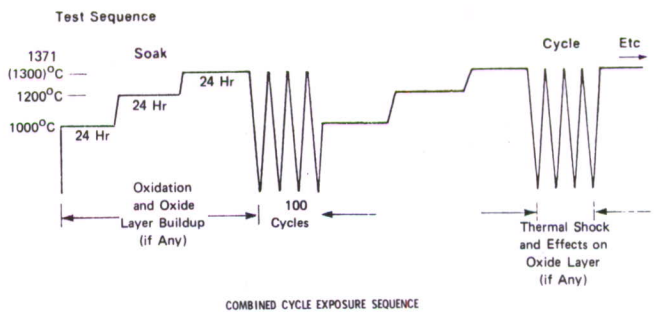

Figure 4. The combined thermal exposure thermal cycling schedule. Five repetitions of the heat soak and 100 thermal fatigue cycles result in an accumulation of 360 hours of soaks from 1000 C to 1371 C and 500 thermal fatigue cycles.

*Dow Chemical Company

6. JOHNSON, C. F., and HARTSOCK, D. L. *Thermal Response of Ceramic Turbine Stators* in Ceramics for High Performance Applications, J. J. Burke, A. E. Gorum, and R. N. Katz, ed., Brook Hill Publishing Company, Chestnut Hill, Massachusetts, 1974, p. 549.

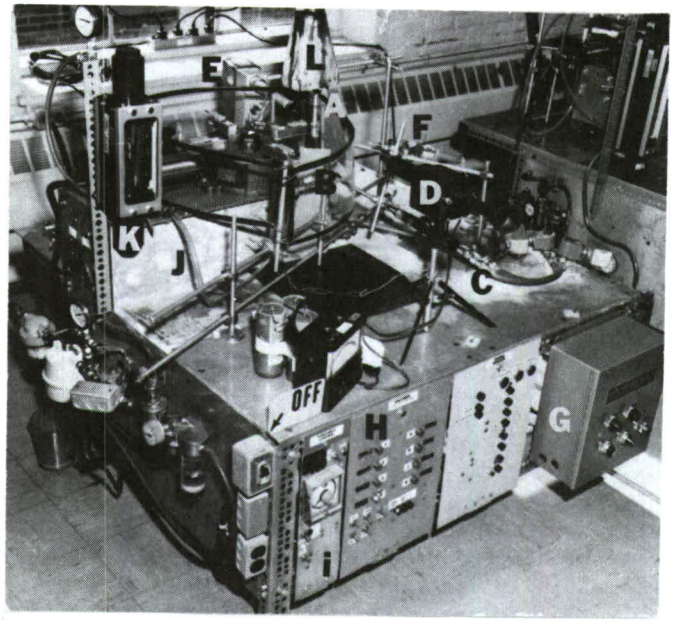

Figure 5. Thermal fatigue rig with: (A) heating station on turntable; (B) quench station; (C) heating torch; (D) Micro-Optical pyrometer; (E) automatic pyrometer; (F) flame sensor; (G) safety control; (H) specimen failure monitor; (I) turntable rotation control; (J) quench line; (K) flowmeter; (L) exhaust duct.

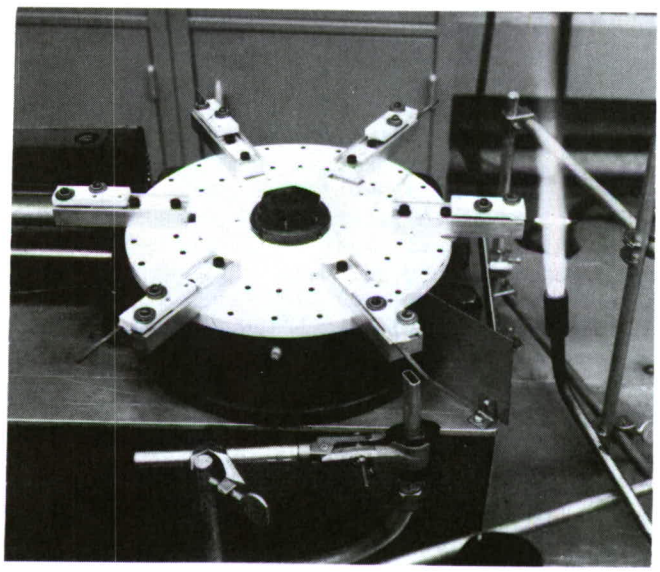

Figure 6. Close-up of the thermal fatigue rig turntable with six samples in place. A single sample is in the heating station and has achieved steady state temperature. The quench station is in the foreground. Much of the peripheral equipment has been removed to simplify this view.

Air is supplied by a compressor through regulators, filters, and a flowmeter. Samples are allowed to accumulate 100 such cycles each and then are removed from the rig for subsequent furnace exposure or final strength testing. Care is taken to insure each sample is remounted in the same orientation each time it is placed on the apparatus.

The apparatus is capable of running unattended indefinitely, but minor adjustments to gas flows are periodically made to maintain correct specimen temperatures. A safety system composed of a flame-on and flame position sensor, oxygen and fuel gas pressure transducers, air line pressure transducer, and electrical power relay, monitors conditions and shuts the rig off if out of norm. Shutdown is accomplished by closing an electrical switch which in turn stops the rotation of the table, closes two solenoid valves (normally closed) in the oxygen and fuel gas lines, and closes an air line solenoid valve.

Temperature was controlled by manually varying the oxygen and fuel gas flows. Temperature is monitored by a manual optical pyrometer* and by an automatic pyrometer† coupled to a recorder. Both are brightness pyrometers that measure light intensity at $\lambda = 0.65$ μm. Since both instruments assume an emissivity of 1.0 at the 0.65 μm wavelength, a correction temperature had to be added to the indicated values. An emissivity of 0.80 was arbitrarily assumed, leading to a correction of 26 C at 1345 C measured.[7] (Had the emissivity been 0.90, the correction would be only 13 C at the same temperature.) The Micro-Optical Pyrometer has a small filament and is capable of making measurements on a region of 0.03 cm. The automatic pyrometer with lens extension tubes can read a target diameter of 0.04 cm, but care must be taken to clamp it into position. A typical steady state temperature distribution for an NC 132 HPSN sample is shown in Figure 7. Heat-up and cool-down rates for several samples are shown

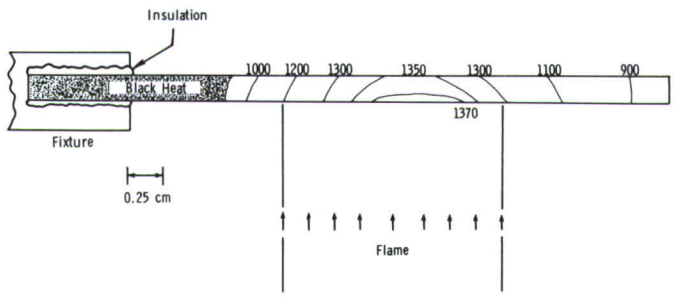

Figure 7. Steady state temperature distribution in NC 132 thermal fatigue specimen. The side view is shown. Isotherm temperatures are degrees centigrade.

*Pyro Micro-Optical Pyrometer, Pyrometer Instrument Company, Northvale, New Jersey.
†Pyro 650, Instrument Development Laboratory, Attleboro, Mass.

7. Instruction Manual 5040 for Pyro 650, Instrument Development Laboratories, Inc., Attleboro, Massachusetts, April 1961.

in Figure 8. Both instruments are used to measure rate of rise and steady state temperatures in the heating station. Neither could be used accurately on quench since the cool-down rates were too high. Cool-down rates were estimated by using a stop watch and visually observing the attainment of black heat temperature. Attainment of room temperature during quench is estimated by manually touching the specimens in situ at progressively shorter times from 20 seconds.

The heat transfer conditions and thermal stress estimates for these test conditions are discussed in Reference 5. In general, however, the peak thermal stresses during the quench portion are not very high due to the regular geometry of the bend bar. Hot-pressed silicon nitride experiences a peak stress of approximately 37 MPa at 0.2 second into the quench; an arbitrary grade reaction-bonded silicon nitride of 2.5 g/cm^3 density experience 79 MPa at 0.15 second; and hot-pressed silicon carbide, 65 MPa at 0.05 second. These peak stresses exist at the surface of the bulk material, however, and stresses on surface oxide layers would be much higher (due to the dissimilar thermomechanical properties). Internal stresses during heat-up are low, also due to the regular sample geometry.

Samples were visually inspected, weighed, and dimensionally checked after each stage of exposure. A small notch at the sample end ensured that the samples were placed in the same orientation on the thermal fatigue machine for each of the five times mounted. After the exposure sequence was completed, samples were tested in four-point bending at room temperature to measure retained strength. Care was taken to insert the most severely damaged face in a tensile manner within the inner load pins.

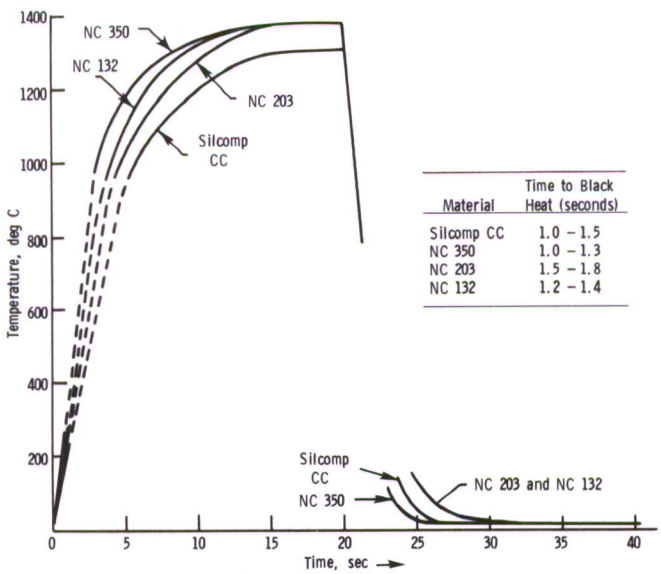

Material	Time to Black Heat (seconds)
Silcomp CC	1.0 – 1.5
NC 350	1.0 – 1.3
NC 203	1.5 – 1.8
NC 132	1.2 – 1.4

Figure 8. Heat-up and cool-down rates of bend bars in the thermal fatigue apparatus.

F. Fractography

The fracture surfaces of all 830 samples broken in this study were examined with a binocular microscope with magnifications up to 200X. The direction of lighting used for such inspection was very important and each sample was rotated or the light source adjusted as necessary for optimum effect. A camera stand was used to photograph a (large) representative selection of sample fractures and flat surfaces at 27X. Lighting for this work was effected with an intense light source equipped with two gooseneck fiber optic aiming appendages. Best results were achieved with low incident angles onto the fracture surfaces which promoted shadows that enhanced the photographs. Nevertheless, none of the photographs are as clear and distinct as what the eye can discern with the binocular microscope.

A representative selection of samples (just over 200) were examined with the scanning electron microscope (SEM). Optical photomicrographs with arrows labelling the defects to be studied were almost mandatory for optimum efficiency in using the SEM. Very often the SEM image lost some of the detail (colors and shading) visible to the eye or even on the light photographs. SEM samples were all coated with a very thin gold palladium coating to provide a conductive surface. All SEM samples for fracture surface examination were mounted with a slight tilt backwards (about 10 to 20°) so that the tensile surface as well as the fracture surface could be viewed. Therefore, true flaw depths cannot be accurately measured, but flaw lengths along the tensile edge could be. (As will be shown later, this did not prevent reasonable estimates of flaw depth.) This was done to permit inspection of oxide layers, machining marks and damage, chamfer chipping, and to observe surface porosity or pitting. For clarity many of the fracture surface photos in this report are labelled with a "T" for the tension edge or face and "C" for compression. "F. S." indicates the fracture surface.

III. MATERIAL CHARACTERIZATION

A quantitative analysis of impurity or additive content was conducted for all thirteen materials and the results are shown in Table 1. The method used was an emission spectroscopy procedure that required the grinding of samples into a powder. The grinding of samples was performed with a tungsten carbide apparatus and it is likely some tungsten was picked up in the process. Characterization details specific to the thirteen materials are discussed in the following sections. The density of each material was determined by measuring the mass and dimensions of the bend bars. Density variations in the materials can be appraised by the standard deviation of the bend bar densities. The phase composition of the materials

Table 1. METALLIC ELEMENT CONTENT (WEIGHT PERCENT) OF SILICON-BASED CERAMICS

	Al	B	Ca	Co	Cr	Cu	Fe	Mg	Mn	Mo	Ni	Ti	V	Zr	Y
a. Silicon Nitride															
Norton NC 132	0.09	∿0.005	0.08	--	<0.03	<0.008	0.13	0.25	<0.02	--	<0.02	<0.03	∿0.05	--	--
Norton NCX 34	0.11	∿0.05	*	--	<0.03	<0.008	0.17	0.006	<0.02	--	<0.02	<0.03	∿0.05	--	6.5
Norton NC 136	0.12	∿0.005	*	--	<0.03	<0.008	0.09	0.008	<0.02	--	<0.02	<0.03	∿0.05	--	9.6
Ford 2.7 RBSN	0.07	∿0.005	0.06	--	<0.04	0.01	1.0	0.003	0.02	--	<0.04	<0.06	<0.03	--	--
KBI RBSN	0.12	∿0.005	0.07	--	<0.04	0.01	0.23	0.004	0.03	∿0.05	<0.04	<0.06	<0.03	∿0.01	--
Norton NC 350	0.08	∿0.005	0.07	--	<0.04	0.01	0.14	0.003	0.01	--	<0.04	<0.06	<0.03	--	--
b. Silicon Carbides															
Norton NC 203	2.0	∿0.005	0.06	--	0.02	0.01	0.31	0.01	<0.02	∿0.05	<0.03	<0.03	∿0.05	∿0.05	--
Carburundum Alpha 1977	0.08	∿0.5	0.10	--	<0.02	0.01	0.13	0.02	<0.02	∿0.01-0.05	<0.06	0.04	<0.02	∿0.01	--
Carborundum Alpha 1978	0.05	∿0.5	0.05	∿0.10	0.03	0.01	0.31	0.02	<0.03	--	0.07	0.02	<0.02	--	--
Norton NC 433	0.05	--	0.05	∿0.10	0.02	0.005	0.05	0.01	<0.02	--	<0.03	0.01	<0.02	∿0.01	--
Norton NC 435	0.04	--	0.06	∿0.10	0.02	0.005	0.12	0.01	<0.02	--	<0.03	0.01	<0.02	∿0.01	--
GE Silcomp CC	0.09	∿0.5	0.04	∿0.5	0.02	0.01	0.22	0.01	0.03	--	<0.03	0.02	∿0.05	∿0.05	--
GE Silcomp CRC	0.11	∿0.5	0.05	∿0.5	0.02	<0.01	0.11	0.01	0.03	--	<0.03	0.02	∿0.05	∿0.05	--

∿ Semiquantitative
-- Not detected or scanned for
* Yttrium interference

was determined by X-ray diffraction, usually on the surface of a bend bar. This provided a reference for subsequent comparison to the surface oxides that formed during high temperature testing. In some cases, as discussed in the text, powdered samples were prepared for the X-ray diffraction procedure. The alpha to be Si_3N_4 phase ratio was quantitatively determined for the reaction-bonded materials by using a method detailed in Reference 8.

A. Norton NC 132 Hot-Pressed Silicon Nitride

Norton hot-pressed silicon nitride grade NC 132 was procured in mid 1976 in the form of several billets of size 15.2 × 15.2 × 2.54 cm. Two samples lots were prepared,* originally both of size 0.216 × 0.280 × 5.08 cm. The first lot of 45 samples was intended for use in both stress rupture and STSR testing; the second lot of 60 samples was prepared for the combined cycle testing. The average density of the stress rupture and STSR bend bar group, Lot A, was 3.23 g/cm^3 with a standard deviation of 0.015. The combined cycle group, Lot B, was not prepared to specifications† and had to be remachined to size 0.203 × 0.280 × 5.08 cm. The average density of this lot was 3.19 g/cm^3 with a 0.011 standard deviation. After the combined cycle trials were completed, excess samples from Lot B were used to supplement the stress rupture testing.

X-ray diffration identified Si_3N_4 present with a minor amount of Si_2N_2O. Emission spectroscopy showed Al, Fe, and Mg present (Table 1a). The magnesium present is the result of magnesia additive used to promote sintering. No porosity was evident when a polished section was observed with a light microscope.

B. Norton NC 136 Hot-Pressed Silicon Nitride

Norton hot-pressed silicon nitride, grade NC 136, was procured in July 1975 in the form of a billet 15.2 × 15.2 × 1.27 cm.‡ This material was hot pressed with a nominal 13% yttria as the pressing additive. The material was an experimental grade and only briefly available. It was developed in response to favorable results obtained with yttria rather than magnesia as the additive.[9] A catastrophic instability at 1000 C was identified for high yttria content compositions however,[10,11] and this composition material was found to be susceptible to the problem.[10] The material was chosen for this study to illustrate the benefit of the STSR test and also to act as a comparison to the later NCX 34 grade.

*It is unclear whether the lots were from the same billet or not.

†The samples were prepared by a different machine shop and were Blanchard ground followed by lapping. Although this led to a mirror-like finish, a few deep transverse scratches remained.

‡The meager results reported in the literature on this 13% yttria grade material do not designate the material as NC 136. The Norton quotation, purchase order, and marking on the billet used in this study had this designation however, and it will be used here for convenience. The use of material grade designations should be encouraged even if the material is short lived. In this manner, ambiguous references such as "Company Y old version silicon nitride," etc., can be avoided.

8. GAZZARA, C. P., and MESSIER, D. R. *Determination of Phase Content of Si_3N_4 by X-ray Diffraction Analysis.* Am. Cer. Soc. Bull., v. 56, no. 9, 1977, p. 777.
9. GAZZA, G. E. *Hot Pressed Si_3N_4.* J. Am. Cer. Soc., v. 56, no. 12, 1973, p. 662.
10. McLEAN, A. F., FISHER, E. A., BRATTON, R. J., and MILLER, D. G. *Brittle Materials Design, High Temperature Gas Turbine.* Ford Motor Company, Contract DAAG-46-71-C-0112, Interim Report No. 8, AMMRC CTR 75-28, 1975, p. 138-139.
11. LANGE, F. F., SINGHAL, S. C., and KUZNICKI, R. C. *Phase Relationships and Stability in the Si_3N_4-SiO_2-Y_2O_3 Pseudoternary System.* J. Am. Cer. Soc., v. 60, no. 5-6, 1977, p. 249-252.

Thirty-six samples of size 0.216 × 0.280 × 5.08 cm were prepared. The average geometric density of these bend bars was 3.37 g/cm^3 with a standard deviation of 0.015. Some mottling was evident on the surfaces, giving the appearance of dense patches surrounded by interrupted wavy lines (Figure 9). A gradient in this mottling indicates a lack of homogeneity in the material. A polished section suggests the mottling is porosity (Figure 10). An attempt to view the markings with the SEM was not successful even though a light photograph of the surface was used to guide SEM examination.

An exact yttrium concentration was determined by X-ray flourescence emission spectroscopy against known AMMRC standards. This test was performed on two samples with the result that 9.6 and 9.7 weight percent yttrium was detected. This corresponds to 12.2 and 12.3 weight percent yttria. X-ray diffraction identified beta Si_3N_4, the H phase,[12] WSi_2, and possibly some $Si_3Y_2O_3N_4$.

C. Norton NCX 34 Hot-Pressed Silicon Nitride

Norton NCX 34 hot-pressed silicon nitride with 8% yttria was procured in June 1977 in the form of a billet 15.2 × 15.2 × 1.27 cm in size. This grade was developed in an effort to retain the favorable properties associated with the yttria additive but to eliminate the 1000 C instability that existed in the earlier grades such as NC 136.[13] Thirty-two bend bars of size 0.216 × 0.280 × 5.08 cm were prepared. Average density was 3.37 g/cm^3 with a standard deviation of 0.008.

X-ray diffraction of a powdered bend bar indicated primarily beta Si_3N_4, prominent WSi_2, and some (clearly identified) H phase.[12] A diffraction pattern on the flat face of a bend bar indicated some preferred orientation with the (101) beta Si_3N_4 line increased in prominence relative to the other major peaks. An exact yttrium concentration was determined by X-ray fluorescence and was measured at 6.4 and 6.7 percent on two bend bar samples. This corresponds to 8.1 and 8.5 weight percent yttria.

D. Norton NC 350 Reaction-Bonded Silicon Nitride

Norton NC 350 reaction-bonded silicon nitride has been available for a number of years[14,15] and is one of the more mature materials tested in this program. The material reportedly has an excellent fabricability[16] and retains good mechanical properties to elevated temperatures.[15] Sixty samples of size 0.203 × 0.280 × 5.08 cm were cut from a billet of size 19 cm round by 0.46 cm thick. Some cracking in the plate occurred during the initial slicing process, suggesting residual stress might be present.* The average density of the bend bars

Figure 9. Light photo of the flat surface of an NC 136 bend sample showing the mottling. The surface is as machined.

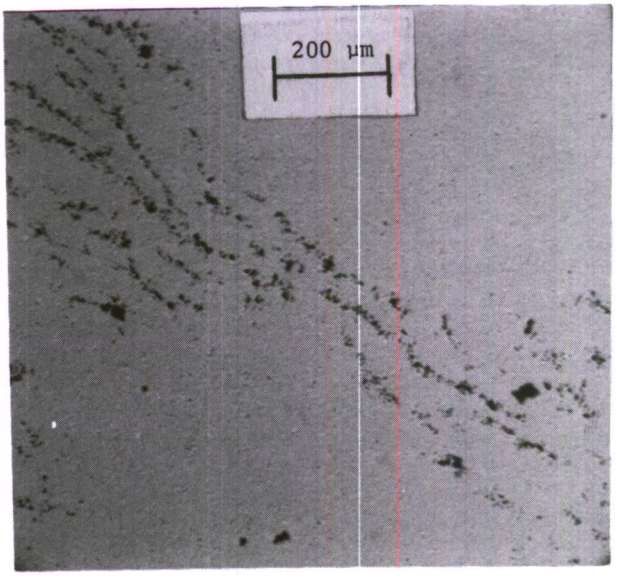

Figure 10. Polished section of a piece of NC 136 showing a close-up of a mottling band.

*This effect was also observed when several other plates were cut for other studies.

12. LANGE, F. F., SINGHAL, S. C., and KUZNICKI, R. C. *Phase Relations and Stability Studies in the Si_3N_4-SiO_2-Y_2O_3 Pseudo-Ternary System.* ARPA-Westinghouse Electric Corporation, Contract N00014-74C-0284, Technical Report No. 6, April 1976.
13. WEAVER, G., and LUCEK, J. *Optimization of Hot Pressed Si_3N_4-Y_2O_3 Materials.* Am. Cer. Soc. Bull., v. 57, no. 12, 1978, p. 1131.
14. WASHBURN, M., FREDRIKSSON, J., and ALLIEGRO, R. *Properties and Applications of Reaction-Bonded Silicon Nitride.* Presented at the 74th Annual Meeting of the American Ceramic Society, Washington, D.C., 6-11 May 1972.
15. WASHBURN, M., and BAUMGARTNER, H. *High Temperature Properties of Reaction-Bonded Silicon Nitride* in Ceramics for High Performance Applications, J. J. Burke, A. E. Gorum, and R. N. Katz, ed., Brook Hill Publishing Company, Chestnut Hill, Massachusetts, 1974, p. 486.
16. HAUCK E., *Future in Ceramic Gas Turbine Design.* Gas Turbine World, September 1974, p. 18.

was 2.53 g/cm^3 with a standard deviation of 0.019. The plate was fabricated by Norton in mid 1975.

Quantitative analysis by X-ray diffraction (on a powdered sample) indicated 74 weight percent alpha silicon nitride with the remainder beta phase. A polished section (Figure 11) reveals the considerable porosity which is well distributed with no excessively large pores or zones of porosity. No residual silicon was evident.

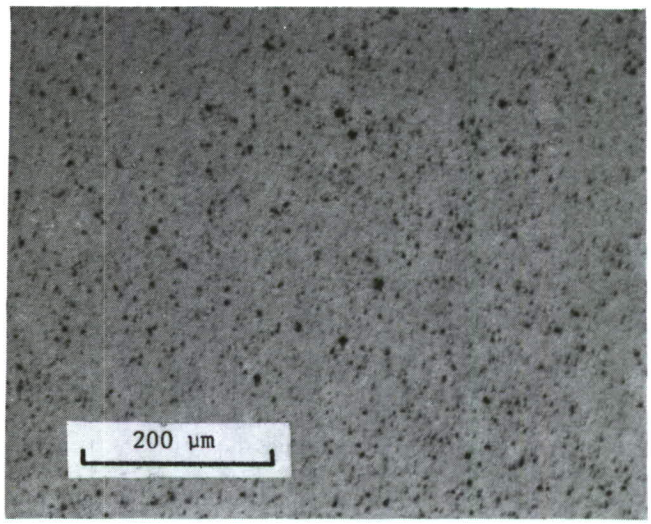

Figure 11. Polished section of NC 350 showing uniform porosity distribution.

E. Kawecki Berylco Industries Reaction-Bonded Silicon Nitride

A billet of Kawecki Berylco Ind. reaction-bonded silicon nitride was procured in January 1977. The billet was 30.5 × 30.5 × 1.27 cm in size and was much larger (particularly in thickness) than billets of the other two RBSN materials tested in this study. It was formed by isopressing a large billet of silicon powder, slicing the 1.27 cm slab from the billet, and finally nitriding the slab. One hundred bend bars of size 0.230 × 0.280 × 5.08 cm were cut from the center (away from the sides) of the billet with at least two samples coming from the thickness of the billet. The average bend bar density was 2.58 g/cm^3 with a standard deviation of 0.043.

A density gradient was evident through the plate thickness as shown in Figure 12 and this probably accounts for the high standard deviation in bend bar density. The billet was least dense in the interior. This gradient was manifested in the bend bars as shown in Figure 13. Polished sections indicated the porosity is irregular in shape with a wide distribution of size. Occasional silicon grains associated with pores were also observed (Figure 14).

X-ray diffraction identified 72 weight percent alpha silicon nitride and the remainder as beta silicon nitride. Emission spectroscopy showed Al and Fe to be the primary impurities or additives (Table 1a).

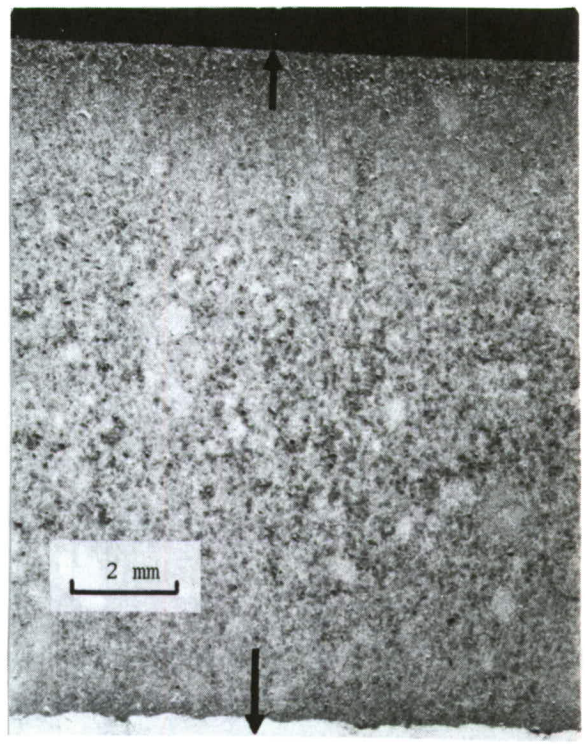

Figure 12. A light photograph of a section through the thickness of a KBI RBSN billet. The two arrows mark the surfaces. The billet is 1.27 cm thick (arrow tip to arrow tip). The gradient is porosity is evident.

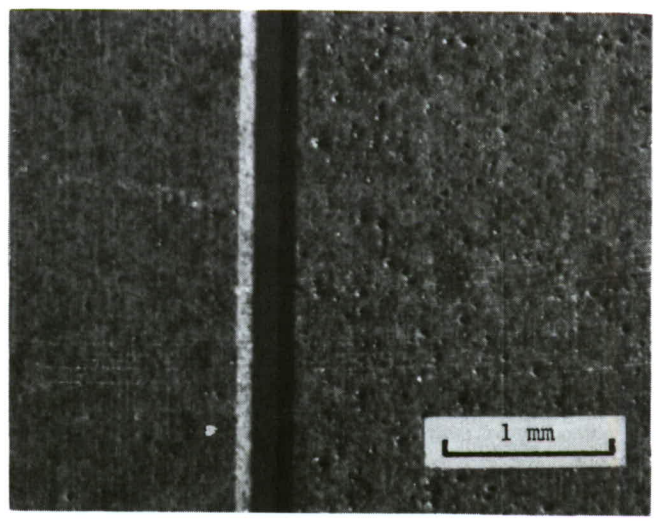

Figure 13. Light photograph of the surface of a KBI RBSN bend bar. After the sample was broken at room temperature, the two halves were placed side by side (with one side inverted) to show the gradient in pore size that exists through a single sample.

F. Ford 2.7 Reaction-Bonded Silicon Nitride

Reaction-bonded silicon nitride of nominal density 2.7 g/cm^3 was obtained from the Ford Motor Company in late 1977. The development of this material has been reported in References 10 and 17 to 21. The material was furnished in many small slabs of size 0.3 × 0.6 × 7.6 cm that were injection molded and nitrided. Sixty-four samples of size 0.216 × 0.280 × 5.08 cm were prepared from 32 of these slabs. Average sample density was 2.77 g/cm^3 with a standard deviation of 0.016. Porosity was uniformly distributed except for large pockets that were often observed (Figure 15). Very little free silicon was observed, although the shape of some pores suggested some meltout may have occurred.[19] X-ray diffraction indicated 80 weight percent alpha Si_3N_4 with 20 weight percent beta Si_3N_4. A few samples had large cracks and were rejected for testing. The relatively high iron content detected by emission spectroscopy (Table 1a) is the result of a three-percent iron oxide addition.[19]

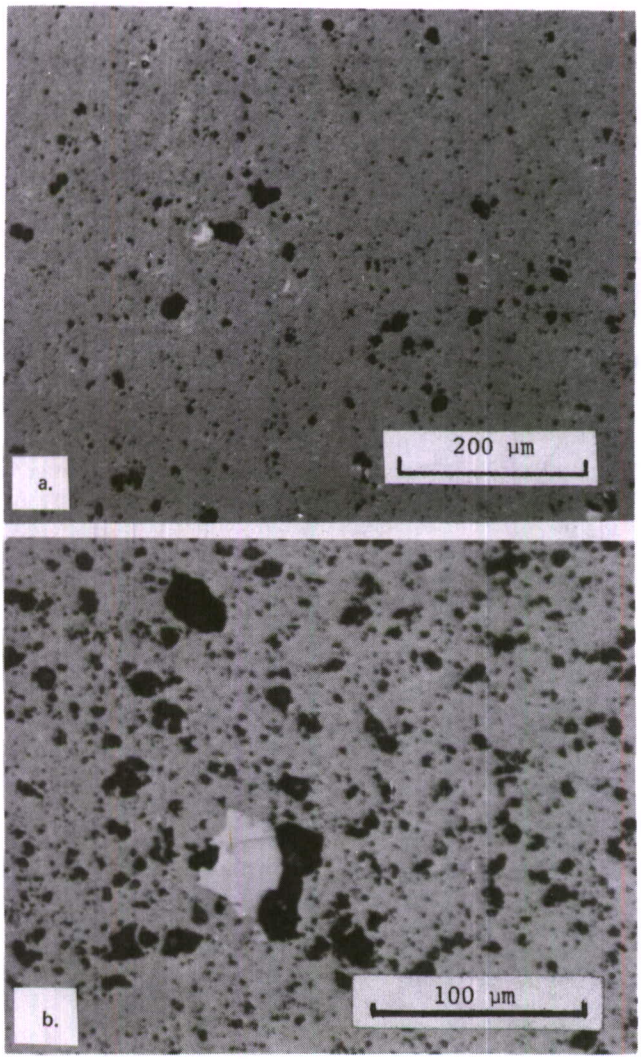

Figure 14. (a) Polished section showing the pore size and shape distribution in KBI RBSN; (b) close-up of a region showing an irregular pore associated with residual free silicon.

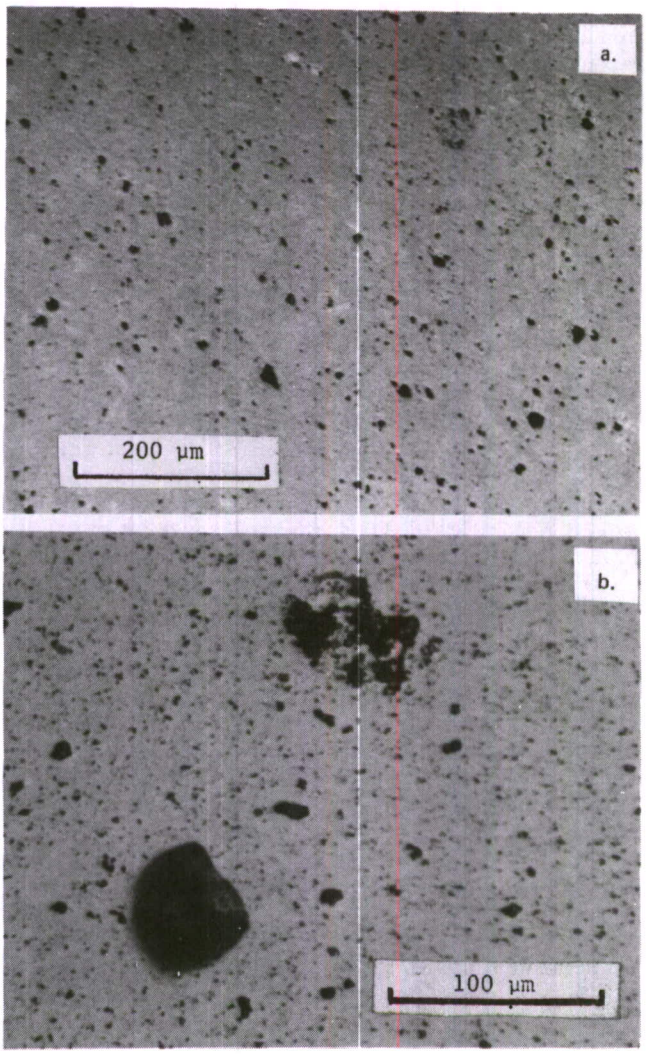

Figure 15. (a). Polished section of Ford 2.7 RBSN showing the distribution of porosity; (b) another section showing the shape of large pores.

17. McLEAN, A. F., FISHER, E. A., BRATTON, R. J., and MILLER, D. G. *Brittle Materials Design, High Temperature Gas Turbine.* Ford Motor Company, Contract DAAG46-71-C-0162, Interim Report No. 7, AMMRC CTR 75-8, July to December 1974.
18. McLEAN, A. F., BAKER, R., BRATTON, R. J., and MILLER, D. G. *Brittle Materials Design, High Temperature Gas Turbine.* Ford Motor Company, Contract DAAG46-71-C-0112, Interim Report No. 9, AMMRC CTR 76-12, July to December 1975.
19. McLEAN, A. F., and BAKER, R. *Brittle Materials Design, High Temperature Gas Turbine.* Ford Motor Company, Contract DAAG46-71-C-0142, Interim Report No. 10, AMMRC CTR 76-31, January to June 1976.
20. McLEAN, A. F., and FISHER, E. A. *Brittle Materials Design, High Temperature Gas Turbine.* Ford Motor Company, Contract DAAG46-71-C-0162, Interim Report No. 11, AMMRC CTR 77-20, July to December 1976.
21. MANGELS, J. *Development of Injection-Molded Reaction-Bonded Si_3N_4* in Ceramics for High Performance Applications II, J. J. Burke, E. M. Lenoe, and R. N. Katz, ed., Brook Hill Publishing Company, Chestnut Hill, Massachusetts, 1978, p. 113.

G. Norton NC 203 Hot-Pressed Silicon Carbides

Hot-pressed silicon carbide, Norton grade NC 203, was procured in June 1977 in the form of billets of size 15.2 × 15.2 × 2.5 cm. Two groups of samples size 0.203 × 0.280 × 5.08 cm were prepared for this study from two separate billets. One group of 60 samples (Lot A) was used for the stress rupture trials while a second group of 34 (Lot B) was applied to the combined cycle procedure. Sample densities averaged 3.36 g/cm^3 for both lots. X-ray diffraction analysis indicated tungsten carbide present in addition to the silicon carbide. Major impurities (or additives) detected by emission spectroscopy were Al, Fe, and W (Table 1b).

H. Carborundum 1977 Alpha Silicon Carbide

A sintered alpha silicon carbide produced by the Carborundum Company was also evaluated. Densities of up to 98% theoretical are claimed and it is reported that the material is suitable for injection molding, transfer molding, extrusion, slip casting, and cold pressing.[22,23] Data reported to date indicates the material retains a four-point flexural strength of 345 MPa to 1500 C.[22,23] Experiments at temperatures up to 1500 C did not detect evidence of slow crack growth.[23] The material was furnished in billets of size 5 × 5 × 0.6 cm and was fabricated in early 1977 by cold pressing followed by sintering. Samples for this study were cut to 0.216 × 0.318 × 5.08 cm and had an average density of 3.11 g/cm^3 with a standard deviation of 0.02.

A typical polished section shows a uniform distribution of porosity with a few uncharacteristically large pores (Figure 16). X-ray diffraction analysis on a bend bar identified only alpha SiC present. Major impurities (or additives) identified by emission spectroscopy include Al, B, Ca, Fe, and W (Table 1b).

I. Carborundum 1978 Alpha Silicon Carbide

A revised grade of sintered silicon carbide has been developed by the Carborundum Company. This newer grade results from a scale-up process to produce larger quantities of sintered silicon carbide than the earlier 1977 efforts, which were research oriented. Ten plates of size 5.08 × 5.08 × 0.63 cm (same size as 1977 lot tested for this program) were received in April 1978 and 100 samples of size 0.216 × 0.280 × 5.08 cm were prepared. This is a substantially greater number than were tested from the 1977 grade and permitted more extensive testing. Average density was 3.13 g/cm^3 with a standard deviation of 0.013.

More recently published data[24] on the sintered alpha SiC has indicated the material experiences "slow crack growth" at 1400 C and above, but no observation of this effect was made at lower temperature. Four-point flexural stress rupture experiments detected static fatigue failures at 1400 C and above, but not at 1200 C. The stresses that caused failure at 1400 C were in the range of 10 to 20 percent less than the fast fracture strength at room temperature; at 1500 C they were 20 to 30 percent less. A fast fracture strength decrease (10%) was noted at 1500 C, unlike the earlier grade.

A polished section of one of the bend bars shows the distribution of porosity in the sample is unlike the earlier grade (Figure 17a). The pore size distribution is wider than that of the earlier grade although the size of the largest pores (which can be expected to be strength limiting) appear similar.

A frequently observed feature (not seen in the 1977 material) was a ringlike porous region (Figure 17b). This defect has been attributed to powder agglomeration due to the spray drying procedure used during powder preparation.[25] In addition, large lenticular SiC grains were evident as shown in Figure 18. X-ray diffraction revealed only alpha silicon carbide. Emission

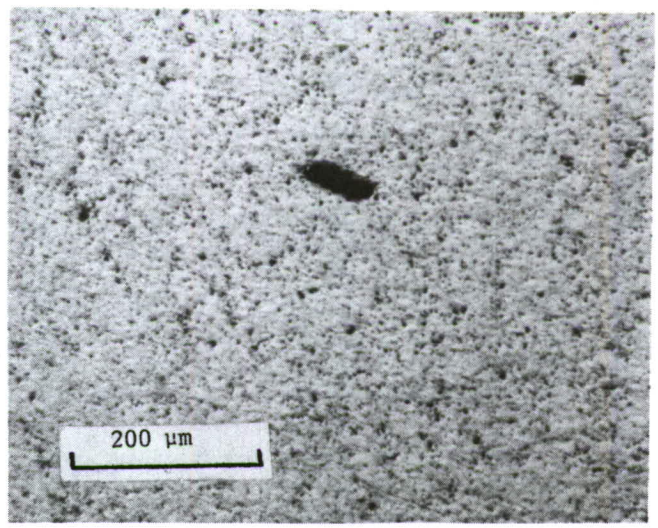

Figure 16. Polished section of Carborundum 1977 alpha silicon carbide.

22. KRAFT, E. H., and DOOHER, G. I. *Mechanical Response of High Performance Ceramics.* Presented at Second International Conference of Mechanical Behavior of Materials, Boston, Massachusetts, 16-20 August 1976.
23. KRAFT, E. H., and COPPOLA, J. A. *Thermomechanical Properties of Sintered Alpha Silicon Carbide* in Ceramics for High Performance Applications II, J. J. Burke, E. M. Lenoe, and R. N. Katz, ed., Brook Hill Publishing Company, Chestnut Hill, Massachusetts, 1978, p. 1023.
24. COPPOLA, J. A., SRINIVASAN, M., FABER, K., and SMOAK, R. *High Temperature Properties of Sintered Alpha Silicon Carbide.* Presented at International Symposium on Factors in Densification and Sintering of Oxide and Non-Oxide Ceramics, Hakone, Japan, October 1978.
25. JANOVICZ, M. A. *Ceramic Applications in Turbine Engines.* Detroit Diesel Allison Division, NASA Contract DEN 3-17, Progress Report, June 1978, p. 39.

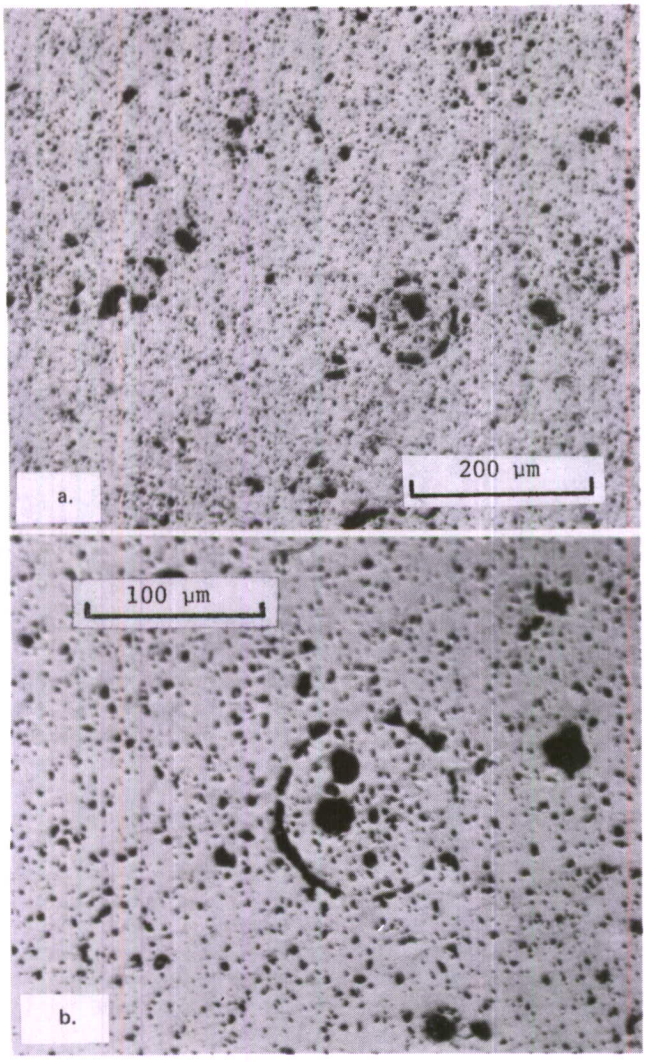

Figure 17. (a) Polished section of Carborundum 1978 alpha silicon carbide; (b) close-up of a common pore geometry observed in the material.

spectroscopy indicated a similar concentration of impurities (or additives) compared to the 1977 grade, except that substantially less tungsten was present in the 1978 vintage and more iron is present.

J. Norton NC 433 Siliconized Silicon Carbide

Norton NC 433 silicon carbide was procured in December 1976 in the form of several billets nominally 10 × 10 × 1.5 cm in size. This material, a variant of NC 400, is a composite fabricated by firing a body with a bimodal distribution of SiC particles into a porous compact. The compact is then infiltrated with silicon such that there is little or no residual porosity.[26,27] The

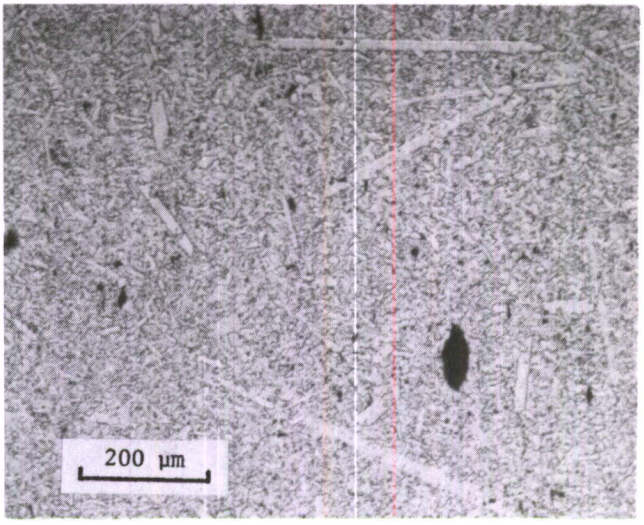

Figure 18. Polished and etched section of Carborundum 1978 alpha silicon carbide showing the elongated grains.

billets did not have a uniform thickness and varied by as much as 0.2 cm, but the most uniform billet was used for this study. Bend bars of size 0.216 × 0.318 × 5.08 cm were prepared. Average density of the samples was 3.063 g/cm^3 with a standard deviation of 0.013.

The microstructure is composed of a multimodal size distribution of bonded silicon carbide grains with a matrix of continuous silicon (Figure 19a). Periodically, large silicon zones are observed (Figure 19b), presumably due to the existence of large pores prior to infiltration. These zones often measure larger than 100 microns and are irregular in shape. Silicon concentration varied from 13 to 25 percent as measured by point analysis on five representative photomicrographs. X-ray diffraction identified alpha SiC, silicon, and probably beta SiC present.

K. Norton NC 435 Siliconized Silicon Carbide

A second grade of densified silicon carbide, Norton NC 435, was also evaluated. This material is similar to NC 433 (and NC 430) with the key difference being that the silicon carbide grain size is unimodal and much finer with higher flexural strengths reported as a result.[16,28] The material was received in May 1977 in the form of several billets of size 10.2 × 10.2 × 0.95 cm as well as several smaller billets. The density of 40 bend bar samples of size 0.216 × 0.280 × 5.08 cm prepared for this study from one of the large billets averaged 2.99 g/cm^3 with a standard deviation of 0.02. The smaller billets were thinner and had densities up to 3.10 g/cm^3.

26. ALLIEGRO, R. A. *Processing and Fabrication of Non-Hot Pressed SiC Ceramics* in Ceramics for High Performance Applications, J. J. Burke, A. E. Gorum, and R. N. Katz, ed., Brook Hill Publishing Company, Chestnut Hill, Massachusetts, 1974, p. 253-264.
27. TORTI, M., LUCEK, J., and WEAVER, G. *Densified Silicon Carbide - An Interesting Material for Diesel Applications.* SAE Technical Paper 780071, presented at SAE Congress and Exposition, Detroit, Michigan, March 1978.
28. TORTI, M. *The Effect of Fabrication Procedures Upon Mechanical Properties of Si_3N_4 and SiC Turbine Components.* Presented at Third Materials Conference Turbine Application, University of Michigan, Ann Arbor, Michigan, November 1974.

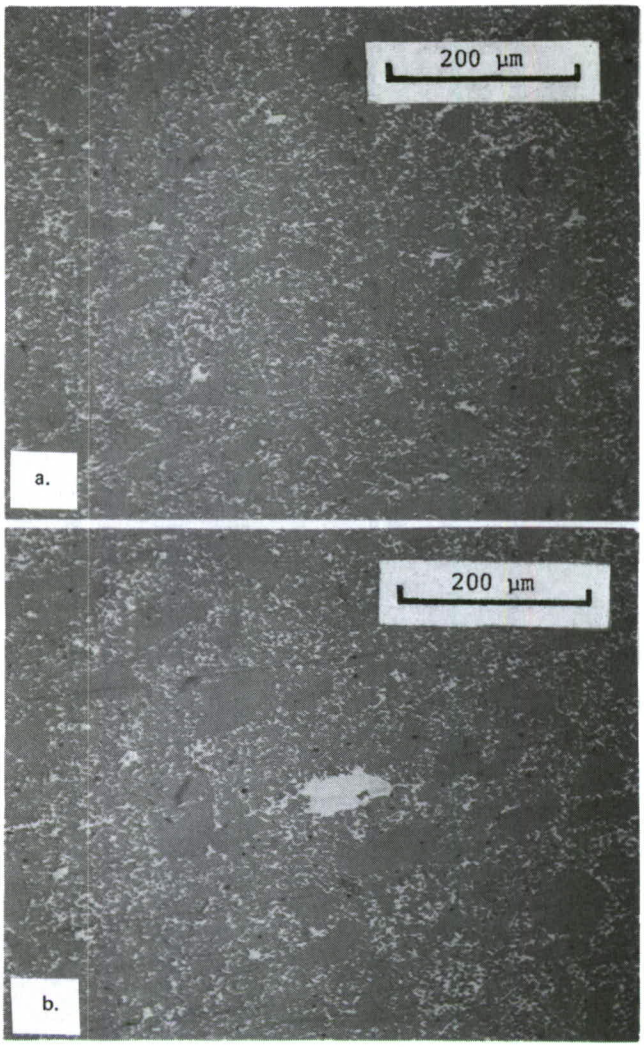

Figure 19. (a) Polished section of NC 433. The grey areas are silicon carbide grains, the white areas are silicon; (b) another section with a large Si zone.

X-ray diffraction indicated alpha silicon carbide (Form II, IV, VI probable), beta silicon carbide, and silicon metal. Although the beta SiC peaks are masked by the alpha lines, the intensity of the 2.51 Å line is so high relative to the other peaks that some is likely present. Emission spectroscopy shows a nearly identical chemistry compared to the NC 433 grade except for Fe content which was higher in the NC 435 (Table 1b).

The microstructure (Figure 20) is composed of much finer bonded silicon carbide grains (than the NC 433 grade) with a silicon matrix. A gradient in microstructure was detected, however, with

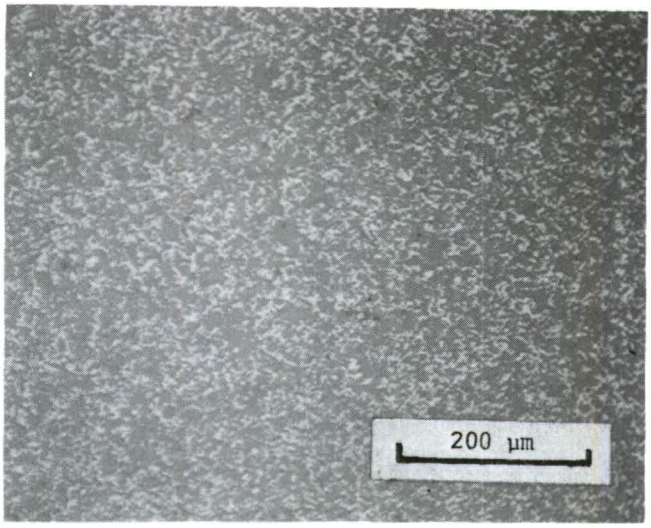

Figure 20. Polished section of NC 435 silicon carbide. The white phase is silicon metal and the grey phase is SiC.

large silicon carbide grains and higher silicon content near the billet surface (Figure 21). Silicon volume fraction near the surface measured by point analysis on three photomicrographs ranged from 30 to 35 percent, whereas two photomicrographs from the interior showed 18 and 25 percent.

L. General Electric Silcomp CRC Siliconized Silicon Carbide

A silicon carbide/silicon composite made by the General Electric Corporation was also tested in this study. The material is fabricated by infiltrating a precursor plate of carbon fibers with silicon metal. The carbon reacts to form silicon carbide crystals that are arranged according to the original carbon fiber arrangement. For example, uniaxially aligned fibers result in uniaxial silicon carbide crystals. Excess silicon forms the matrix but some residual carbon may be present. A variety of microstructures are possible depending upon the nature of carbon fibers of the precursor. Similar G.E. grades are described in References 29 to 32.

The particular grade tested for this study was designated CRC and resulted from infiltration of a random carbon fiber precursor with silicon. Forty samples of size 0.203 × 0.280 × 5.08 cm were obtained from G.E. in May 1977. The samples were fabricated by cutting a preform into approximately a dozen bend bar precursors and then infiltrating the individual bars with silicon. Because of this, the results of this study may not reflect the actual behavior or problem areas to be expected with thicker or larger billets. In addition, these

29. MEHAN, R. L. *Anistropic Behavior of Si/SiC Ceramic Composites.* Am. Cer. Soc. Bull., v. 56, no. 2, 1977, p. 211.
30. MEHAN, R. L. *Effect of SiC Content and Orientation on the Properties of Si/SiC Ceramic Composites.* J. Mat. Sci., v. 13, 1978, p. 358.
31. HILLIG, W. et al. *Silicon/Silicon Carbide Composites.* Am. Cer. Soc. Bull., v. 54, no. 12, 1975, p. 1054.
32. HILLIG, W. *Tailoring of Si/SiC Composites for Turbine Applications* in Ceramics for High Performance Applications II, J. J. Burke, E. M. Lenoe, and R. N. Katz, ed., Brook Hill Publishing Company, Chestnut Hill, Massachusetts, 1978, p. 989.

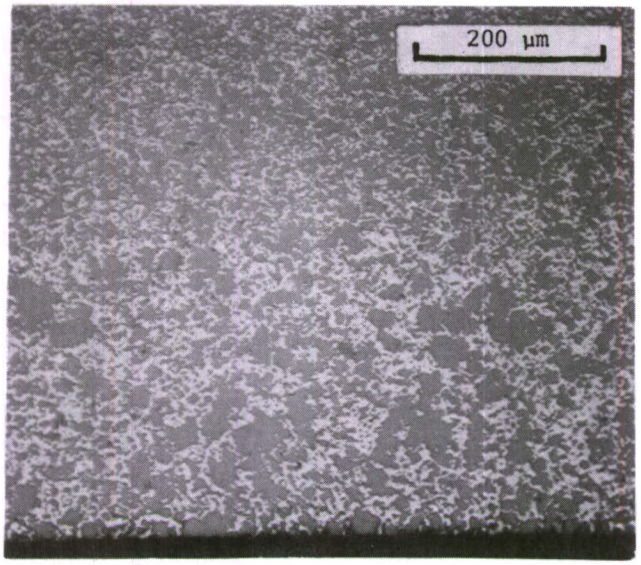

Figure 21. Polished section of NC 435 showing a gradient of SiC grain size and also Si content as the sample is traversed from interior to the surface. The surface is indicated by the black border.

samples were, unlike the other materials tested in this study, subjected to a proof testing scheme applied by G.E. The proof test involved applying a three-point loading of 276 MPa. Some samples were also discarded by G.E. on the basis of low density. The 40 samples delivered represent a 68 percent yield from the samples actually fabricated. Densities of the 40 samples averaged 2.98 g/cm^3 with a standard deviation of 0.046 (relatively high).

A polished section (Figure 22) shows the distribution of SiC, Si, and void. The void may in fact be carbon pullouts. Regions of higher void or carbon content were often detected as shown in Figure 23. X-ray diffraction analysis indicated beta SiC as the primary component with some silicon present. Emission spectroscopy identified Al, B, Co, and Fe as the major impurities (Table 1b).

M. General Electric Silcomp CC Siliconized Silicon Carbide

A second grade of General Electric Corporation Silcomp, designated CC, was also evaluated. This grade was fabricated in a similar manner to the CRC grade except that the precursor was made up of a carbon cloth (rather than random fibers). Carbon fiber ribbons were woven into mattes with a perpendicular alignment of the ribbons (such as a chaise lounge outdoor seat). Several such sheets were laid on top of each other to form the precursor. The end result after infiltration is a composite structure very similar to woven roving fiberglass epoxy plates used as ceramic armor back-up plate. Figure 24, as well as the fracture surfaces discussed below, illustrates the arrangement and orientation. As with the CRC grade, infiltration was performed on individual bars cut from the precursor. The bend bars delivered had been ground after infiltration to provide a suitable surface and final sample dimensions. The microstructure shown in Figure 25 illustrates the typical features, including elongated SiC fibers, excess silicon, and residual carbon.

Sixty samples of size 0.198 × 0.280 × 5.08 cm were obtained from G.E. in May 1977. Average density was 2.95 g/cm^3 with a standard deviation of 0.036. The samples of this grade were also survivors of a proof testing scheme that G.E. applied. The proof testing scheme involved three-point bending to 276 MPa. Samples with low densities were also discarded. The 60 samples delivered represent a 58 percent yield after the three-point proof test procedure.

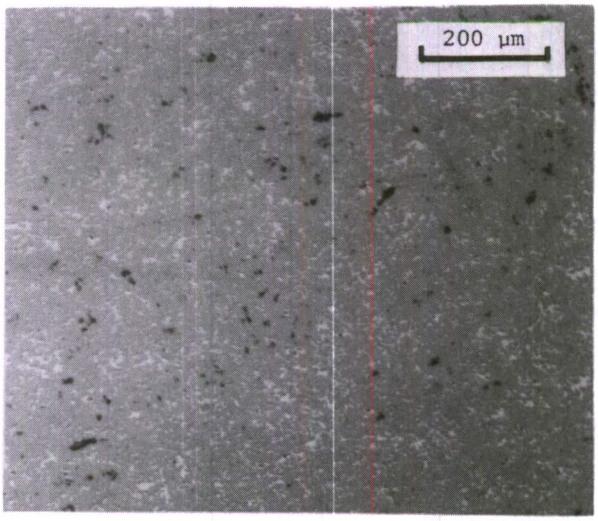

Figure 22. Polished sections of Silcomp CRC siliconized silicon carbide. The grey is SiC, white is silicon, and the black is carbon-void.

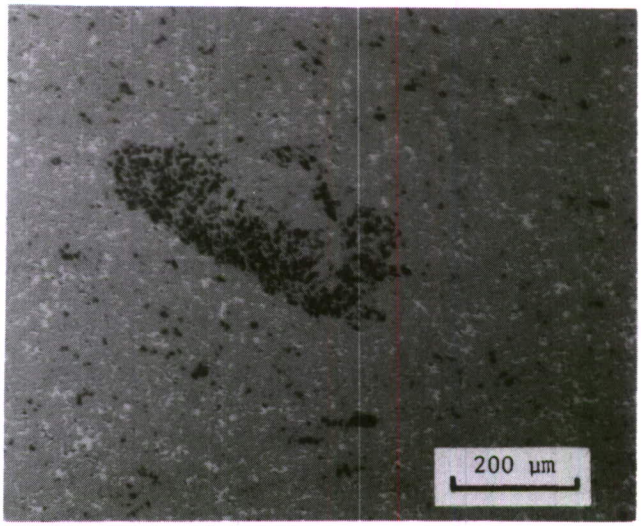

Figure 23. Alternate section of Silcomp CRC showing a a high carbon-void concentration.

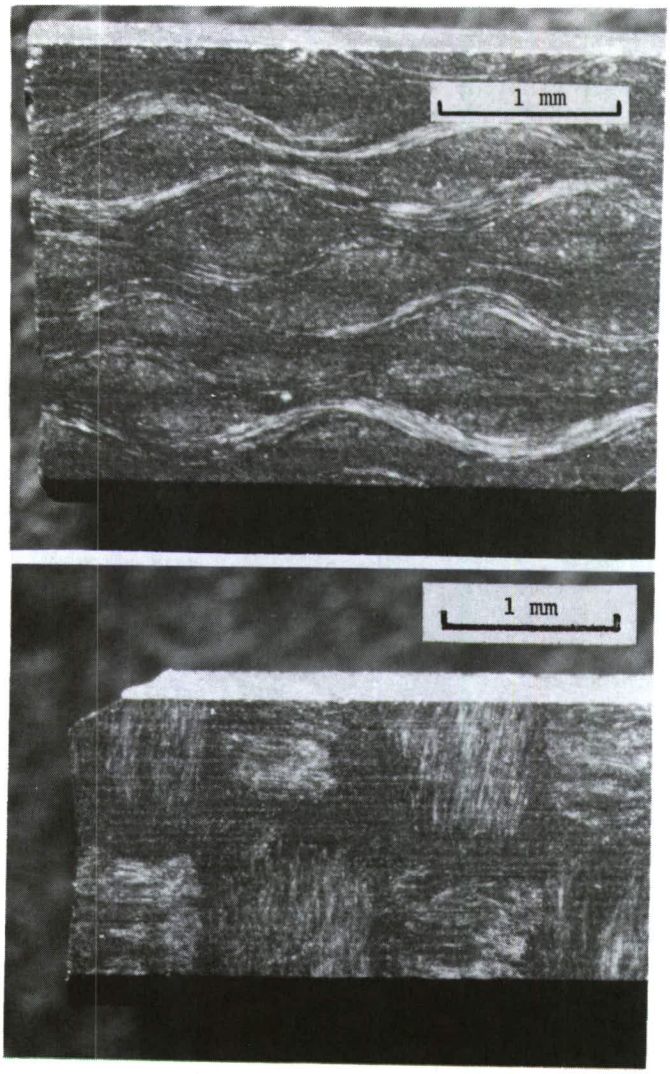

Figure 24. Photos of the top (a) and side (b) of a Silcomp CC bend bar showing the fiber arrangement. This sample failed at 20 hours during a 1200 C stress rupture trial. Oxidation highlights the fiber markings.

X-ray diffraction identified beta silicon carbide, some silicon metal, and no alpha silicon carbide. Emission spectroscopy identified Al, B, Co, and Fe as the major impurities (Table 1b).

IV. RESULTS AND DISCUSSION

A. Norton NC 132 Hot-Pressed Silicon Nitride

1. Control Strengths

Two control groups of reference strengths were generated, one for each lot of samples prepared. Twenty-four room temperature flexural strengths were obtained from 16 of the stress

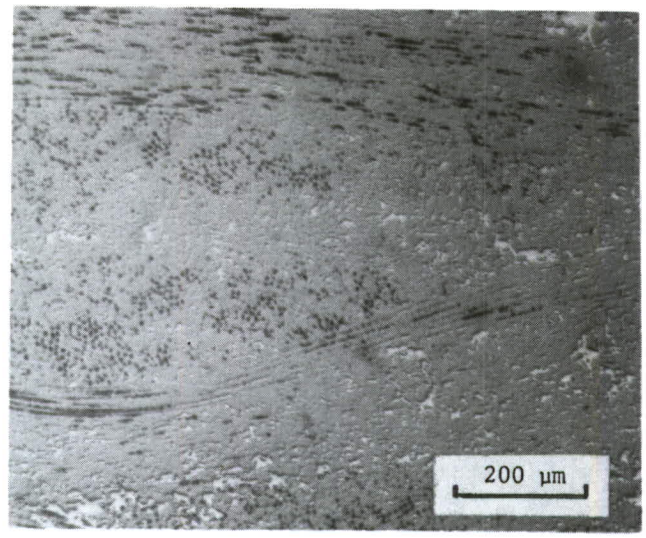

Figure 25. Polished section of Silcomp CC sample. The grey is SiC, the white is silicon, and the black is carbon-void.

rupture and STSR group (Lot A).* Average strength was 825 MPa with a rather high standard deviation of 137 MPa. The Weibull plot of the data shows a distinctly multimodal nature (Figure 26). The samples often fragmented into several pieces and in a few cases it was difficult to positively identify the initiation site. Nevertheless, nearly all fractures originated within the gage length of the bend fixtures. The bimodal character seemed to relate to a tendency to break from a corner or noncorner-located flaw. Binocular microscope inspection revealed that all but one of the higher strength fractures originated from a corner defect. Despite distinctive mirrors, a specific defect could not be identified in any sample, although small chips along the corner chamfer may have contributed to some failures (Figure 27). Machine marks along the chamfer were not longitudinal, an effect that probably contributed to the chipping. The lower strength samples generally fractured into two pieces only. These samples had distinct mirrors well away from the corners, but were near the tensile edge. A critical stress intensity formulation can be used to predict an expected flaw size:

$$K_{Ic} = M \sigma_a \sqrt{c}$$

where K_{Ic} = the critical stress intensity

M = a geometric factor

σ_a = the applied stress

c = the flaw depth or size.

*Half the samples broke so a second test was possible on the longest fragment.

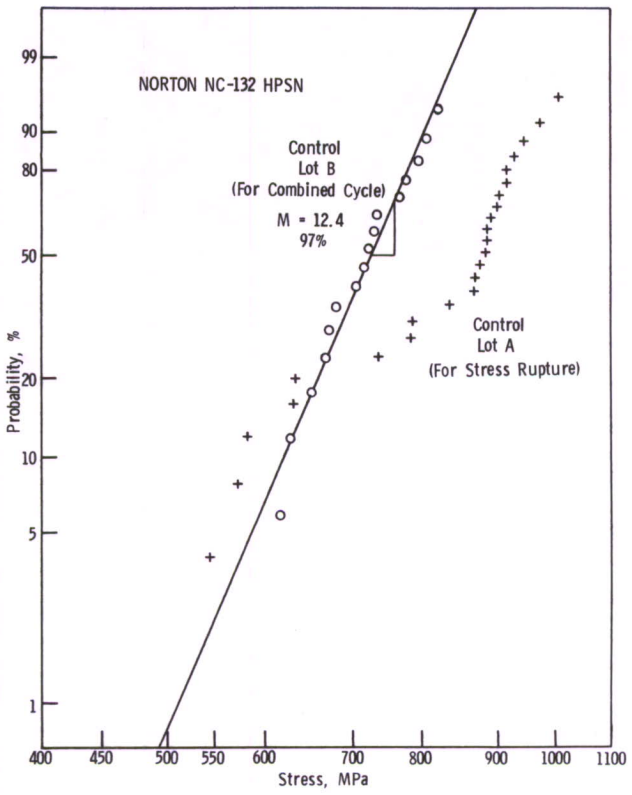

Figure 26. Control strength data for two lots of NC 132 hot-pressed silicon nitride. The vertical axis is cumulative probability of failure. The axes have been chosen so that if the data is fit by a Weibull two-parameter function, it will appear as a straight line. The slope of the line is the Weibull modulus and is fitted by a least squares procedure with a correlation coefficient as shown. Each point represents one strength test.

For a shallow semicircular surface defect in a beam in bending, M = 1.16 at the deepest point.[33] If $K_{Ic} \approx 5.0$ MN/m$^{1.5}$ (References 34 to 36), then the flaw depth should be $\approx$ 18 to 63 μm (according to the range of strengths for NC 132 Lot A samples: 543 to 1010 MPa). Specific flaws of appropriate size could not be identified, but a common feature was observed: a dent in the surface at the mirror center and on both fracture halves (Figure 28). This defect, although too small in itself to cause fracture, is likely the result of machining damage that may have caused a deeper crack to form. The outline of the deeper crack was not evident on any of the SEM photos, however. (As will be shown later, such a defect was observed for other hot-pressed materials tested in this study.)

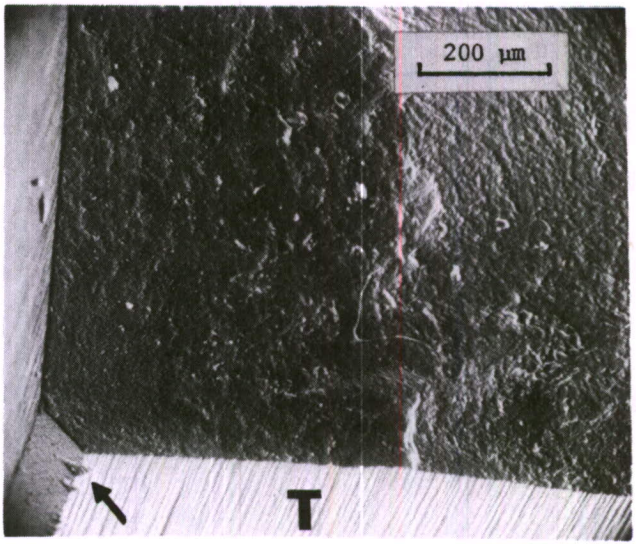

Figure 27. Fracture surface of a room temperature control fracture showing the mirror and corner chipping. Bend strength was 543 MPa.

The second control group, Lot B, was for the combined cycle set of samples. Ten samples yielded 16 fractures with an average of 714 MPa and a standard deviation of 60 MPa, both of which are lower than the Lot A results. The Weibull plot was unimodal and a least-squares fitted line of slope 12.4 had a correlation coefficient of 97 percent (Figure 26). All fractures were within the gage length and originated from corners. Most were either from machining striation damage or from chip-outs.

2. Stress Rupture, 1200 C

Forty-five stress rupture trials at 1200 C were conducted and the results are shown in Figure 29. Eighteen samples from Lot A (specimens originally intended for stress rupture) were used, but 30 samples from Lot B that were excess to the combined cycle testing were also used to supplement the data. A consistent trend of shorter lifetime with higher applied stress is evident. A least-squares fitted line (all points except the failure on loading and the survivors) implies the following relationship:

$$t_f = B\,\sigma_a^{-11.5}$$

where t_f = the time to failure

B = a constant

σ_a = the applied stress.

33. SMITH, F., EMERY, A., and KOBAYASHI, A. *Stress Intensity Factors for Semicircular Cracks, Part II - Semiinfinite Solid.* J. Appl. Mech., Trans. ASME Series E, v. 34, December 1967, p. 953.
34. HENSHALL, J., ROWCLIFFE, D., and EDINGTON, J. *The Measurement of K_{Ic} and Subcritical Crack Propagation Rates in Hot-Pressed SiC and Si_3N_4* in Fracture, 1977, v. 3, ICF4, Waterloo, Canada, June 1977, p. 875.
35. EVANS, A., and WIEDERHORN, S. *Crack Propagation and Failure Prediction in Silicon Nitride at Elevated Temperatures.* J. Mat. Sci., v. 9, 1974, p. 270.
36. LARSEN, D., and WALTHER, G. *Property Screening and Evaluation of Ceramic Turbine Engine Materials.* IIT Research Institute, AFML Contract F33615-75-C-5196, Interim Report No. 6, July 1978, p. 667.

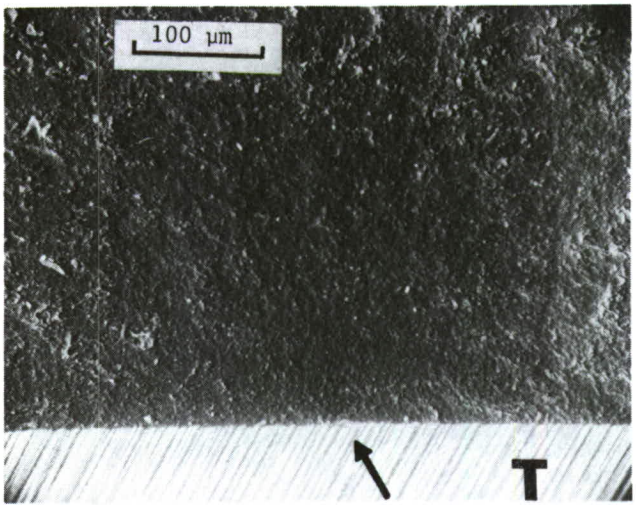

a. SEM low power photo of the entire mirror. The arrow points at a feature at the center of the mirror.

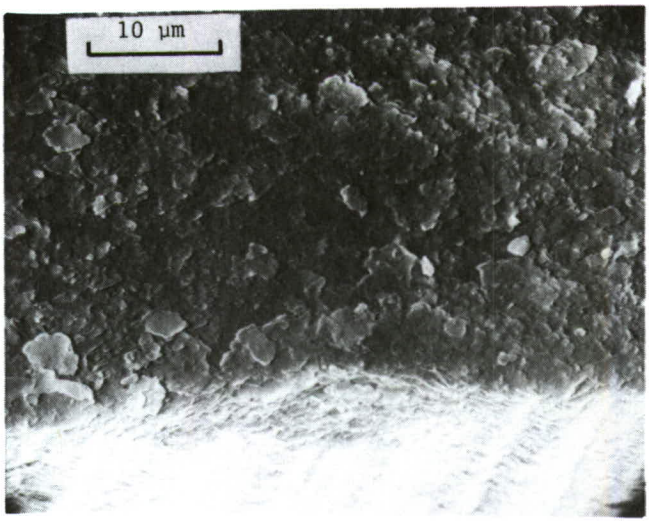

b. A close-up of (a) shows a slight dent in the surface. A matching dent was observed in the mating fracture half.

Figure 28. Fracture surface of an NC 132 room temperature control sample which broke at 630 MPa.

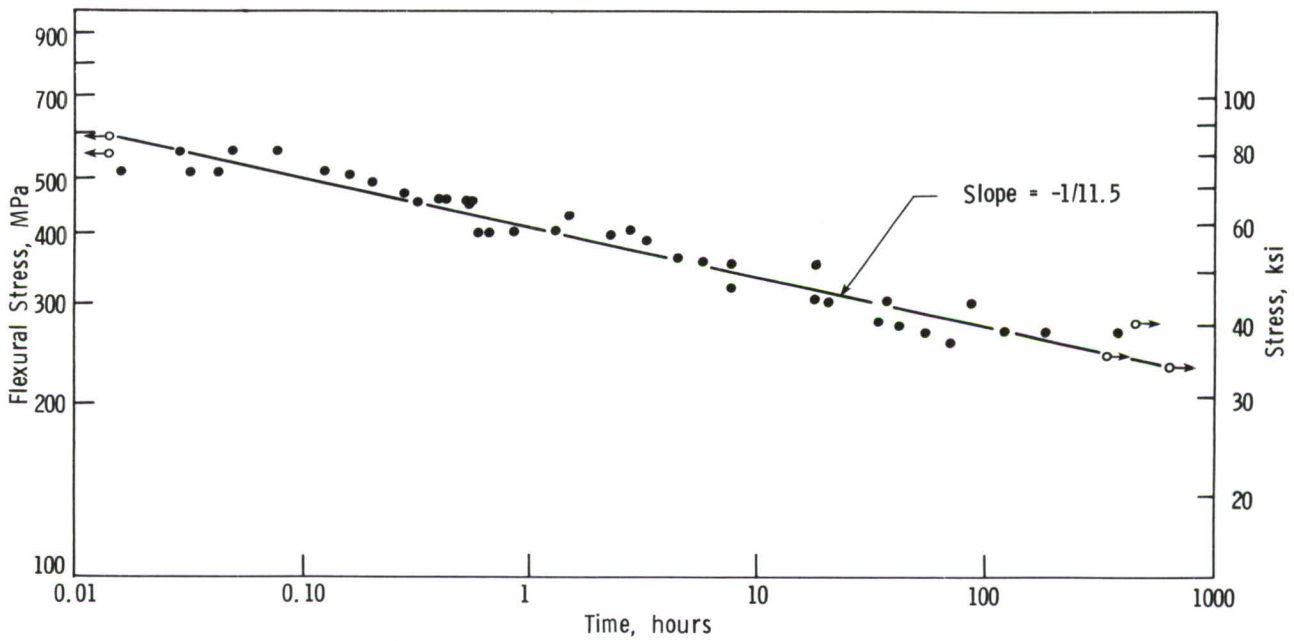

Figure 29. Flexural stress rupture at 1200 C for Norton NC 132 hot-pressed silicon nitride.

It can be shown (see, for example, References 37 and 38) that the linear behavior of the log time-log stress plot is expected if the power law crack velocity-stress intensity relationship applies:

$$V = A\ K_I^N$$

where V = the crack velocity

A, N = constants

K_I = the stress intensity.

The (inverse) slope of the stress rupture plot (11.5) is in fact the exponent N.

37. DAVIDGE, R., McLAREN, J., and TAPPIN, G. *Strength Probability Time (SPT) Relationships in Ceramics.* J. Mat. Sci., v. 8, 1973, p. 1699.
38. RITTER, J., Jr. *Engineering Design and Fatigue Failure of Brittle Materials* in Fracture Mechanics of Ceramics IV, R. Bradt, D. Hasselman, and F. Lange, ed., Plenum Press, New York, 1978, p. 667.

Care must be taken in the interpretation of the above stress rupture data, however, despite the excellent fit of the line to the data. Considerable permanent deformation was evident in samples that endured for 100 hours or more. The creep that accounts for this deformation may also act to reduce the maximum tensile stress that acts within the bend sample. As stated earlier, all the stresses reported in this work are calculated from the elastic solution where stresses vary linearly from compression to tension across the sample thickness. The *actual* peak tensile stress may be considerably less. The reduction can be expected to be greater the longer the sample is under load. (See, for example, Figure 2-52 of Reference 1.) Thus the elastic stresses listed in Figure 29 are upper limits and the longer runs may have effectively had lower stresses. If the corrections could be made, it would result in a line of steeper downward slope in Figure 29. This would correspond to a *lower* value for the stress intensity-crack velocity exponent.

A further complication is the violation of the assumptions that the crack shape and stress state around the crack front do not change as the crack grows. These assumptions may be suitable for very large samples that can be treated as semi-infinite plates, but may not be suitable with samples of small cross section. As will be discussed below, the crack fronts for the long-time samples grew to become significant fractions of the cross-section dimensions. The stress intensity at the deepest point of the crack will *diminish* as a result of penetrating into the area of lower stresses toward the neutral axis. The same applies for the stress intensity at any other part of the crack front periphery. (See Figure 6 of Reference 33, for example.) This effect would also tend to cause the slope of the line in Figure 29 to be an upper limit; that is, the exponent N should be a smaller number.

The least-squares line in Figure 29 was generated by assuming that time was the independent variable. Allowing stress to be the independent variable resulted in a line of slope 10.8, but the line in this case fits poorly at either end; that is, at the long or short times to failure. That a change in the manner of analysis can result in a significantly different exponent indicates care should be applied in interpretation. Alternate statistical approaches such as reported in References 39 to 41 may help.

The intermixing of samples from the two sample lots is a procedure of uncertain validity.* As stated in the introduction of the NC 132 data (Section III-A), it is not known whether Lot A and Lot B came from the same billet. A number of redundant trials were conducted over the entire range of stresses using samples from both lots. *No* tendency for different behavior was evident.†

The results of the first 24 trials were published in a preliminary form in References 2 and 5. The slope reported at that time was 9.2, but was based on only sixteen data points. The survival of several of the samples at the long times prompted an interpretation that a static fatigue limit may apply. The addition of tests using Lot B samples (excess from combined cycle testing) indicates otherwise. It is evident the three samples which did not fail may have done so if allowed to remain under load.

The SCG (slow crack growth) exponent reported here (11.5) is somewhat lower than the values reported in the literature for 1200 C. It has been shown[35] that the SCG exponent for hot-pressed silicon nitride can vary from 10 (±2) for double torsion experiments conducted at 1250 C to 1400 C to a much higher value at 1200 C. The stress intensities involved for the 1200 C experiments shown in Figure 29 of this report are small. By applying the stress intensity formula, substituting in the range of applied stresses and the range of initial flaw sizes, it can be shown that the initial stress intensities are of the order of 1.0 to 5.5 $MN/m^{1.5}$. Most of the samples with high initial stress intensities ($\approx$5 $MN/m^{1.5}$) will fail rather quickly due to the high exponent that applies to that range of velocity-stress intensity data. These samples will fail on loading or in short times. The bulk of the stress rupture data involves stress intensities in the range of 2 to 4 $MN/m^{1.5}$. Re-examining the crack growth data in Reference 35 indicates it is quite plausible that the 1200 C behavior also could have the lower exponent at the low velocities and low stress intensities. The 1200 C data plot of Reference 35 could shift slopes as did the 1250 C and 1300 C results. Indeed, the lower stress intensities and crack velocities (inherent to the stress rupture process) are of much greater importance to the designer than the data usually furnished by double torsion experiments. Similar conclusions apply regarding the comparision of the low exponent reported here (11.5) to those values reported in Reference 34 (HS 130, 1000 C, N=90);

*It is at least known that the initial control strengths vary, but this may be due to minor differences in the machining preparation.

†We do have data, however, that shows a definite difference in lifetime with samples cut from different billets. This result is based on a third lot of samples from a billet not used in this study.

39. RITTER, J., Jr,, and JAKUS, K. *Overview of Lifetime Predictions for Silicon Nitride.* Proceedings of 1977 DARPA/NAVSEA Ceramic Gas Turbine Demonstration Engine Program Review, Castine, Maine, MCIC 78-36, August 1977, p. 701.

40. JAKUS, K., COYNE, D., and RITTER, J., Jr. *Analysis of Fatigue Data for Lifetime Predictions for Ceramic Materials.* J. Mat. Sci., v. 13, 1978, p. 2071.

41. JAKUS, K., and RITTER, J., Jr. *Static Fatigue of Si_3N_4.* J. Am. Cer. Soc., v. 61, no. 5-6, May 1978, p. 274.

Reference 42 (NC 132, 1204 C, N=30); and Reference 43 (NC 132, 1200 C, N=30). On the other hand, the exponent reported herein is in good agreement with the 9.5 value obtained in Reference 44 from controlled flaw experiments on bend bars (HS 130, 1200 C, in vacuum); with the 9.5 value obtained in Reference 45 from controlled flaw experiments on bend bars (NC 132, 1200 C, in air), and with the 12.4 obtained from pure tension static fatigue experiments (NC 132, 1200 C, in air).[45]

Fracture surfaces showed prominent slow crack growth zones (Figure 30). Outside of the SCG zone, fracture surfaces were relatively smooth and not jagged. The samples generally broke into only two pieces. As will be shown below, a Griffith criterion of failure may account for the enormous size of these flawed areas, but as discussed in References 43, 46, and 47, the notion of an ideally sharp crack propagating through the material is unrealistic. In general, the longer the time to failure, the larger the SCG zone. The short-time-to-failure samples (Figure 30a-f) had a semicircular (or quarter circle from the corner) SCG shape. This shape gradually evolved sideways under the influence of tensile stress, first to an ellipse and then to a linear crack front as additional time elapsed prior to failure. SCG zones were observable in samples which endured more than 10 minutes, but samples which failed in less than that time showed no prominent SCG zone and instead assumed a fast fracture-like appearance (smooth mirror - jagged fast fracture zone). In at least one case, two independent SCG zones grew on the same fracture surface. While in some samples the SCG grew from a corner, at least half of the samples had SCG growing from a location either on the tensile edge or internally.

The three samples that survived intact had prominent permanent deformation. The 234 MPa sample that survived 610 hours had 1.4 percent maximum outer fiber strain (Figure 31). When subsequently fractured at room temperature the retained strength was 247 MPa.* The 247 MPa survivor (331 hours) had a retained strength of 420 MPa and a maximum strain of 1.1 percent. The third survivor, 277 MPa (431 hours), was broken in handling but had a 0.9 percent permanent strain. Of special interest is that the first two showed SCG markings on the room temperature fracture surface and that these were *subsurface* (Figure 32). These SCG zones evidently grew during the 1200 C stress rupture loading, but not enough to reach a fast fracture condition. On subsequent testing for room temperature retained strength, the SCG zones were loaded to failure. Based upon the fracture surface markings on the samples which did fail, it is likely other samples had SCG that originated below surface and grew to intersect the surface. The presence of SCG zones in the survivors suggests that if the samples were allowed to remain under load, they eventually would have failed.

In the samples which did fail, it was often observed that the SCG boundary was unsymmetrical and undulating rather than semicircular or elliptical (Figure 30h). This suggests variations in the microstructure or sample chemistry that might have affected crack growth conditions. In a number of samples, cracks originally away from a corner would assume irregular shapes once they grew large enough to be influenced by an unbalanced stress state due to the corner. In a few cases nonuniform loading on the sample (fixture misalignment) could have accounted for the unsymmetrical shape.

All fracture surfaces were analyzed for percentage of area consumed by SCG and the results are shown in Figure 33. A general trend of greater growth with longer time to failure (lower stress) is clear, but the scatter is large. A critical stress intensity formulation can be used to predict the final crack size. Again, applying the critical intensity K_{Ic} for a semicircular surface crack in a semi-infinite plate in tension at 1200 C with $K_{Ic} \approx 6.0$ MN/m$^{1.5}$ (References 34 and 35) and for the higher applied stresses ($\approx$600 MPa), the final crack depth is predicted to be 78 μm. It is not surprising that the short-time-to-failure samples had a fast fracture appearance. At the lower applied stresses ($\approx$250 MPa), a similar calculation for a semicircular flaw leads to a final crack size of 450 μm. Such a crack would extend well into the specimen cross section and the crack shape and uniform stress field assumptions are not valid. To examine this case more correctly, the finite dimensions of the beam

*The actual stress value is of little validity due to the excessive curvature. The samples were fractured primarily to detect any gross strength loss and to determine if SCG had occurred.

42. ANNIS, C., and CARGILL, J. *Modified Double Torsion Method for Measuring Crack Velocity in NC 132 (Si_3N_4)* in Fracture Mechanics of Ceramics IV, R. Bradt, D. Hasselman, and F. Lange, ed., Plenum Press, New York, 1978, p. 737.
43. TIGHE, N. *The Structure of Slow Crack Interfaces in Silicon Nitride.* J. Mat. Sci., v. 13, 1978, p. 1455.
44. MENDIRATTA, M. G. *Use of Controlled Surface Flaws in Studying Slow Crack Growth in Ceramics.* Systems Research Laboratories, AFML Contract F33615-75-C-1005, Quarterly Progress Report 3165-10, May 1977.
45. GOVILLA, R., and ELDER, R. *Tensile Stress Rupture Testing of Hot-Pressed Si_3N_4 at 1200°C.* Presented at the 81st Annual Meeting of the American Ceramic Society, Cincinnati, Ohio, 2 May 1979.
46. RICE, R. et al. *Fractography of Si_3N_4 and SiC* in Ceramics for High Performance Applications II, J. J. Burke, E. M. Lenoe, and R. N. Katz, ed., Brook Hill Publishing Company, Chestnut Hill, Massachusetts, 1978, p. 669.
47. RICHERSON, D., and YONUSHONIS, T. *Properties of Silicon Nitride Rotor Blade Materials.* Proceedings of the 1977 DARPA/NAVSEA Ceramic Gas Turbine Demonstration Program Review, Castine, Maine, MCIC 78-36, August 1977, p. 193.

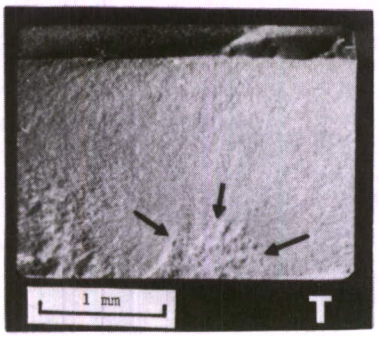

a. Applied stress: 483 MPa; failure at 0.20 hour

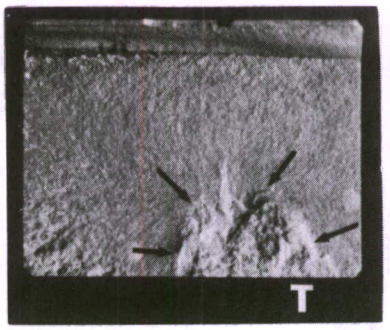

b. 448 MPa at 0.55 hour

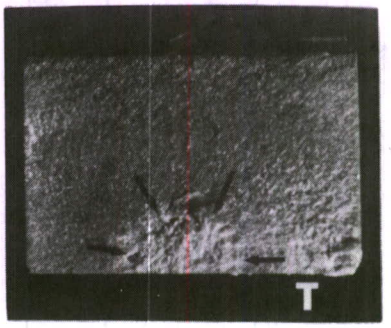

c. 400 MPa at 1.25 hours

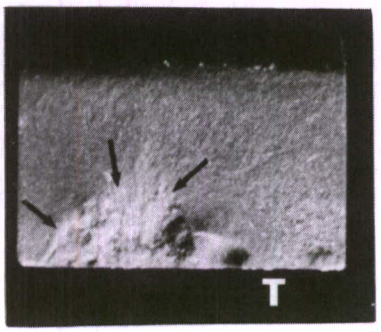

d. 400 MPa at 2.65 hours

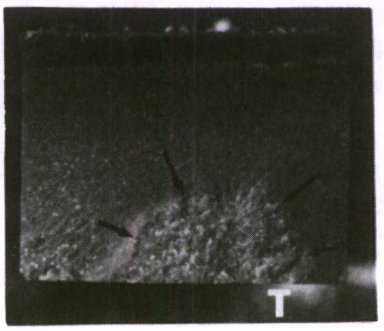

e. 393 MPa at 2.26 hours

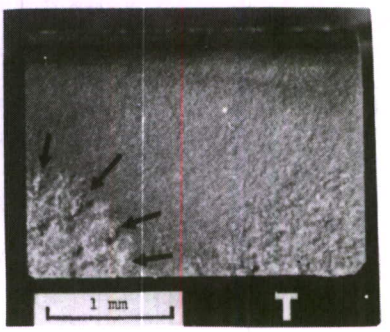

f. 386 MPa at 3.20 hours

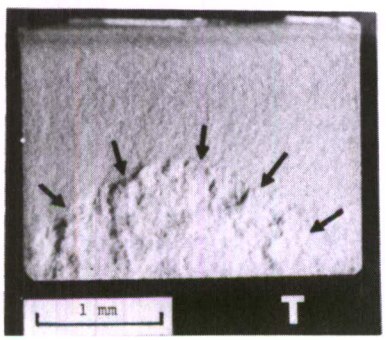

g. 317 MPa at 7.25 hours

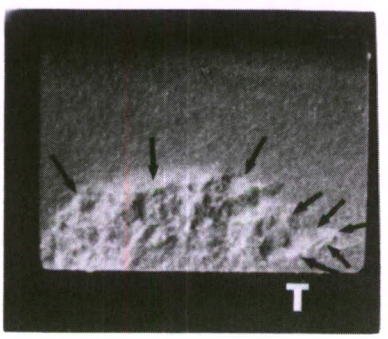

h. 270 MPa at 110 hours

Figure 30. Fracture surfaces showing slow crack growth at 1200 C in NC 132. Arrows outline the SCG zones. T denotes the tensile edge.

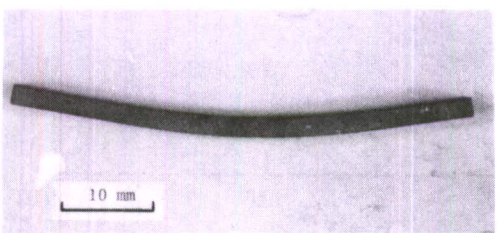

Figure 31. Side view of the stress rupture sample which survived intact for 610 hours while sustaining 234 MPa. The creep deformation is such that the maximum outer fiber strain in the gage length is 1.4 percent.

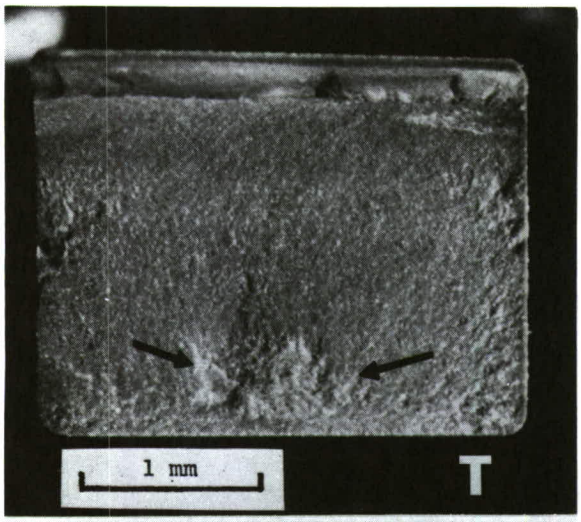

a. Light photomicrograph for a fracture surface of a sample which survived 247 MPa for 330 hours.

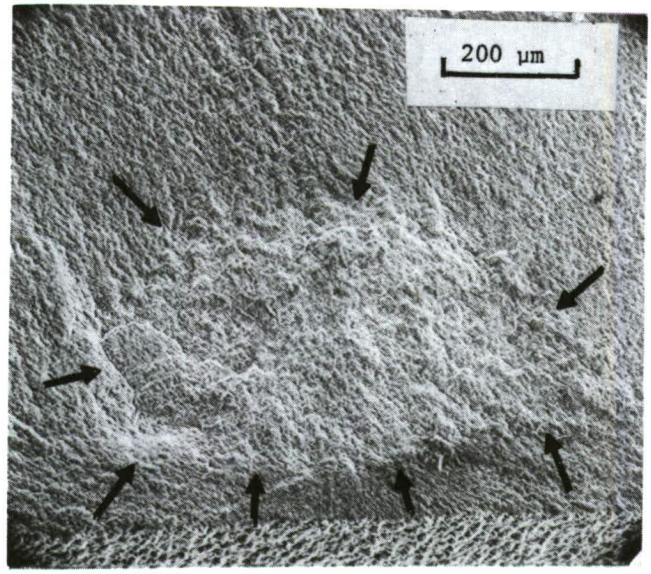

b. Same fracture surface, SEM close-up.

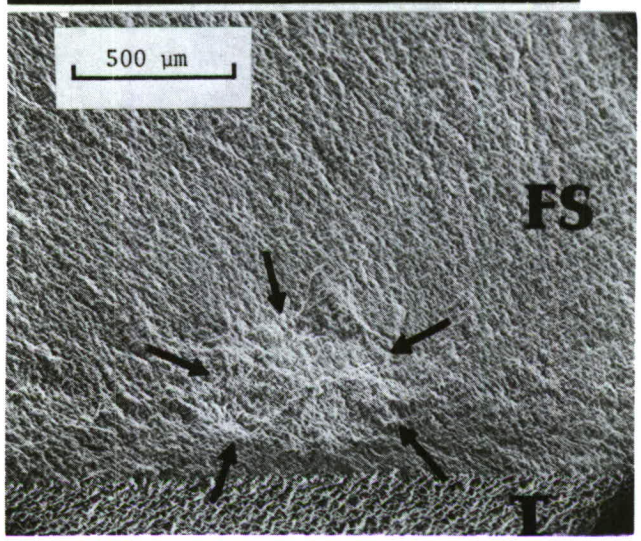

c. 234 MPa survivor at 610 hours, SEM close-up of subsurface SCG.

Figure 32. Subsurface slow crack growth in NC 132 at 1200 C. T denotes the tensile edge and FS marks the fracture surface.

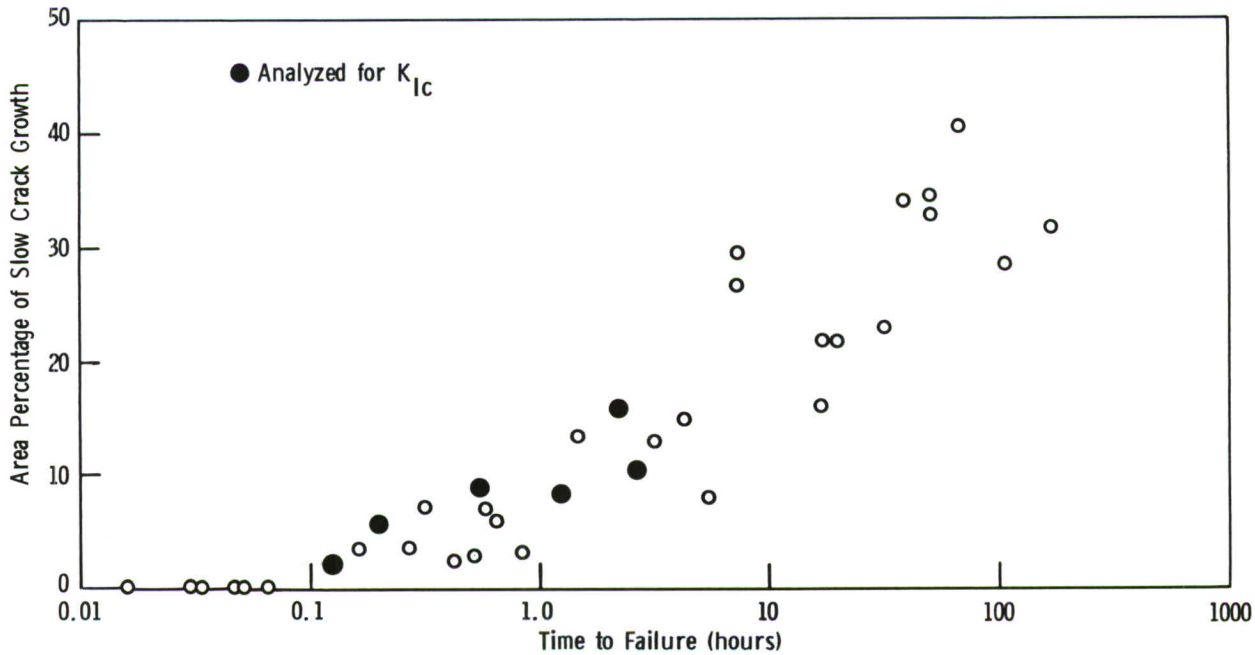

Figure 33. NC 132 static fatigue sample data showing the extent of slow crack growth as a function of time at 1200 C.

and the large crack size relative to these dimensions must be considered, such as in References 33, 48 to 50. While it is commonly understood that the flaw depth for a semicircular or semi-elliptical surface flaw directly determines the stress intensity that exists, it is not widely recognized that the maximum stress intensity may *not exist* at the deepest point of the flaw. The stress intensity that exists varies with position along the boundary of such flaws. This effect is incorporated at the geometric factor M that is in the stress intensity formula:

$$K_I = M \sigma_a \sqrt{c}.$$

Geometry factors for semicircular and semi-elliptical flaws are available in References 33 and 48 to 50. As shown in Figures 4 and 6 of Reference 33, the stress intensity around a semicircular surface flaw is always greatest at the crack intersection with the *surface* and *not* the deepest point into the cross section. This is true whether the crack is deep or not and whether or not the beam is in bending *or* tension. This is not necessarily true for a semi-elliptical flaw. A semi-elliptical flaw may have a more severe stress intensity at its surface or at its greatest depth depending upon its shape and depth into the bend sample cross section (finite size). (See Figure 2 of Reference 48.) For example, a shallow (relative to the sample thickness semi-ellipse will tend to have more severe intensity at the depth if its ratio of minor axis to major axis length is less than approximately 0.8. It is not clear if other investigators have made this important distinction in the use of stress intensity factors for analyses of ceramic failure. As will be shown below, the differing usage of the stress intensity factor can cause a major shift in K_{Ic} calculations. (In the case of semicircular shallow surface flaws, the difference is 17%.)

For the SCG zone shown in Figure 30a, the crack depth-to-width ratio is nearly 0.5 and the crack depth-to-sample thickness ratio is 0.24. This sample was chosen since its SCG zone is easily discerned, is away from the corners, is moderately large, and is nearly semicircular. References 33 and 48 treat the case of a deep semicircular crack in a beam in bending. The stress intensity geometric factor M for the deepest part of the crack is 0.79 so that:

$$K_I = 0.79 \sigma_a \sqrt{c}.$$

That the crack tip protrudes well toward the neutral axis (reduced tensile stress) accounts for the smaller magnification factor when compared to a shallow crack. The above factor fails to account for the finite width of the sample, however, and Reference 49 must be consulted to get a correction factor for the effect. For this case, the factor is 1.17 so that the correct expression for K_I at the deepest point of the SCG zone is:

$$K_I = (1.17)\ (0.79)\ \sigma_a \sqrt{c} = 0.93\ \sigma_a \sqrt{c}.$$

Substituting the applied stress and the size of the SCG zone:

$$K_{Ic} = (0.93)\ (483\ \text{MPa})\ (530 \times 10^{-6})^{\frac{1}{2}}$$
$$= 10.3\ \text{MN/m}^{1.5}.$$

The above formulation assumes the maximum stress intensity is at the deepest point of the crack front. This is not correct in this case as shown by References 33, 48 to 50. The maximum stress intensity for the crack is in fact at the surface. The magnification factor in this case results in:

$$K_{Ic} = (1.59)\ (483\ \text{MPa})\ (530 \times 10^{-6})^{\frac{1}{2}}$$
$$= 10.3\ \text{MN/m}^{1.5}.$$

Since the greater stress intensity is at the surface, fast fracture in principle should have initiated from this point and therefore K_{Ic} should be reported from the surface and not depth data. Examination of the fracture surface shows no indication of whether the fast fracture initiated from the surface or the deepest part of the crack front. In truth, the sample probably failed when the crack geometry as a whole became critical, not merely one portion of the crack front periphery. Thus a K_{Ic} formulation that integrates the whole crack front is likely to be more valid. A smooth halo surrounds the SCG zone. This halo is likely analogous to the smooth mirror that surrounds strength-controlling defects from modulus of rupture or tension testing. The mirror or halo is the result of a fast fracture crack that is initially straight but which eventually branches, giving a ragged appearance to the fracture surface.

Five other fracture surfaces were analyzed in the same fashion, with the results listed in Table 2. These five were chosen since they also had symmetric SCG shapes that were away from sample corners. All other fracture surfaces had unsatisfactory SCG shapes that would be nearly impossible to analyze. The average K_{Ic} at 1200 C based upon the stress intensity at the crack-tensile surface intersection is 14.9 $\text{MN/m}^{1.5}$.

48. MARRS, G., and SMITH, C. *A Study of Local Stresses Near Surface Flaws in Bending Fields* in Stress Analysis and Growth of Cracks, Proceedings of 1971 National Symposium on Fracture Mechanics, Part I, ASTM STP 513, 1972, p. 22.
49. GRANDT, A., and SINCLAIR, G. *Stress Intensity Factors for Surface Cracks in Bending* in Stress Analysis and Growth of Cracks, Proceedings of 1971 National Symposium on Fracture Mechanics, Part I, ASTM STP 513, 1972, p. 37.
50. PARIS, P., and SIH, G. *Stress Analysis of Cracks* in Fracture Toughness Testing and Its Applications, ASTM Special Technical Publication No. 381, 1964, p. 30.

Table 2. K_{Ic} CALCULATIONS FROM FINAL CRACK SIZE FOR NC 132 HOT-PRESSED SILICON NITRIDE AT 1200 C.

Maximum Outer Fiber Stress (MN/m^2)	Time to Failure (hr)	SCG Percent of Cross Section Area	Maximum Flaw Depth (μm)	Approximate Flaw Shape (depth/total width)	Figure	K_{Ic} Depth ($MN/m^{1.5}$)	K_{Ic} Surface ($MN/m^{1.5}$)
510	0.12	2.0	325	semicircle	-	9.0	12.6
483	0.20	5.8	530	semicircle	30a	10.3	17.7
448	0.55	8.8	620	semicircle	30b	8.9	16.0
400	1.25	8.3	526	ellipse (0.44)	30c	8.6	13.0
400	2.65	10.5	561	ellipse (0.40)	30d	9.5	13.0
393	2.26	15.9	801	semicircle	30e	8.0	17.2
					Average	9.1	14.9

That this K_{Ic} value is much greater than commonly reported in the literature for hot-pressed silicon nitride at 1200 C suggests the K_{Ic} formulation may not strictly apply to the final failure of a sample with extreme SCG. The stress intensity magnification factors may be in error to a certain extent ($\sim$5 to 10 percent), but this cannot account for the large difference. One possible explanation is that the elastic-linear stress distribution assumed may not be valid due to creep relaxation of tensile stress. This effect could be significant, since the samples were under load for a considerable time (although not enough for much permanent deformation). If the maximum tensile stresses were reduced, then the K_{Ic} values reported here would be correspondingly reduced. The conclusion that the K_{Ic} formulation may not apply is in contrast to that reported in Reference 51 where SCG zones were used (in a similar fashion as above) to calculate K_{Ic} values (Norton HS 130 grade, 1200 C in air, K_{Ic} $\sim$6.0 $MN/m^{1.5}$). It was not reported in that reference whether the critical stress intensity was calculated for the deepest portion of the crack or at the surface. It was reported that SCG zones extended well into the cross section. As shown in this report, the difference can be considerable.

The stress intensity geometry factor at the crack tip gets smaller as the crack grows into the cross section while the surface stress intensity does not, which suggests the crack will grow faster at the surface. Flaws which are initially semicircular at the surface will evolve into a semi-elliptical shape with the long axis along the tensile edge. This was observed in this work as well as in References 51 and 52. The SCG zone in Figure 30a is still semicircular suggesting that the initiating defect may have been subsurface such as in Figure 32.

The scatter in the times to failure for samples that are identically loaded can be attributed to:

1. variation in initial flaw type;
2. variation in initial flaw size;
3. spatial variation in slow crack growth properties (such as chemistry variations in a billet);
4. furnace-to-furnace temperature error; and
5. furnace-to-furnace stress variation.

The furnace-to-furnace stress variation can be estimated as follows. As shown in Section II, a two percent possible variation in applied stress is possible. (This likely is an upper limit.) If the power relationship between time to failure and applied stress applies as shown in Figure 29, then then a stress that is actually 0.97 of what was calculated would result in a 42 percent increase in the time to failure. Alternately, a stress that is 1.03 of what was calculated would result in a 29 percent decrease in the time to failure ($t_f = (1.02 \times \text{applied stress})^{-11.5}$).

The error due to temperature variation can be treated as follows. If slow crack growth is assumed to be the mechanism of failure, then the empirical power law crack velocity-stress intensity relation can be used (see, for example, Reference 52):

$$V = A K_I^N \exp(-Q/RT)$$

where V = crack velocity

A, N = constants

K_I = the stress intensity

Q = the activation energy

$R = 1.99 \times 10^{-3}$ kcal/mole °K

T = absolute temperature.

Integration leads to an expression for time to failure in terms of temperature:

$$t_f \propto \exp(Q/RT).$$

51. PETROVIC, J., JACOBSON, L., TALTY, P., and VASUDEVAN, A. *Controlled Surface Flaws in Hot-Pressed Silicon Nitride.* J. Am. Cer. Soc., v. 58, no. 3, 1975, p. 113.
52. EVANS, A., RUSSEL, L., and RICHERSON, D. *Slow Crack Growth in Ceramic Materials at Elevated Temperatures.* Met. Trans., v. 6A, April 1975, p. 707.

If T = 1200 C and Q = 170 kcal/mole (Reference 52), then a five-degree centigrade error will cause a 22 percent difference in the time to failure:

$$t_f^{1200\ C} / t_f^{1205\ C} = 1.22.$$

A ten-degree difference causes a 48 percent change. As stated in Section II, care was taken in this study to limit the actual error to 2 C or less.

The variation due to initial flaw size scatter can also be estimated as follows. Assuming the crack velocity-stress intensity power law relationship applies (see, for example, Reference 37):

$$t_f \propto (c_i)^{N-2/2}$$

where c_i = the initial flaw size and

N = the slow crack growth exponent.

If the initial flaw size varies from 18 to 63 microns (see the discussion of flaw size in the control data, Lot A, presented above), then:

$$\frac{t_{f,\ 63\ \mu m}}{t_{f,\ 18\ \mu m}} = \left(\frac{63\ \mu m}{18\ \mu m}\right)^{11.5-2/2} = 384.$$

This variation is strong.

The possible variations in material structure or chemistry that result in crack growth variations are unknown. Their effect could be significant, however. Other phenomena may enhance or retard the slow crack growth process, and variables that affect these other phenomena may in turn alter slow crack growth. For example, the creep of viscous grain boundary phases ahead of a crack tip can lead to slow crack growth.[35] Factors which influence the creep rates may affect the rate of slow crack growth. Alternately, the creep may reduce the stress intensification ahead of the crack tip, thus retarding crack growth.* Oxidation is another phenomenon that could enhance or retard crack growth. Spatial variations in impurity content (within a billet) that can cause variation in creep or oxidation rates could in turn cause slow crack growth variations from sample to sample (or even within a sample).

Thus it is not surprising that the scatter in time to failure in the data of this report is about one order of magnitude. The necessity of maintaining a good experimental procedure is evident. That all the above factors can contribute to significant variations in time to failure should be of concern to designers and researchers who devise models of life prediction.†

3. STSR

Stepped temperature stress rupture tests on NC 132 showed failures occurred over all temperature ranges from 1000 C to 1400 C (Figure 34). Samples exposed to 1400 C exhibited gross permanent deformation (>1%) even for very low stresses. Samples that reached 1100 C showed little or no permanent deformation; samples that survived to 1200 C had measurable strains of the order of a few tenths of a percent and from a few tenths to one percent for samples in the 1300 C range.

The STSR samples loaded to 345 MPa failed at 4.87 and 4.42 hours into the 1200 C step as compared to an expected time of 7.0 hours from the stress rupture trials (Figure 29). The shorter lifetime at 1200 C for the STSR samples reflects the prior exposure to 1000 C and 1100 C.

Prominent SCG zones were again evident. In two samples, independent zones on the same fracture surface were observed. In general, the longer the time to failure the larger the zone. In some cases the SCG emanated from corners but many did not. The 486 MPa sample at 1100 C had two prominent independent SCG zones. The 551 MPa sample at 0.55 hr in the 1100 C step had a very small SCG zone. The 1000 C samples (which lasted one or more hours) did not show SCG zones but resembled fast fracture-room temperature breaks (mirror-jagged surface). As shown previously, slow crack growth could have occurred at 1000 C, but the size of the SCG zone can be very small.

4. Combined Cycle Procedure

A thick oxide layer identified by X-ray diffraction as alpha cristobalite and enstatite formed on the NC 132 hot-pressed silicon nitride combined cycle samples (Figure 35). A dark discoloration around the flame-impinged zone suggested carbon or some other impurity from the flame. This coloration was minor and disappeared each time the samples were subjected to the furnace heat soak. Some erosion of the oxide layer, exposing the matrix, was evident at the corners of the sample. An average weight gain of 0.005 gram out of 0.9200 gram was observed on the first soak cycle with insignificant gain thereafter on the soak cycles. A slight weight loss (approximately 0.0005 gram) was observed with each set of 100 thermal fatigue cycles.

A significant loss in strength compared to the untreated samples was observed. Average strength of the exposed samples was 348 MPa (±36), whereas the average for the control (Lot B) was 714 MPa (±60). A least-squares line of slope

*It has been occasionally observed in other work conducted in this laboratory that hot-pressed silicon nitride samples, when loaded to low stresses over 1200 C, may creep excessive amounts (see, for example, Figure 31). Such samples often have enormous cracks in the tensile face of bend samples, but the sample does not rupture.

†To further examine this matter, an independent research program was recently conducted by G. Quinn and E. Lenoe at AMMRC. A large number of stress rupture trials were conducted on NC 132 samples with controlled flaws introduced via a Knoop indenter. This would serve to eliminate the initial flaw size as a variable. Quite surprisingly, the scatter in time to failure was still of the order of one magnitude in time.

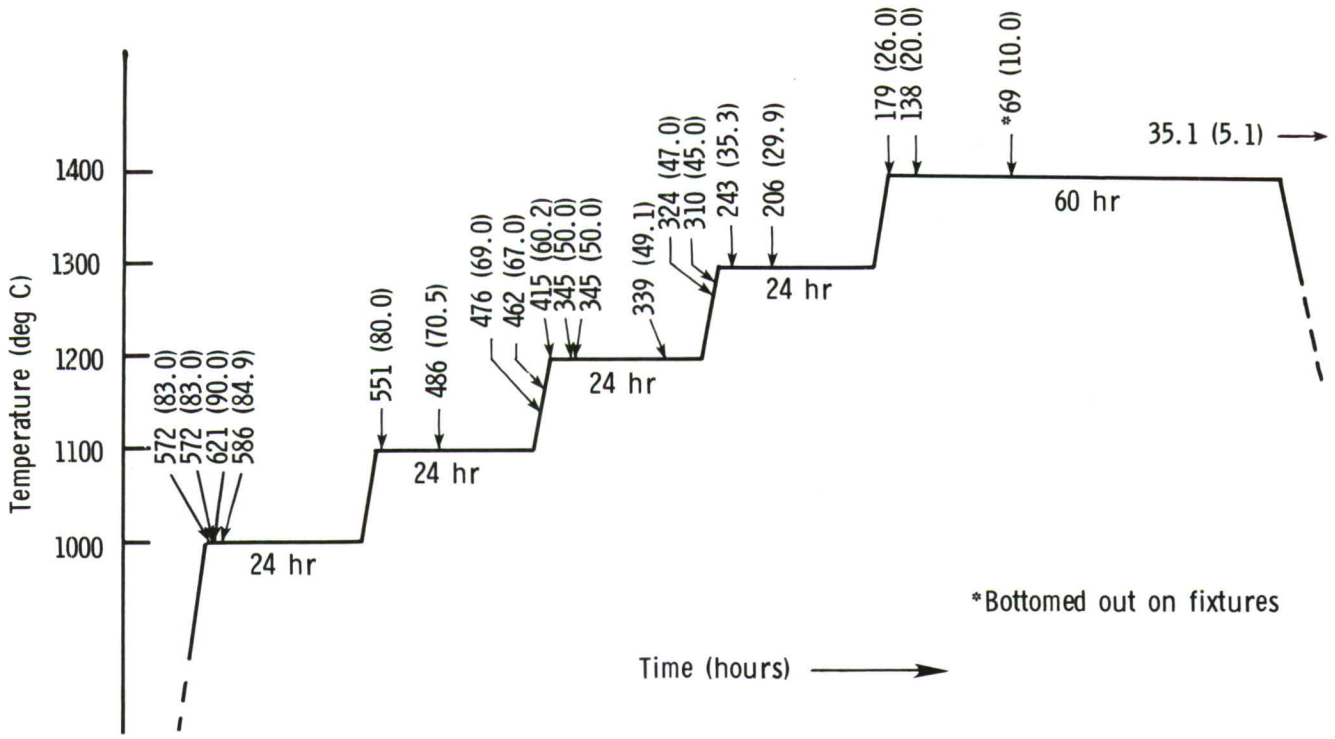

Figure 34. Stepped temperature stress rupture data for NC 132 HPSN. Arrows indicate failure times, arrow labels specify stress on sample in MPa (ksi).

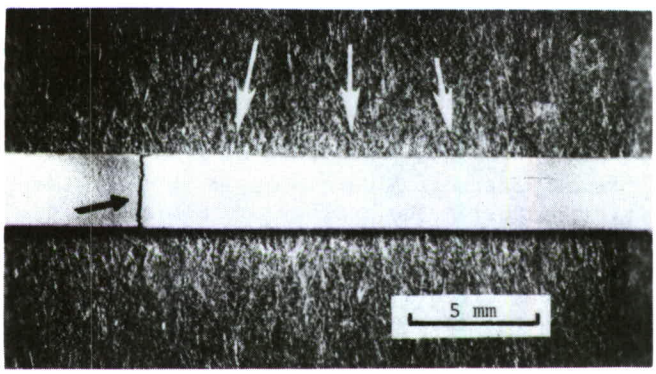

a. Combined cycle NC 132 sample photomicrograph showing badly damaged tensile surface. The fracture from subsequent retained strength measurement is marked by the black arrow. The lighter colored zone is the flame impinged area (white arrows).

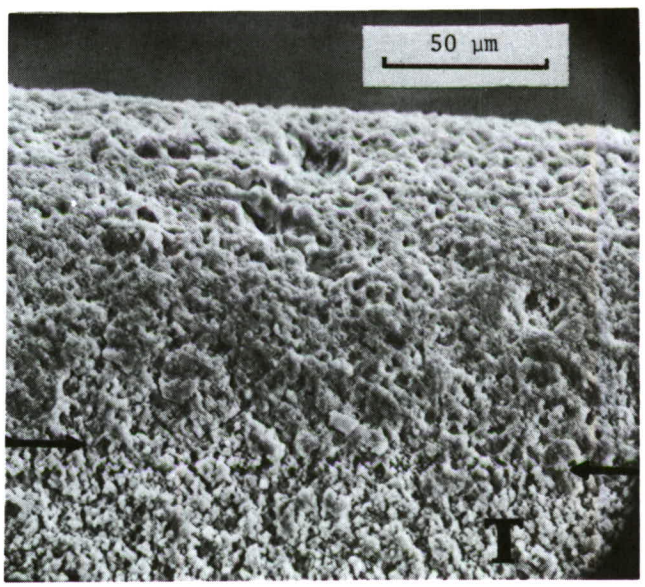

b. Close-up of corner showing badly pitted material. The oxide extends only as far as the arrows. The matrix material is exposed at the corner. T marks the tensile face during the retained strength test.

Figure 35

9.6 was an excellent 98.5% fit to the combined cycle data when plotted on a Weibull graph (Figure 36). The difference between the Weibull modulus and that of the control group (12.4) suggests the initiating flaws causing failure have changed.

Fractography confirmed this interpretation. Eight samples failed from pits located at the corner of the sample (Figure 37). The corner pits were continually exposed to damage by the action of the thermal fatigue portion of the combined cycle. Higher heat transfer rates at the corner caused greater thermal shock damage to the oxide layer or, alternately, the corrosion-erosion effect of the flame caused the corner to be more severely damaged. Four samples failed from pits on the bottom tensile face or on the side (Figure 38) of the sample. Similar pitting as the result of oxidation and the cause of strength reduction has been reported previously.[10,48,53-55]

5. Discussion

The control room temperature strengths were different for the two lots, but reported average strengths and standard deviations also vary widely in the literature. The average strength of the stress rupture and STSR Lot A compares well with the 837 MPa (±81) reported in References 19 and 56, but is well above the 620 MPa average reported in Reference 57. On the other hand, the standard deviation in the latter case was also high: 110 MPa. Flexural average strengths reported in Reference 58, where trials were conducted on ten billets, ranged from 905 to 1060 MPa with standard deviations ranging from 87 to 165 MPa. The probable reason for these variations is that the material is sensitive to machining variations.

Slow crack growth was observed at temperatures of 1100 C and above and may exist at 1000 C as well. Four STSR samples failed at that temperature and although SCG markings were not evident, such markings may be very small. Samples tested longer than ten hours at 1200 C resulted in SCG zones extending through a major fraction of the fracture surface. In some cases multiple zones were observed on the same fracture surface. Samples which were exposed to 100 hours or more had significant permanent deformation which led to multiple creep cracks (or

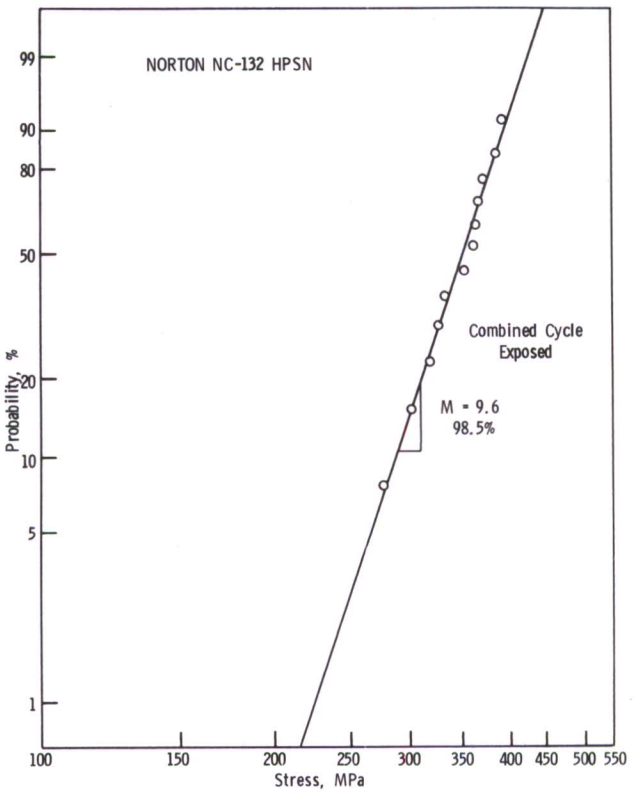

Figure 36. Weibull plot of retained strength of the NC 132 combined cycle samples.

SCG cracks) on the tensile face. Significant permanent deformation occurred at 1200 C and above. Stress rupture trials at 1200 C showed a distinct and reproducible trend of diminishing load-carring capacity with time. A power-law relationship between stress and time to failure represents the data quite well. A log-log representation (as used in Figure 29) gives a slightly better fit to the data as opposed to a linear stress-log time plot. Although the data yields a slow crack growth exponent of 11.5 and the fit to the data looks good, several assumptions may not be valid. A lower value of the exponent could be expected as discussed above.

The applicability of the longer time to failure data is uncertain since significant stress relaxation probably occurred due to the creep

53. FREIMAN, S., MECHOLSKY, J., McDONOUGH, W., and RICE, R. *Effect of Oxidation on the Room Temperature Strength of Hot Pressed Si_3N_4/MgO and Si_3N_4-ZrO_2 Bodies* in Ceramics for High Performance Applications II, J. J. Burke, E. M. Lenoe, and R. N. Katz, ed., Brook Hill Publishing Company, Chestnut Hill, Massachusetts, 1978, p. 1069.
54. RICHERSON, D., and YONUSHONIS, T. *Environmental Effects on the Strength of Silicon Nitride Materials.* Proceedings of the 1977 DARPA/NAVSEA Ceramic Gas Turbine Demonstration Program Review, Castine, Maine, MCIC 78-36, August 1977, p. 247.
55. FREIMAN, S., WILLIAMS, A., MECHOLSKY, J., and RICE, R. *Fracture of Si_3N_4 and SiC.* Proceedings of the Sixth International Materials Symposium, Ceramics Microstructures, 1976, University of California, Berkeley, California, August 1976.
56. WILLIAMS, R., and UY, J. *Ceramic Materials Characterization* in Ceramics for High Performance Applications II, J. J. Burke, E. M. Lenoe, and R. N. Katz, ed., Brook Hill Publishing Company, Chestnut Hill, Massachusetts, 1978, p. 151.
57. WADE, T. *Property Screening and Evaluation of Ceramic Vane Materials.* IIT Research Institute, AFML Contract F33615-75-C-5196, Interim Report No. 2, July 1976.
58. TORTI, M. *The Effect of Fabrication Procedures Upon Mechanical Properties of Si_3N_4 and SiC Turbine Components.* Presented at Third Materials Conference, Turbine Applications, University of Michigan, Ann Arbor, Michigan, October 1974.

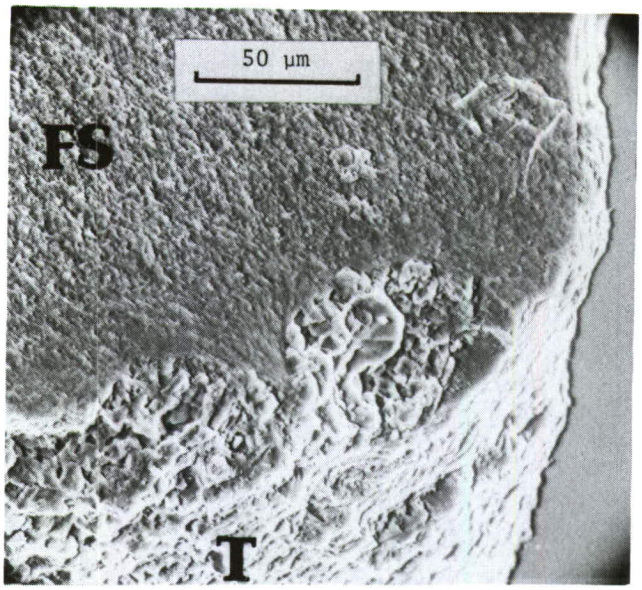

Figure 37. Combined cycle NC 132 sample fracture surface showing a pit on sample corner. Fracture stress was 303 MPa.

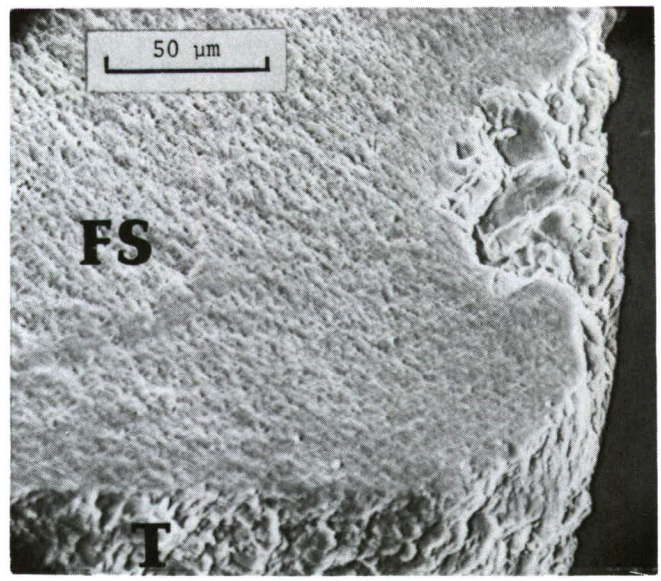

Figure 38. SEM photo of the fracture surface of NC 132 combined cycle sample that had a retained strength of 321 MPa.

mechanisms that were operative. In addition, once significant deformation had occurred, the elastic beam formula may no longer be valid due to second-order curvature effects. Thus the true maximum stress acting on the sample may have been considerably less than the value calculated from the elastic solution. Since these effects are time-dependent (and will cause greater deviation with longer time), the slope of the stress rupture plot may not be a correct value to use for the crack velocity-stress intensity relationship. The value of 11.5 obtained from the 1200 C data should be regarded as an upper limit. Tests of duration greater than 1000 hours may not even be possible since samples would bottom out on the fixtures prior to failure. These observations, derived from the 1200 C data, apply to the higher temperatures as well.

A major strength loss (≈50 percent) was observed in the combined cycle procedure. The strength-controlling defect was surface pitting that was accelerated by the cycling procedure. Such defects were not evident in the less aggressive static fatigue experiments where failure was from a different mechanism.

That this material can fail from different flaws in several modes is a major problem for life prediction modeling. Room temperature failures were from machining defects. Combined cycle failures occurred from surface pits that have no correlation to machining defects. Stress rupture failures occurred as a result of slow crack growth from sources that may have been surface machining damage, but in at least several cases were from unidentified subsurface sources. Reliable life prediction models must account for each of these failure modes.

B. Norton NC 136 Hot-Pressed Silicon Nitride

1. Control Strengths

Ten control samples yielded fourteen fractures with an average of 737 MPa and a very high standard deviation of 253 MPa. (Some of the samples broke so that a second test was possible on the longest fragment.) Three points were uncharacteristically low: 253, 383, and 478 MPa. When these three are deleted, the average strength is 836 MPa with a standard deviation of only 46 MPa. A Weibull plot with the eleven highest points gave a modulus of 18.0 with a correlation coefficient of only 95 percent (Figure 39). The high strength, coupled with the high scatter, compares well with the 810 MPa average with 248 MPa standard deviation reported in Reference 10.

Most samples had poorly defined mirrors outlining the initiation site, but in general the fracture surfaces were quite irregular. Many of the samples failed from corner-located flaws, but specific flaw identification could not be made. Machining damage associated with longitudinal grinding striations is the presumed defect as shown in Figure 40. The three low strength samples failed from defects that could not positively be identified, although processing cracks are suspect (Figure 41). The three fracture surfaces were unlike those of the higher strength samples. For example, the 253 MPa fracture surface was undulating and at an angle not perpendicular to the applied tensile stress.

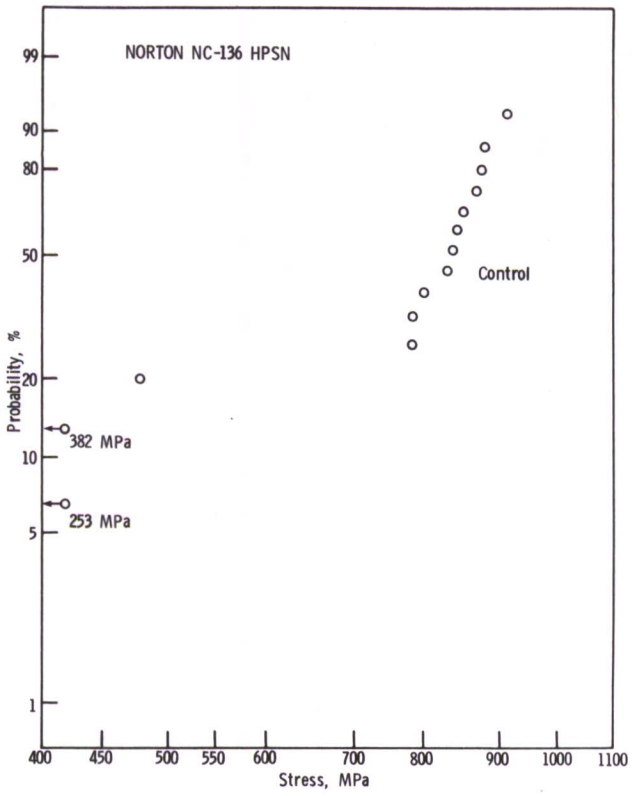

Figure 39. Control room temperature strengths of NC 136 HPSN.

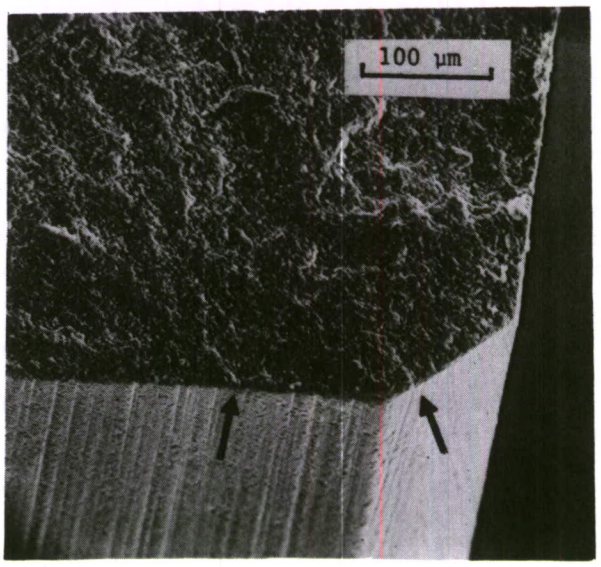

Figure 40. SEM photo of the fracture surface of an NC 136 control sample that failed at 866 MPa. No defect is obvious although this photo shows the mirror. Machining damage is suspect (arrows). Note the nonlongitudinal chamfer striations.

a. Light photo of the flat surface of an NC 136 bend bar showing processing cracks (arrows). This particular sample was fractured at the other end of the piece.

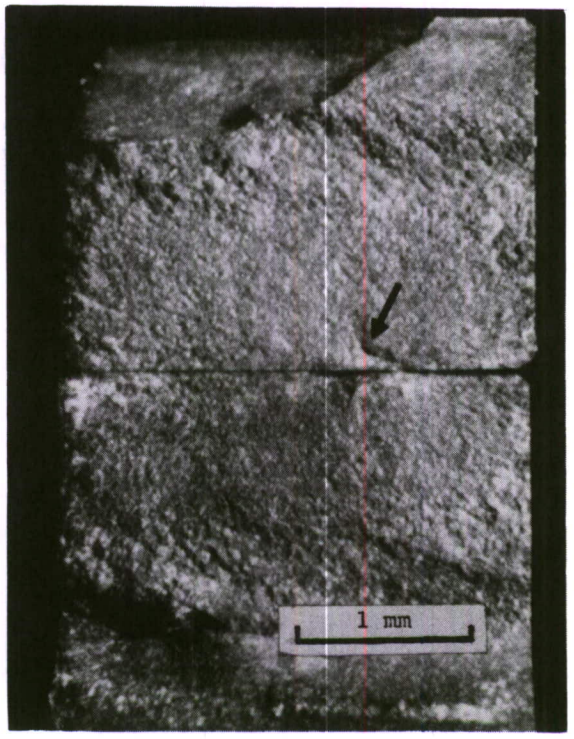

b. Light photograph of the fracture surface of the sample in (a). Failure occurred from an irregular zone near the tensile face (arrow) which likely is a processing crack. The two fracture halves of the sample are mounted back to back on the tensile edge in this view.

Figure 41.

2. Stress Rupture, 1200 C

Very little static fatigue behavior was observed at 1200 C, with about 500 MPa acting as a cutoff level (Figure 42). This value is considerably less than the control room temperature strengths. Some overlap occurs with, for example, samples loaded at 517 MPa failing on loading, surviving 300 hours, or failing in between. The five survivors all had permanent deformation of the order of 0.1 to 0.2 percent. The retained strengths were 758, 831, 847, 982, and 996 MPa. The latter two are higher than any of the control group, and the average (863 MPa) is substantially greater than the control strength (737), which suggests flaw healing was occurring.

Oxidation markings were variable and followed the variations observed in the samples prior to exposure (Figure 43). An X-ray diffraction pattern indicated alpha cristobalite present in addition to the phases in the reference sample. Fracture surfaces of the two time-dependent failures showed extremely irregular, jagged markings across the entire face.

3. STSR

STSR results (Figure 44) demonstrate the instability of this grade material. Of eight samples tested, seven failed in the 1000 C step at stresses of 345 MPa and below. The 69 MPa sample failed at 19.7 hours and had gross cracks through the entire sample. The 1000 C failures can be plotted in a standard stress rupture format as shown in Figure 45. In this representation, the data implies the material would have no load-carrying capacity if exposed to more than 65 hours. Static heating trials on bend bars (without loading) reported in Reference 10 indicate this material has no strength after 100 hours exposure to 982 C in an oxidizing environment. This procedure is tantamount to a stress rupture test with zero load and is shown as the arrow in Figure 45, consistent with the findings of this report. The samples which broke at 1000 C failed from long linear features (possibly cracks) that ran through the fracture surface (Figures 46 and 47). The survivor sample had permanent deformation of 0.4 percent maximum strain. The retained strength was 767 MPa.

Oxidation surface markings were quite variable. Two X-ray diffraction patterns were generated for the sample which failed at 14 hours at 1000 C. One pattern (from the mottled face shown in Figure 48) was very similar to the reference pattern except the beta Si_3N_4 (101) peak was much diminished. The second pattern (from the snowflake crystallite face) gave similar results except that the H phase and WSi_2 peaks were slightly more distinct. No cristobalite was evident in either pattern. A similar diversity in markings existed on the survivor sample. The dichotomy of markings from face to face was similar, but a thicker oxide layer obscured the mottling and snowflake features. A strong alpha cristobalite peak was present on patterns taken from both sides of the sample. In addition, strong 5.37 and 1.80 Å peaks appeared on the pattern generated from the mottled face, but not at all on the other.

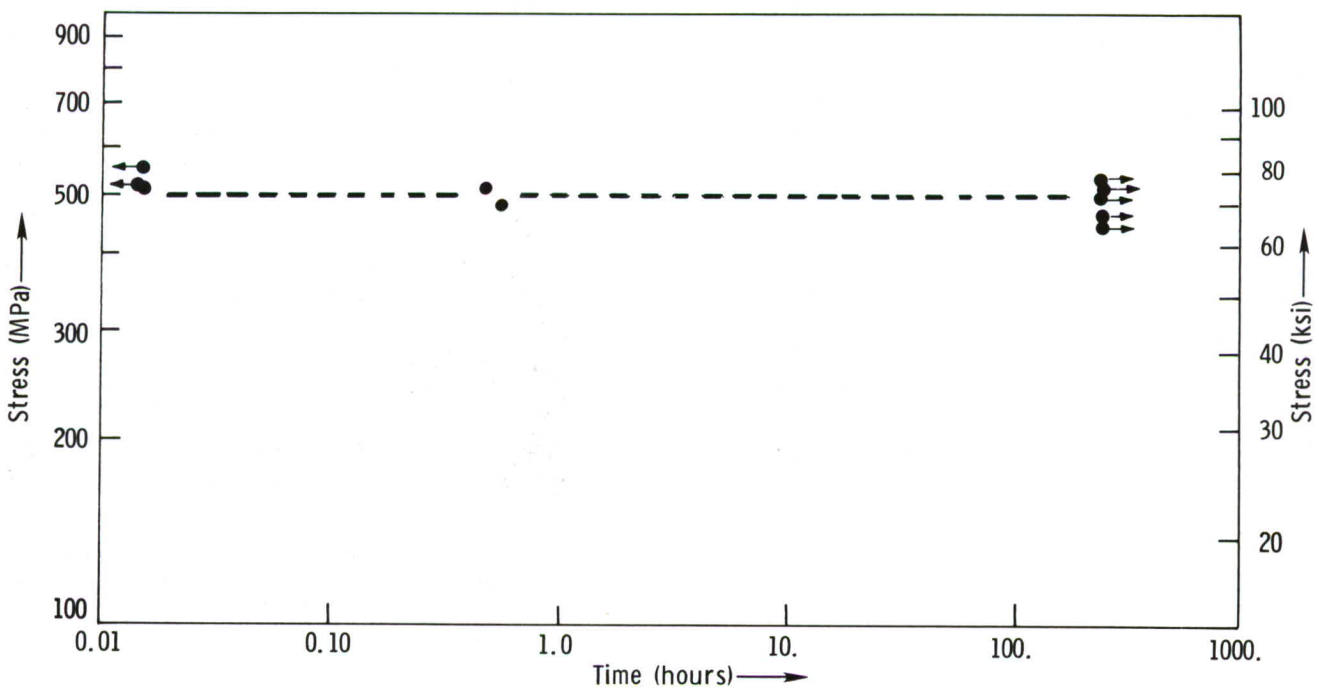

Figure 42. Flexural stress rupture at 1200 C for NC 136 hot-pressed silicon nitride with yttria additive.

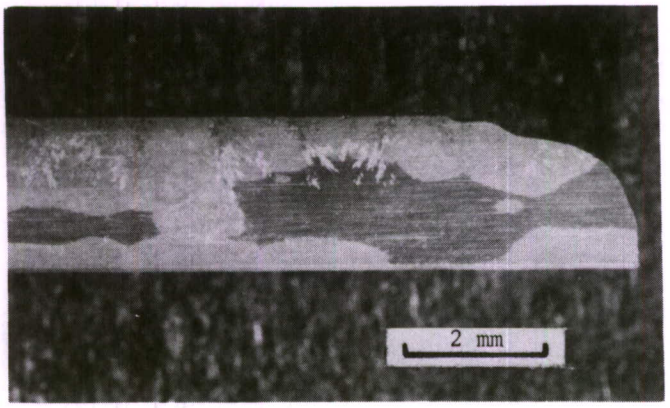

Figure 43. Light photo of the side of an NC 136 stress rupture sample that broke at one half hour at 1200 C. Note the strong gradient in oxidation surface markings.

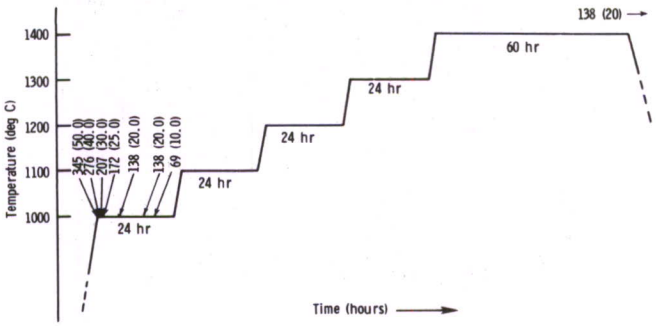

Figure 44. Stepped temperature stress rupture data for NC 136 hot-pressed silicon nitride with yttria additive.

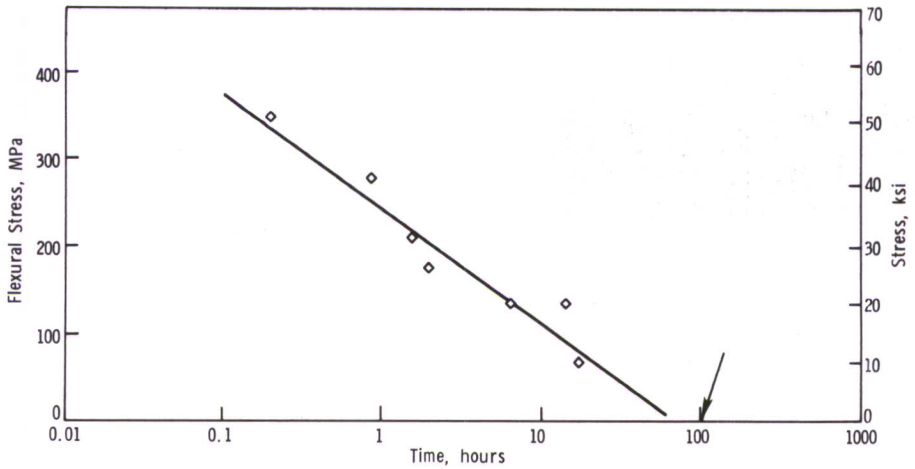

Figure 45. Semilogarithmic representation of STSR-1000 C failures of NC 136 HPSN. The arrow marks the results of the oxidation exposure experiments reported in Reference 9.

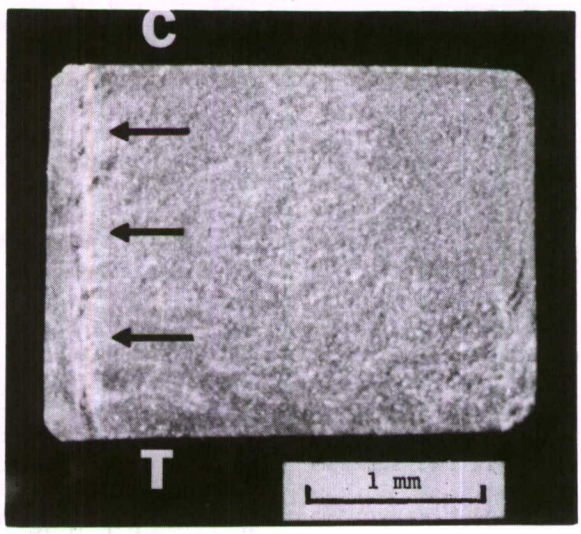

Figure 46. Light photo of the fracture surface of an NC 136 STSR sample which failed at 0.86 hour at 1000 C. Note the long crack up the side of the sample (arrows). The size distortion is real and not an optical effect. T marks the tensile edge; C the compressive edge.

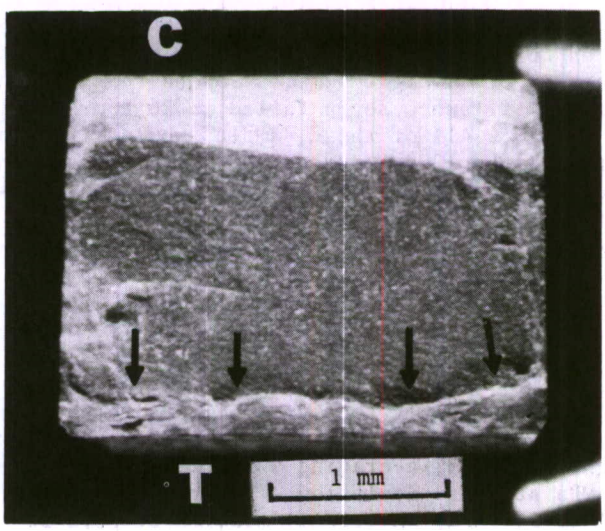

Figure 47. Light photo of an NC 136 STSR sample which failed at 14 hours at 1000 C. Note the crack which runs across the sample (arrows).

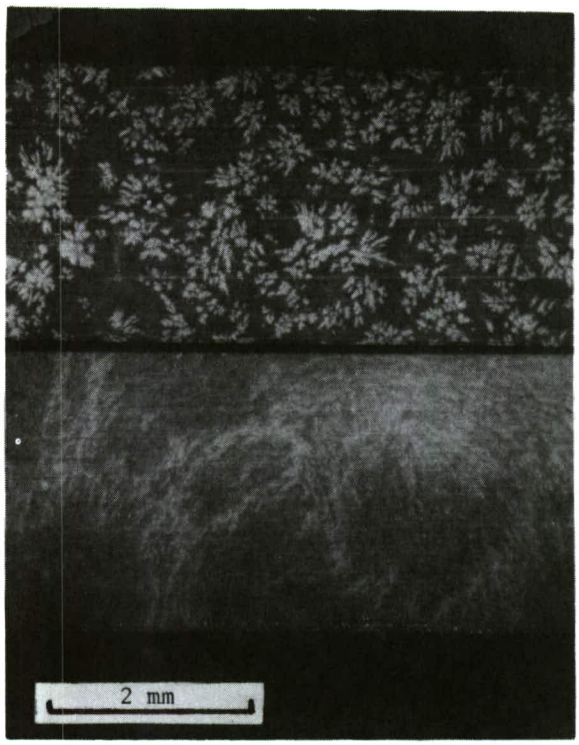

Figure 48. Light photograph of the flat surface of a single STSR sample which failed at 14.0 hours at 1000 C. The two pieces of the sample were placed side by side for this photo but were inverted so that one piece shows the oxidation markings on one side, the other half the markings on the opposite face.

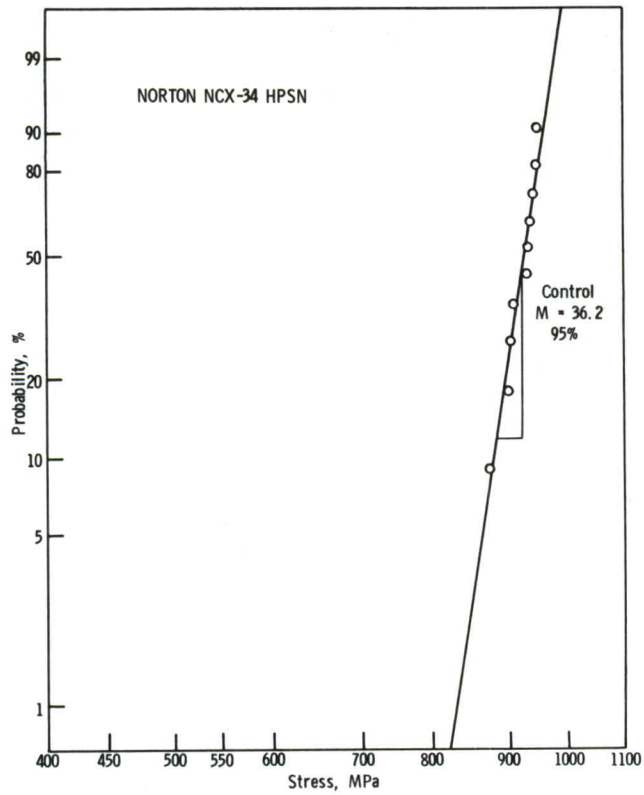

Figure 49. Room temperature flexural strength data for Norton NCX 34 hot-pressed silicon nitride.

4. Discussion

Based upon the stress rupture trials at 1200 C, one would normally expect that this material would be outstanding at loads below 500 MPa and temperatures below 1200 C. The STSR results indicate otherwise. Of eight samples loaded to stresses of 345 MPa or lower, seven failed in 20 hours or less at 1000 C. All of these samples would likely have survived the 1200 C stress rupture trials for hundreds of hours. Several investigators have attempted to identify the cause of the 1000 C instability.[11-13,59,60]

C. Norton NCX 34 Hot-Pressed Silicon Nitride

1. Control Strengths

Although only ten strength measurements were made, room temperature control samples had very high strengths, averaging 921 MPa with only a 24 MPa standard deviation. The range was from 871 to 947 MPa. A Weibull modulus of 36.2 resulted from a least-squares line with a coefficient of determination of 0.95 (Figure 49).

Fracture surfaces showed distinct mirrors which indicated five fractures initiated from corner chamfer flaws. The five other fractures initiated at the sample surface but away from corners. Although at first no specific defect could be found, the strength-controlling flaw was probably subsurface damage induced by the longitudinal machining marks (Figure 50). At the center of the mirrors was a feature often observed by SEM. Emanating from a deep longitudinal striation is an angled line that extends back into the fracture surface (white arrows, Figure 50b). Often it was observed that the angled line would then curve back and intersect the surface at another deep machining mark. Thus the defect extends considerably deeper into the sample than the actual striations. These markings were also observed in several of the other high strength materials tested in this study (where a mirror could be found but no specific defect could be identified). The defect is understandably common to several materials since all the samples for this study were machined in the same manner.

An exact measurement of the flaw depth in Figure 50b is not possible due to the tilt of the sample, but an estimate may be made. The sample

59. KNOCH, H., and GAZZA, G. E. *Carbon Impurity Effects on the Thermal Degradation of a Si_3N_4-Y_2O_3 Ceramic.* Submitted to Amercian Ceramic Society.
60. GAZZA, G. E., KNOCH, H., and QUINN, G. D. *Hot Pressed Si_3N_4 with Improved Thermal Stability.* Am. Cer. Soc. Bull., v. 57, no. 11, 1978, p. 1059.

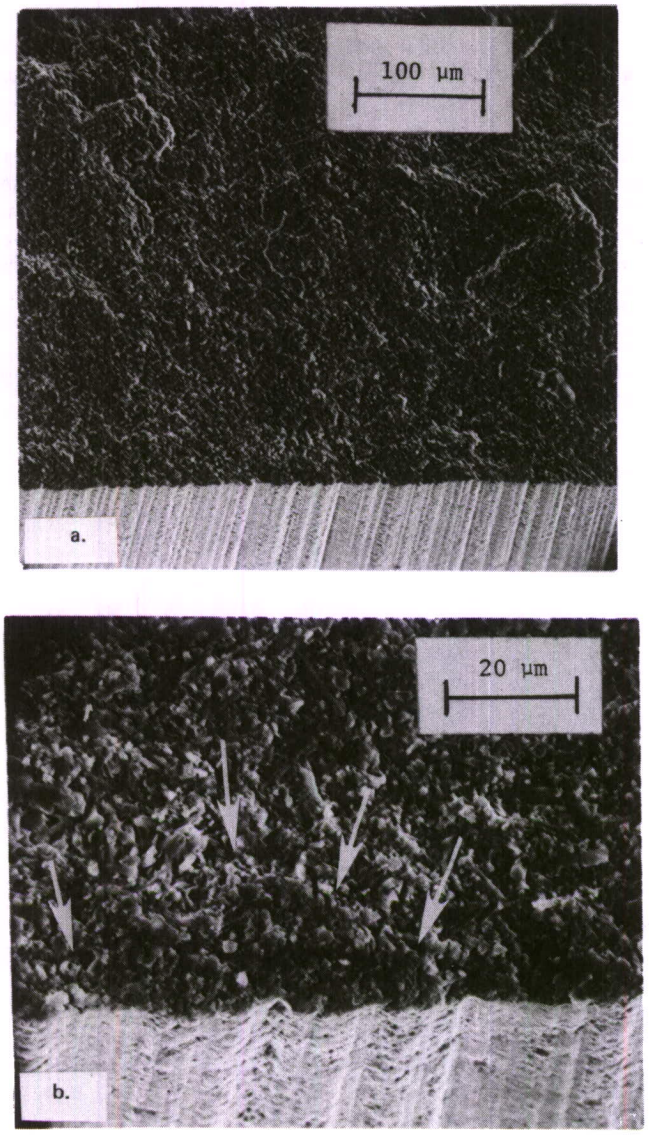

Figure 50. (a) SEM photo of fracture mirror on a fracture surface of an NCX 34 bend sample broken at room temperatures; (b) close-up view of deep machining striations and damage below surface.

was cut so that the tilt was approximately 20° off normal. The cosine correction for this angle is small and the measured 20 μm flaw depth on the figure can be adjusted to 21.3 μm. If the tilt were a few degrees different from 20°, the flaw depth would be only slightly different. As before, the formulation for the stress intensity for a semi-elliptical flaw in a semi-infinite plate in tension can be written:

$$K_I = M \sigma_a \sqrt{c}.$$

(Of interest is that the formulation in References 50 and 61 for the stress intensity around an elliptical crack is in part incorrect. The definition of the angle β in Figure 10 of the former reference and Figure 1 of the latter is in error and should be defined as in the original Reference 62 or as shown in Figure 179 of Reference 63. The nature of the incorrect definition is that *correct* numerical results will be obtained at the major and minor axes (where most interest lies) but all angles in between will be wrong. The incorrect definition has been propagated in a number of references.)

For the semi-elliptical flaw (depth = 21.3, length = 60 μm) the shape factor is a maximum at the deepest point and is 1.38.[48-50] At failure σ_a = 945 MPa and thus:

$$K_{Ic} = (1.38)\ (945\ \text{MPa})\ (21.3 \times 10^{-6}\ \text{m})^{\frac{1}{2}}$$
$$= 6.0\ \text{MN/m}^{1.5}.$$

A similar calculation on another sample gave K_{Ic} = 5.8 MN/m . The evidence and photos are not conclusive, but this feature was repeatedly observed associated with deep longitudinal striations. Occasionally several such elliptical zones intersected due to multiple deep striations.

2. Stress Rupture, 1200 C

Of ten samples tested in stress rupture at 1200 C, six failed in a time-dependent manner over a narrow stress range (Figure 51). The critical stress is approximately 440 MPa, a value that is less than half the room temperature flexural strength. The fracture surfaces of several of the failed samples showed "slow crack growth" zones similar to those observed for the magnesia-additive hot-pressed silicon nitrides. The zones were located away from the corners of the samples but were probably centered on the surface flaws. Close-up examination with SEM on both the inside and outside of these zones showed similar appearances. Failure was primarily intergranular in the SCG zone but mixed transgranular-intergranular in the fast fractured portion. Elongated grains were prominent. Light microscope examination more readily revealed the SCG zones as they were lighter in color (probably due to the oxidation of exposed material).

Three samples survived intact to 300 hours, but had permanent deformation of the order of 0.4 percent maximum strain. Retained flexural strengths were 736, 844, and 955 MPa. Very little oxide developed on the surface and the surface retained a matte (virgin-like) appearance. A subtle

61. BANSAL, G. K. *Effect of Flaw Shape of Ceramics.* J. Am. Cer. Soc., v. 59, no. 1-2, 1976, p. 87.
62. IRWIN, G. *Crack Extension Force for a Part Through Cracking Plate.* Trans. ASME, Series E, 1962, p. 651.
63. ROOKE, D., and CARTWRIGHT, D. *Compendium of Stress Intensity Factors.* Published by Her Majesty's Stationery Office, Ministry of Defense, Hillington Press, Uxbridge, Middlesex, United Kingdom, 1976.

mottling was evident as lighter and darker zones, however. X-ray diffraction indicated alpha cristobalite present in addition to the phases originally present. Very weak 6.1 and 5.4 Å d spacings were also observed.

3. STSR

STSR testing showed NCX 34 failures over the 1000 C to 1300 C temperature range (Figure 52). No failures at 1400 C were obtained although this may be the result of the limited number of samples tested. Four samples tested at stresses from 566 to 621 MPa either failed on loading or very shortly thereafter. These stress levels are substantially lower than any of the room temperature control strengths. The 572 MPa sample that broke at 16 seconds at 1000 C failed from a corner defect and the fracture surface had a fast fracture appearance. The 552, 566, and 483 MPa samples at 1100 C probably failed from corner origins. The fracture surfaces for the 414 MPa at heatup to 1200 C, the 379 MPa at 1300 C, and a faulty run (not shown on Figure 52), all showed prominent SCG markings away from the sample corners. The faulty run, which involved a sample loaded to 400 MPa, was a successful trial except that the exact time of failure was not noted; records indicate it must have been between 5 and 21 hours at 1300 C. Figure 53 shows a SCG zone which may have emanated from a surface machining defect as described previously.

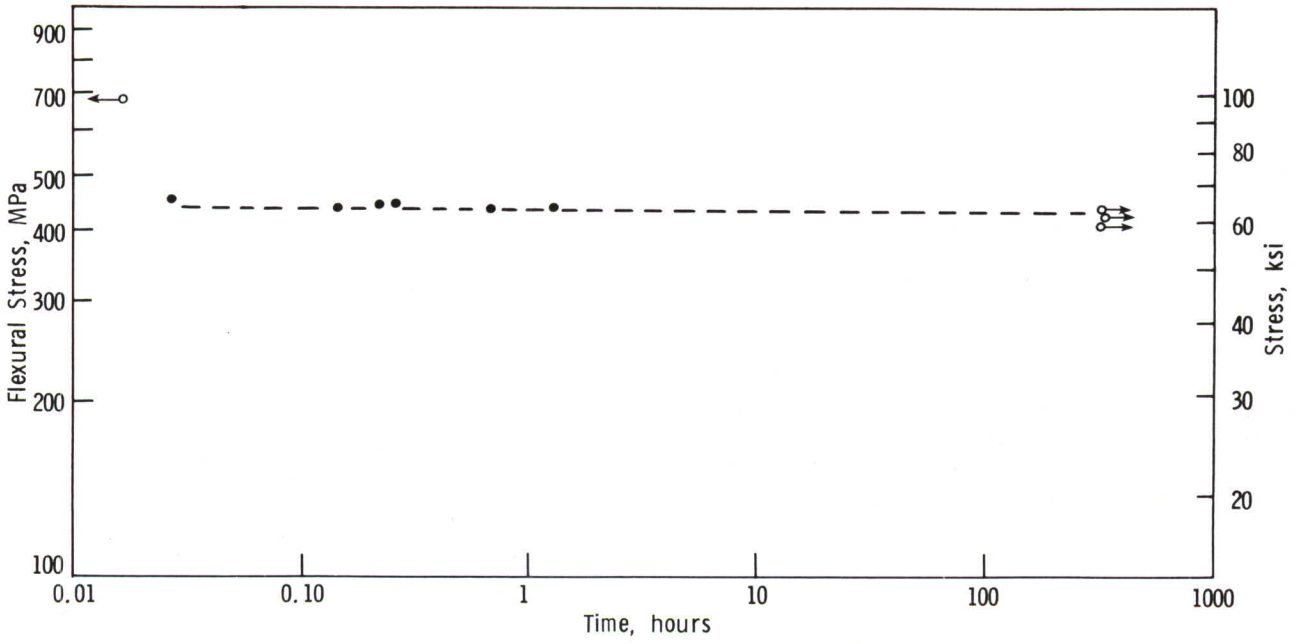

Figure 51. Flexural stress rupture at 1200 C for Norton NCX 34 hot-pressed silicon nitride.

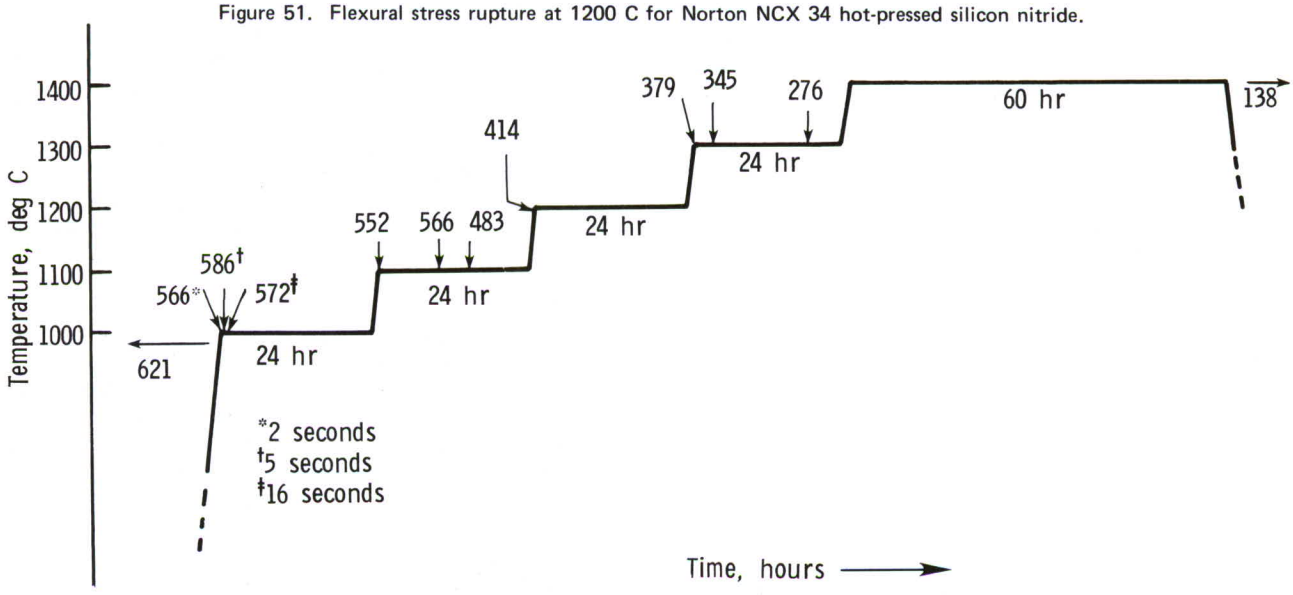

Figure 52. STSR results for Norton NCX 34 hot-pressed silicon nitride.

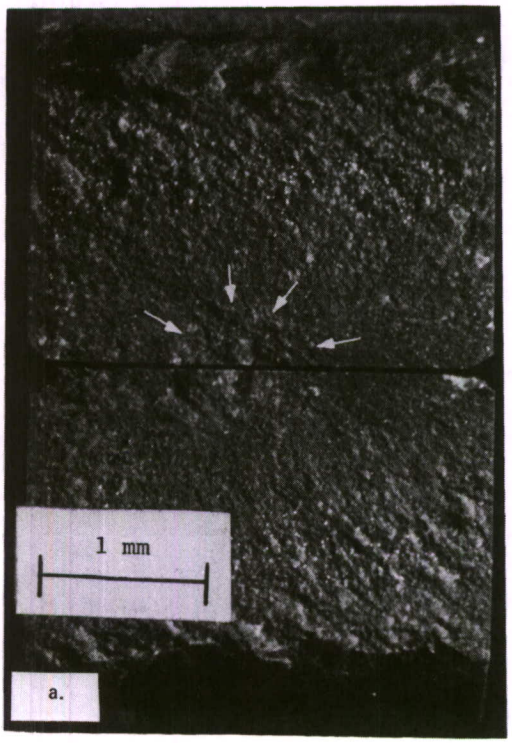

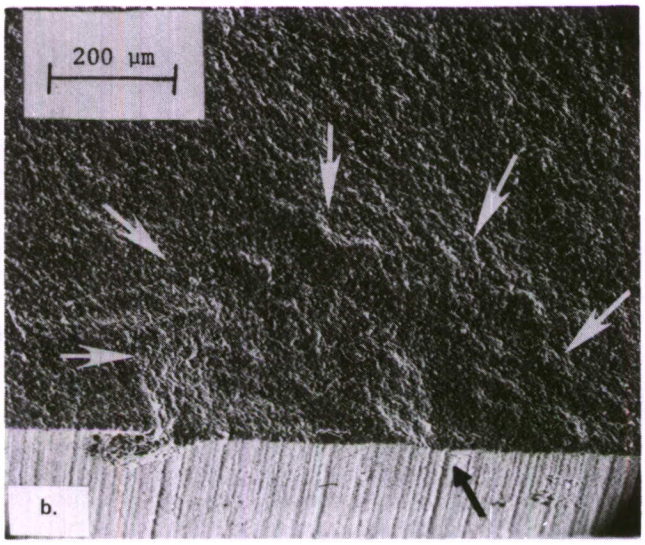

Figure 53. (a) Light photograph of the two fracture surfaces of an NCX 34 STSR sample showing a slow crack growth zone (white arrows). The sample failed between 5 and 21 hours at 1300 C. The fracture halves are mounted back to back on their tensile faces; (b) SEM close-up of slow crack growth zone. The black arrow shows a possible initiation site (machining damage). The item on the surface at the left is contamination pickup which resulted when the sample fell onto the furnace floor.

Several other samples, 345 and 276 MPa at 1300 C, the 138 MPa survivor, and a faulty 207 MPa trial, all had an unusual band of material that occupied 1 to 3 mm of the length of the bend bar (Figure 54). The faulty 207 MPa run failed during heatup to 1400 C (at 1397 C), but four hours elapsed during this heatup from 1300 C due to worn furnace elements (normal heatup time is 1/2 hour). Curvature of the bend bars with such a feature was not uniform and a distinct kink was observed in the nonuniform bands, indicating the zone was much less creep resistant than the remainder of the sample. Light microscopy revealed small lateral cracks in the zones running normal to the applied stress field. Occasionally a large crack would be observed (Figure 55). SEM examination of the crack reveals it to be wide and meandering. This cracking may be due to excessive creep deformation since the cracks are uniformly distributed and normal to the applied stress. Contrary evidence is indicated in Figure 56 which shows a cracked region extending along one side of the sample well into the compressive zone of the bend bar. This appearance is similar to cracks observed in some of the NC 136 fracture surfaces (Figures 46 and 47). An X-ray diffraction pattern from the material of the zone was identical to a pattern generated from outside the zone. It is possible the oxide layer was thick enough to obscure the phases present beneath the zone. The nonuniform zone was not observed in STSR samples that broke before reaching 1300 C and was not observed in the 1200 C stress rupture samples.

In general, samples that reached 1300 C developed gross curvature. The sample that survived the entire pattern intact had a maximum strain of more than 1 percent (nonuniform as well,

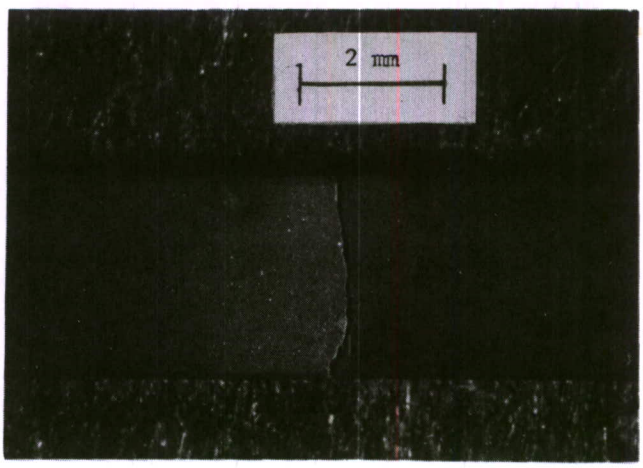

Figure 54. Light photo showing the tensile face of an NCX 34 STSR sample which failed on heatup to 1400 C. Failure occurred from the light colored band.

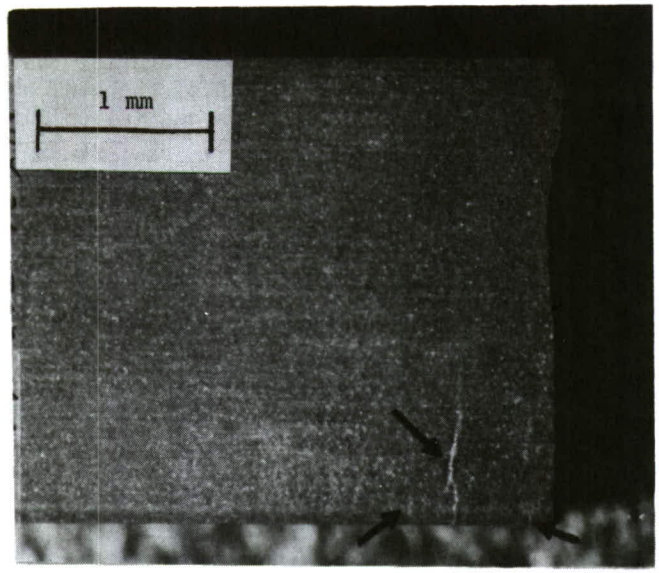

Figure 55. Close-up light photomicrograph of an NCX 34 STSR sample showing cracks in a nonuniform band of material. The nonuniform band occupies the entire photo. The sample was loaded to 345 MPa and failed at 2.9 hours at 1300 C.

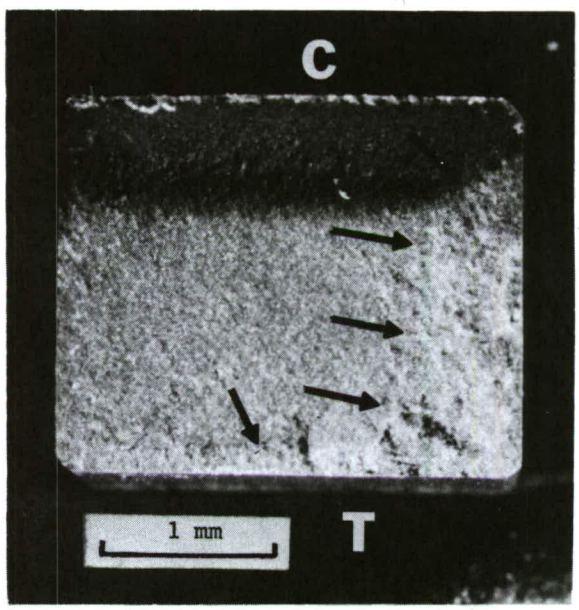

Figure 56. Fracture surface of the sample shown in Figure 55. Cracking extends along the tensile face and up the side of the sample (arrows).

due to the creep susceptible zone). Samples with the nonuniform zone tended to fail from the zone. Once temperatures of 1300 C were attained, a thick oxide layer began to develop. The sample that survived had a thick, glossy, faceted layer that appeared crystalline. X-ray diffraction indicated strong beta Si_3N_4 peaks, prominent alpha cristobalite, and a strong unidentified phase characterized by peaks shown in Table 3. No H phase or WSi_2 (both present in control samples) were observed. The prime peaks of the unidentified phase were stronger than the cristobalite prime peak.

Table 3. NCX 34 STSR UNIDENTIFIED OXIDE PHASE FROM X-RAY DIFFRACTION

(Other peaks may be shared with beta Si_3N_4 or alpha cristobalite.)

d Spacing, Å	Prominence
5.37	Major (most prominent)
3.03	Minor
2.65	Minor
2.22	Minor
1.79	Major

4. Discussion

This grade of hot-pressed silicon nitride has the highest strength at room temperature of any of the thirteen materials tested in this study. The strength distribution is very narrow as well. The strength-controlling defect appears to be damage induced by the machining process. An important observation is that the machining damage extends considerably deeper into the sample than the depth of the striation.

Unfortunately, this material does not retain the high strength at elevated temperatures. Stresses of 566 to 621 MPa caused failure on loading at 1000 C in the STSR trials and represent a strength loss of 40 percent. At 1200 C the load-carrying ability is even less, with 440 MPa acting as a cut-off value: a 52 percent decrease with respect to the room temperature values. Since the strengh-controlling defect is machining damage, these values can be expected to vary with the quality of machining, but the strength degradation will still be evident. Similar large reductions in strength with temperature have been reported in References 64 and 65.

64. LARSEN, D., and WALTHER, G. *Property Screening and Evaluation of Ceramic Turbine Engine Materials.* IIT Research Institute, AFML Contract F33615-75-C-5196, Interim Report No. 5, January 1978.

65. RICHERSON, D., SCHULDIES, J., YONUSHONIS, T., and JOHANSEN, K. *ARPA/NAVY Ceramic Engine Materials and Process Development Summary* in Ceramics for High Performance Applications II, J. J. Burke, E. M. Lenoe, and R. N. Katz, ed., Brook Hill Publishing Company, Chestnut Hill, Massachusetts, 1978, p. 625.

No unusual temperature sensitivity was detected at 1000 C, but time-dependent failures occur at 1100 C and above. Many, but not all, fracture surfaces for failures in the 1100 C to 1300 C range showed slow crack growth markings similar to those observed in NC 132. The remainder of the fracture surfaces for samples that failed in that range were quite irregular and the origin could not be identified. Several failures at 1300 C and above are from a nonuniform zone in the sample where excessive creep had occurred. These zones and their effect on mechanical behavior were not evident at elevated temperature but a slight mottling was visible. Further work on this material should be directed at identifying the nature of the nonuniform zones and attempting to eliminate them. Testing in this study was limited by the small number of samples prepared.

Oxidation buildup was relatively minor at 1200 C and lower temperatures, but became substantial at 1300 C and above. Comparing the creep and STSR results at temperatures above 1200 C for NCX 34 to those for NC 132 shows little or no improvement in the high temperature performance of the yttria-additive material.

A recent study of this material has identified a severe instability at temperatures between 600 C and 850 C.[66] The STSR trials reported in this study did not detect this effect and suggest that a broader range of temperatures should have been utilized than the 1000 C to 1400 C actually employed. To investigate this matter further, several additional samples were loaded in an STSR test sequence, but with a modified temperature schedule. Two samples loaded to 450 MPa were exposed to a temperature sequence starting at 700 C and increasing to 1000 C in 50-degree increments. Twenty-four hours at each 50 C step were allowed to elapse. One sample survived intact, the other failed at 9.6 hours at 950 C. Neither had any unusual features or markings. An additional sample at 450 MPa was exposed to an STSR sequence with temperatures from 900 C to 1020 C in 20-degree increments, again with 24 hours at each step. The sample survived intact. Finally, a last sample was placed in the flame-heating station of the thermal fatigue machine. One end was heated to 1371 C while the other end was maintained well below black heat temperatures (700 C to 800 C). After 20 hours of steady state heating (no cycling or quenching), a gradient of oxidation markings was evident on the surface, but no severe degradation was observed. Presumably, billet-to-billet variations are accounting for the difference in the results of Reference 66 and this report.

D. Norton NC 350 Reaction-Bonded Silicon Nitride

1. Control Strengths

Thirteen samples were used to obtain 16 control fractures at room temperature. Average strength was 294 MPa with a 41 MPa standard deviation. The data, when plotted on a Weibull graph, is well fitted (98% correlation coefficient) by a least-squares line of slope 7.2 (Figure 57). This average strength is somewhat higher than the 264 MPa reported in Reference 14. It is considerably higher than the 162, 213, and 234 MPa values (three separate batches) reported in Reference 67 or the 214 MPa reported in Reference 68. In the former case, density variations from billet-to-billet may account for the discrepancy. In addition, a higher fraction of machining defects caused failures in that study than in this report.

Failure origins were readily discernible from the clear mirrors that were on fracture surfaces.

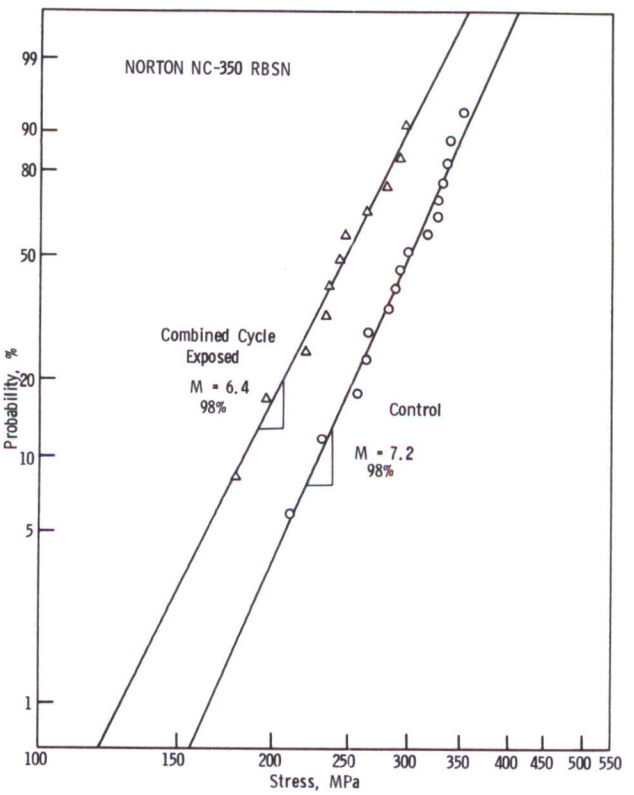

Figure 57. Room temperature control strengths of NC 350 RBSN samples.

66. BENN, K. W., and CARRUTHERS, W. D. *3500 Hour Durability Testing of Commercial Ceramic Materials.* Third Quarterly Progress Report, September to November 1978, AiResearch Manufacturing Company of Arizona, NASA Contract DEN 3-27, 15 December 1978.
67. LARSEN, D., BORTZ, S., RUH, R., and TALLAN, N. *Evaluation of Four Commercial Si_3N_4 and SiC Materials for Turbine Applications* in Ceramics for High Performance Applications II, J. J. Burke, E. M. Lenoe, and R. N. Katz, ed., Brook Hill Publishing Company, Chestnut Hill, Massachusetts, 1978, p. 651-668.
68. YONUSHONIS, T., and RICHERSON, D. *Strength of Reaction-Bonded Silicon Nitride.* Proceedings of the 1977 DARPA/NAVSEA Ceramic Gas Turbine Demonstration Engine Program Review, Castine, Maine, MCIC 78-36, August 1977, p. 219.

Although the Weibull plot suggests a single distribution of defects, examination of the fracture surfaces revealed two distributions: pores and machining defects. Eight fractures originated at pores such as shown in Figure 58. In four of these samples, pores were quite light in color when viewed with the unaided eye. Binocular microscope examination showed these to be partially filled with material (both pore halves in the two fracture halves). When subsequently examined with SEM, the pores no longer had interior material evident, probably due to the sonic vibration cleaning applied to all samples prepared for SEM. The porous areas may be regions of incomplete reaction. Seven samples failed from machining damage. One of these failed from a scratch on the sample side. The six others failed due to damage induced by relatively deep striations at the corner chamfer (Figure 59). Some of the chamfer striations were not longitudinal, but were at an angle of 10 to 20° to the long axis. The final sample failed from a processing crack that existed in the bend bar.

2. Stress Rupture, 1200 C

Of nine trials, none failed in a time-dependent manner (Figure 60). The cut-off stress level is 345 MPa, a value considerably higher than the room temperature average strength (294 MPa). A slight permanent deformation in the 300-hour survivors was noted, an amount that corresponds to maximum strains of 0.08 percent for the 207 MPa sample, 0.11 percent for the 276 MPa sample, and 0.15 percent for the 345 MPa sample.

All six survivors were subsequently broken to measure retained strengths. Table 4 shows an interesting trend of higher retained strength with higher stress rupture loading. This trend may be in part a proof testing effect or a chance statistical outcome. The four highest retained strengths are greater than any control strength. (As always, care was taken to ensure the tensile face of the stress rupture loading was also the tensile face on subsequent retained strength loading.) Insufficient data is available, however, to draw any conclusions.

Very little oxide formation occurred at the specimen surfaces. The samples appeared only slightly lighter in coloration than the control samples. X-ray diffraction identified the oxide as alpha cristobalite and SEM examination of the oxide indicated it is a smooth coherent layer (Figures 61 and 62). The 207 and 276 MPa survivors failed from subsurface pores (Figure 61). The 241 and 345 (300 hr) MPa survivor samples failed from surface-connected pores (Figure 62). The 310 and 345 (267 hr) MPa survivor samples failed from unidentified flaws, but were probably related to machining damage.

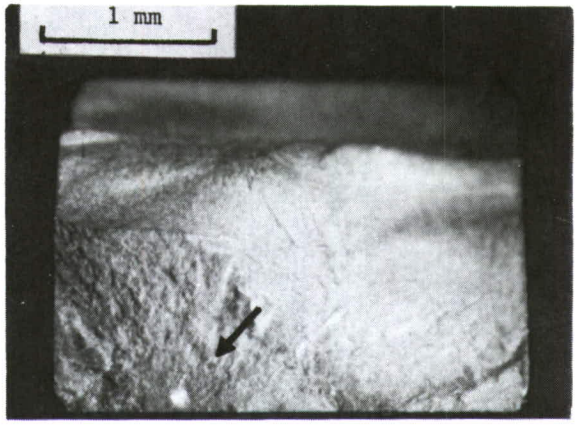

a. Light photo showing a prominent subsurface defect in the mirror (arrow).

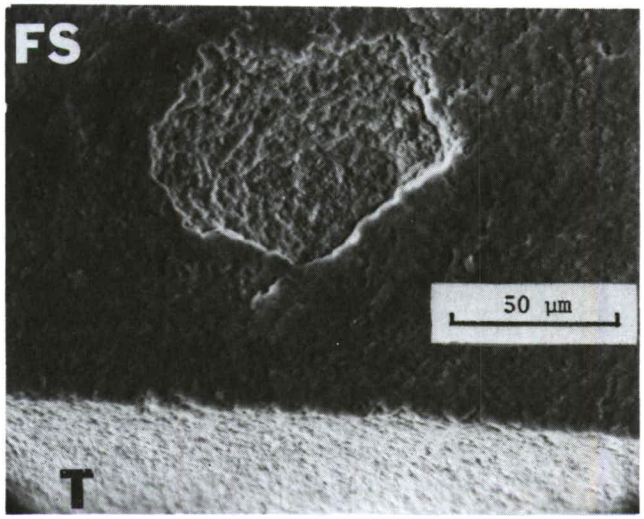

b. SEM close-up of the defect of (a). Fracture stress for this sample was 316 MPa.

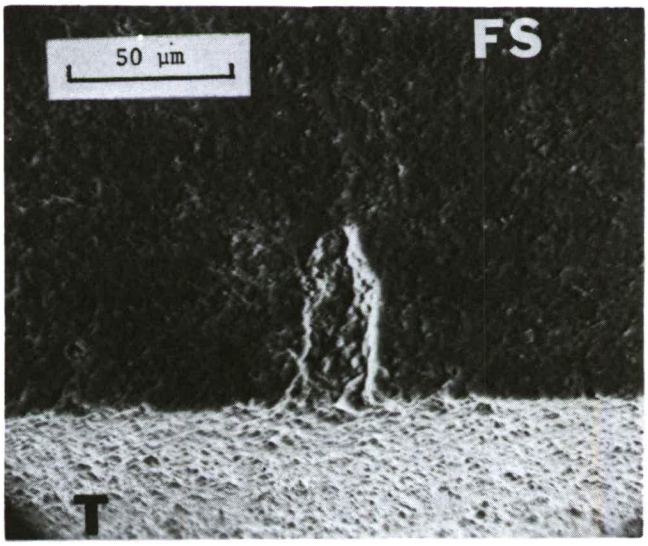

c. SEM close-up of a defect that initiated failure at 326 MPa in a different sample.

Figure 58. Fracture surfaces of room temperature control samples of NC 350.

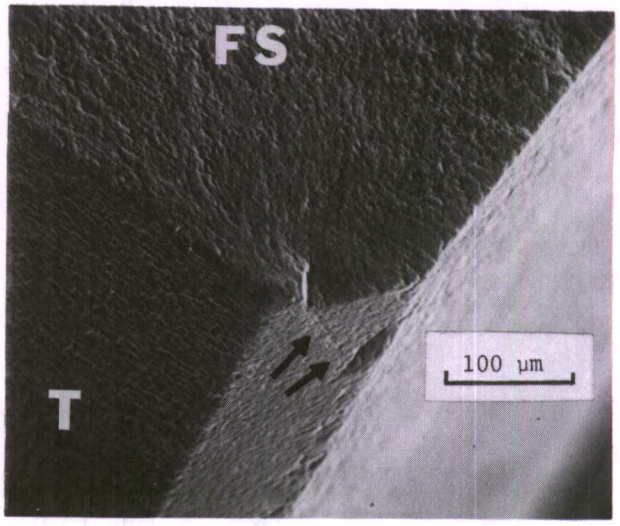

a. Machining mark on the chamfer is associated with the shoulder that is subsurface damage.

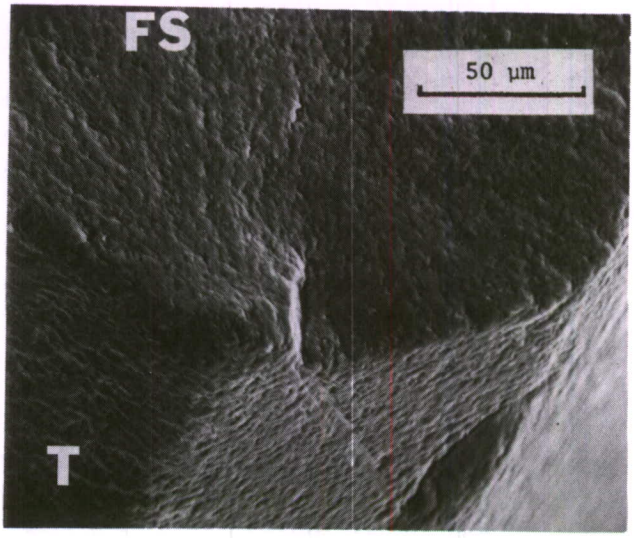

b. Close-up of (a).

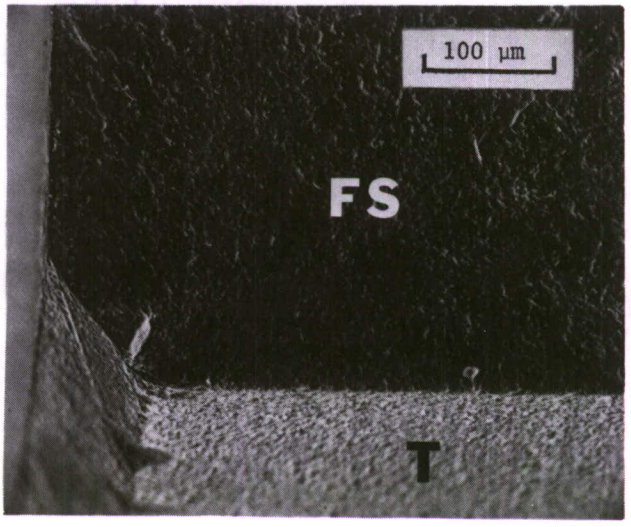

c. Opposite and mating fracture half showing the shoulder and a second machining mark nearby.

Figure 59. SEM photos of the fracture surface of a room temperature control sample of NC 350. Fracture stress was 264 MPa. The sample has been strongly tilted to gain a better view of the chamfer. The tension face is labeled T, the fracture surface FS.

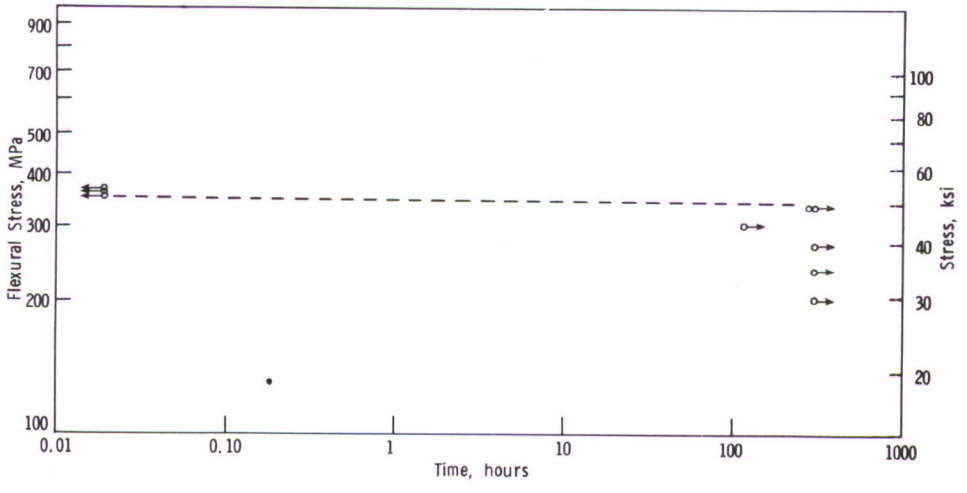

Figure 60. Flexural stress rupture at 1200 C for Norton NC 350 reaction-bonded silicon nitride.

Table 4. NC 350 STATIC FATIGUE SURVIVORS

Stress Rupture Loading (MPa)	Survival Time (hour)	Room Temperature Retained Strength (MPa)	Room Temperature Failure Source
345	300	470	*Surface-Connected Porosity
345	267	427	*Machining damage?
310	118	454	*Machining damage?
276	300	373	Subsurface porosity
241	300	257	*Surface porosity
207	300	256	Subsurface porosity

*Flaw-healing potential

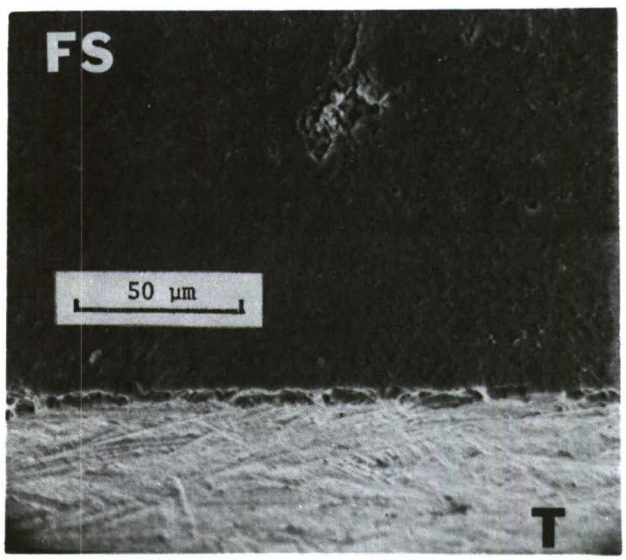

Figure 61. Fracture surface of an NC 350 1200 C stress rupture survivor. Retained strength was 373 MPa. The strength-controlling defect is a subsurface porous region.

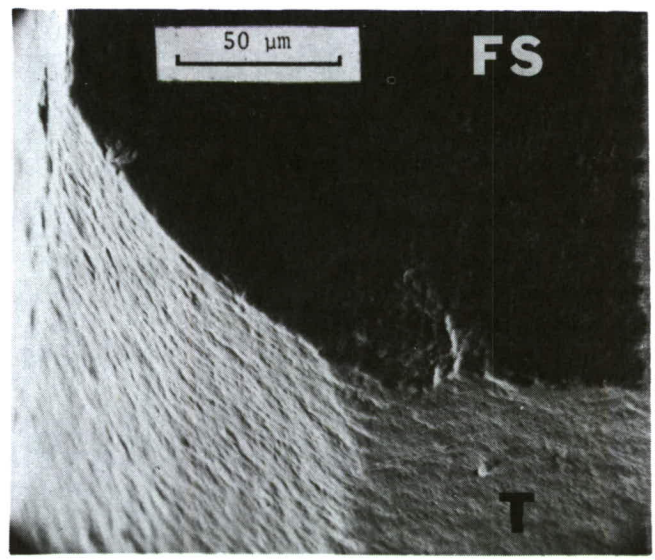

Figure 62. Fracture surface of another NC 350 survivor which shows a surface connected pore that limited the retained strength to 257 MPa.

3. STSR

Stepped temperature stress rupture trials also demonstrated a high resistance to static fatigue failure (Figure 63). Only two samples out of fourteen failed in a time-dependent manner. Both failures appeared to fail from surface-connected porosity (Figures 64 and 65). Both pores were shallow and may have actually been pits. A similar shallow feature was observed in one of the survivors (Figure 66).

The survivors had some permanent deformation and retained strengths were all higher than the average room temperature strength as shown in Table 5.

The oxide layer caused only a slight lightening in sample coloration and again was identified as alpha cristobalite. The layer was somewhat more rippled than the 1200 C stress rupture trials however, but still appeared uninterrupted (compare Figures 64 and 65 to 61 and 62).

4. Combined Cycle Procedure

Twelve combined cycle samples survived intact with very little change in appearance compared to their original condition (Figure 67). Slight pitting and erosion were evident at the edges where the flame and quench air washed over the sample. An initial mass loss (an average of 0.013 gram each sample out of an initial mass of 0.734 gram) was recorded on the first heat treating period. This was followed by a steady increase in mass on each subsequent heat soak or thermal cycling pattern. The initial mass loss may be due to the burn-off of residual wax from the machining process. Net mass gain subsequent to the first heat period was 0.004 gram per sample.

The retained flexural strength of eleven samples (one was broken in handling) averaged 244 MPa with a standard deviation of 37.2 MPa. This represents a 17% strength loss compared to the control strength. The Weibull graph (Figure 57) again indicated a unimodal distribution and a

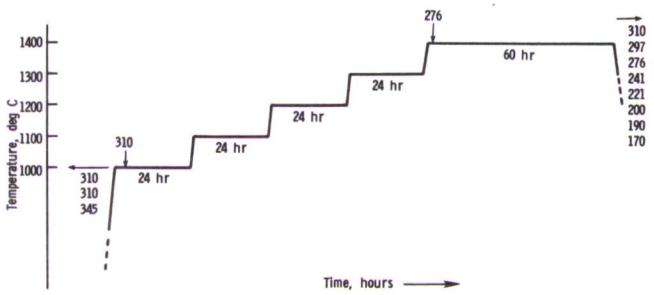

Figure 63. STSR results for Norton NC 350 reaction-bonded silicon nitride.

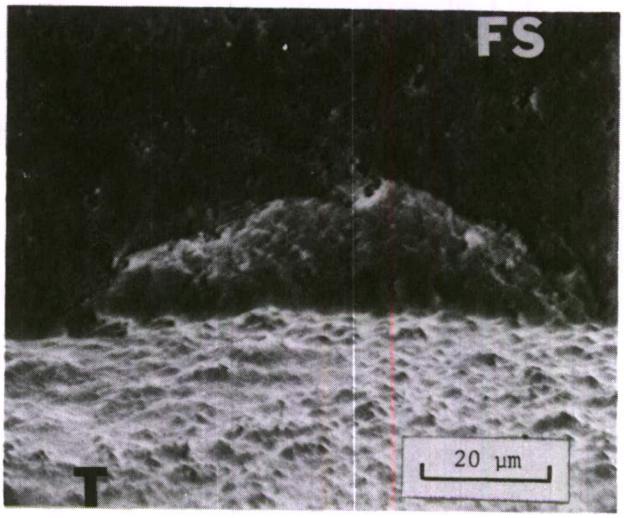

Figure 64. NC 350 STSR sample which failed at 1 hour at 1400 C. SEM examination of the fracture surface shows a shallow pit or porous region that was the initiation site.

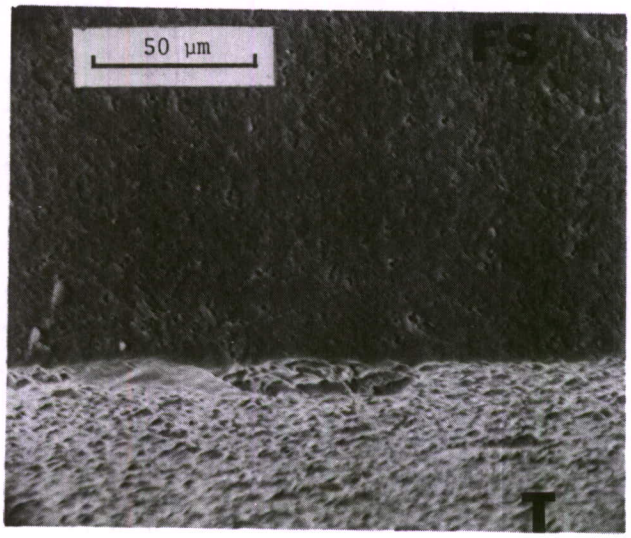

Figure 65. SEM photo of the initiation site of the STSR sample that failed at 3 hours at 1000 C. A distinct mirror clearly pinpointed this site.

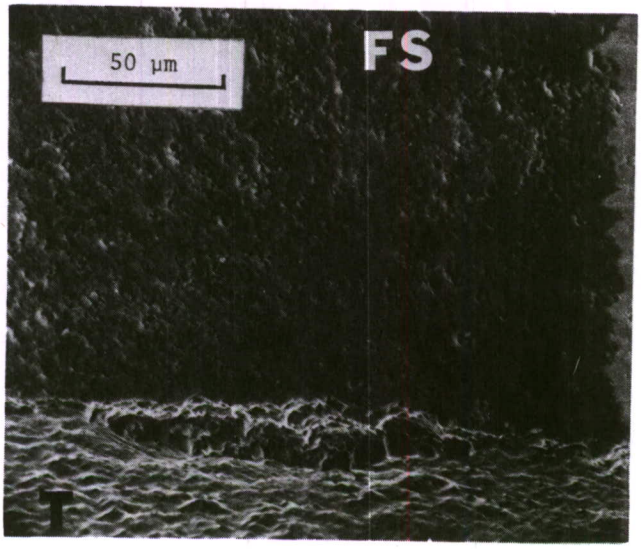

Figure 66. NC 350 STSR survivor sample. Sample was loaded to 200 MPa and had a retained strength of 343 MPa. The fracture initiation site is a shallow pit at the surface as shown on this SEM photo of the fracture surface.

Table 5. NC 350 STSR SURVIVOR DATA

Stress Rupture Loading (MPa)	Room Temperature Retained Strength (MPa)	Maximum Tensile Strain (%)	Room Temperature Failure Source
310	343	0.12	*Chamfer machine mark
310	Broke on cooldown	-	*Surface pore?
297	349	-	*Surface pore filled with oxide
276	387	-	*Surface pore?
241	Broke on cooldown	-	*Corner defect
221	319	0.15	*Surface pore filled with oxide
200	343	-	*Surface pore filled with oxide
190	312	-	Shiny spot in mirror - Silicon?
170	305	0.2	*Chamfer machine mark

*Flaw-healing potential

Figure 67. Light photograph of the exposed surface of an NC 350 combined cycle sample. The crack is the break point on subsequent retained strength testing. Some damage to the surface, particularly at the corners, is evident.

least-squares line of slope 6.4 was an excellent fit to all data (98% correlation coefficient). A shift in failure sites relative to the control group was apparent. Eight of the eleven samples failed from surface-connected porosity as shown in Figure 68. The pores were often sealed over by the oxide layer; but the layer itself was porous, not smooth (Figures 68 and 69), and was very much unlike the stress rupture oxide layers. One other sample failed from a pore beneath the surface that may or may not have been surface connected. The remaining two samples failed from unidentified sources, but were probably initiated at the corners.

5. Stress Rupture, 1000 C

A sufficient number of samples remained so that the stress rupture behavior at 1000 C could be further investigated. The two other grades of RBSN tested in this study seemed to show a sensitivity to this temperature and although NC 350 showed little propensity for failure at 1000 C, it is possible too few samples were tested. The results of trials on ten samples are shown in Figure 70 and only one additional failure was obtained. That failure occurred at a large surface-connected pore located away from the corner chamfer. The critical stress level is 310 MPa, a value less than the 345 MPa observed for 1200 C testing, but still above the room temperature average strength (294 MPa).

The survivors had negligible permanent deformation after 500 hours and were only slightly lighter in coloration than the virgin samples. Retained strengths of the four survivors were: 348 MPa for the 280 MPa loaded sample, 382 and 373 MPa for the 300 MPa loaded samples, and 399 for the 310 MPa loaded sample. Failures were from an inclusion at the surface, a surface pore, an unidentified surface defect, and a corner chip from machining, respectively. An average mass loss of 0.015 gram was sustained by the samples (possibly wax loss).

6. Discussion

Norton NC 350 reaction-bonded silicon nitride has a high resistance to static fatigue failure at temperatures of 1000 C to 1400 C. The material is able to sustain higher stress levels at elevated temperature than at room temperature. Subsequent strength at room temperature is also significantly improved for many of the survivor samples. These observations are consistent with reports that the strength of NC 350 increases with temperature[15,64,67-70] and with high temperature oxidation exposure (room temperature strength).[54,65,71] The fractographic evidence indicates the samples which had significantly improved strengths during or after exposure to high temperature had strength-controlling defects at the surface. These defects were either machining-related or surface-connected porosity. Samples which showed little or no improvement in strength compared to the control group had strength-controlling defects, usually porosity, in the interior. Thus an oxidizing heat treatment *cannot* be relied upon to improve the strength of *all* samples. Examination of the oxide layer that forms shows it is a coherent, smooth, and thin layer of alpha cristobalite. In some cases the oxide layer filled the surface porosity. Thus the evidence indicates that the oxide formation is a strong aid in crack blunting or flaw healing. Sufficient time for oxidation was presumably available (during heatup to temperature) for the stress rupture trials at 1000 C to attain an improvement in strength. A further improvement is experienced for stress rupture testing at 1200 C, probably due to the longer time to reach temperature (more oxidation time).

On the other hand, the combined cycle results show the hazard in applying such conclusions from static oxidizing environments to an aggressive thermal environment more likely to be encountered in service. The combined cycle process leads to an oxide layer that is not smooth, but porous, irregular, and cracked by the thermal cycling. At sample edges much of the oxide is eroded away.

69. LARSEN, D., and WALTHER, G. *Property Screening and Evaluation of Ceramic Vane Materials.* IIT Research Institute, AFML Contract F33615-75-C-5196, Interim Report No. 4, October 1977.
70. McLEAN, A., FISHER, E. A., and BRATTON, R. J. *Brittle Materials Design, High Temperature Gas Turbine.* Ford Motor Company, Contract DAAG46-71-C-0162, Interim Report No. 6, AMMRC CTR 74-59, September 1974.
71. LARSEN, D., and WALTHER, G. *Property Screening and Evaluation of Ceramic Vane Materials.* IIT Research Institute, AFML Contract F33615-75-C-5196, Interim Report No. 5, January 1978.

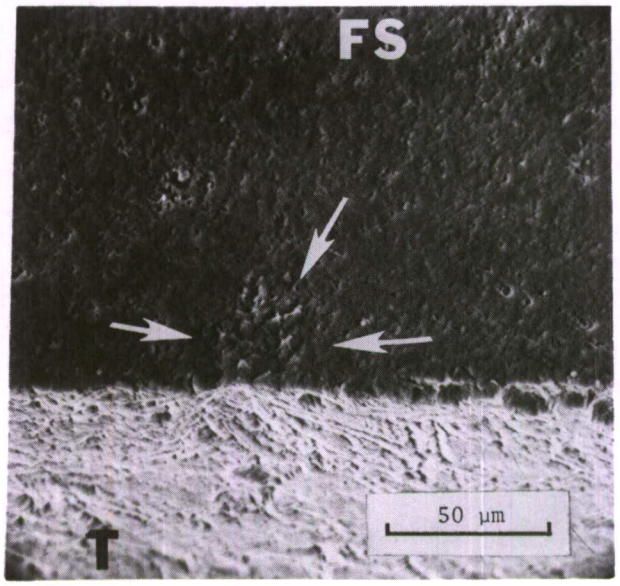

Figure 68. Failure initiation site (arrows) of a combined cycle NC 350 sample. The porosity is surface connected. Retained strength was 195 MPa.

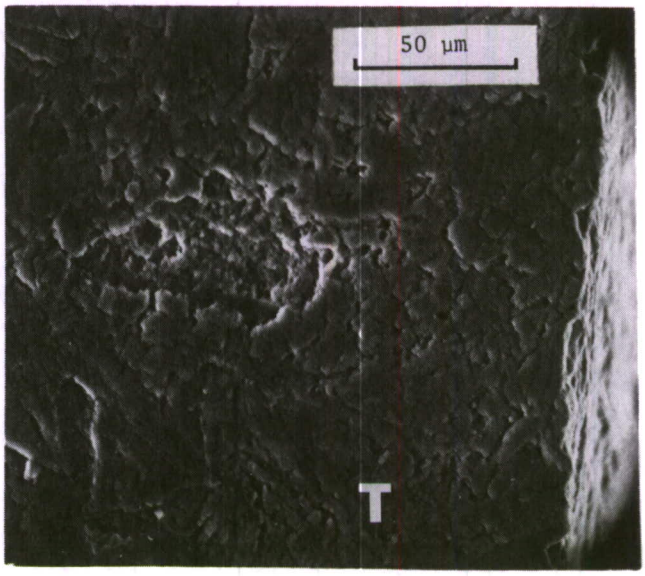

Figure 69. SEM photo of the flat tensile surface of the combined cycle sample shown in Figure 68. The oxide layer is badly damaged.

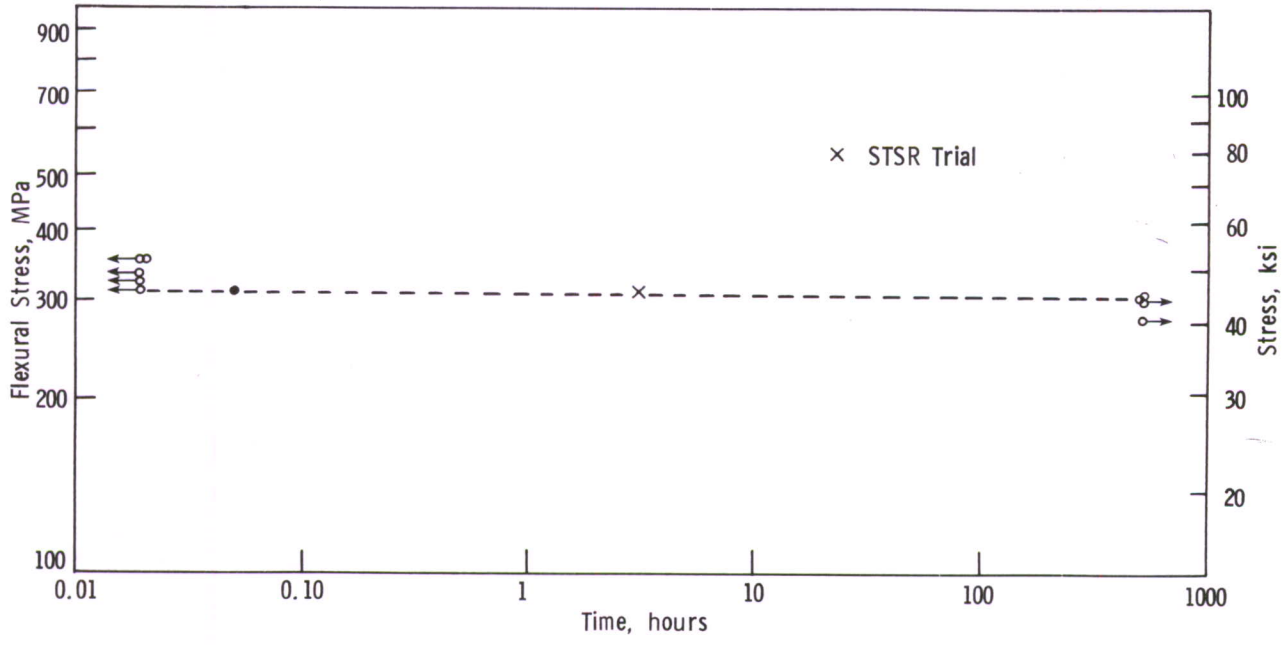

Figure 70. Flexural stress rupture at 1000 C for Norton NC 350 reaction-bonded silicon nitride.

Ten of eleven samples failed from surface-connected porosity or machining damage that may have grown in size due to repeated oxidation attack and the failure to retain a protective oxide layer. Unlike the samples from the static oxidation experiments, the combined cycle samples thus experienced a measurable decrease in strength. This result reinforces the contention that proper materials evaluation requires exposure to dynamic oxidizing environments.

Although the bulk of the data generated indicates passive oxidation of surface defects leads to an improvement in strength, the converse may also be true. In the two cases where fatigue failure occurred at 1000 C, the failure site was surface-connected porosity. Just what was occurring to these porous regions that led to sample failure is not clear, but the possibility that oxidation was a contributing factor cannot be ruled out.

E. Kawecki Berylco Industries Reaction-Bonded Silicon Nitride

1. Control Strengths

Nineteen samples yielded 25 room temperature MOR values. Average strength was 206 MPa with a standard deviation of 15. A two-parameter Weibull line with a slope-modulus of 14.8 was an excellent fit (98% correlation coefficient) to all data (Figure 71). Fracture initiation sites were identified by the presence of a very large but poorly defined mirror. Despite the unimodal Weibull plot, at least two strength-controlling defects were identified. Fifteen fractures initiated from large pores such as shown in Figure 72. Some of the pores were surface connected, others were not, and a volume distribution of this defect (as opposed to surface) is appropriate. Six samples had initiation sites that were pores associated with presumably unreacted silicon that gave the appearance of an inclusion (Figure 73). The initiation site of four other fractures could not be identified. All fractured samples had shiny reflective spots distributed throughout the fracture surface. These spots are likely either free silicon or large silicon nitride grains.

One would expect that based upon the porosity gradient as shown in the polished section (Figure 13) that a bimodal effect on strength would result, depending upon whether the samples were placed one way or the other into the fixtures (large pores in tension or compression). During testing samples were randomly positioned, thereby insuring an unbiased selection of sample orientation. That the bimodal effect is not apparent in the Weibull plot is not surprising since several samples came out of each thickness of the billet and the pore gradient was evenly distributed in the samples.

2. Stress Rupture, 1200 C

Results of 1200 C stress rupture testing are shown in Figure 74 and indicate good resistance to static fatigue. Twelve samples failed on loading or survived hundreds of hours. A critical stress level of 180 to 200 MPa applied, a value only slightly below the room temperature average strength.

Three samples survived 500 hours and none had any measurable permanent deformation. The surface of the samples was slightly lighter in coloration than the control samples. The surface was a smooth, coherent, and clear layer occasionally interrupted by depressions or holes that correspond to large pores underneath. X-ray diffraction identified the surface layer to be alpha cristobalite. The 500-hour survivors were fractured at room temperature and had retained strengths of 219, 208, and 191 MPa for the samples loaded to 207, 193, and 150 MPa, respectively. Failures initiated at an unidentified site, a pore, and an unidentified site, respectively. The 200 MPa sample which survived 300 hours had a retained strength of 198 MPa and also failed from a large pore. These retained strength values are not very different from the

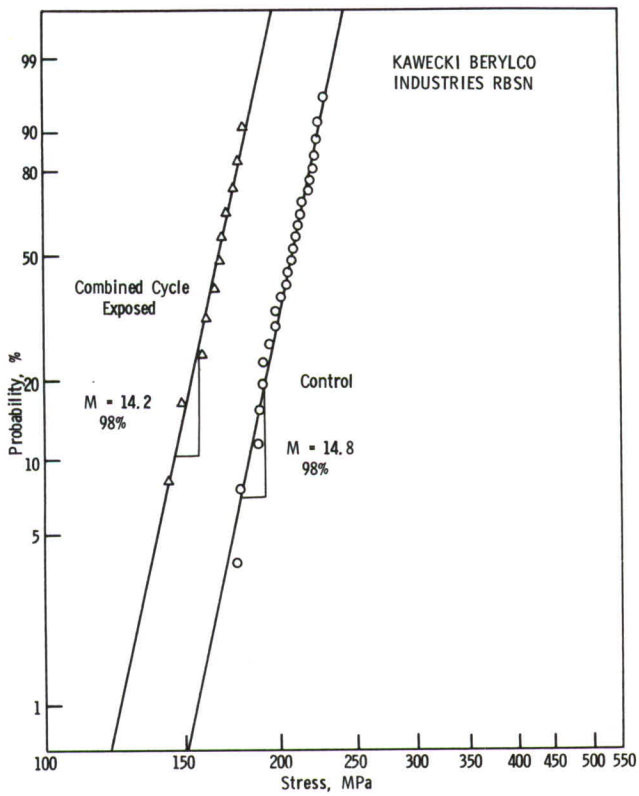

Figure 71. Room temperature control strengths of KBI RBSN bend samples.

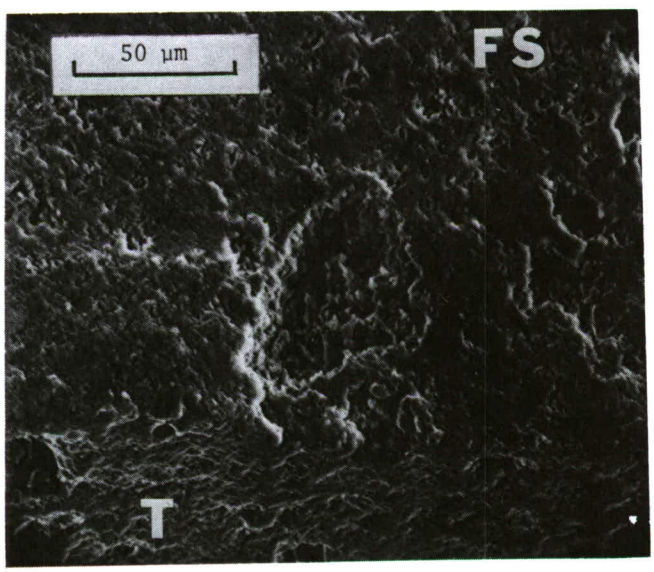

Figure 72. SEM photo of the fracture surface of a KBI control sample that failed at 214 MPa. The large pore was strength controlling. T marks the tensile face while FS marks the fracture surface.

average room temperature control strength (206 MPa) and indicate very little strength degradation. Of interest is that in each case the retained strength was just above the load applied to the sample in the stress rupture trial!

Two samples failed in a time-dependent manner; one loaded to 193 MPa broke at 27 hours, the other loaded to 180 MPa broke at 118 hours. The fracture surfaces were similar in appearance to a fast fracture sample and showed no evidence of slow crack growth. The failure origin could not positively be identified in either.

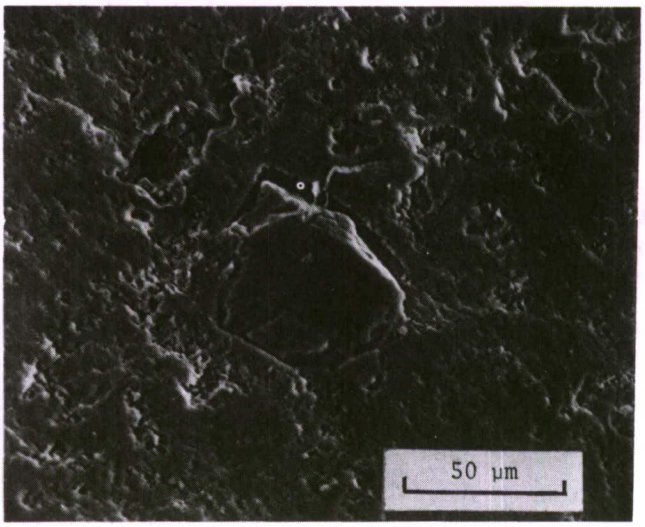

Figure 73. SEM photo showing a subsurface pore with a filling inclusion that probably is silicon. This defect limited the strength of this control KBI sample to 225 MPa.

3. STSR

The twelve STSR trials conducted did show a susceptibility to static fatigue failure (Figure 75). Eight samples loaded to 172 MPa tended to fail either in the 1300 C to 1400 C range or at the low temperature end of the pattern. That no failures occurred at 1200 C is in accord with the stress rupture trials conducted at that temperature. The samples that failed in the 1300 C to 1400 C range (and the two survivors) exhibited a slight creep deformation (0.05 to 0.10 percent tensile strain). The sample that failed after 44 hours at 1400 C had a maximum strain of about 0.07 percent. No common defect was observed for all the failures, although in three cases a small clear-white glassy formation associated with a pore was detected at the initiation area. This feature was visible only when viewed by low power optical microscopy (with any type of lighting). SEM examination failed to discern this feature, however, even when light photomicrographs were used to guide SEM examination (Figure 76). (The whitish-clear appearance may be an optical effect that is lost when the samples are gold coated and then viewed by SEM.) In one other sample a large version of this feature, a white band, extended through a significant portion of the fracture surface. Two other samples, 14 hours at 1300 C and 44 hours at 1400 C, had unidentified failure initiation zones.

The retained strength of one survivor was 196 MPa (very similar to control strengths) and it failed from a surface-connected pore. The

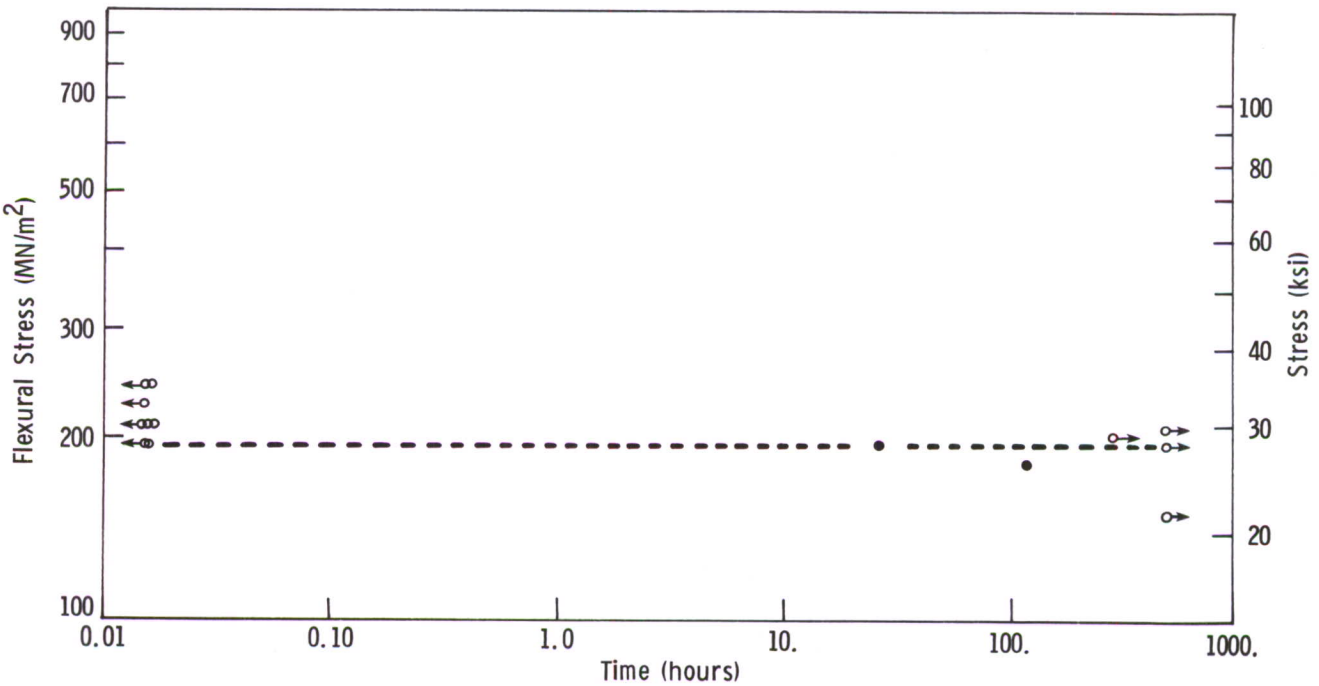

Figure 74. Flexural stress rupture at 1200 C for KBI reaction-bonded silicon nitride.

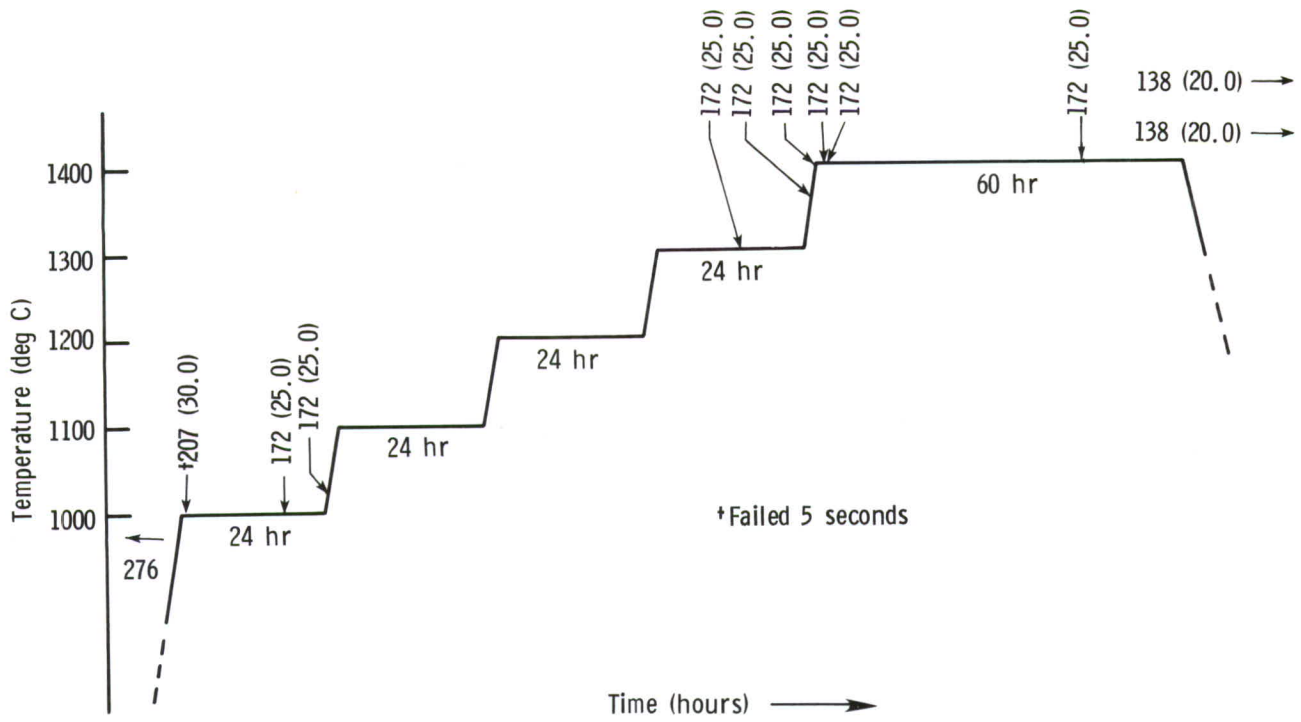

Figure 75. Stepped temperature stress rupture data for KBI reaction-bonded silicon nitride.

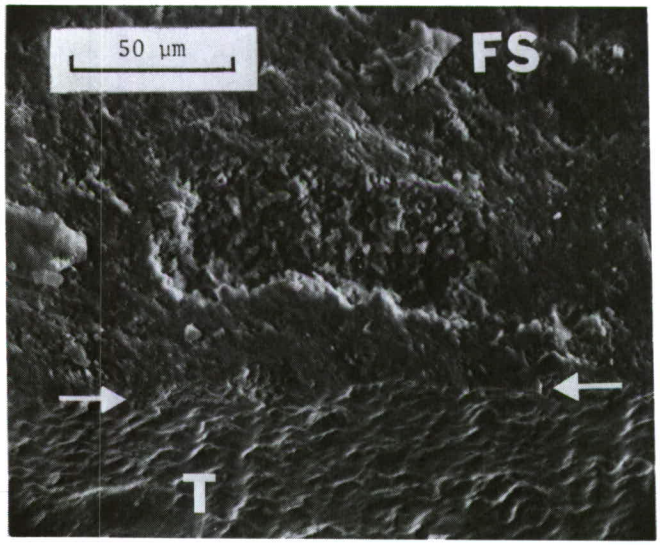

Figure 76. SEM photo of the failure initiation site for a KBI RBSN sample that failed during heatup to 1400 C in an STSR trial. Sample was loaded to 172 MPa. The defect is just below the surface (which is marked by the two arrows) but is likely connected via pore channels to the surface. When viewed with the light microscope this defect appeared white.

other survivor was broken in handling during removal from the furnace. The oxide layer was identified as alpha cristobalite by X-ray diffraction and covers nearly all the surface of the survivors with a smooth transparent layer. All but the largest pores are sealed over.

The two 1000 C failures were initiated at surface-connected pores (Figure 77). The third sample which failed at low temperature (on heatup to 1100 C) failed from an unidentified source. An unusual feature not observed on the samples exposed to higher temperature (either STSR or 1200 C stress rupture trials) was faint red banding that developed on the material after a few hours at 1000 C. The red was often seen associated with surface-connected porosity.

4. Combined Cycle Procedure

Eleven samples were subjected to the combined cycle procedure. (One sample was broken in handling part way through the test.) The average retained strength was 166 MPa with a standard deviation of 11.5 MPa. The average is 20 percent lower than the control strength. The Weibull modulus for the exposed samples was 14.2 (98% correlation coefficient), a value similar to the 14.8 of the control samples (Figure 71).

Fractography determined that surface-connected porosity caused most failures (at least seven). A typical defect is shown in Figure 78 and it is apparent the oxide attack has altered the shape of the pore. Thus the mechanism of strength degradation is probably the uniform enlargement of the porosity already in the material. This mechanism is consistent with the observation that the distribution of strengths of the combined cycle and control samples are nearly identical (same Weibull moduli and standard deviations).

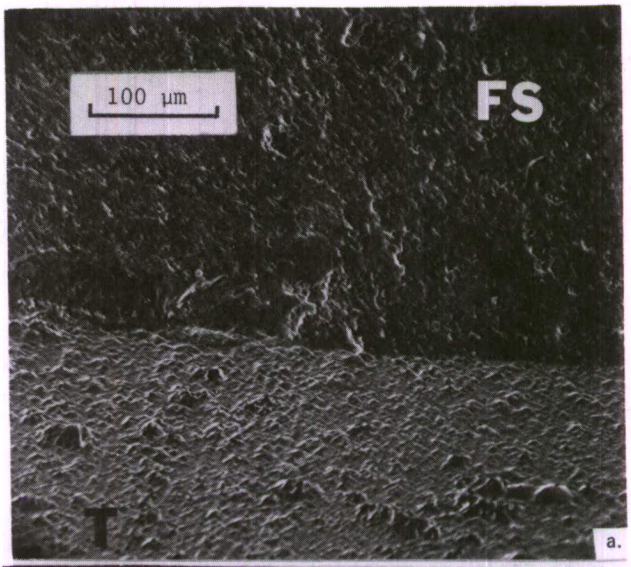

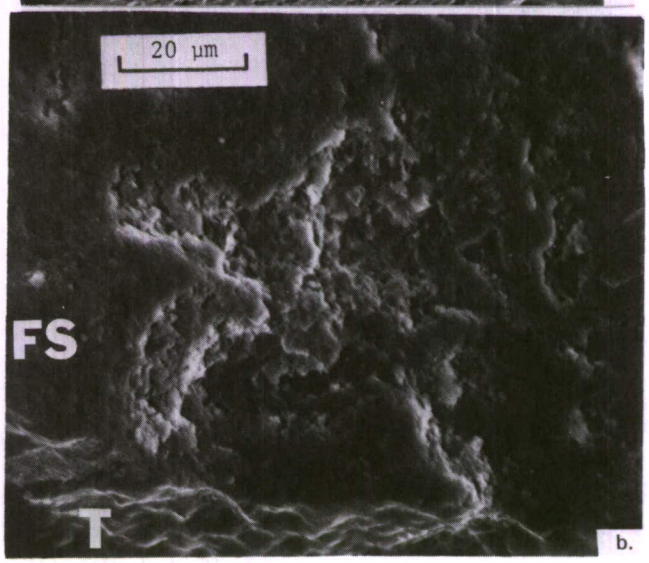

Figure 77. SEM photos of the fracture surface of the KBI STSR sample that failed at 17.2 hours at 1000 C: (a) shows the defect which caused failure; a porous region connected to the surface. Note the other surface-connected porosity in the vicinity; (b) is a close-up of the pore.

The oxide layer that formed was quite irregular and damaged in the region which was subjected to the flame attack-air quench. At the ends of the samples (away from the flame-air streams) the oxide layer was glossy, smooth, and coherent, but nearly all samples had the bright red spots on the surface. These spots were not evident in the flame-attacked zone. An initial mass loss of 0.0005 gram per sample was recorded on the first heat treating cycle, but was followed by mass gains on each heat treat or thermal fatigue portion of the pattern. A net gain of 0.0022 gram (out of an average initial mass of 0.7445 gram) was attained.

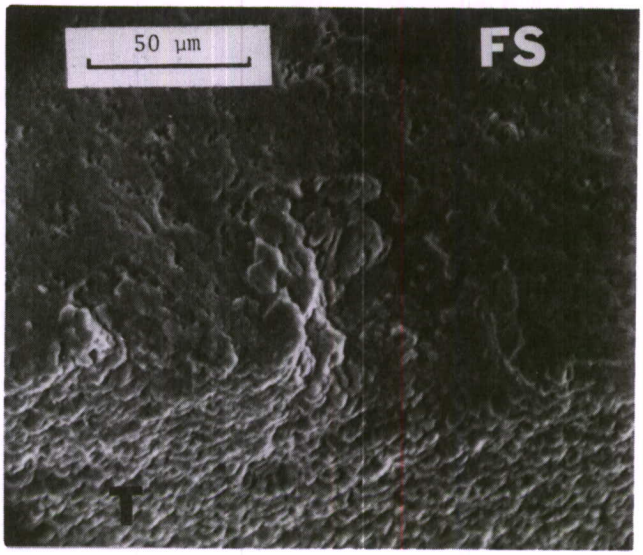

Figure 78. SEM photo of the fracture surface of a KBI combined cycle sample broken for a retained strength measurement of 150 MPa. The strength-controlling defect is a large surface-connected pore that has reacted with the surface oxide. The oxide layer is badly damaged.

5. Stress Rupture, 1000 C

Sufficient samples remained to permit additional testing at 1000 C. Seventeen stress rupture trials were conducted at 1000 C with the result that only two additional failures were attained (Figure 79). The critical stress level again is in the 170 to 210 MPa range. The initiation site of the 207 MPa failure at 0.9 hour was a large subsurface pore, again with an associated white band of material (Figure 80). The initiation site in the 197 MPa sample at 18.1 hours was indeterminate.

The red surface discoloration became more prominent with longer time at 1000 C. The 200-hour survivors had bright red markings that again were in bands. A semiquantitative analysis of the surface by X-ray fluorescence and emission spectroscopy indicated the surface had approximately 15 percent more iron than the surface of a control sample. X-ray diffraction indicated alpha cristobalite in addition to alpha and beta Si_3N_4. An SEM close-up of a red zone is shown in Figure 81. Retained strength of the sample loaded to 197 MPa which survived 119 hours was 221 MPa, for the 200 MPa sample at 138 hours was 234 MPa, and for the 159 MPa sample at 200 hours was 191 MPa. None had any measurable permanent deformation. The other two survivors were not available for retained strength measurement.

The samples which broke on loading generally failed from surface-connected porosity. An oxide layer tended to form very quickly.* An illustrative example is shown in Figure 82 which shows the

*The samples reached 1000 C very quickly and were held at temperature for about 5 minutes prior to loading. Heat-up time from 900 to 1000 C was about 5 to 10 minutes.

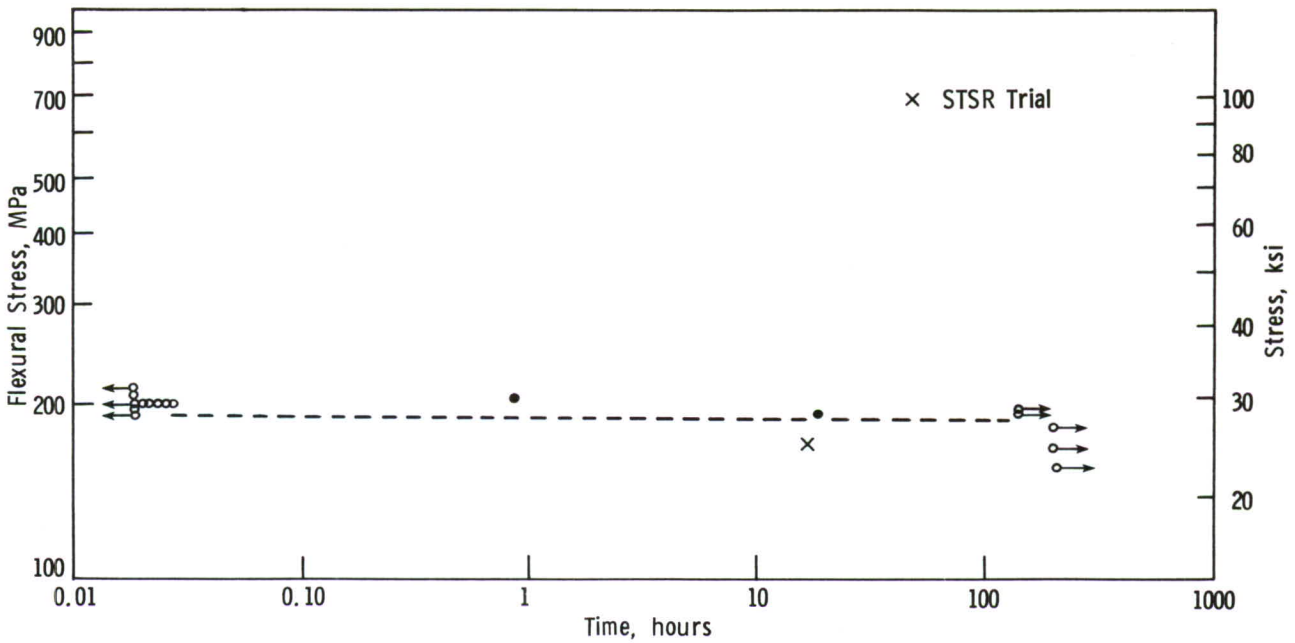

Figure 79. Flexural stress rupture at 1000 C for KBI reaction-bonded silicon nitride.

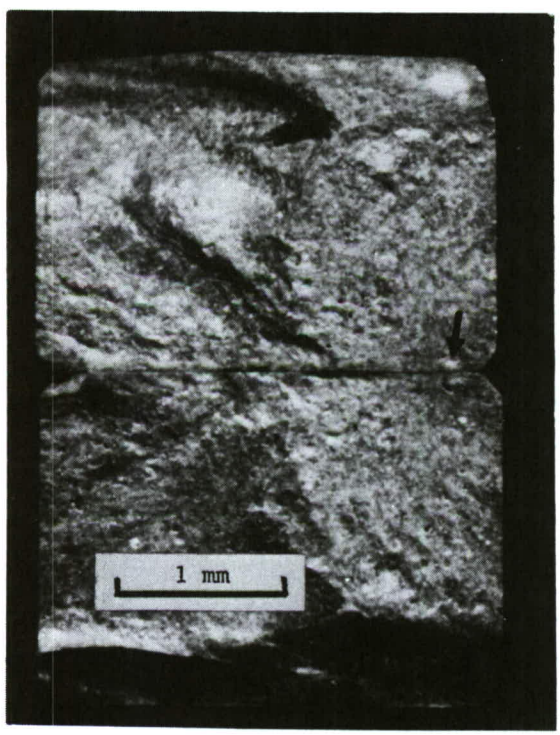

Figure 80. Light photo of the back-to-back fracture halves of a KBI sample that failed at 0.9 hour at 1000 C while carrying a stress of 207 MPa. The white coloration of the defect is evident. The halves share their tensile edge.

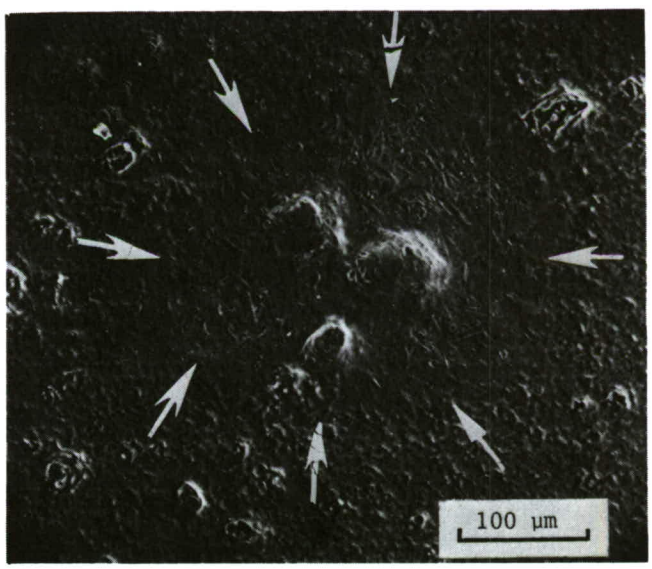

Figure 81. SEM photo of the surface of a 1000 C stress rupture sample that survived intact of 118 hours. A red patch is outlined by the arrows.

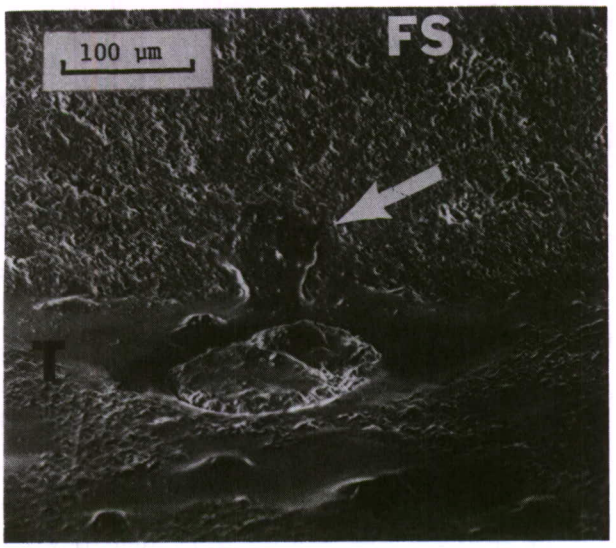

Figure 82. SEM photo of the tensile (T) and fracture surface (FS) of a 1000 C stress rupture sample that failed at 1 second. The arrow indicates an oxide filled pore at the surface. The exposed surface is developing a clear oxide layer in patches.

origin of failure of a sample loaded to 200 MPa. The initiating defect is a surface-connected pore that has been filled with oxide.

6. Discussion

The Kawecki Berylco Industries RBSN material tested in this study was sampled from a relatively large plate. Despite the thickness, a density of 2.58 g/cm^3 was achieved. A gradient in structure existed, however. Polished sections of the microstructure indicated a wide distribution of pore size and shape. Large pores, sometimes associated with silicon, were strength-limiting at room temperature and elevated temperature. Average room temperature strength was 206 MPa, a value higher than the 145 MPa reported in References 67 and 69. However, in Reference 69, the material was of much lower density: 2.4 g/cm^3. Despite these factors, the strength scatter was quite small as evidenced by the low standard deviation and high Weibull modulus. Evidently, although the overall pore distribution is large, the high end (strength-controlling) of the distribution is narrow.

Little or no strength degradation occurs at temperatures lower than 1300 C under static thermal conditions. This is unlike the Norton NC 350 grade which tended to improve in strength with exposure. These observations on the KBI material are similar to those reported in References 67 and 69 (which reported high temperature flexural MOR results). In the case of NC 350, fractographic evidence herein indicates that surface oxide formation is effective in sealing over or filling the strength-controlling defects which were machining marks and porosity. The strength-controlling defects for the KBI material were pores that were larger than those in the NC 350 grade. Thus the KBI pores are harder to seal or fill, and therefore are not as amenable to the healing effect of the oxidizing environment.

A tendency of the KBI RBSN to fail in the 1000 C to 1100 C range as well as the high temperature range of 1300 C to 1400 C was noted. Failures for both regimes were from surface or surface-connected porosities although the mechanisms of failure may be different. Regarding the lower temperature failures, it is reported that the oxidation mass gain on some grades of RBSN can be far greater at 1000 C to 1100 C than at higher temperatures.[17,18,72] This effect is likely due to the failure to develop a protective oxide layer, thus permitting oxidation into the interior via continuous porosity.[17,18,73-75] Oxidation attack may act to enlargen the surface-connected pores leading to static fatigue failure. Whereas negligible creep deformation was noted for the RBSN samples during the 1000 C and 1100 C exposures, noticeable permanent curvature was observed on samples that were exposed to the higher temperatures. (Creep deformation was such that the maximum tensile strain was of the order of 0.1 to 0.2 percent.) The high temperature failures may be related to this macroscopically observed creep. Creep along oxide grain boundary layers may act to enlargen the surface-connected pores. Grain boundary sliding has been observed in RBSN in the 1300 C to 1450 C range[73,74,76] (and at lower temperatures from earlier 2.3 g/cm^3 grade material[77]).

On the other hand, recent work suggests the creep and oxidation phenomena are interrelated. lated.[73,74] It is possible that the low temperature failures are related to the formation of oxide grain boundary (throughout the interior) which results in creep deformation at the low temperatures. The creep rate in the bulk material may not be significant enough to cause overall sample deformation, but in a microscopic region near a surface-connected pore, locally

72. DAVIDGE, R. *Mechanical Properties of Reaction-Bonded Silicon Nitride* in Nitrogen Ceramics, F. Riley, ed., Proceedings of NATO Advanced Study Institute on Nitrogen Ceramics, Canterbury, United Kingdom, August 1976.
73. GRATHWOHL, G., and THUMMLER, F. *Creep of Reaction-Bonded Silicon Nitride.* J. Mat. Sci., v. 13, 1978, p. 1177.
74. GRATHWOHL, G., and THUMMLER, F. *Creep of Reaction-Bonded Silicon Nitride* in Ceramics for High Performance Applications II, J. J. Burke, E. M. Lenoe, and R. N. Katz, ed., Brook Hill Publishing Company, Chestnut Hill, Massachusetts, 1978, p. 573-592.
75. WARBURTON, J., ANTILL, J., and HAWES, R. *Oxidation of Thin Sheet Reaction-Sintered Silicon Nitride.* J. Am. Cer. Soc., v. 61, no. 1, 1978, p. 67.
76. DIN, S. U., and NICHOLSON, P. S. *Creep Deformation of Reaction-Sintered Silicon Nitride.* J. Am. Cer. Soc., v. 58, no. 11-12, 1975, p. 500.
77. MANGELS, J. *Development of a Creep-Resistant Reaction-Sintered Si_3N_4* in Ceramics for High Performance Applications, J. J. Burke, A. E. Gorum, and R. N. Katz, ed., Brook Hill Publishing Company, Chestnut Hill, Massachusetts, 1974, p. 195-206.

higher creep rates (possibly due to a higher impurity concentration) could cause pore enlargement.

In the more thermally aggressive combined cycle procedure, a strength degradation of 19 percent was noted for the KBI RBSN. The similarity of Weibull moduli both for exposed and virgin samples as well as the fractographic evidence indicate pore enlargement as the mechanism of degradation. The degradation is very similar to the 17 percent observed in this study for the Norton NC 350 grade material.

Some red blotching, usually in bands, was apparent in samples exposed to temperatures in the 1000 C range (STSR, stress rupture at 1000 C, and combined cycle exposed). This effect was not related to any origin of failure, however.

F. Ford 2.7 Reaction-Bonded Silicon Nitride

1. Control Strengths

Sixteen control fractures were obtained at room temperature. Average strength was 288 MPa with a 38 MPa standard deviation. The Weibull two-parameter plot indicated a bimodal strength distribution (Figure 83). A least-squares line through the 13 highest points yields a Weibull modulus of 14.1 (but only 7.3 when fitted through all 16 points.

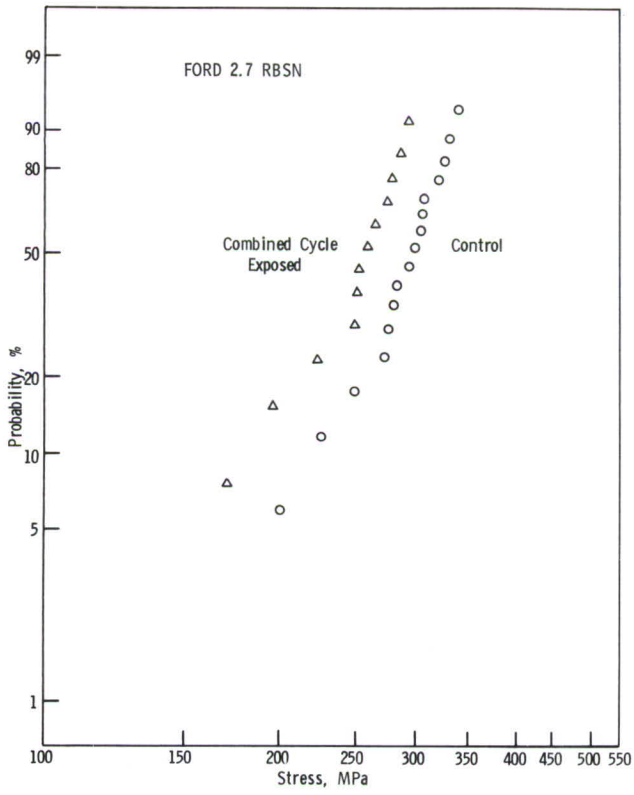

Figure 83. Room temperature control strengths of Ford 2.7 RBSN samples.

Failure initiation sites were often readily indicated by mirrors as shown in Figure 84. Unfortunately, the strength-controlling defects of the three lowest strength samples were not identifiable. Two of these failed from corner sites and one of them might have failed from a corner machining chip. The higher strength samples failed from pores or defects associated with pores (Figure 85). Often the defects appeared like white inclusions when viewed with the light microscope. When examined by SEM, however, these zones were revealed

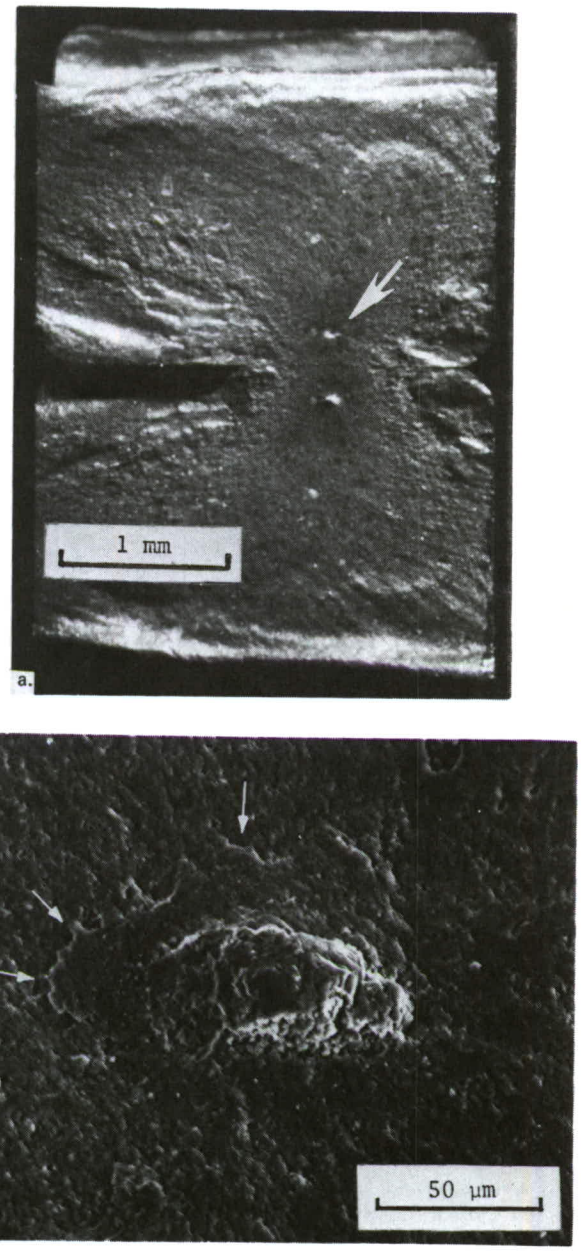

Figure 84. (a) Matching fracture halves for a control sample that broke at 273 MPa; (b) SEM close-up of the strength-controlling defect. The defect appears to be a porous region with inclusions or free silicon. The shapes of some of the features (arrows) suggest a melting effect.

to be porous regions (Figure 86). Several samples had features that appeared to be inclusions but may be silicon pockets associated with porosity (Figure 84b).

2. Stress Rupture, 1200 C

Of twelve tests, three samples failed on loading, five survived intact, and four failed in a time-dependent manner (Figure 87). No cut-off stress can be specified as there is some overlap. No major strength degradation compared to the room temperature values is evident. Three time-dependent failures occurred from surface-connected defects: two from white-appearing pores (Figure 88) and one from a corner pit-pore. The fourth, 0.028 hour at 228 MPa, shattered into many pieces on failure. All but the failure-on-loading samples had oxide layers that sealed over most porosity (Figure 88). The oxide was identified by X-ray diffraction as alpha cristobalite.

The survivors had very little permanent deformation. The retained strengths and sources of failure are identified in Table 6. The 241 MPa survivor did not fail during the stress rupture trial despite a large (longitudinal) crack which ran the length of the sample. On subsequent retained strength testing, the initiation site was at the intersection of the crack with the tensile surface. The failure initiation site for the 207 MPa sample is shown in Figure 89. The consistency of the retained strengths is remarkable.

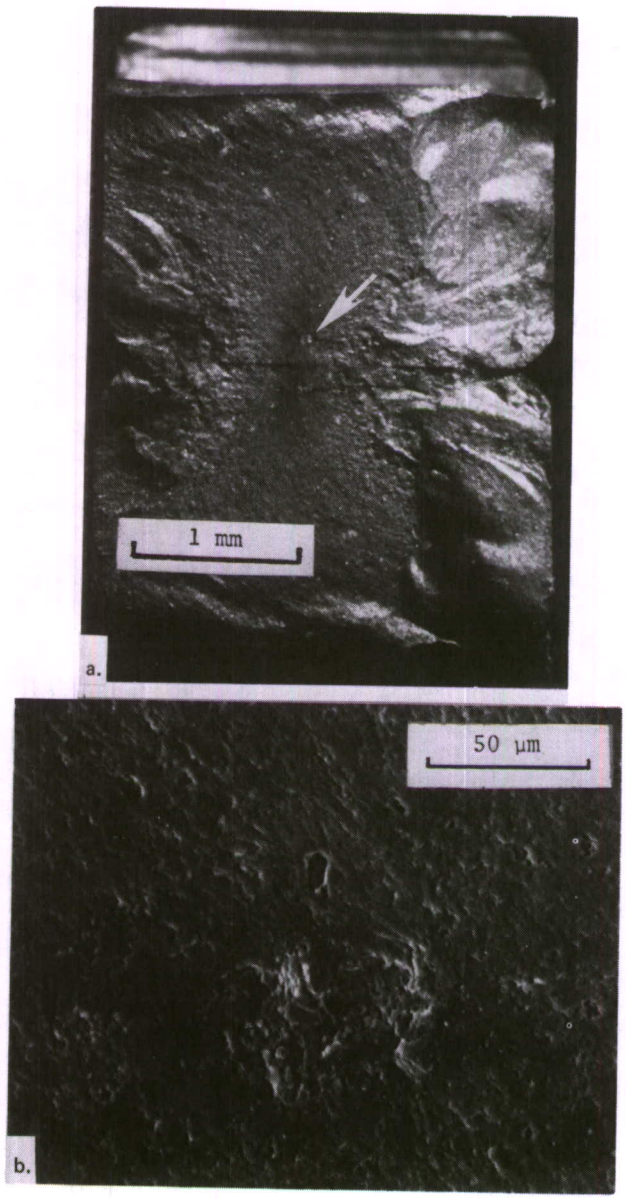

Figure 85. (a) Matching fracture halves of a Ford 2.7 RBSN sample which failed at 307 MPa. The defect is well below the tensile edge; (b) SEM close-up of the defect in (a).

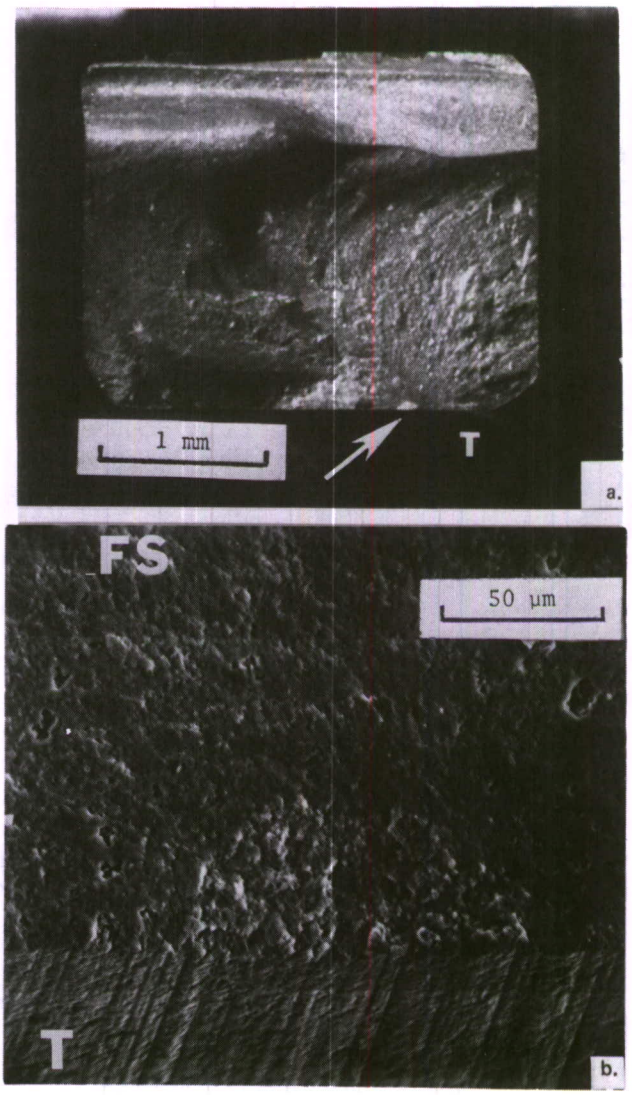

Figure 86. (a) Light photo of a Ford control sample fracture surface. Stress at failure was 321 MPa. Defect is at the tensile edge and is marked by the arrow; (b) SEM close-up of the defect in (a) shows the fault is a porous zone.

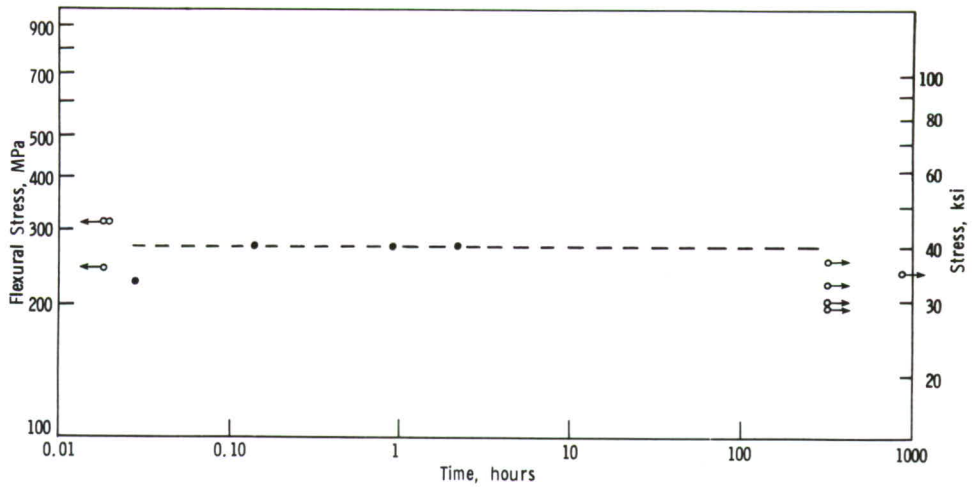

Figure 87. Stress rupture at 1200 C for Ford 2.7 reaction-bonded silicon nitride.

Figure 88. SEM close-up of the defect that caused a Ford 2.7 RBSN sample to fail at 0.9 hour at 1200 C. The defect is a surface-connected porous zone. A smooth oxide layer seals the surface.

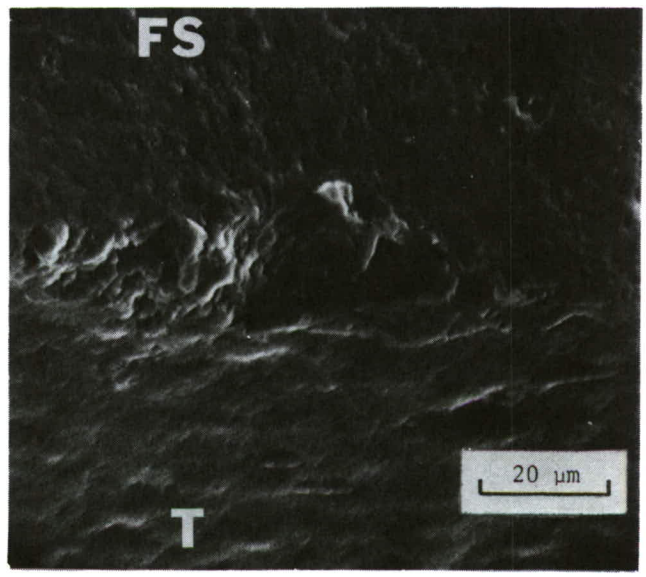

Figure 89. Strength-controlling defect for a stress rupture survivor. This SEM close-up shows the defect is a surface pore/pit. Retained strength at room temperature was 336 MPa.

Table 6. FORD 2.7 RBSN 1200 C STRESS RUPTURE SURVIVOR DATA

Stress Rupture Loading (MPa)	Survival Time (hour)	Maximum Tensile Strain (%)	Room Temperature Retained Strength (MPa)	Room Temperature Failure Source
200	308	-	342	Surface pore/pit
207	308	-	336	Surface pore/pit (Figure 89)
228	307	-	337	?
241	847	0.15	343	Crack
255	300	0.12	340	Subsurface Inclusion (silicon?)

The average is 340 MPa with a standard deviation of 3 MPa. This average is well above the room temperature control strength (288 MPa).

3. STSR

STSR trials indicated the Ford 2.7 RBSN was susceptible to time-dependent failure at 1000 C to 1100 C (Figure 90), which is common with the KBI RBSN and to a lesser extent the NC 350 RBSN. However, unlike those two samples, no Ford sample failed in the 1300 C to 1400 C range. Some reduction in load-carrying capacity compared to control strengths is evident.

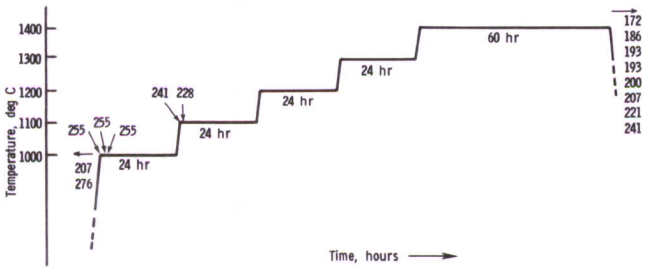

Figure 90. STSR results for Ford 2.7 reaction-bonded silicon nitride.

Eight samples survived, with seven intact (the eighth, loaded to 241 MPa, failed during furnace cooldown). A slight curvature, of the order of 0.1 to 0.2 percent, was detected in all. Retained strengths (in order of lowest to highest applied stress) were 254, 276, 240, 279, 284, 287, and 248 MPa. These average 267 MPa (with a standard deviation of 19 MPa), which is somewhat less than the 288 MPa control strength. At least six of these samples failed from surface-connected pores that were partially or completely oxide filled. The oxide layer was smooth and glossy in appearance and was identified by X-ray diffraction to be alpha cristobalite.

Time-dependent failures were initiated from surface or near-surface defects. Four failed from white-colored porous zones that were difficult to observe with SEM (Figures 91 and 92). These white zones are similar to those observed at room temperature. The specific mechanism that involved these porous regions and that results in failure could not be identified. The fifth sample, after 16 minutes at 1100 C, failed from a subsurface porous zone which had a dark black zone (light microscopy) near it (Figure 93). When viewed with SEM, the dark zone is less evident, but close examination shows it probably is a melted silicon zone. A coherent oxide layer formed in patches on the sample.

4. Combined Cycle Procedure

The average retained strength of twelve combined cycle samples was 246 MPa and the standard deviation was 25.1 MPa. The average is 15 percent less than the control value (288 MPa). The Weibull plot (Figure 83) shows a striking similarity to the control distribution. The bend in the control data seems to be translated to the exposed samples. The uniform shift of strength values suggests that the combined cycle procedure acted to enlarge the flaws that were strength-controlling at room temperature.

Fractography identified all of the strength-controlling defects. All but one were surface or surface-connected flaws. Five failures occurred from surface pits (or enlarged pores) located at the corner of the sample. The greatest erosion-corrosion occurred at the corners and led to a significant rounding of the corners (Figures 94 and 95). Six other samples failed from porosity that appeared as a white patch when viewed with the binocular microscope (Figure 96). These pits were sometimes sealed over by oxide and the oxide at least partially filled the pore. The lowest strength sample was one of the six samples which

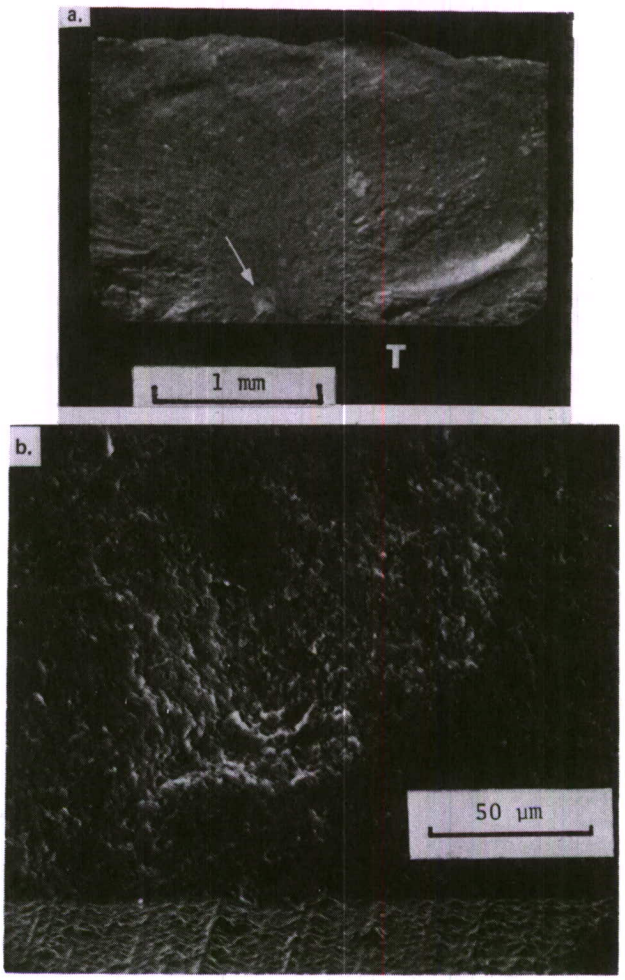

Figure 91. Fracture surface of a Ford 2.7 RBSN STSR sample that failed at 8.5 seconds at 1000 C: (a) is a light photo of the surface showing a white spot at the initiation site. Other such spots were often observed scattered throughout the surfaces; (b) SEM close-up of the strength-controlling defect shows it is a porous region.

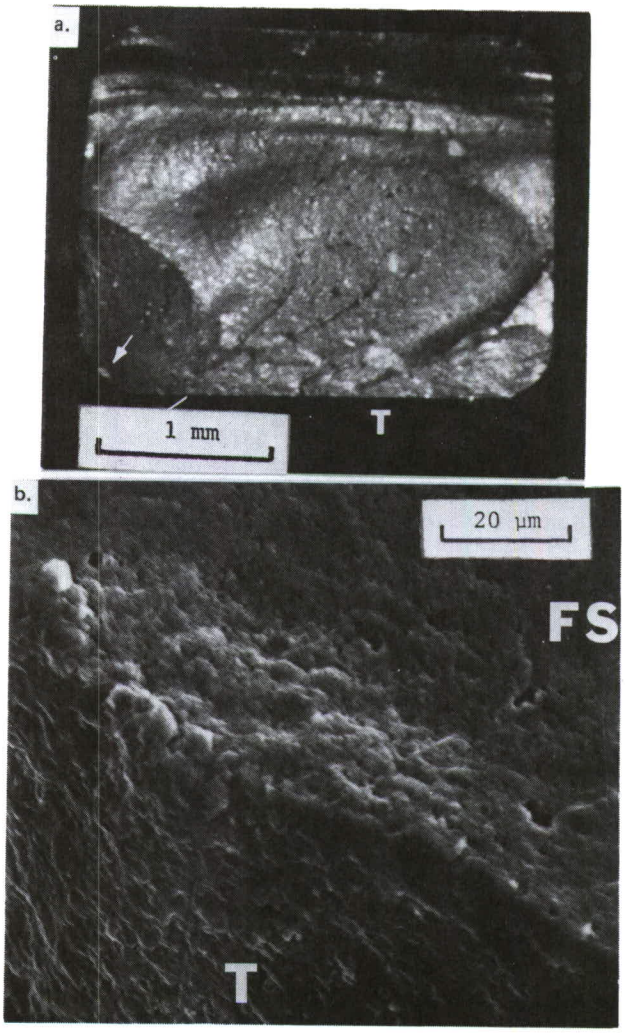

Figure 92. Fracture surface of a Ford 2.7 RBSN sample which failed at 1.8 hours at 1000 C. The macrophoto (a) pinpoints the strength-controlling defect at the corner (arrow). The SEM close-up of the flaw is shown in (b) where the sample has a strong tilt.

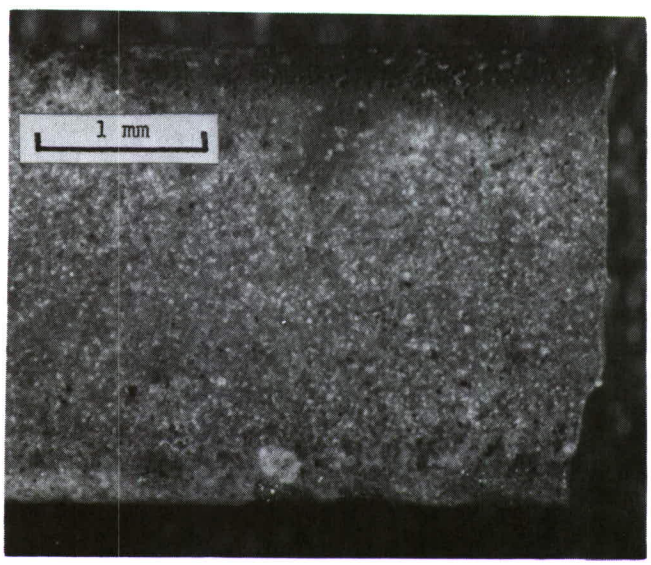

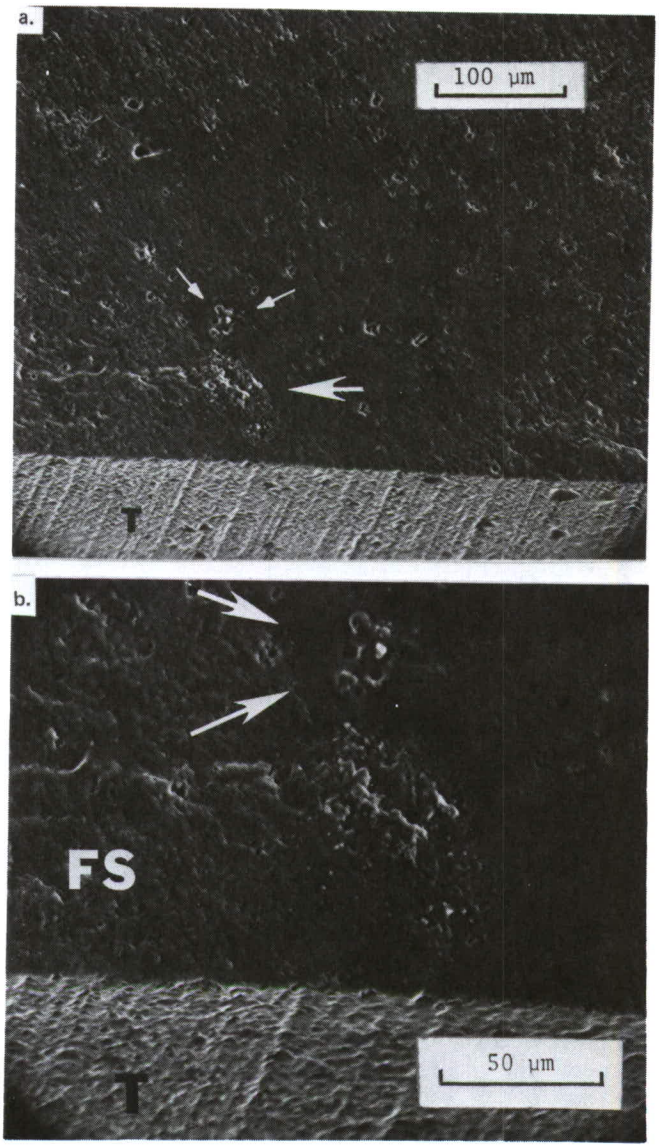

Figure 93. Fracture surface of a Ford 2.7 RBSN STSR sample that failed at 0.27 hour at 1100 C: (a) is a low power SEM view showing the fracture mirror. The large arrow marks the probably strength-controlling defect while the small arrows indicate a feature that appeared black when viewed with a light microscope; (b) is a close-up showing the faults more clearly.

Figure 94. Light photo of the exposed surface of a combined cycle sample of Ford 2.7 RBSN.

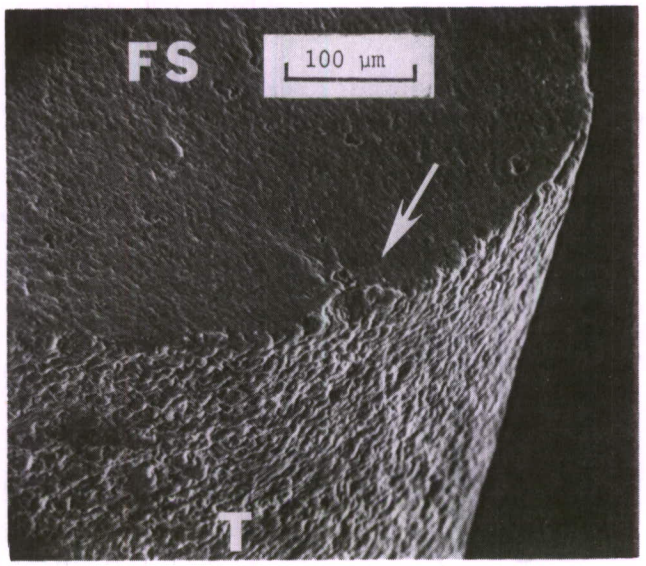

Figure 95. SEM photo of the fracture surface of a Ford 2.7 RBSN combined cycle sample showing the strength-controlling defect is located at the corner. Retained strength was 223 MPa. The sample has been given a tilt to show the damaged surface oxide.

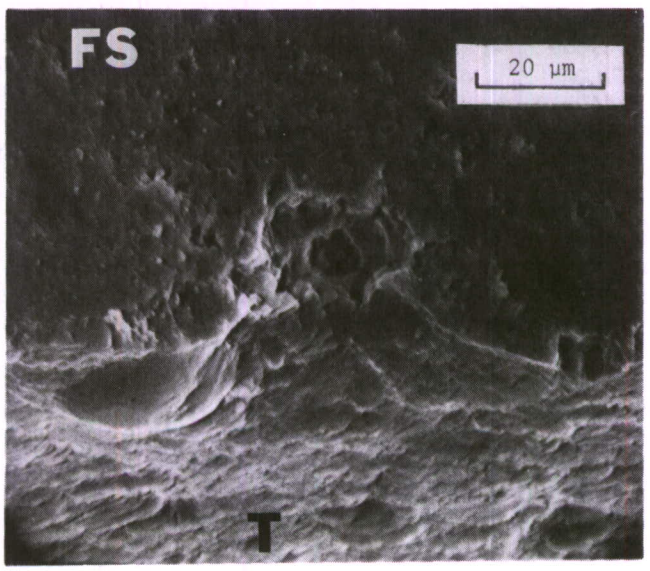

Figure 96. Ford 2.7 RBSN combined cycle sample that had a retained strength of 278 MPa. This SEM photo shows the strength-controlling defect is a surface-connected pore that has reacted with surface oxide.

failed from a surface-connected (white colored) pore that was away from the corner. The next to lowest strength sample failed from a large subsurface pore (Figure 97).

The flaws in the three lowest strength samples are no different than those in the other samples except that they may be larger. Thus the kink in the Weibull plot is not caused by a shift in the nature of the defect (such as from a machining defect as opposed to a pore). It is probably the result of a minor or undetected change in some processing variable. Since the original slabs (from which samples were machined) were not all made simultaneously this explanation is plausible. Alternately, the variation may be due to a spatial variation in sintering furnace temperature or some injection molding parameter.

Away from the flame-impinged zone, the oxide layer was smooth, coherent, and glossy in appearance. At the impinged zone, significant attack occurred resulting in an irregular and damaged oxide layer. The corners were well rounded and more pores (pits) were evident. At the corners the oxide layer was gone, exposing matrix material to the attack. During the first heating cycle an average mass loss of 7 milligrams (out of 0.843 gram) was experienced (possibly due to wax burnoff). Thereafter, a slight mass gain was evident after each static heating or thermal cycling sequence. A net mass gain of 2.5 milligrams was recorded not counting the initial mass loss.

5. Discussion

Although the Ford 2.7 RBSN has a higher density (2.77) than the Norton NC 350 RBSN (2.53), it has a nearly identical strength and standard deviation. This again points out the desirability of maintaining a uniform porosity distribution

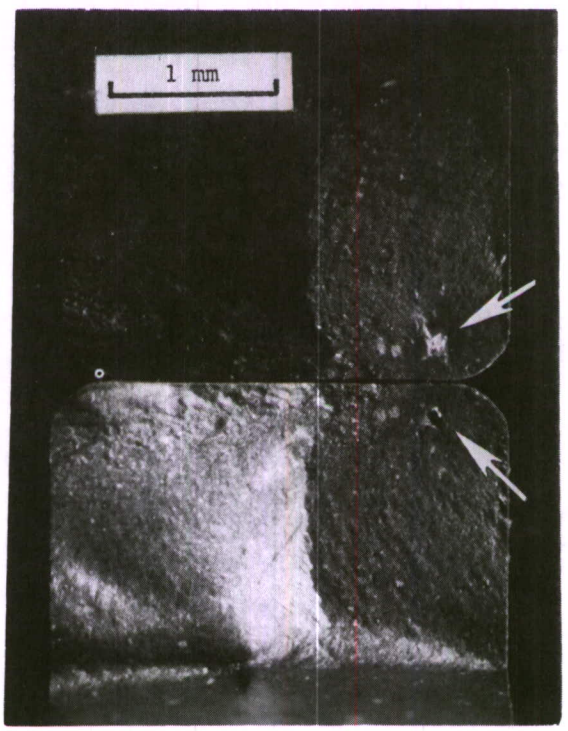

Figure 97. The only Ford 2.7 combined cycle sample with a subsurface defect that controlled the retained strength. Fracture stress was 195 MPa.

rather than simply a higher density. The strength-controlling defects in the Ford 2.7 RBSN are large pores that can assume a variety of sizes and shapes. The kink in the Weibull plot is not due to a change in flaw character, but probably is the result of batch-to-batch variations. Samples were cut from a number of separate small pieces, unlike the NC 350 and KBI materials tested in this program (which were cut from a single billet each). Similar strength-controlling defects are shown in Figure 14 of Reference 21 where poor control of the injection molding process was blamed.

Stress rupture trials showed static fatique failure can occur at 1200 C although the STSR results do not so indicate. Four-point flexural stress rupture trials conducted on the same material are reported in Reference 19. No time-dependent failures were attained in tests at 1038 C, 1149 C, and 1204 C, but the stresses employed (138 to 207 MPa) were substantially lower than those which caused failure in this study. Failures at 1200 C most often occurred for samples loaded to 276 MPa. Based upon Figure 90, similarly loaded samples in the STSR trials would likely fail immediately or in the 1000 C to 1100 C range. Thus the lower temperature failures in the STSR trials may *mask* the 1200 C failure tendency. The material may have less load-carrying capacity at 1000 C to 1100 C than at 1200 C. No failures were sustained at higher temperatures despite eight STSR trials. It may also be true that the same STSR masking effect applies to the higher temperatures as well.

Retained strengths after 1200 C stress rupture trials were remarkably consistent and well above control values. The surface oxide formation tended to seal over and partially fill the surface-connected pores which were strength-controlling. Alternately, the retained strengths of the STSR survivors were less consistent and showed no improvement relative to control values. This occurred despite the oxide surface layer which again sealed and filled surface pores.

These results contrast with data reported in Reference 18. In the latter case, samples exposed to 1260 C in a static oxidizing environment experienced an average 22 percent MOR loss. No MOR change was reported for samples similarly exposed but at 1037 C. The data in Reference 18 was for as-fired surfaces whereas this study used machined surfaces.

The combined cycle procedure caused a 15 percent strength reduction. Surface-connected porosity was modified or enlarged by the process. Portions of the sample away from the flame-impinged zone had a smooth, glossy oxide formation. At the impinged zone, considerable erosion and damage to the oxide layer (particularly at the corners) occurred, exposing the matrix material.

Insufficient samples were available to conduct 1000 C stress rupture testing.

G. Norton NC 203 Hot-Pressed Silicon Carbide

1. Control Strengths

Two control groups of room temperature flexural samples were broken for hot-pressed silicon carbide, corresponding to the two billets from which samples were machined. The control group which acted as a reference for the stress rupture trials (Lot A) numbered 24 fractures while the reference group for the combined cycle procedure (Lot B) was 10 breaks. The average stress measured was significantly different for the two groups: 582 MPa (Lot A) compared to 683 MPa (Lot B), although the standard deviations were similar, 62 and 65. Such a variation is consistent with billet-to-billet variations reported elsewhere.[58] The Weibull moduli (least-squares fitted lines) are almost alike: 10.1 (Figure 98) versus 9.9 (Figure 99), suggesting a similar distribution of flaws in each case. If, on the other hand, the data is combined and plotted similarly, the slope becomes 8.8 and the least-squares line is a poor fit to the tails of the distribution. Therefore it is concluded that there is a basic difference in the two sample lots in either the billets or in the machining damage which occurred during preparation.

Fractography of the broken samples was difficult due to extensive fragmentation. Often a mirror emanating from the tensile edge was evident, yet no distinct flaw could be detected at the mirror center. In one case, however, a semi-elliptical flaw associated with a longitudinal machine mark on the tensile edge was identified at the mirror center (such as reported in Reference 46). The flaw measured approximately 20 microns deep by 80 microns in width (Figure 100). The maximum stress intensity for the shape of this flaw exists at the deepest portion of the flaw using a geometry factor from Reference 48:

$$K_{Ic} = 1.55\ \sigma_a \sqrt{c}$$
$$= (1.55)\ (649\ MN/m^2)\ (20 \times 10^{-6}\ m)^{\frac{1}{2}}$$
$$= 4.5\ MN/m^{1.5}$$

This value is in good agreement with values reported in References 34 and 78. Therefore, the semi-elliptical flaw of Figure 100 is a plausible strength-controlling defect. Since it is located at the center of the mirror, we conclude it is the controlling defect. The striation itself probably did not cause the subsurface defect, but

78. EVANS, A. G., and LANGE, F. F. *Crack Propagation and Fracture in SiC.* J. Mat. Sci., v. 10, 1975, p. 1659.

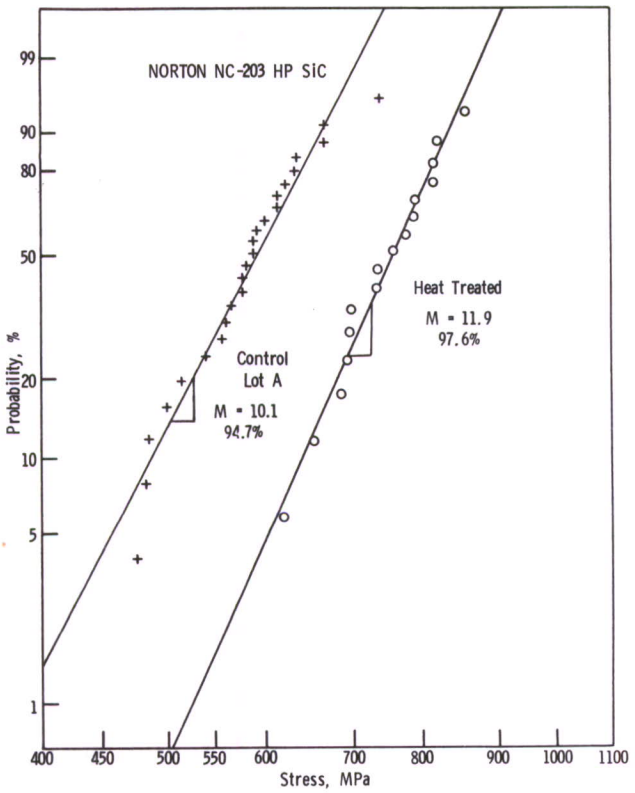

Figure 98. Room temperature control strengths for the NC 203 HP SiC stress rupture testing (Lot A). Also shown is the strength data of heat-treated samples as described in the text.

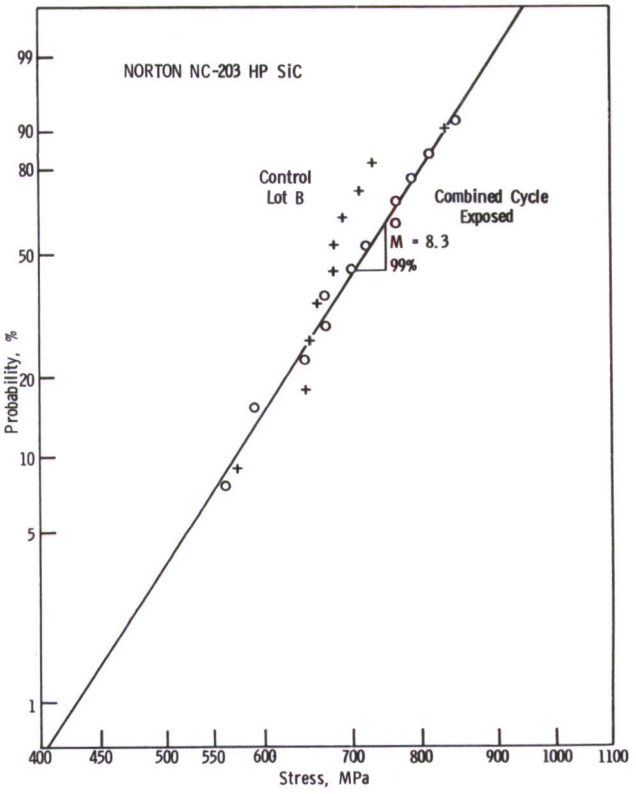

Figure 99. Room temperature control strengths for the NC 203 combined cycle trials (Lot B). The crosses are the control strength and can be described by a least-squares line of slope 9.9 with a poor 87% correlation coefficient (not shown). Also shown (circles) are the strengths of samples after exposure to the combined cycle procedure.

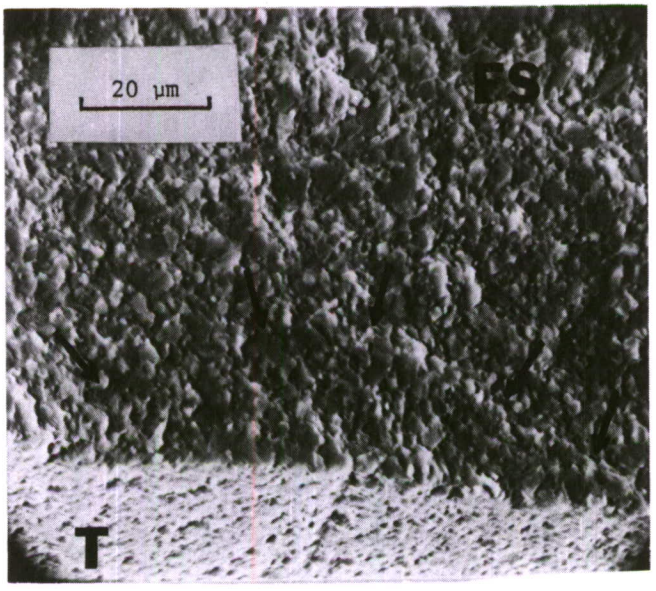

Figure 100. SEM close-up of the fracture surface of an NC 203 control fracture. Failure stress was 649 MPa. The black arrows delineate a difficult-to-discern semi-elliptical fault centered on a deep machining striation. The specimen has been tilted back slightly to show the longitudinal striation on the tensile face.

both are manifestations of the same machining step. Even if the surfaces were subsequently lapped and the striation removed, the subsurface defect would still remain. It is probable that this effect has happened with many of the samples prepared in this and other studies. Coarse initial machining can introduce such damage and subsequent final machining can remove many of the striations and other surface markings. Thus although a surface may look satisfactory (mirror finish), subsurface machining damage may be present! Similar defects are reported in the NCX 34 results section.

2. Stress Rupture, 1200 C

Seventeen trials were conducted for hot-pressed silicon carbide and the results are shown in Figure 101. Two samples failed on loading, four survived several hundred hours, and the remainder failed at times from 0.037 to 244 hours. Considerable overlap occurs; samples loaded to 435 MPa either failed on loading, survived intact, or failed in a time-dependent manner. These stresses are considerably lower than the average room temperature strength of 582 MPa. The survivor samples exhibited no discernible permanent deformation. The survivors were loaded at 455 and 370 MPa for 300 hours and also 370 and 300 MPa for 500 hours. Their retained strengths were 979, 942, 887, and 903 MPa, respectively, all well above any value achieved for the control samples. X-ray diffraction of the surface revealed cristobalite as well as the SiC and WC originally present. Low power and SEM inspection of the surface revealed a thin coherent layer of cristobalite with a few, very rare, pits. The pits are shallow and blunt and do not appear to significantly penetrate the matrix. In none of the samples was a fracture observed emanating from such a pit.

The fracture surfaces of the samples which failed in a time-dependent manner were less jagged or irregular in appearance than the control group. Fracture surface markings were intergranular. Mirrors were not as distinct, but the area of fracture initiation was generally evident. No features were evident that can identify the mechanism of time-dependent failure. No zones of slow crack growth were observed, even for the sample which failed after 244 hours. The fracture surface of this sample is shown in Figure 102 and is typical of the group. A number of the failures (including the latter) were not initiated at the corners. Inclusions and subsurface machining damage may be involved, but the size of these observed features seemed less than what is expected from a K_{Ic} formulation. It was observed in some samples that a deep machining striation oxidized differently (irregular - broken oxide layer) than the overall surface and these striations were quite distinct in appearance. One sample which failed after 4 hours had such a machine mark associated with the origin of failure.

3. STSR

Seventeen STSR trials were conducted (Figure 103). Fourteen failed in a time-dependent manner over all temperatures tested with no sensitivity to one temperature. A single sample survived intact and had no discernible permanent deformation. The surface was covered with a glassy glaze that was again identified as cristobalite. The retained strength of the sample was 743 MPa, a value greater than any from the control lot. Two of the time-dependent failures (448 MPa at 1200 C and 386 MPa at 1300 C) were associated with unusually deep machining striations (Figure 104). Distinct mirrors were evident

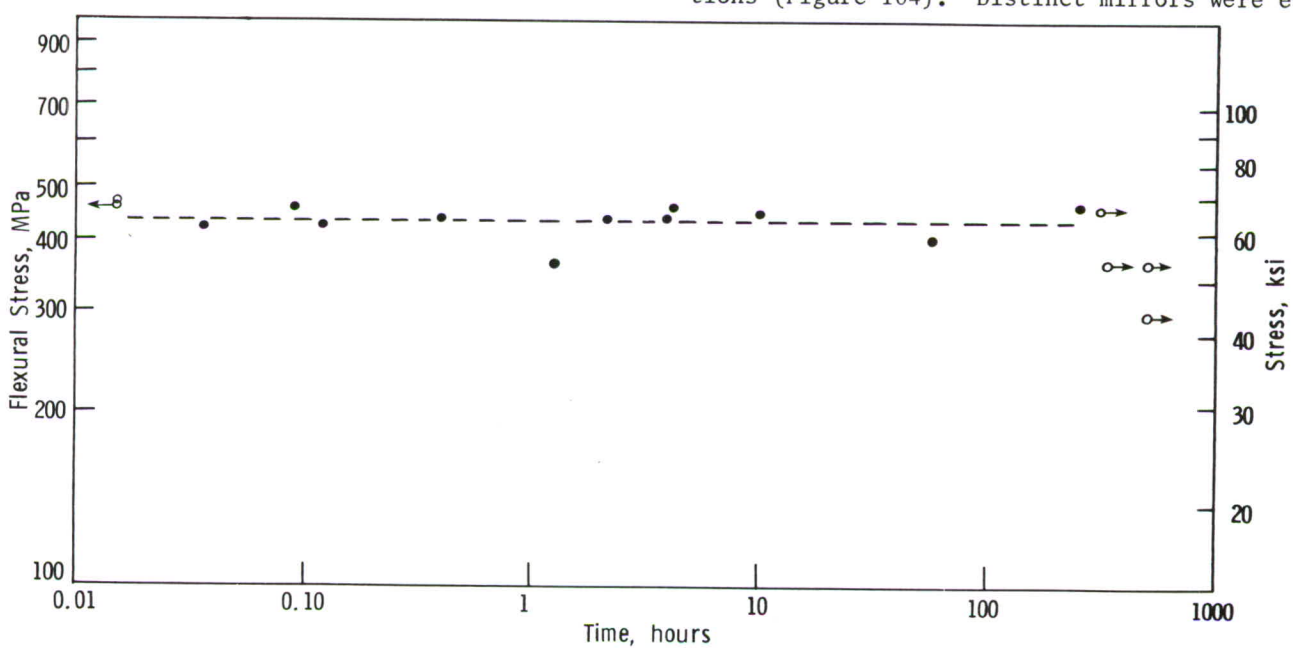

Figure 101. Flexural stress rupture at 1200 C for Norton NC 203 HP SiC.

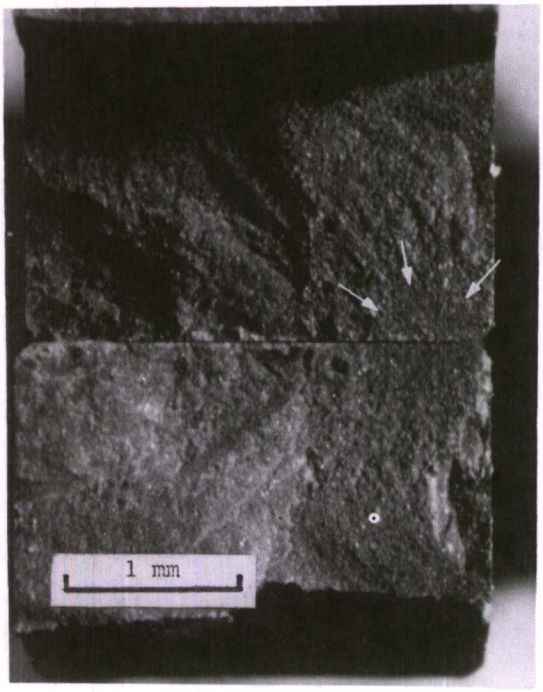

a. Light photo of the two fracture halves. The arrows mark the mirror.

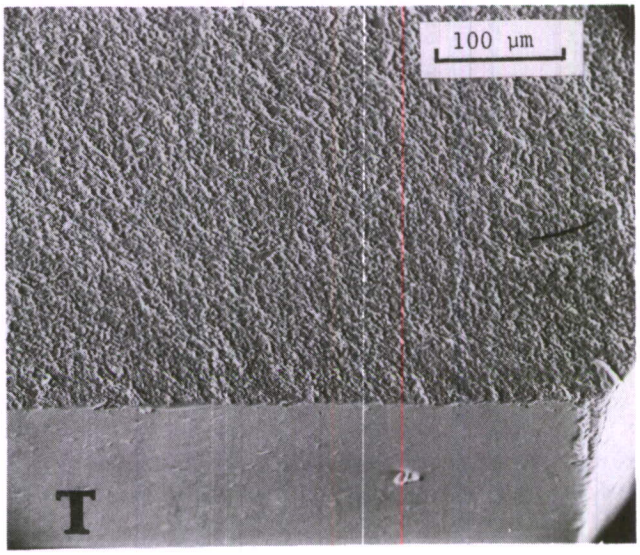

b. SEM close-up of the mirror. No defect of suitable size is evident.

Figure 102. Fracture surface of an NC 203 SiC sample which failed at 1200 C while bearing a load of 462 MPa.

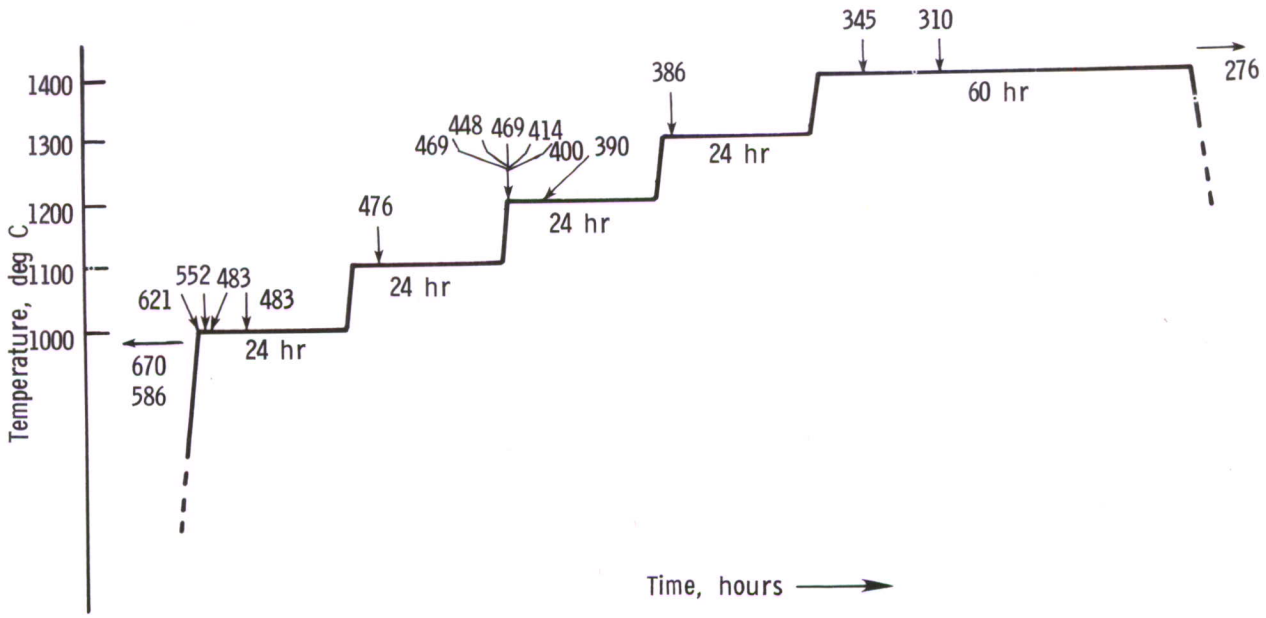

Figure 103. STSR results for Norton NC 203 HP SiC.

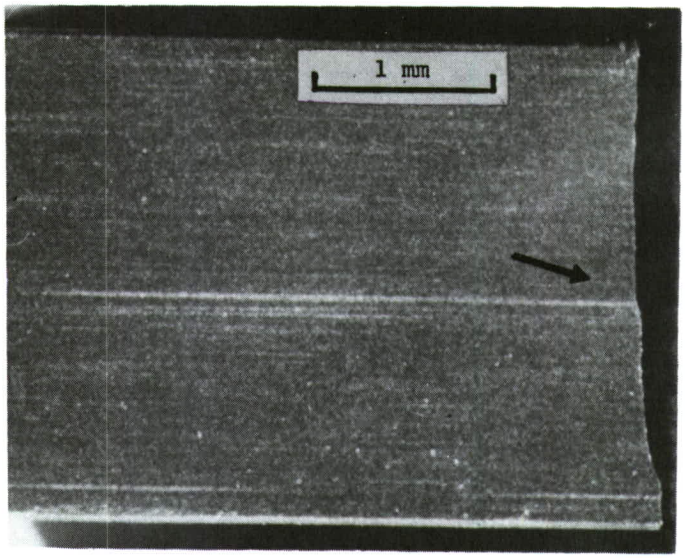

a. Light photograph of the tensile face shows the distinctly different oxidation along the deep machining striations. The arrow points to the fracture surface.

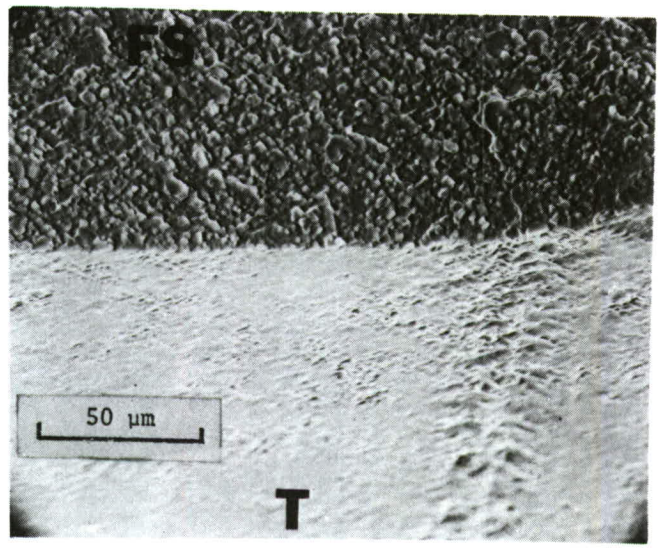

b. SEM close-up of the fracture surface (FS). The sample has been tilted back to show the machining striations along the tensile face (T).

Figure 104. NC 203 STSR sample which was loaded to 386 MPa and failed at 1.8 hours at 1300 C.

(away from the corners) on many other fracture surfaces but closer inspection with SEM failed to find similar machine marks nor identify an alternate mechanism. No prominent zones of slow crack growth were observed. Fractures were entirely intergranular. Pitting was observed but was rare and not associated with the fracture surfaces.

4. Combined Cycle Procedure

The twelve combined cycle samples of NC 203 all oxidized with a clear glossy layer except in a zone which was subjected to the thermal fatigue treatment. At that point the surface was quite dull in appearance. A weight gain of 0.0013 gram out of 0.9694 gram was recorded on the average on the first heat treatment with significantly less gain thereafter. After each of the five thermal fatigue executions of 100 cycles a minor weight loss (0.0001 gram) was observed, reflecting the localized erosion or damage of the flame attack-thermal shocking.

The retained flexural strength of the samples averaged 706 MPa (standard deviation of 84.5 MPa) which is slightly *higher* than the reference group (683 MPa). The Weibull plot yielded an excellent fit (99% coefficient of determination) to a least-squares line of slope 8.3 (Figure 99). The samples did not always break in the middle of the zone that received the severest thermal fatigue damage, but often offset to one side (still within the inner pins of the flexural fixtures, however). Low power optical microscopy revealed semicircular fracture mirrors for nine of the samples, usually away from the corners of the sample. Of four samples inspected with SEM, only one positive flaw identification was made. A surface pit (Figure 105) was positively identified as the cause of failure of the weakest sample. An SEM energy dispersive analysis was not successful in identifying a concentration of impurity or second phase at the pit. Two other samples probably failed from much smaller pits or pores observed within the fracture mirror.

5. Discussion

Norton NC 203 hot-pressed silicon carbide NC 203 has the highest room temperature flexural strength of the silicon carbides tested. A variation in strengths between two sample lots reflects either a billet-to-billet variation or the effect of machining. The material does exhibit time-dependent failure at temperatures from 1000 C to 1400 C, but does not have unusual temperature sensitivity to any temperature. The mechanism(s) of time-dependent failure was difficult to assess. Slow crack growth has been observed in this material at high temperatures,[34,46,78,79] but does not manifest itself on the fracture surface as clearly as in hot-pressed silicon nitride at similar temperatures. Rice et al.[46] report the onset of such prominent slow crack growth markings only at temperatures of 1650 C and above. If failure occurred in an ideally brittle manner from semicircular

79. McHENRY, K. D., and TRESSLER, R. E. *Subcritical Crack Growth in Silicon Carbide.* J. Mat. Sci., v. 12, 1977, p. 1272.

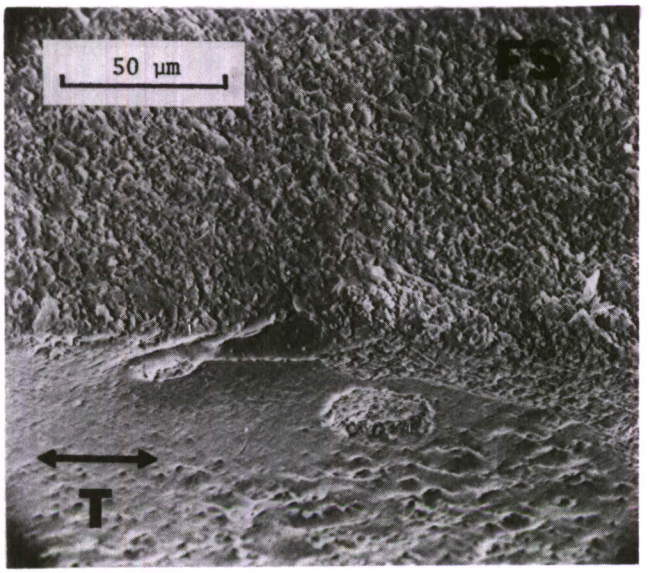

Figure 105. SEM close-up of the fracture surface of an NC 203 combined cycle sample. Retained strength at room temperature was 560 MPa. The lower portion of the photo (arrow) shows the interrupted oxide layer on the tensile face (T). The strength-controlling flaw is the pit which is partially filled with surface oxide.

flaws at the tension face at an applied stress of 460 MPa, and K_{Ic} is assumed to be in the range 4.0 $MN/m^{1.5}$ (Reference 78) to 5.0 $MN/m^{1.5}$ (Reference 34) at 1200 C, then the fracture surfaces of the stress rupture samples at 1200 C should reveal faults that grew to 41 to 64 microns in depth. A feature of such size should be readily detected, but was not apparent with SEM inspection.

The short-term failures (of the order of 0.01 hour or less) are qualitatively similar to results showing a decrease in flexural strength from room temperature to 1200 C.[78] The limit stress for survival of 300 hours at 1200 C for the bend bars in this study is between 400 and 450 MPa, a level considerably less than the average room temperature flexural strength. The shallow slope of the stress-time to failure data suggests a high exponent in the crack velocity-stress intensity power relation. The scatter in data precludes any estimate and is presumably due to variations in initial flaw size or property variations in the original billet.

Weight gain data, X-ray diffraction analysis and microscopic inspection indicate a coherent layer of cristobalite forms on the samples. The layer retards further oxidation and may help heal machining damage. Similar observations were made in Reference 10. The survivors of stress rupture testing had strengths considerably greater than the control lot. To test the hypothesis that oxidation of the surface may improve flexural strength, a group of twelve samples were given a heat treatment of 1200 C for 305 hours in the same style static environment test furnace. The strength of the samples relative to their control values (samples were from the stress rupture lot) is shown in Figure 98. A significant improvement is apparent with the average flexural strength 742 MPa with a standard deviation of 65 MPa compared to the control values of 582 MPa and 62 MPa, respectively. The Weibull modulus is improved as well with a 97 percent correlation to a line of slope 11.9. Fractography revealed that most samples again failed from corners, possibly from machining marks. At least four failures were not due to corners but were initiated along the tensile edge or subsurface.

The retention of high strength despite the combined cycle thermal exposure treatment again suggests the oxide layer is protective. Oxide erosion and spalling was observed in the flame-exposed zone, but it may be that too few cycles were applied to cause damage to the matrix (bulk material). In a parallel program conducted by this laboratory* similar samples were exposed to thermal fatigue cycling *only*, with the results indicated in Figure 106. Little or no strength loss was observed until *greater than* 100 cycles had been applied. In the combined thermal exposure treatment reported here, only 100 cycles were applied prior to static furnace heat treating. With 10,000 consecutive cycles, strength had been reduced to 345 MPa with little scatter. Failure in the high cycled samples was clearly attributed to pits associated with a corrosion-erosion process that severely degraded the specimen surface.* The combined cycle samples in this program accumulated 500 cycles overall, but did not experience the strength loss that samples exposed to 500 consecutive cycles suffered. This suggests the interim oxidation heat treatments were restorative in effect. Thus the evidence shows that although a static heat treatment in a furnace may be beneficial, a prolonged aggressive flame-gas exposure-thermal cycling procedure is detrimental.

H. Carborundum 1977 Alpha Silicon Carbide

1. Control Strengths

The flexural strengths of the control group of alpha silicon carbide samples averaged 375 MPa with a standard deviation of 52 MPa. When plotted on a Weibull graph, the data reveals a pronounced slope change indicative of a multimodal flaw distribution (Figure 107). Fractography was directed at identifying the flaws causing the bimodal effect, but no firm conclusion could be made. Origins of failure could be identified by a poorly defined mirror. Very large pores were often the causes of failure (Figure 108), but did not

*G. Quinn, unpublished research.

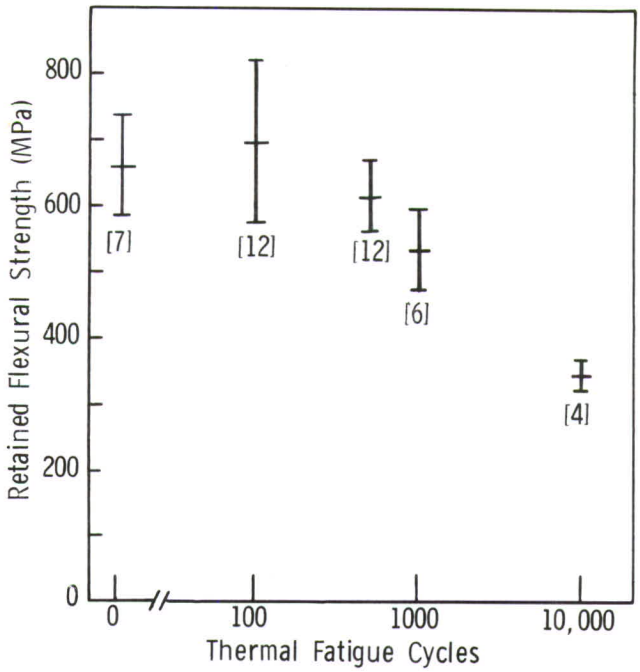

Figure 106. Effect of thermal fatigue cycling on NC 203 bend samples. Retained strength as a function of the number of applied cycles is shown. The number in parenthesis is the total number of samples tested at each condition. Error bars are one standard deviation.

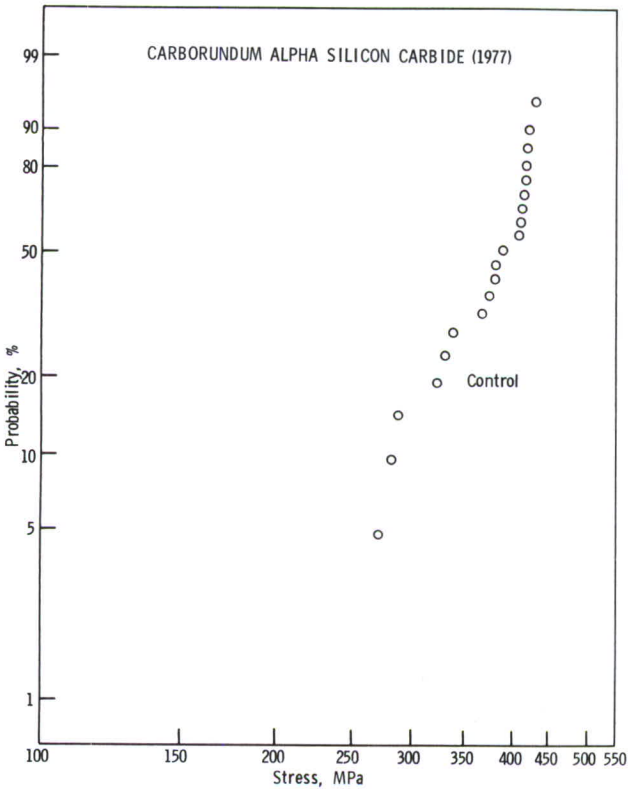

Figure 107. Room temperature flexural strengths of Carborundum 1977 alpha silicon carbide.

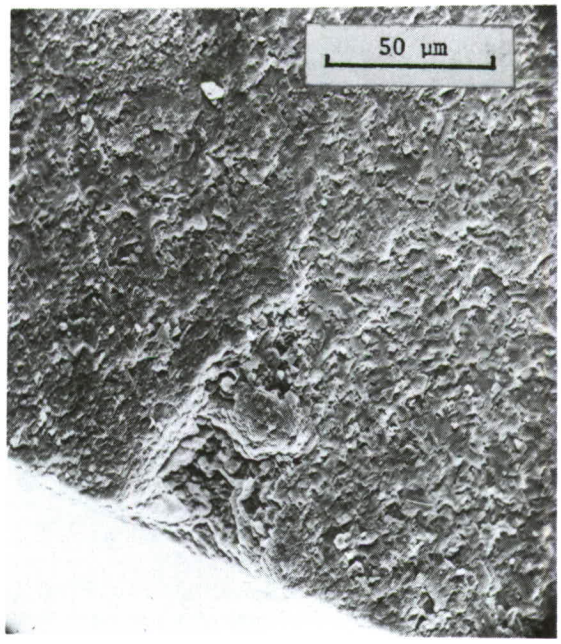

Figure 108. Fracture surface of a Carborundum 1977 alpha silicon carbide control sample. The large pore was strength controlling. Flexural strength was 411 MPa.

exclusively account for the lower strengths. Some samples had inclusions, unreacted material, or large grains which collectively may have acted as a flaw (Figure 109). An SEM energy-dispersive analysis on one such inclusion detected only silicon. A few of the high strength samples fractured from corner origins, but no specific flaw could be detected. Similar observations regarding the room temperature flexural strength of this material have been reported in References 23 and 32.

2. Stress Rupture, 1200 C

Eleven stress rupture tests at 1200 C were conducted on the 1977 alpha silicon carbide (Figure 110). Five samples failed in a time-dependent manner. A stress of 300 MPa is critical for this material under the test conditions applied. Somewhat above that value, failures are instantaneous; somewhat below, samples survive hundreds of hours. This stress is below the room temperature flexural strength of 375 MPa obtained from the control group.

Fractography was not conclusive in identifying the failure mechanism. Minor pitting was observed in rare patches of about a dozen pits in some of the samples. The pits were shallow and were not as severe as those that have been observed in hot-pressed silicon nitride tested under similar conditions, and could not be correlated with any of the failures. For two of the samples that failed, large pores acted as the initiating sites. When examined by SEM one such sample, which survived

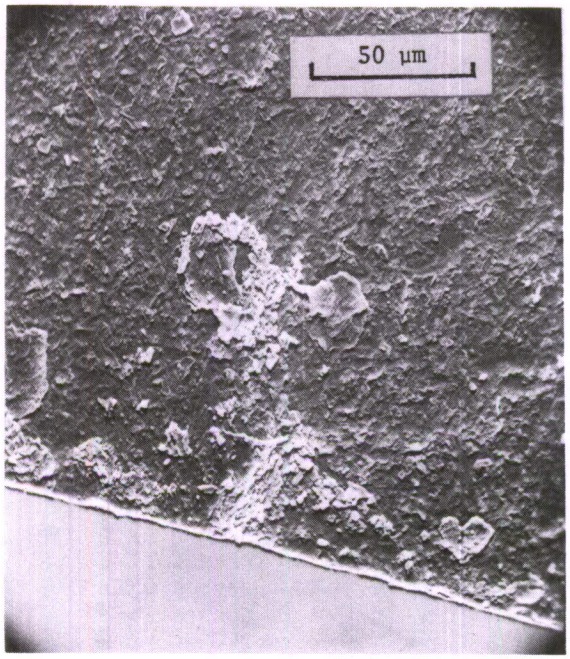

Figure 109. Fracture surface of a Carborundum 1977 control sample showing the strength-controlling defect. Flexural strength was 413 MPa.

for several hundred hours prior to failure, showed a small region of intergranular roughness extending from the pore toward the direction of maximum tensile stress (Figure 111). This may be a zone of slow crack growth or a zone of not fully reacted material. The pore is approximately 150 µm long and 175 µm below the surface.

The two surviving samples did not exhibit any significant permanent deformation. The retained strengths were 499 and 527 MPa, both of which are greater than any control group value. Light microscope observation of the fracture surface suggested a pore in one sample and a cluster of small pores in the other acted as the initiating flaws.

X-ray diffraction of the surface of the 276 MPa sample that survived 500 hours indicated significant alpha cristobalite and an unidentified phase of less prominence. The unidentified phase had peaks typical of a metal ion silicate compound, but no specific phase was found that could match the peaks in this case. The major unidentified peaks were at 3.21, 1.97, and 1.93 Å. An attempt to identify the surface elements via emission spectroscopy, relative to an untreated specimen, was unsuccessful.

3. STSR

Nine stepped temperature stress rupture trials were performed with stresses ranging from 207 to 414 MPa (Figure 112). Failures occurred over the 1100 C to 1400 C temperature range. The 207 MPa sample survived the entire pattern intact and had

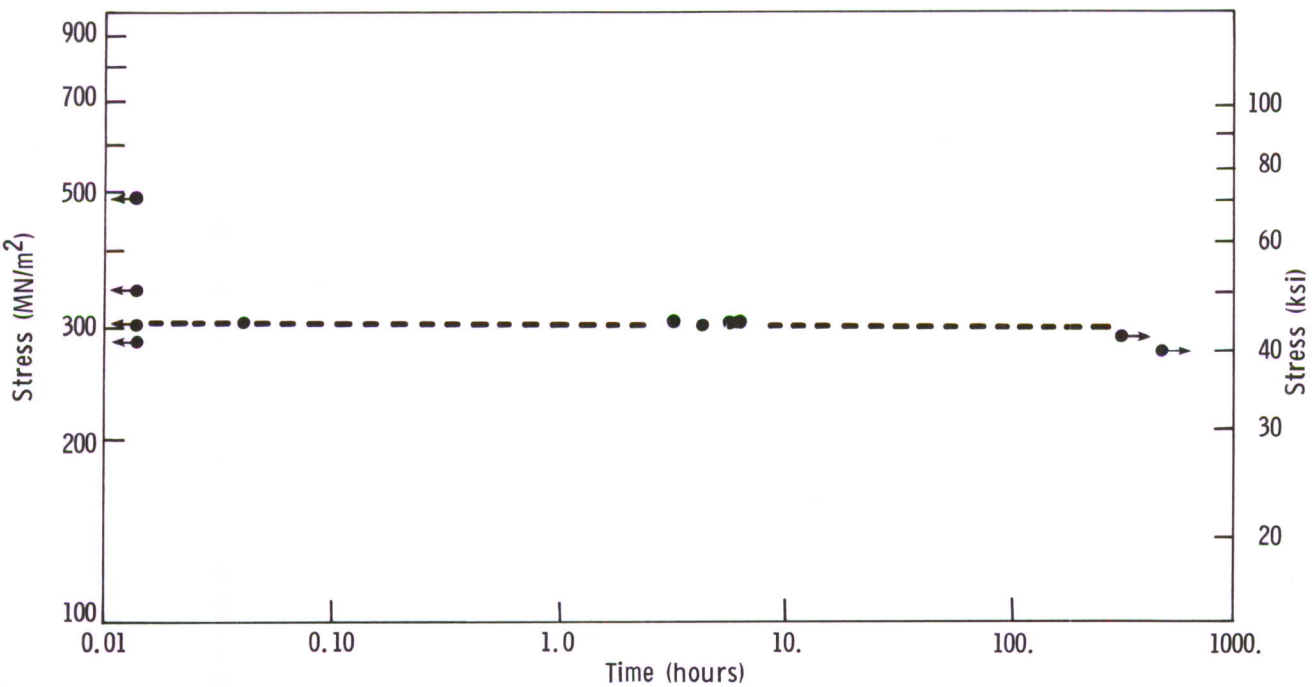

Figure 110. Flexural stress rupture at 1200 C for Carborundum 1977 SiC.

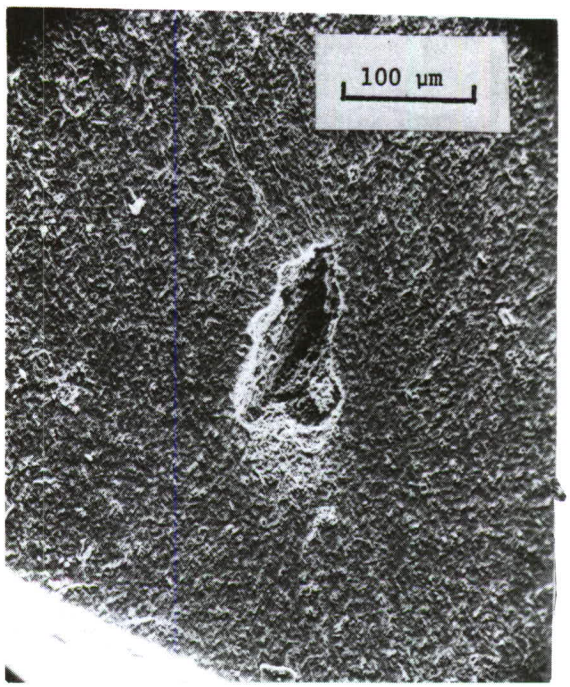

Figure 111. Fracture surface of a Carborundum 1977 SiC sample that broke at 3.25 hours at 1200 C when loaded to 303 MPa. The pore was the strength-controlling defect. A small zone of intergranular markings extends toward the tensile edge (corner of photo).

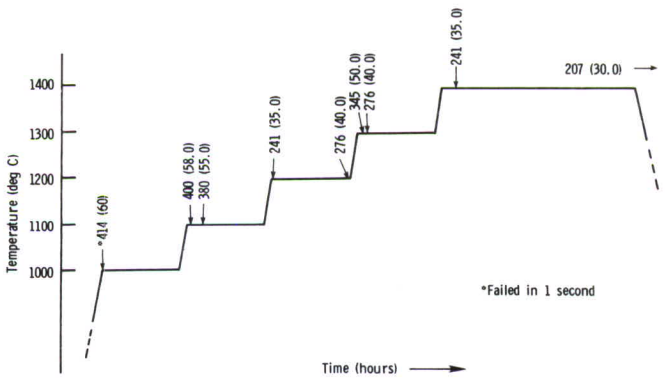

Figure 112. Stepped temperature stress rupture for Carborundum 1977 SiC.

negligible permanent deformation. Retained strength at room temperature was 469 MPa, a value well above any in the control group. In several cases a sample loaded to a higher stress survived longer than a lower stressed sample. This variation may be due to scatter in the initial flaw size distribution.

Fractography was successful in identifying many of the initiating flaws. The 414 MPa sample which failed one second after loading at 1000 C broke at a subsurface pore (one third the way from the tensile edge to the neutral axis). The 241 MPa sample which failed at 0.35 hour at 1200 C failed from a large processing crack that extended through the sample. (This was the only sample of this material with such a feature.) The 276 MPa sample which failed in the 1200 C step had a subsurface porous zone with some intergranular markings in the adjacent zone. It was unclear in this latter case whether any porosity reached the surface. The 241 MPa sample which failed at 4.6 hours at 1400 C failed from a defect (probably a surface-connected pore) that is surrounded by a semi-elliptical zone of intergranular slow crack growth (Figure 113a). Beyond the semi-ellipse, the markings are transgranular, indicating fast fracture (Figure 113b). This semi-elliptical SCG zone was large and visible to the naked eye. It appeared white whereas the remainder of the fracture surface appeared an iridescent red. This iridescent coloration was often observed on fracture surfaces and even the whole sample exterior if the surface was exposed to high temperature for a short time only. It is the result of a very thin oxide layer. The semi-elliptical SCG zone was exposed for a longer time and the thicker oxide layer was transparent. The intergranular zone is approximately 125 μm deep. The intergranular zones observed emanating from flaws in other samples discussed above imply slow crack growth may be operative at lower temperatures as well. In the former cases, flaws grew only a little larger prior to fast fracture, unlike the latter case at 1400 C where the markings are well developed.

The sample that survived intact fractured into three pieces on subsequent strength testing. It had a retained strength of 469 MPa which is well above the control strength. An inclusion was evident as a source on one fracture surface and a pore or pit at the surface on the other fracture face. X-ray diffraction of the sample surface again showed prominent alpha cristobalite and also a prominent unknown phase which is *different* from the unknown phase in the 1200 C stress rupture trials. The d spacings in this case were 3.76, 3.16, 2.16, 1.96, and 1.92 Å. Emission spectroscopy of the surface did indicate an excess of Ca at the surface.

4. Discussion

The 1977 vintage alpha silicon carbide by Carborundum Company is susceptible to static fatigue at temperatures from 1100 C to 1400 C. The critical stress level at 1200 C is 300 MPa, a value lower than the room temperature flexural strength (375 MPa). Samples that survive the stress rupture procedure had little or no permanent deformation and apparently have higher strengths as a result of the oxidation environment. The oxide layer that forms is very thin and coherent at the surface, and is composed of cristobalite and an unknown phase which may be a silicate with a combination of metal ions that has not been indexed. The phase that forms at 1200 C is different from the phase observed in samples exposed to 1400 C.

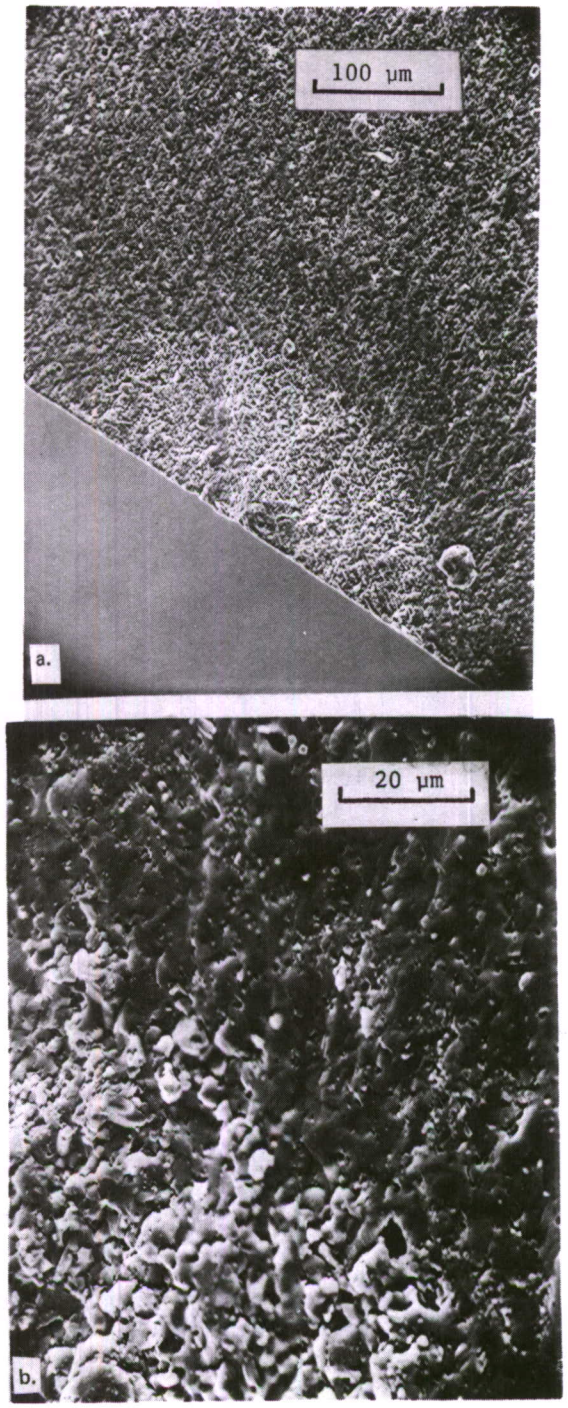

Figure 113. (a) Fracture surface of a Carborundum 1977 SiC STSR sample. An elliptical slow crack growth zone is evident; (b) SEM close-up of the boundary of the elliptical zone. Crack growth inside the zone is intergranular; outside the zone (the half with the size marker) the crack traveled transgranularly.

Fractures originated from several type flaws, but primarily from pores which occasionally were very large. Time-dependent failures were usually associated with the porosity (most often when the pores intersected the surface), but in at least two cases samples failed in a time-dependent manner from subsurface pores. Evidence of slow crack growth was prominent in one sample which failed at 1400 C and less evident in two other samples which failed at lower temperatures.

I. Carborundum 1978 Alpha Silicon Carbide

1. Control Strengths

Thirty-six control fractures were obtained from 26 samples tested at room temperature. (Several of the samples broke such that a second test was possible on the longest fragment.) Average flexural strength was 363 MPa with a standard deviation of 45 MPa. When plotted on the Weibull graph, the data appears unimodal with the exception of one low strength value (Figure 114). A least-squares fitted line to the 35 highest points gives a line of slope 10.6 with a correlation coefficient of 96 percent.

Although the Weibull plot suggests an unimodal distribution of flaws, fractography was successful in identifying two flaw populations

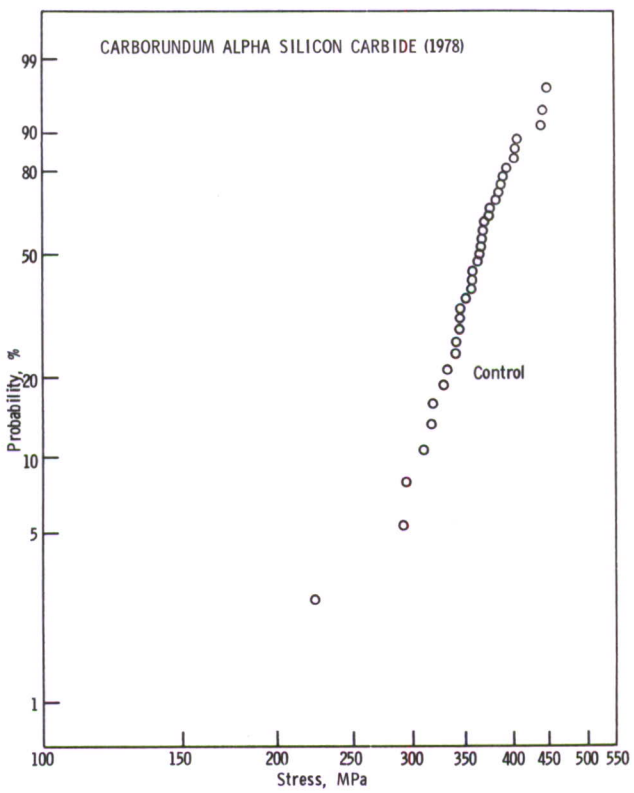

Figure 114. Room temperature flexural strengths of Carborundum 1978 alpha silicon carbide.

that caused failure: large pores and large silicon carbide grains. Fracture origins were located by observing where sample halves joined (reconstruction after fracture), ridge lines, and the somewhat smoother circular zone surrounding the initiation site. This mirror zone was vague in definition.

The large pores are usually equiaxial in shape and aften quite spherical (Figures 115 and 116). Figure 116 shows a common pore morphology that has a spherical core inside and is probably

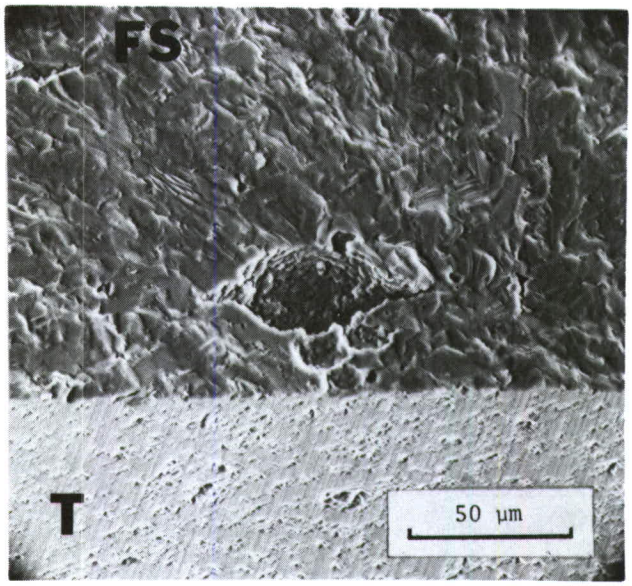

Figure 115. Fracture surface of a Carborundum 1978 SiC control sample that failed at 408 MPa.

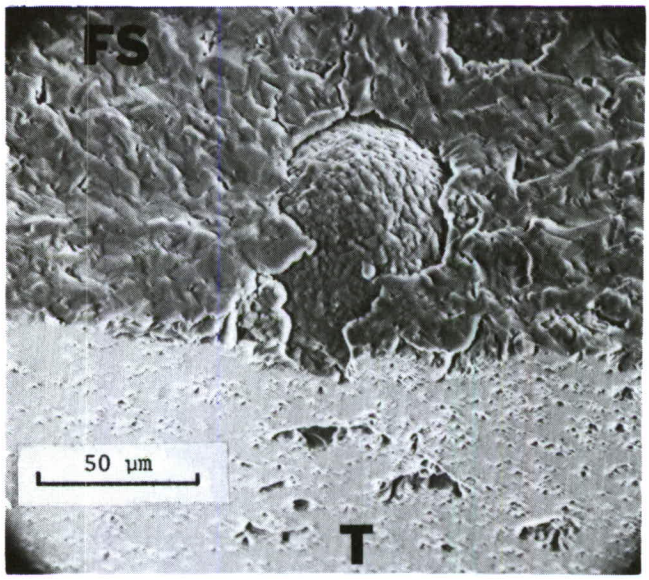

Figure 116. Fracture surface of a Carborundum 1978 control sample. Surface-connected porosity exists both at the strength-controlling defect and also below it along the tensile face of the sample.

the powder agglomeration feature observed in the polished section shown earlier (Figure 18). Although some of the pores were surface-connected, most seemed to be subsurface with a random bulk volume statistical placement.

Large grains, often needlelike or alternately penny-shaped on the fracture surface, also caused failure (Figure 117a to 117c). These grains were very reflective and easy to spot with the naked eye, indicating cleavage that was confirmed by SEM examination. The lowest strength sample (that appeared uncharacteristic of the group on the Weibull plot) failed from such a feature that had the worst possible orientation with respect to the maximum tensile stress (Figure 117c). Other samples had large grains of comparable dimensions, but in less severe orientations and sometimes in the compressive zone or near the neutral axis. If additional samples were tested, it is likely more of these "uncharacteristically" low strengths would be obtained. Thus this single low-strength sample cannot be ignored. It measured more that 300 µm deep and 850 µm across. River markings on the grain indicate fracture initiated at one end of the grain where it intersected the surface. A Laue back-reflected photograph was generated by a beam focused on the defect and indicated it was polycrystalline silicon carbide. An SEM energy dispersive analysis on the spot indicated silicon only and the intensity on a location outside of the zone was similar. The large grains were often associated with porosity and it could not be determined which acted as the initiating flaw (Figure 118). In some cases river markings in the large grain pointed back toward the pore, however. Of all the fractures, 14 occurred from porosity, 7 from large grains, and the remainder were not identifiable.

2. Stress Rupture, 1200 C

Unlike the earlier grade of alpha silicon carbide the 1978 grade does have a definite trend toward decrease in load-carrying capacity with time at 1200 C (Figure 119). Thirty-five tests were conducted; 22 specimens failed in a time-dependent manner (out to 720 hours), 11 on loading, 2 aborted, and none survived intact. A least-squares fitted line of slope -1/40.8 was a reasonable fit to all data points, particularly in the extremes.

Fracture surfaces had appearances similar to those of the room temperature fractures. None had prominent SCG markings. Of the 11 samples that failed on loading, 10 were from pores or pores with cores, and the other sample had its fracture surface contaminated when it landed on the furnace floor, precluding origin location. At least 18 of the time-dependent failures occurred from pores located at the surface or very near to it (Figure 120a to 120c). All the pores

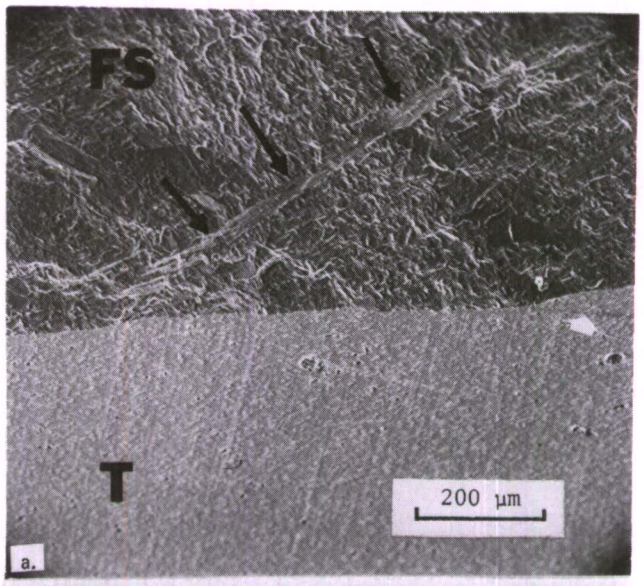

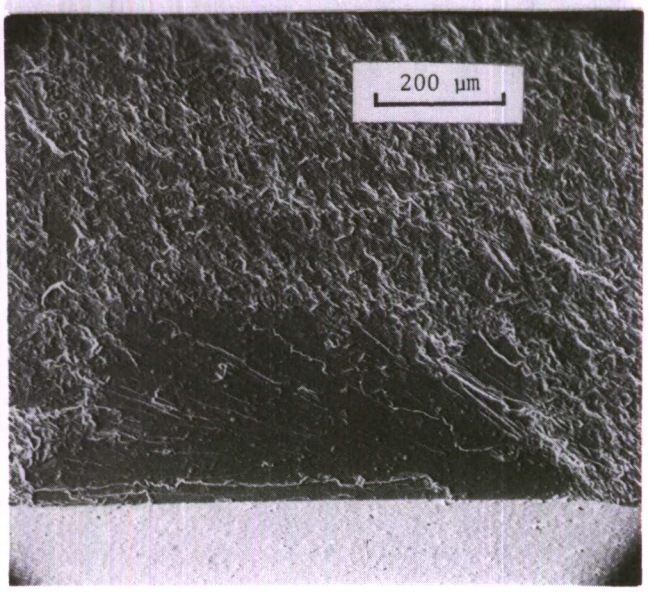

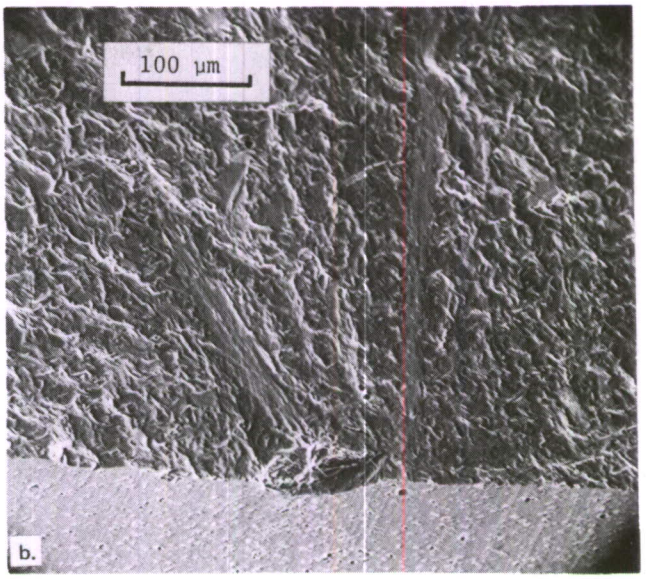

Figure 117. (a) Fracture surface of a Carborundum 1978 control sample that failed at 352 MPa. The long grain may have initiated failure (arrows). A secondary fracture crack is on the tensile face (small arrow); (b) fracture surface of a control sample that failed at 394 MPa. Either the large grain or the pore at the surface (or both) acted as the strength-controlling flaw; (c) fracture surface of a control sample that failed at the lowest strength observed: 224 MPa. The large SiC grain was the strength-controlling defect.

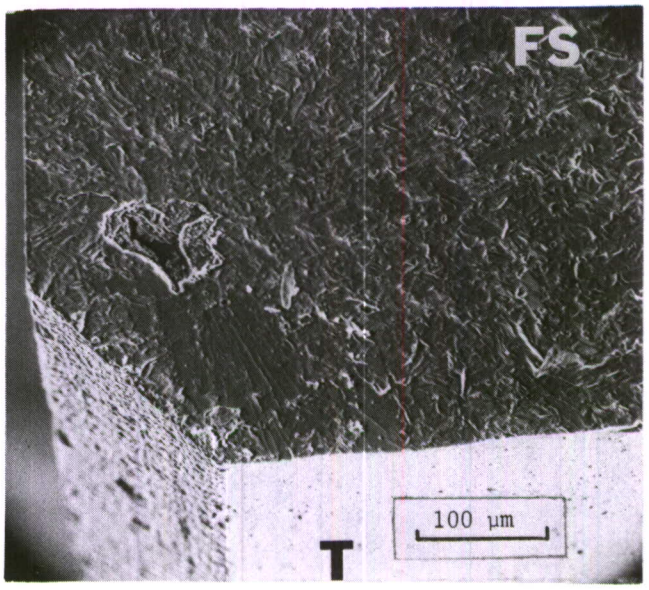

Figure 118. Fracture surface of a Carborundum 1978 control sample that broke at 449 MPa. Either the large grain or the pore acted as the strength-controlling flaw.

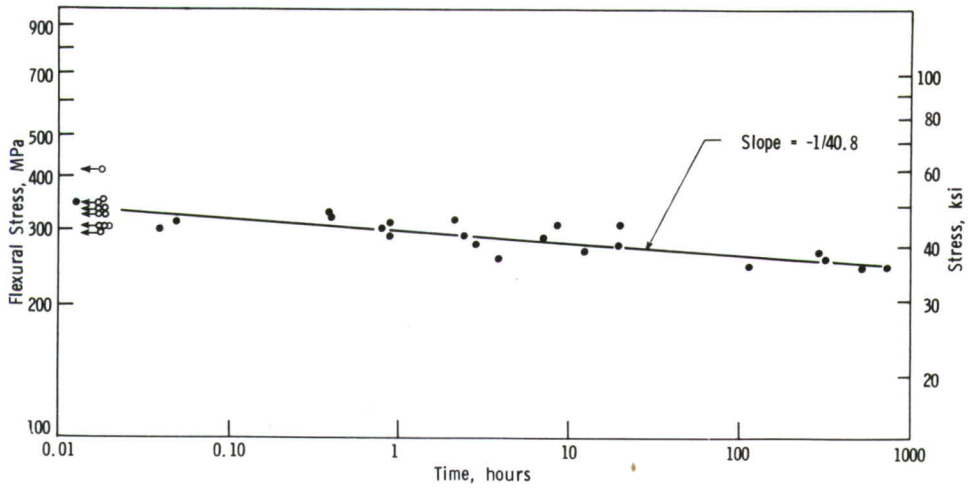

Figure 119. Flexural stress rupture at 1200 C for Carborundum 1978 alpha silicon carbide.

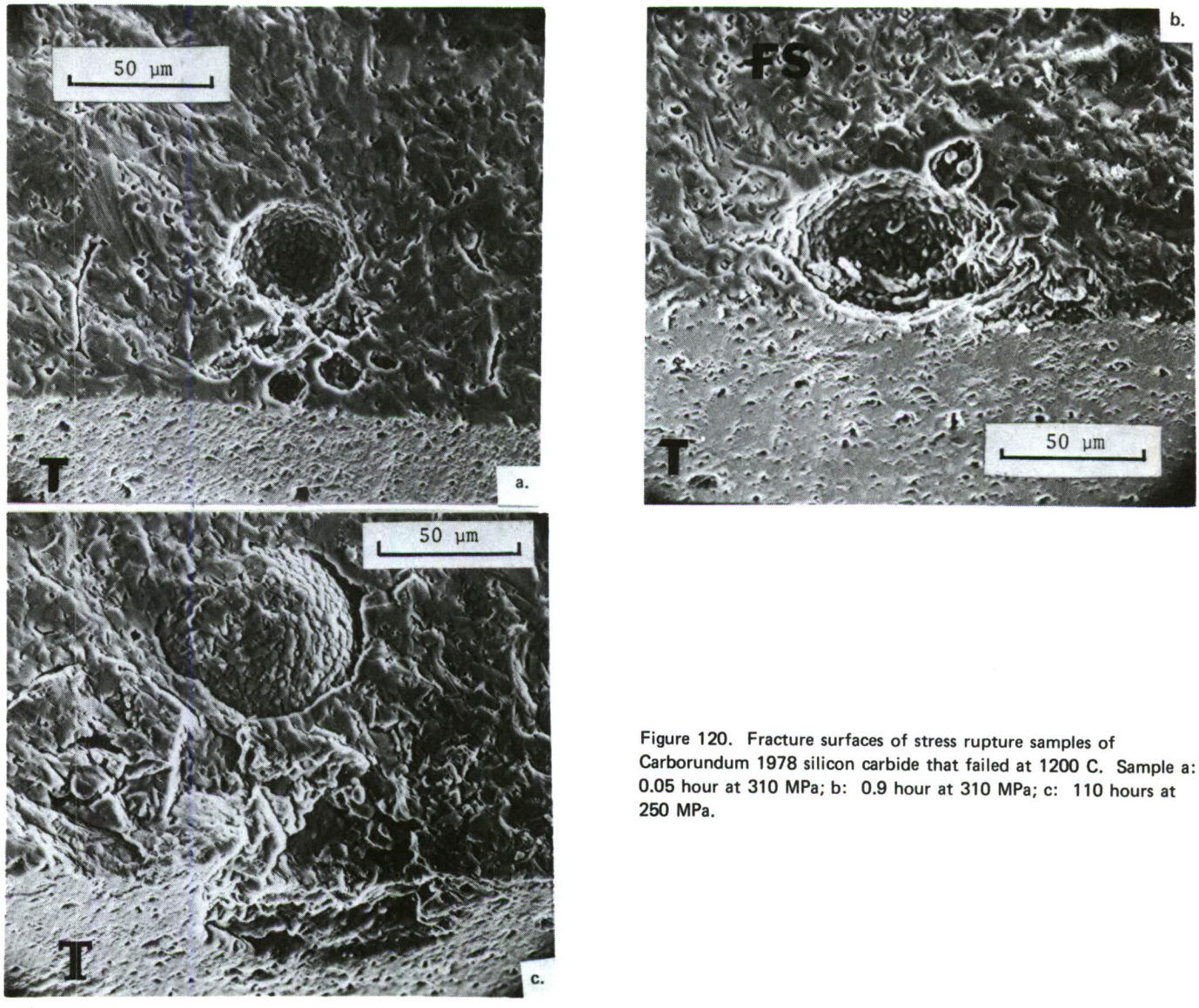

Figure 120. Fracture surfaces of stress rupture samples of Carborundum 1978 silicon carbide that failed at 1200 C. Sample a: 0.05 hour at 310 MPa; b: 0.9 hour at 310 MPa; c: 110 hours at 250 MPa.

beneath the surface were connected to the surface by other porosity. The pores showed no markings different from pores in the samples that failed at room temperature. Several other samples failed either from a pore at the surface or at an adjacent large grain (Figure 121).

The oxide that formed on the surface partially sealed many of the large pores and most of the small pores after a few hours. The oxide was identified by X-ray diffraction as alpha cristobalite. Samples exposed to short times at 1200 C tended to have an iridescent and colorful surface sheen. Often the fracture surfaces would have this sheen due to the short time the fresh surface was exposed (the furnace would lose all power when a sample failed).

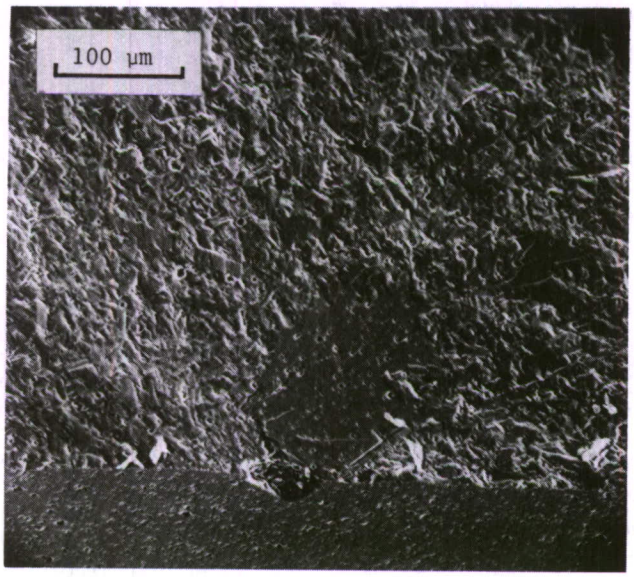

Figure 121. Failure site for a stress rupture sample of Carborundum 1978 SiC which failed at 7 hours at 1200 C. The defect is either the large grain or the adjacent pore.

3. STSR

STSR failures occurred over all temperature regimens for stresses ranging from 240 to 320 MPa (Figure 122). As with the earlier grade, considerable overlap was observed, but a general trend of longer lifetime with lower stress is apparent. As with the stress rupture and room temperature samples, the origin area could usually be located and the specific flaw often identified. The 1000 C and 1100 C failures were all from pores that were connected to the surface (Figure 123a and b). Higher temperature failures were from pores and sometimes pores associated with large SiC grains (Figures 124 and 125). SCG markings were prominent in one sample (250 MPa) which failed at 0.7 hour at 1400 C (Figure 126). Of the three samples that survived intact, one (280 MPa) failed during furnace cooldown. The other two (both loaded to 220 MPa) had very little permanent deformation (<0.1%) and both had retained strengths of 403 MPa. One failed from a surface pore; the other initiating flaw could not be positively identified. The oxide layer that formed is thin and coherent. It was identified on a survivor sample as alpha cristobalite only.

4. Discussion

Room temperature strength-controlling defects are large pores or large SiC grains. The large grains are in fact polycrystalline as indicated by the Laue photograph and also by the SEM pictures. The shape of the large grains is

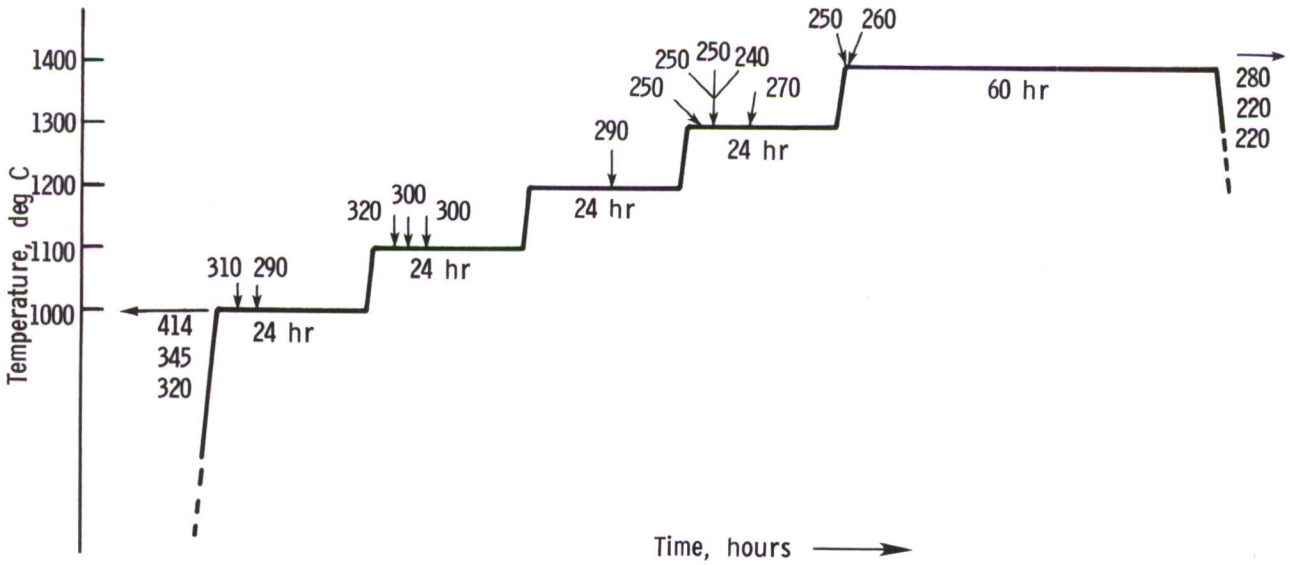

Figure 122. STSR results for Carborundum 1978 alpha silicon carbide.

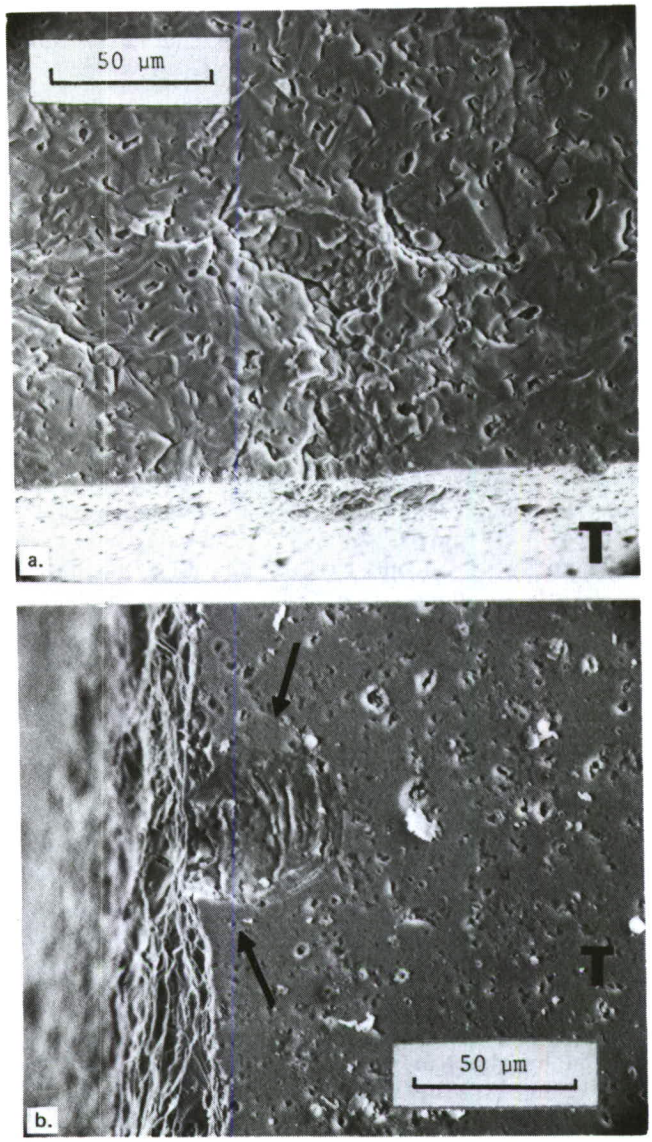

Figure 123. (a) Carborundum 1978 silicon carbide STSR sample fracture surface showing the failure initiation site is a pore that is surface connected. Applied stress was 300 MPa with failure at 5 hours at 1100 C; (b) the opposite matching half of the same sample, but viewed on the tensile face. The surface-connected porosity is being sealed by the oxide layer. The arrows point to the pore that initiated fracture.

difficult to access, but since both circular and linear sections were observed on the fracture surfaces, the defect may be disk-like. In only one case did a room temperature sample fail from such defect that may have been in the worst possible orientation and position, but this result *cannot be ignored* since more trials would likely have resulted in additional such failures.

Very little variation in average strength or in scatter between the 1977 and 1978 grades existed. The strength-controlling defect in the earlier grade was large porosity as well as an unidentified defect. The morphology of the

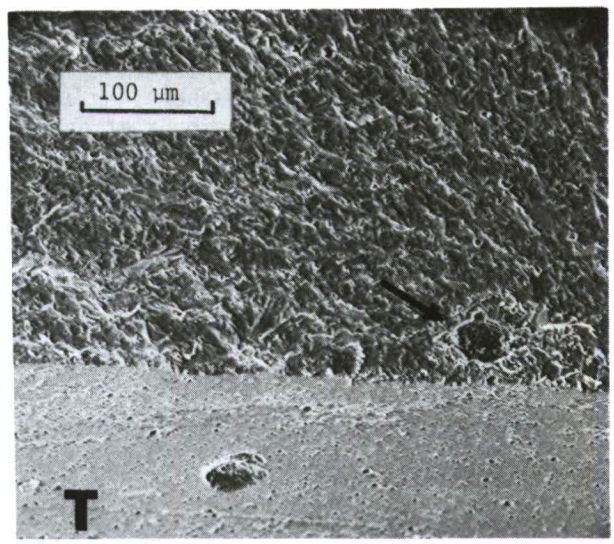

Figure 124. Fracture surface of a Carborundum 1978 SiC STSR sample which failed at 4.8 hours at 1300 C. The arrow indicates the fracture initiation site, a pore possibly with SCG markings. Sample was loaded at 250 MPa.

porosity in the new grade is quite different, however. Furthermore, a higher frequency or concentration of moderately large pores exists in the 1978 grade (see polished sections, Figure 17a and b). These differences, as well as the fact that less tungsten exists in the 1978 grade, are the result of the change in powder preparation from a grinding-milling procedure to a spray-drying process.

Both the 1977 and 1978 grades of Carborundum silicon carbide exhibit static fatigue failure at 1200 C. The newer grade seems *more* susceptible to strength decay with time, however. Time to failure of the 1978 grade is proportional to applied stress raised to the -1/40.8 power. STSR trials showed both materials tend to fail over all temperatures in the 1000 C to 1400 C range. At 1200 C and above, no meaningful difference was observed, but at 1000 C to 1100 C the newer 1978 grade may be more susceptible to failure at lower stresses. Both the 1978 and 1977 vintages showed evidence of SCG at the higher temperature (≈1400 C), but little or no evidence at lower temperatures. In the case of the twenty-two 1200 C stress rupture failures in the 1978 material, no evidence of SCG was observed on *any* of the samples. An alternate mechanism must account for the failures.

Since nearly all the static fatigue failures of the 1978 grade silicon carbide and some of the 1977 grade silicon carbide specimens involve surface-connected porosity, it is likely the mechanism of failure involves some attack on or enlargement of the pores. It is possible that quite simply since there are more surface-connected pores in the newer version, it experiences more static fatigue failures. It may be that oxidation attack upon weakly bonded material occurs

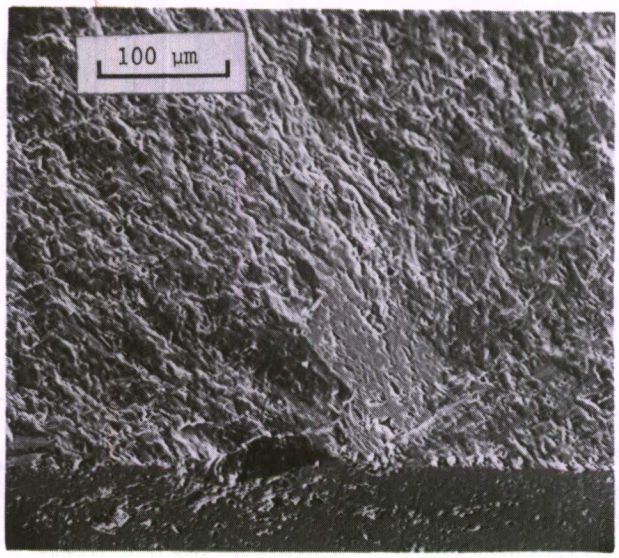

a. The initiation site is either the large grain or the pore next to it.

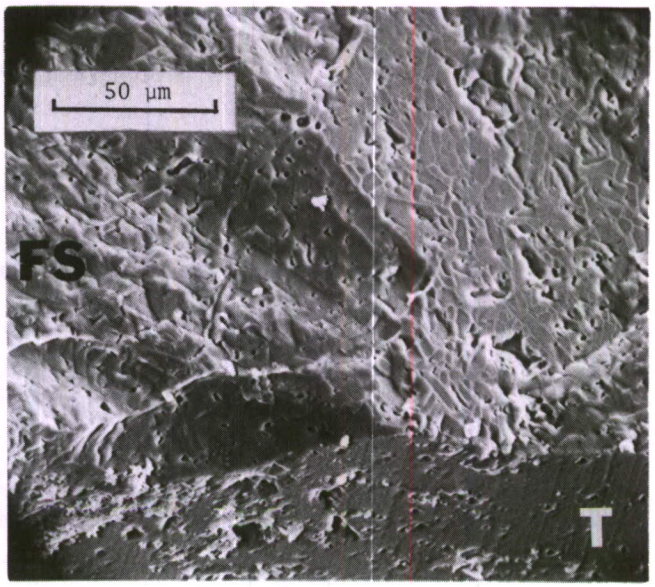

b. Close-up shows the faceted nature of the large grain which may in fact be a zone of recrystallized material or the result of excessive grain growth.

Figure 125. Fracture surfaces of a Carborundum 1978 STSR sample which failed at 2.4 hours at 1300 C. Sample was loaded to 250 MPa.

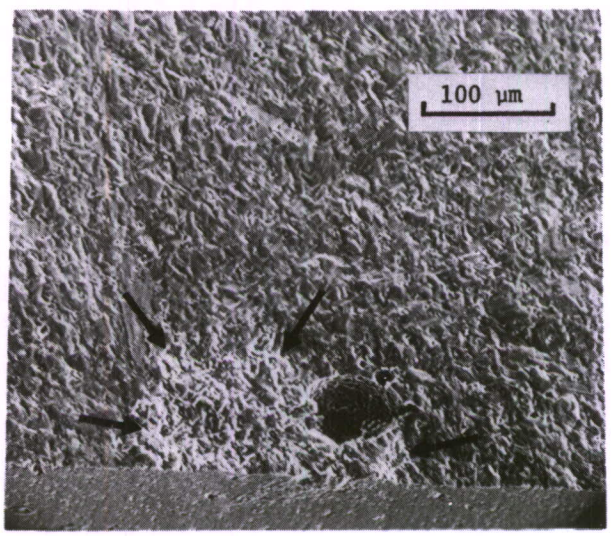

Figure 126. SEM view of the fracture surface of an STSR sample (250 MPa) which failed at 0.7 hour at 1400 C. The arrows delineate an SCG zone which may have emanated from the side of the pore.

around the large pores. No difference in pore appearance was noted when SEM photos of the samples were compared with similar pores in room temperature fracture surfaces, but the effect may be subtle.

These results, particularly the 1200 C stress rupture data, at first seem to be in disagreement with the findings of Reference 24. No static fatigue behavior was observed in the latter work, despite the fact that stress rupture trials with four-point bending at 1200 C were also used. Failures were obtained at temperatures of 1400 C and above, and the mechanism responsible was "slow crack growth" (such as shown to exist in a few of the STSR samples tested in this study). The key to understanding the apparent discrepancy lies in one important difference in the experimental procedure. In Reference 24, artificially induced flaws were used to preferentially influence the location of failure. In that procedure a Knoop microindenter is used to indent the sample, resulting in an ideally sharp crack that is much larger than the indent itself. These induced cracks were sufficiently large to reduce the fast fracture strength of the material at 1200 C to 192 MPa. The stress rupture testing reported herein was on beams *without* such controlled flaws and the samples failed from *naturally* occurring defects: surface-connected pores. If the material is sensitive to surface-connected porosity at 1200 C, why didn't some of the samples in Reference 24 break in a time-dependent manner at the surface pores that undoubtedly existed? The answer is that the data reported in that work involved stresses that, while close to fast fracture K_{Ic} conditions for the artificially induced flaws, were too low to activate the surface-connected porosity. Most of the samples in Reference 24 were loaded at stresses of 192 MPa or less, values that would result in samples surviving thousands of hours according to the data in Figure 119. Therefore it is not surprising that no static fatigue failures occurred from samples tested at 1200 C in Reference 24.

The conclusion is that sharp cracks such as those caused by the microindenter (or possibly machining damage) will not grow in this material until temperatures of 1400 C or above are reached. Above that temperature, the "slow crack growth" mechanism is dominant. On the other hand, an *alternate* mechanism can operate at lower temperatures. This mechanism, detected in the experimental work reported herein, can occur at 1200 C and involves surface-connected porosity. In fact, based upon the STSR results, this alternate mechanism can occur at temperatures *as low as 1000 C*. The exact nature of the low temperature failures is not known, but may involve oxidation attack on surface porosity. This mode of failure was not detected by the controlled flaw method and indicates that such testing should be cautiously interpreted. High temperature failures on the 1977 vintage of this material were from both mechanisms.

The retained strength of the 1977 grade survivors was significantly greater than strengths of the virgin materials. The same effect, but not as significant, was observed for the newer vintage. Similar observations are reported in Reference 71. Thus, although the oxide formation might react with pores and cause static fatigue failure, it can cause a retained strength enhancement at room temperature. Oxide that forms on the grain boundaries (possibly weakly bonded material adjacent to pores) could act to blunt crack tips on subsequent low temperature strength testing. Alternately, prolonged exposure under load may cause failure of the grain boundaries.

Light microscope inspection showed an oxide layer tended to form a thin seal over surface-connected porosity. Very often a small white spot on the surface would be evident over a pore and is an optical effect of the transparent oxide layer. On occasion a partially sealed-over pore would have a white ring at the surface corresponding to a lip of oxide forming over the pore. The oxide layer that forms is very thin and coherent. In the 1978 vintage, it is alpha cristobalite only, but the earlier grade has an additional unidentified phase, probably a metal ion silicate. The 1978 grade has less impurity content (particularly tungsten), however.

Further investigations are required to pursue these matters. Static fatigue testing in an inert atmosphere may be valuable. Although the analysis is not conclusive, it does seem clear some property alterations are occurring as the result of the scale-up procedure from the earlier 1977 research effort.

J. Norton NC 433 Siliconized Silicon Carbide

1. Control Strengths

A total of 37 control fractures were obtained for the NC 433 grade of silicon carbide. The average flexural strength was 317 MPa with a standard deviation of 65 MPa. When plotted for a Weibull representation, the data revealed a distinctly bimodal distribution (Figure 127). Three failures were at uncharacteristically low strengths. Fractography was directed at determining the contributing flaws. Mirrors were not evident, either with the SEM or the light microscope and origins could only occasionally be identified by river markings.

The fracture surfaces were quite rough with many undulations. Numerous large silicon carbide grains (up to 100 μm) were well dispersed and readily observed (due to their high reflectivity) with light microscopy. On some samples zones with higher than normal concentrations of these silicon carbide grains were observed. The four lowest strength samples had very large silicon carbide grains as the initiating flaw (Figure 128). The grains were quite circular in appearance on the fracture surface (no attempt was made to determine if the pockets were spherical) and measured up to 250 μm in diameter. The grains were cleaved in half. Similar large grains were

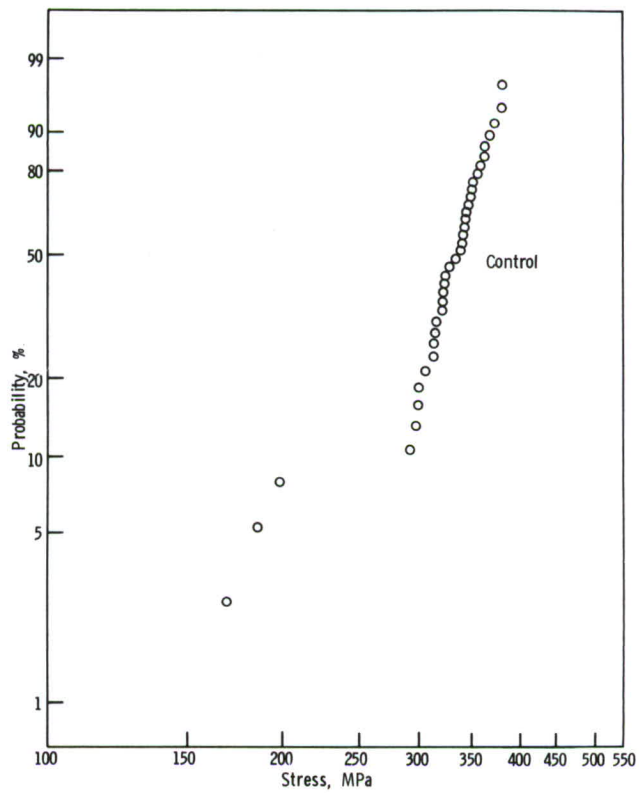

Figure 127. Room temperature flexural strengths of NC 433 silicon carbide.

observed in several of the higher strength samples, but were located near the neutral axis or in the compressive side and thus did not act as the initiating flaw. Therefore these defects, and thus the low strength samples, cannot be ignored.

Higher strength samples failed from flaws that could not be positively identified. The initiating flaw is probably a silicon carbide grain (or group of grains) such as shown in Figure 129. The absence of any mirror or other markings made identification of an individual site difficult. Often when the sample halves were placed together at the fracture surface, and the tensile edge examined, small pieces were missing near the probable region of initiation, suggesting a fragmentation of the initiating site. Most samples did not break from corners and no correlation with machining marks could be made.

2. Stress Rupture, 1200 C

High temperature testing showed almost no time-dependent failure operative in NC 433 silicon carbide. Of 14 samples tested at 1200 C, 10 failed on loading and 4 survived intact for 300 hours (Figure 130). The critical stress level was 310 MPa; two samples at that stress failed on loading, two survived intact. This stress is quite comparable to the control strength (317 MPa). The retained strengths of the survivors were: 345, 415, 422, and 441 MPa. These values are well above the stresses that the samples bore at 1200 C and three are substantially above the highest virgin strength measured: 383 MPa. On the other hand the samples exhibited permanent deformations of the order of 0.2 percent (256 MPa - 0.19%, 297 MPa - 0.23%, 310 MPa - 0.22%, 310 MPa - 0.22%).

3. STSR

The stepped temperature stress rupture tests were conducted over the range of 1000 C to 1300 C only and again revealed very little time-dependent effects (Figure 131). Of 15 trials, 6 survived the entire pattern, and 8 broke during loading or in less than 30 seconds, and only one failed at 26 hours into the 1300 C step. The failure origin could not be determined for this sample. There was some overlap of stresses with, for example, a sample loaded to 310 MPa which did not fail while samples at lower stresses broke on loading. This is consistent with the scatter in strength of the control samples. The surviving samples again exhibited permanent deflections of the order of 0.2 percent; although at 1200 C for only 24 hours, these were exposed to 1300 C for 60 hours.

The retained strengths of the survivors were: 375, 390, 395, 409, 421, and 439 MPa, all well above the stresses they bore at temperature and considerably above the control strengths. Fractography failed to demonstrate whether the higher retained strengths of the stress rupture and STSR survivors were due to healing of an initial flaw distribution. Large shiny circular zones were again observed scattered through some of the samples (about one quarter of the fracture surfaces examined for this material). In none of them was such a zone found to intersect the specimen surface (although some of the control samples had such placement).

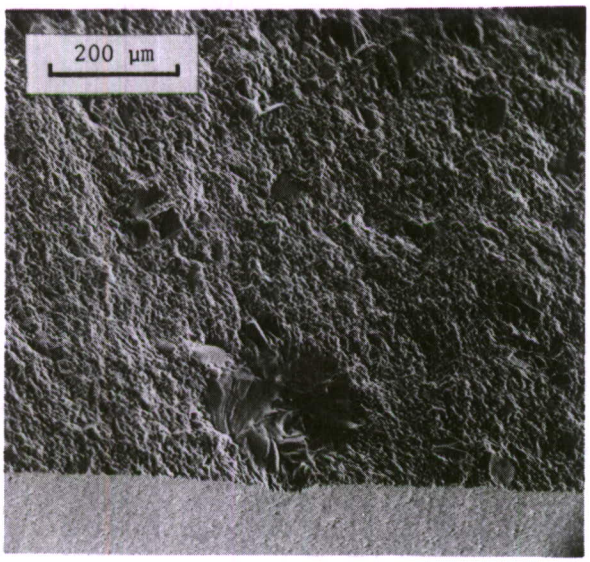

Figure 128. Fracture surface of an NC 433 room temperature sample showing a large silicon carbide grain which acted as the strength-controlling flaw. Fracture stress was 169 MPa.

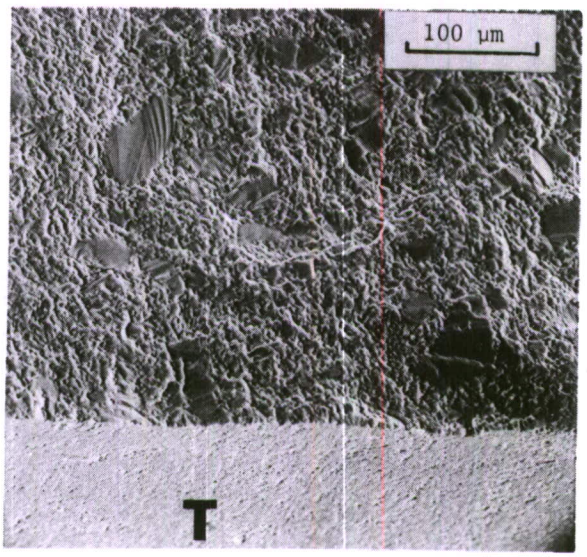

Figure 129. Fracture surface of NC 433 control sample. Fracture stress was 322 MPa.

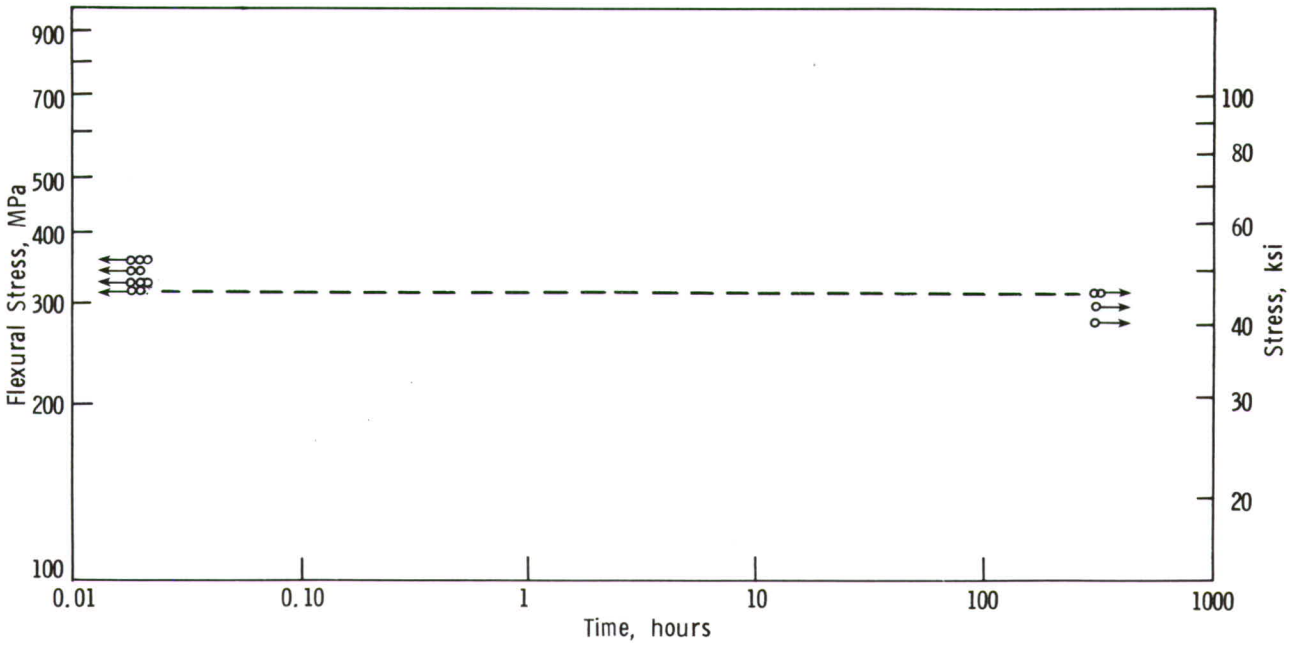

Figure 130. Flexural stress rupture at 1200 C for Norton NC 433 silicon carbide.

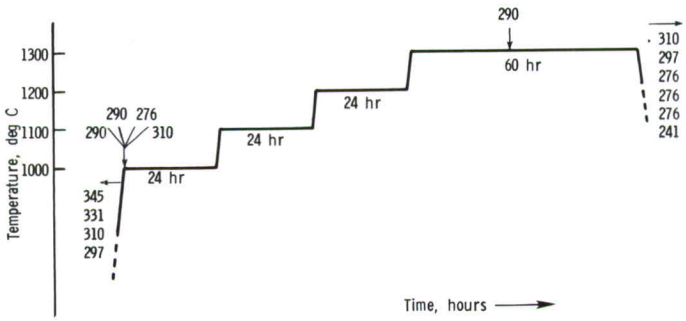

Figure 131. STSR results for Norton NC 433 silicon carbide.

X-ray diffraction showed the appearance of significant amounts of cristobalite at the surface of stress rupture and STSR samples exposed for long times and no major phase other than the original constituents. The surface appearance of the samples which survived appeared mottled as shown in Figure 132. Closer examination with SEM revealed a coherent surface layer of glass interrupted by irregular glassy zones which gave the mottled appearance (Figure 133). Rare pits were observed, sometimes in clusters, but in no sample did fracture initiate from such a pit. The single sample which failed in a time-dependent manner did not show any features on the fracture surface which would indicate the mechanism of failure.

4. Discussion

NC 433 siliconized silicon carbide has very little susceptibility to static fatigue under the conditions applied in this study. Little or no strength degradation is evident at 1200 C compared to room temperature. Significant creep occurs, however, for samples under load at temperatures of 1200 C and above. The low strength flaws that account for the bimodal flaw distribution are large silicon or carbide grains which could possibly be eliminated by careful processing. If the samples which failed from such defects are eliminated, the average strength of the reference samples would then be 337 MPa with a standard deviation of 24 MPa. A Weibull two-parameter modulus would then be 15.5 with a correlation coefficient of 94 percent. The surface layer that develops in an oxidizing environment is cristobalite, which forms a coherent surface layer with some mottling.

K. Norton NC 435 Siliconized Silicon Carbide

1. Control Strengths

Fourteen control fractures at room temperature gave an average flexural stress of 342 MPa, a slight improvement over the NC 433 grade. Despite such a small number of data points, the Weibull plot suggests a multimodal distribution of flaws (Figure 134). Fractography identified the low strength samples (half the number tested) as having veins of silicon running through the fracture surface (Figure 135). The veins are of uniform width and in one sample was as large as 75 μm wide. Although the veins ran perpendicularly through the fracture surface, markings indicate the fracture initiated where the vein intersected the tensile face. The veins, presumably the result of infiltration of a compact that had cracks from prior processing, are completely infiltrated and exhibit no residual

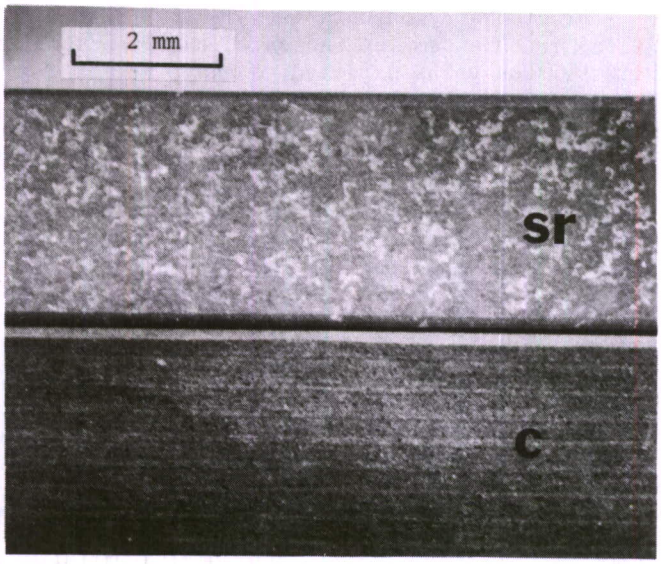

Figure 132. Light photomicrograph of the surface of a 300-hour NC 433 stress rupture survivor (sr) adjacent to a control sample (c).

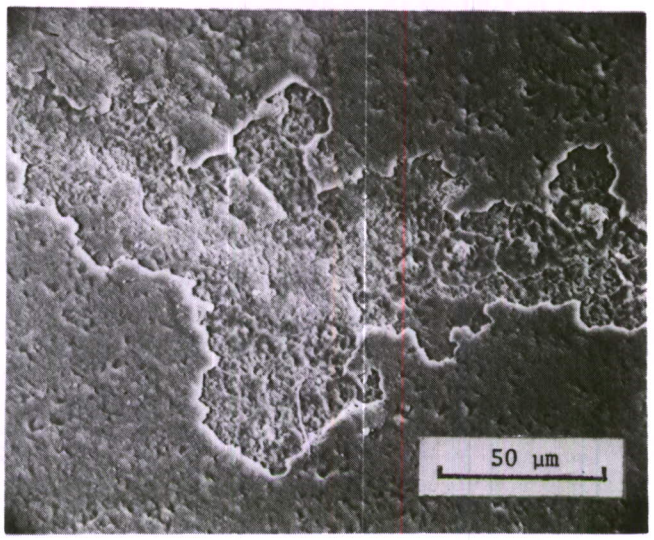

Figure 133. SEM close-up of the mottled surface of a 300-hour NC 433 stress rupture survivor.

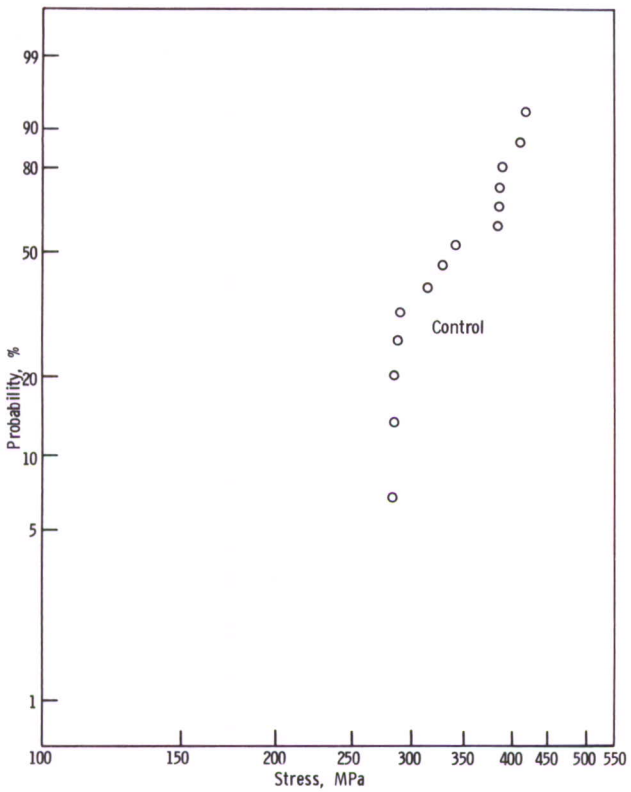

Figure 134. Room temperature flexural strength data for Norton NC 435 silicon carbide.

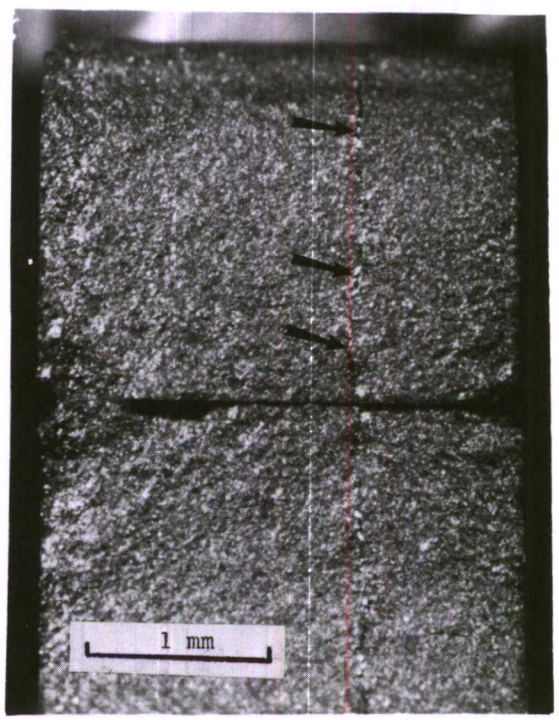

Figure 135. Matching fracture surfaces of an NC 435 control fracture. The pieces are mounted back to back so that they share the tensile edge. Flexural strength was 282 MPa. Strength-controlling flaw was the silicon vein (arrows).

porosity. Failure origins were not evident on the samples without the veins. Fracture surfaces were quite rough and no mirrors were evident. Discontinuities were present yet neither light microscopy or SEM examination could specifically identify the initiating flaw.

2. Stress Rupture, 1200 C

Unlike NC 433, the NC 435 grade of siliconized silicon carbide did exhibit delayed failures at 1200 C. Of 18 samples, 14 carrying stresses ranging from 317 to 395 MPa failed at times from 0.20 to 17 hours (Figure 136). One sample survived 300 hours despite a silicon vein extending through the piece, but had a 0.25 percent permanent deflection. The retained strength of the survivor sample at room temperature was 359 MPa. Failure in that case originated at the intersection of the vein and the tensile edge face.

3. STSR

Stepped temperature testing showed failures at all temperatures from 1000 C to 1300 C (Figure 137). Three samples survived without failure, but had significant curvature. The sample loaded to 241 MPa exhibited a 0.3 percent maximum strain and had a retained strength of 442 MPa. The creep deformation was 50% greater than similarly loaded NC 433 samples. The other two samples broke during furnace cooldown. A sample loaded to 296 MPa failed at 22 hours into the 1300 C step and had a 0.7 percent permanent strain. This sample had nonuniform curvature in the inner gage length, however, and is not typical (it did not have a silicon vein).

Fractography on both the STSR and 1200 C stress rupture samples indicated that the samples with silicon veins oxidized so that, at least at the surface, the veins were transformed to cristobalite. Lateral cracks were observed to emanate on the tensile face from these veins (Figure 138) in a direction normal to the tensile stress. These lateral cracks were most evident on the samples which were exposed to a few hours at 1200 C or higher and are manifested on the surface by different oxidation appearance. The size of the lateral cracks varied with position: they are roughly constant in size between the inner pins of the flexural fixtures, but have a gradient to zero size at the outer pins. This size difference corresponds to the stress gradient along the tensile face. These samples had pronounced permanent curvature, with maximum tensile strains of the order of tenths of a percent. The cracks are presumably the result of this excessive creep deformation. Time-dependent failures in the 1200 C stress rupture and STSR trials were due to these lateral cracks in the samples that had silicon veins (approximately half of all samples tested).

Samples without silicon veins also failed under stress rupture and STSR conditions and also developed lateral cracks (Figure 139), which were again most evident in the samples with considerable permanent deflection. Such lateral cracks were not observed in any of the NC 433 samples tested at high temperature.

Fracture surfaces showed distinct features that highlighted a slow crack growth zone associated with the lateral cracks. A dark matte zone

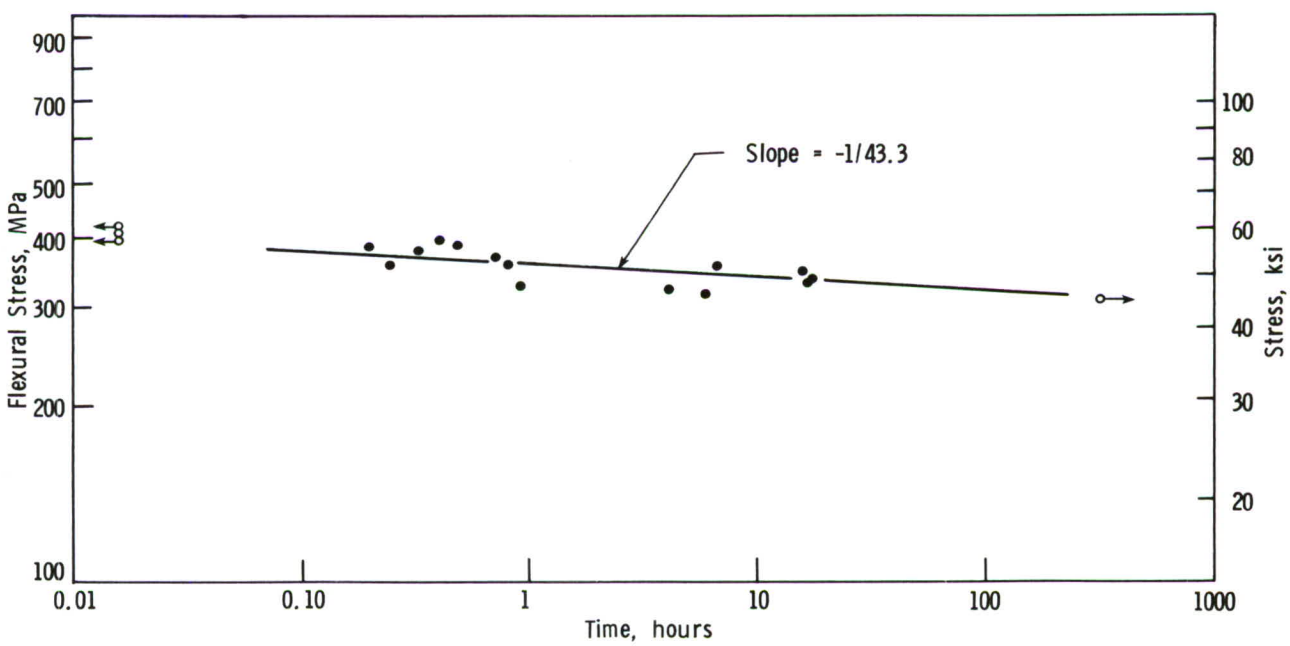

Figure 136. Flexural stress rupture at 1200 C for Norton NC 435 silicon carbide.

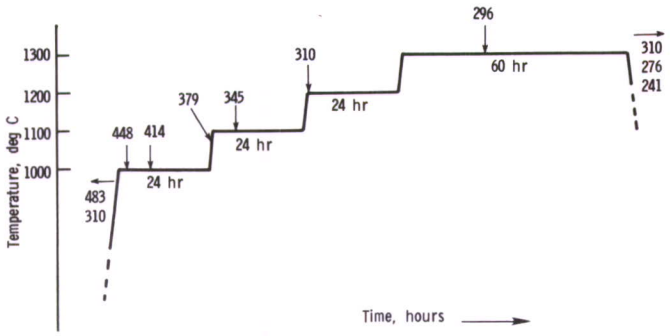

Figure 137. STSR results for Norton NC 435 silicon carbide.

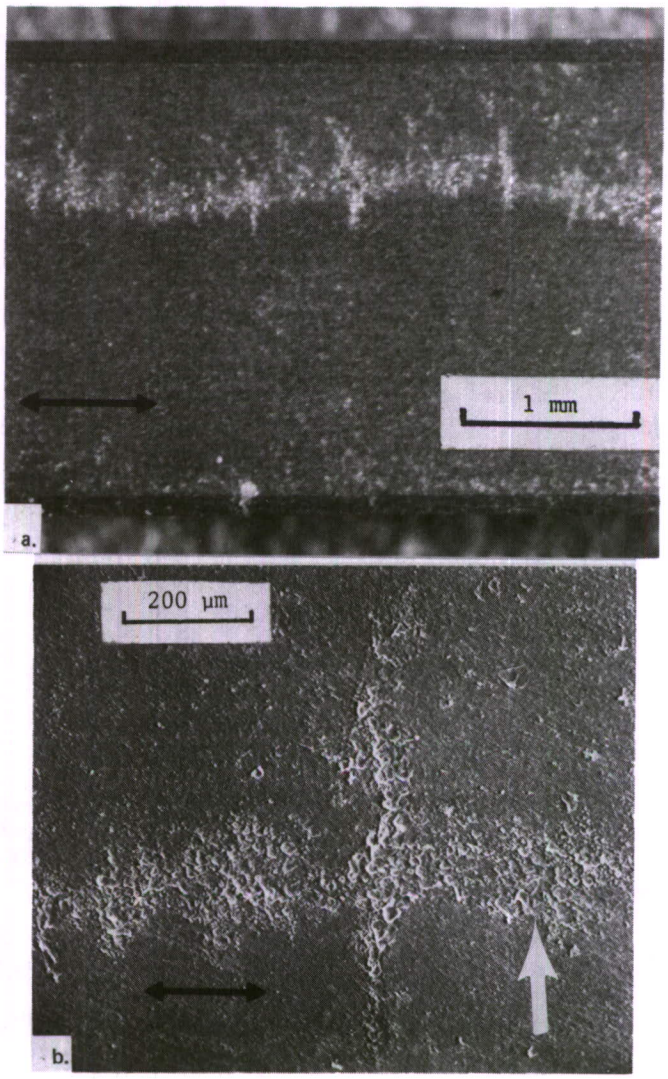

Figure 138. (a) The tensile face of an NC 435 sample loaded in flexural stress rupture to 331 MPa at 1200 C. The direction of maximum bending tensile stress is shown as the black arrows. The vein runs approximately in the same direction, but lateral cracks extend sideways from the vein. Failure occurred from one such crack after 12.0 hours. These cracks do not exist on the compressive face even though the vein was present; (b) SEM close-up of the same sample. The crack is emanating perpendicularly to the applied stress (marked by the double arrow). The white arrow marks the vein.

Figure 139. NC 435 STSR sample that was loaded to 296 MPa and failed at 22 hours at 1300 C. The flat tensile face is shown and lateral creep cracks are evident. Tensile bending stresses were in the direction indicated by the double arrow.

(often visible to the naked eye, but best viewed with a binocular microscope with lighting from directly above the sample) emanates from the tensile face to varying extents depending upon the times to failure and temperatures (Figure 140). Short-time-to-failure samples had small zones, yet long-time-to-failure, high temperature samples had zones that often extended to the neutral axis of the sample. These zones are not evident with SEM examination. The dark matte zone often had regions or pockmarks within that resembled the fast fracture zone, suggesting the slow crack growth did not entirely cleave the sample but worked around and beyond strong points or well-bonded areas in the sample (Figure 141). This mode of crack propagation is unlike the slow crack growth observed in hot-pressed silicon nitride.

On several samples a two-tiered fracture surface resulted as the fast fracture from a SCG zone in one cross section jogged down to a parallel zone in another cross section of the sample. Often a second distinctly different dark zone was evident within the dark matte SCG zone. The difference is subtle, is visible only with light microscopy, and is difficult to photograph. Finally, the samples with the silicon veins had whitish fine-grained markings within (usually centered) the dark matte SCG zone. These may be subsurface cristobalite pockets; the result of oxidation into the veins.

X-ray diffraction of the surface oxide indicated alpha and beta silicon nitride, alpha

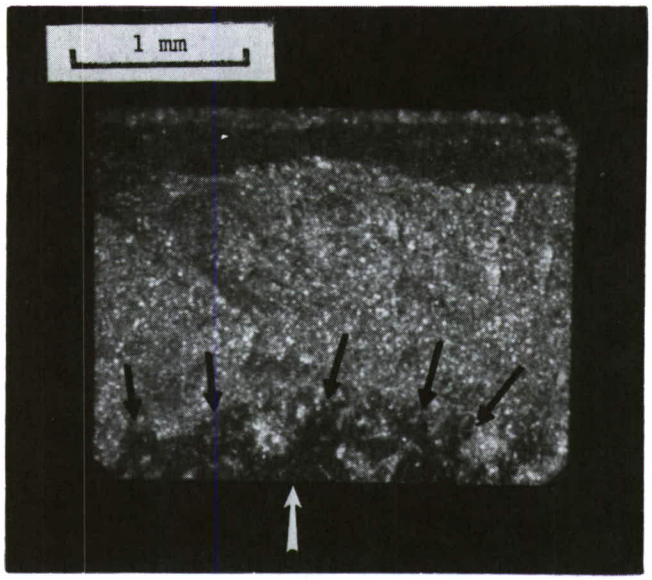

Figure 140. Fracture surface of an NC 435 STSR sample that broke at 22.5 minutes at the 1200 C step. The black arrows outline an irregular matte black "slow crack growth" zone. The white arrow on the tensile edge marks the probable initiation zone. This latter zone, when viewed with the light microscope, appears to have a slightly bluish tint. It does not photograph well.

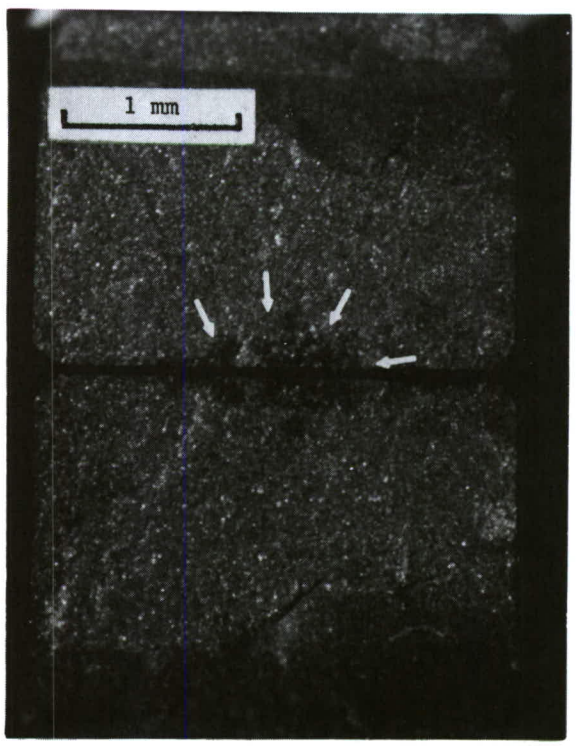

Figure 141. Fracture surfaces of an NC 435 STSR sample that failed at 5.5 hours at 1100 C. The white arrows outline the slow crack growth zone in one half. The two fracture halves share their tensile edges.

cristobalite, and a fifth minor unidentified phase with broad peaks at 4.65, 3.75, 3.22, and 2.40 Å. These latter peaks were not observed on the NC 433 (exposed sample) patterns.

4. Discussion

Fine-grained siliconized carbide, grade NC 435, does have a slightly higher room temperature strength than NC 433 (coarse grain), but the results were obscured by the existence of silicon veins in half the samples. The veins are probably related to a cracking problem during initial firing of the silicon carbide compact prior to infiltration. The material also exhibited a gradient in microstructure with coarse grains of SiC and higher Si concentration near the billet surface. If the large SiC grains act as flaws, then it is not surprising that the material has a strength similar to NC 433. The evidence thus suggests that this material is not being satisfactorily processed at the 0.95 cm thickness.

NC 435 does exhibit static fatigue failure, unlike NC 433. Failures were observed over all temperatures from 1000 C to 1300 C. Scatter precludes accurate curve fitting but a general trend of less load-carrying capacity with time at 1200 C is evident. Although many samples had silicon veins which affected both room temperature and high temperature performance, many other samples without silicon veins also exhibited static fatigue failures. The chemistry of the two grades NC 435 and NC 433 are similar except that the silicon content of the NC 435 grade is higher. The greater silicon content may make the samples more susceptible to oxidation attack along the silicon into the interior, thereby leading to time-dependent failure. Alternately, the greater silicon content may lead to higher creep rates and thus faster creep cracking. On the other hand, a conventional creep-grain size explanation may be appropriate. The finer grain size NC 435 did creep more than the coarse grained NC 433. The NC 435 grade developed cracks resulting from excessive creep, whereas no such cracks developed in the NC 433 samples similarly loaded. The fracture surfaces of static fatigue failed samples were rich with markings whose meaning are as yet unclear. Thus, even if the processing is improved to eliminate the veins and coarse grains, the material may still prove less capable of resisting static fatigue at elevated temperatures than NC 433. Further studies on thinner billets may verify this conclusion.

L. General Electric Silcomp CRC Siliconized Silicon Carbide

1. Control Strengths

Thirteen room temperature fractures were obtained for Silcomp CRC silicon carbide. Average

strength was 389 MPa with a standard deviation of 64 MPa. A least-squares line of slope 5.9 was a good fit for the data when plotted on a Weibull representation (Figure 142). Eight low-strength failures originated from porous zones such as shown in Figure 143. The aligned fiber arrangement inside the pore suggests a clump of fibers existed in the precursor (rather than the random arrangement) and that silicon failed to fully infiltrate the zone. A machining chip at the chamfer accounted for another sample failure and zones of small inclusions caused failures in three others. A single sample failed from a silicon zone (Figure 144) that may have resulted from infiltration of a crack that existed in the precursor (similar to NC 435). Another such zone was observed as the initiating site on a secondary fracture (outside the gage length) on a different sample. Shiny speckles of transgranularly fractured silicon grains were evident on all fracture surfaces when inspected with the optical microscope.

2. Stress Rupture, 1200 C

Of nine samples tested in flexural stress rupture at 1200 C, only one failed in a time-dependent manner (Figure 145). The critical stress is about 240 MPa. Samples at 206, 221, and 228 MPa survived 300 hours and subsequent retained strength measurements at room temperature gave values of 321, 373, 268 MPa, respectively. These values are lower than the average control strength (389 MPa). Failure origins were porous zones associated with fiber clump and were similar to those observed in the control group.

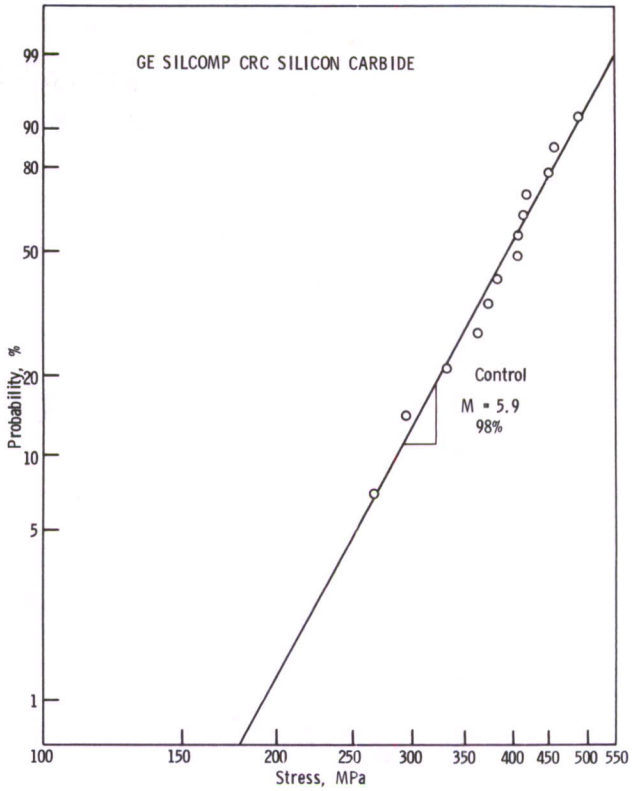

Figure 142. Room temperature control strengths for Silcomp CRC silicon carbide.

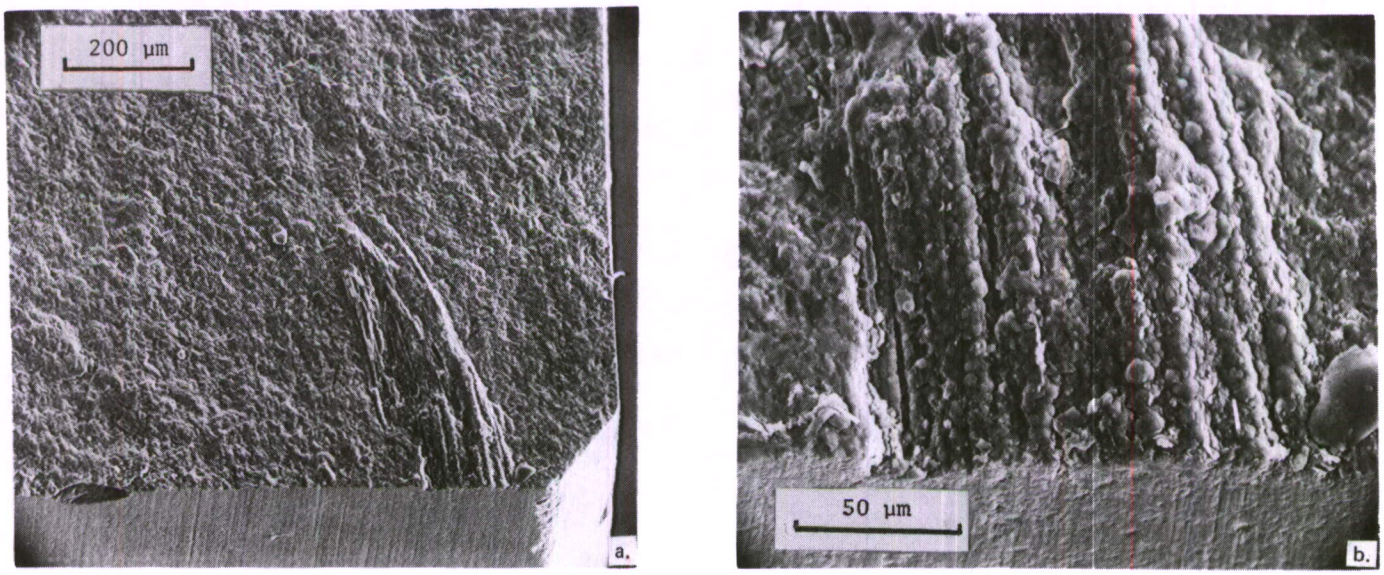

Figure 143. (a) Fracture initiation site for a Silcomp CRC control sample. Fracture stress was 266 MPa; (b) close-up of the porous region. The aligned nature of the SiC crystallites suggests that a clump of fibers occurred during original processing as opposed to the desired random arrangement.

Permanent deformations were significant: 0.23, 0.21, and 0.28 percents, respectively. The material oxidized at the surface to form a thick glassy layer that was characterized by a wide, shallow cristobalite peak on a X-ray diffraction pattern (SiC and Si gave peaks that were much more prominent). The surface layer was nonuniform and had sharply different features on the same sample (Figure 146). Most of the surface had a coherent glass layer occasionally interrupted by porous regions. The samples also had a sharp gradient from a coherent layer to a platelike, porous glass layer which was due to the failure to form a smooth layer over the more porous zones.

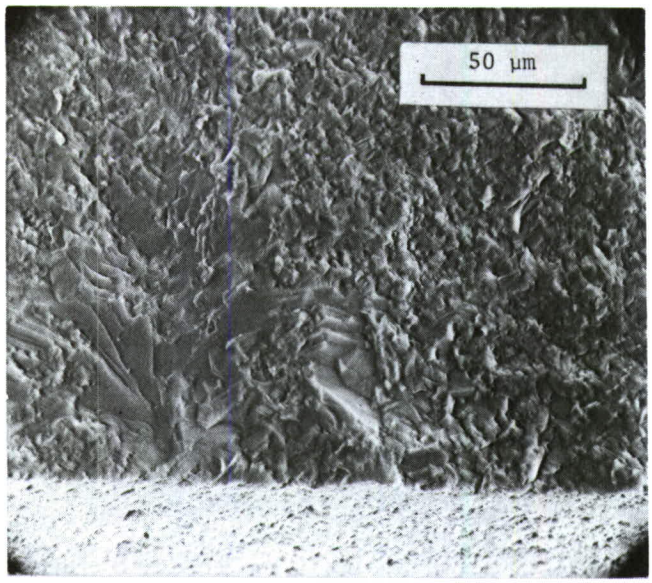

Figure 144. SEM photo of the fracture initiation site of a Silcomp CRC control sample which failed at 455 MPa.

The single sample that ruptured was loaded to 241 MPa and failed after 159.6 hours. The fracture surface was very ragged and an initiation site could not be determined. Considerable excess silicon was present, however, judging by the high reflectivity of some zones. In one portion a large, poorly defined silicon vein was evident.

3. STSR

STSR results confirmed the results of the 1200 C stress rupture trials: no samples failed at 1200 C and only one sample failed at 0.53 hour into the 1000 C step (Figure 147). Static fatigue effects only became important once temperatures of 1250 C were exceeded. Of the seven samples that failed on loading, five were from porous zones and the initiating sites on the other two were unclear. The sample which failed in the 1000 C step had a surface-connected pore as the initiating site. The failure pore was the largest in a zone of greater porosity than elsewhere on the sample surface. Although SEM inspection showed the flaw to be about 70 μm deep, connected porosity associated with it extended much deeper into the sample (possibly one third the way through). The oxidation layer on that sample was coherent except over the porous region, giving rise to a mottled appearance.

The samples which failed during heatup to or early in the 1300 C step had very irregular and jagged fracture surfaces. Considerable difficulty was experienced in pinpointing origins of failure. The 276 MPa sample which ruptured after 1/2 hour at 1300 C failed from a pore associated with a lateral crack that resulted from excessive

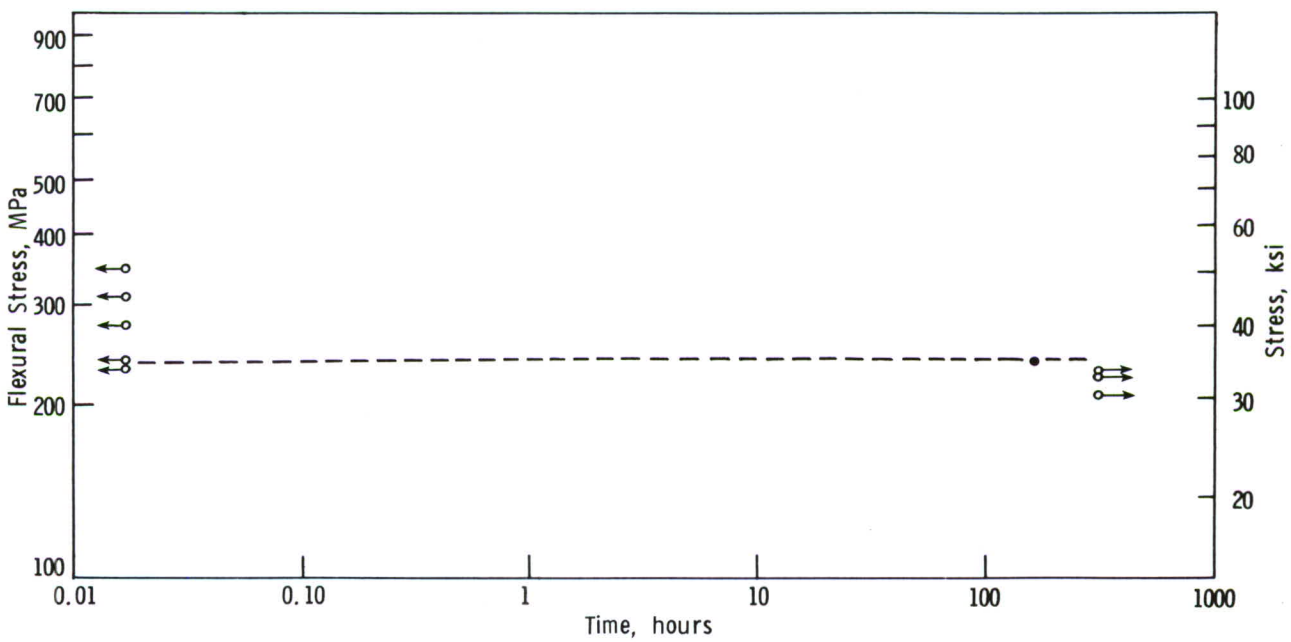

Figure 145. Flexural stress rupture at 1200 C for Silcomp CRC silicon carbide.

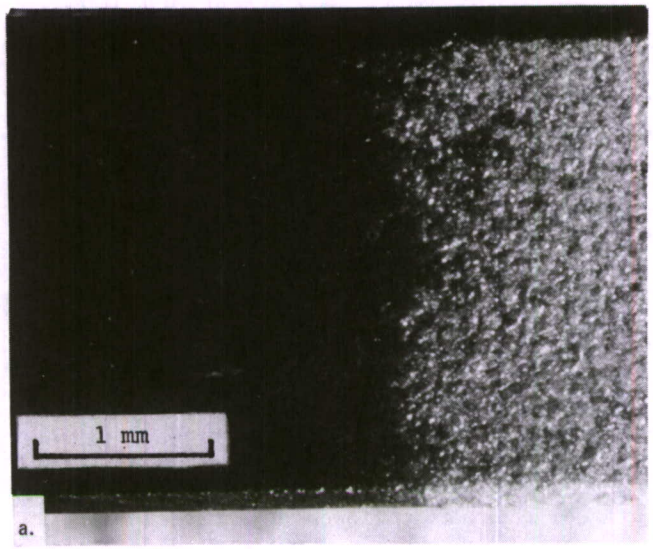

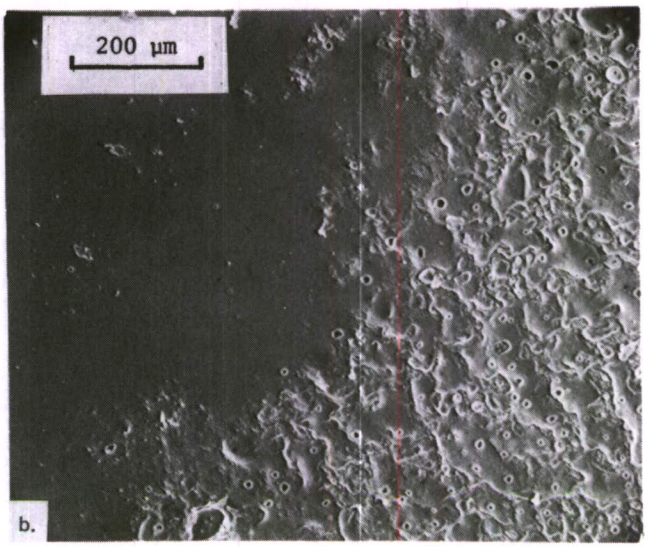

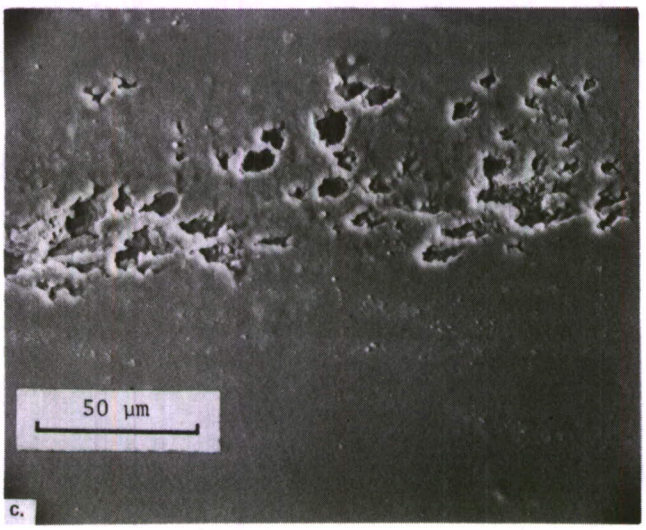

Figure 146. (a) Light photo micrograph of the tensile face of Silcomp CRC bend bar that survived 300 hours intact. A sharp gradient in the oxide layer is evident; (b) SEM close-up of the transition zone. The oxide is coherent and smooth at one end of the sample, but is porous, platelike, and irregular at the other end; (c) close-up of an interrupted zone of the otherwise smooth portion of oxide layer on the surface. A porous zone associated with fiber clump is likely underneath.

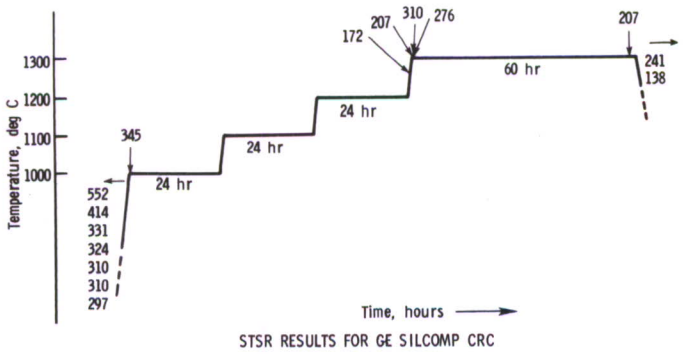

Figure 147. STSR results for Silcomp CRC silicon carbide.

creep deformation (Figure 148). Similar markings were not evident on the others, although the 207 MPa sample failed from a porous region of the sample. The fracture surfaces showed a shiny, fast fracture zone and a large, irregular dark zone in the tensile half.

The 207 MPa sample that failed at 56 hours into the 1300 C step had gross permanent deformation (0.7%) and small lateral cracks along the tensile face. The fracture surfaces showed three areas including a fast fracture zone; a prominent light-colored SCG zone and a dark zone extending from the tensile edge to roughly one third the height of the sample (Figure 149). The originating flaw was not discernible. The large dark zone was a common feature on the samples that failed in a time-dependent manner, but prominent SCG zone appeared only in this sample. The surface beyond the SCG and dark zones appears shiny and is the fast fracture zone.*

*The furnaces are programmed to shut off power immediately upon sample failure, resulting in a rapid cooldown. This serves to preserve fracture surface.

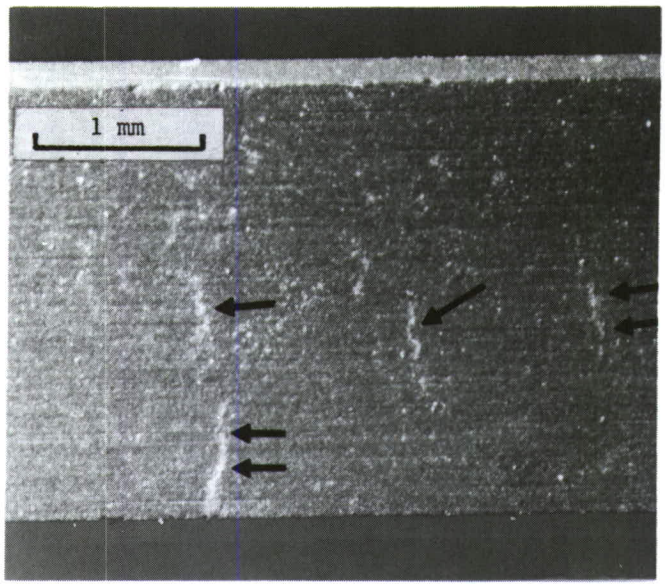

Figure 148. Tensile face of Silcomp CRC STSR sample which failed at 1300 C. Lateral cracks (arrows) run perpendicular to the applied tensile stress. Failure occurred from such a crack.

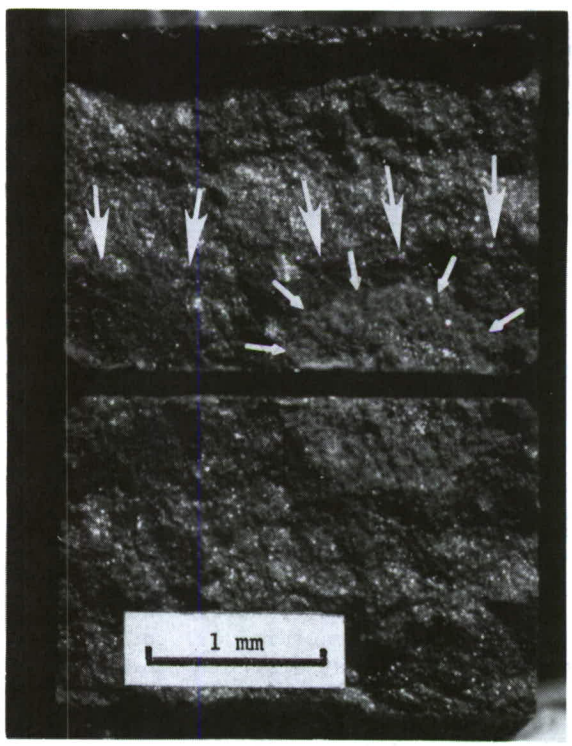

Figure 149. Light photomicrograph showing the two matching fracture surfaces of a Silcomp CRC STSR sample which failed after 55.8 hours at 1300 C. The halves are mounted back to back on the tension edge. The small white arrows delineate a light-colored slow crack growth zone. The larger white arrows show a dark colored matte zone of unidentified nature. The zone appears dark no matter what direction the lighting is from. The distinctions between the zones are best seen with the eye and some resolution is lost in the photography.

Unlike the optical observations, SEM inspection failed to clearly delineate the SCG or dark zone. Using the light microscope photo as a guide, the SCG and dark matte zones are entirely intergranular, whereas the fast fracture zone showed transgranular fracture. The lighter appearance of the fast fracture zone is due to the high reflectance of the transgranular surface while the intergranular dark zone scatters incident light. The SCG zone is intergranular but is likely oxidized with a thin glass layer giving rise to the light coloration. The coloration is lost when all SEM samples are coated with gold.

It is possible the fracture of this sample proceeded in three steps. The original flaw grew by a very slow process (SCG) to the elliptical shape, allowing time for oxidation of the exposed surface; this was followed by an accelerated creep cracking, that in turn lead to fast fracture. The dark zone, accelerated creep cracking, is likely stress-dependent and occurs across the entire fracture face, not just around the SCG zone. A stress concentration exists at the tip of the SCG zone, allowing the stress-dependent dark zone to penetrate deeper into the cross section (Figure 149). That this dark matte portion of the fracture surface is not well oxidized indicates it was not exposed to high temperature for very long. The other statically fatigued samples showed dark markings, but prominent SCG zones were not evident. They may have been present, but much smaller, below the resolution of the binocular microscope, and as stated above, the SEM is of little value in finding the SCG zone.

The two survivor samples had gross deformation as well: the 138 MPa sample had 0.49 percent, the 241 MPa sample had 0.36 percent. On subsequent retained strength testing both samples failed from a surface-connected porous zone (Figure 150). Neither showed the dark accelerated creep or SCG zones, but both were entirely smooth transgranular fast fracture. Small lateral creep cracks were not evident on either. The retained strengths were 249 and 363 MPa, respectively. X-ray diffraction on one survivor indicated only cristobalite in addition to SiC and Si.

4. Discussion

Silcomp CRC grade siliconized silicon carbide is a research grade material. A screening procedure was used by G. E. to weed out low strength and low density samples. The samples were individually infiltrated and not cut out of a plate. Despite this, the scatter of control strengths is high, nonuniform zones of porosity (fibers) exist, and creep deformations are not consistent from sample to sample. Failures are primarily from pores that had an aligned fibrous

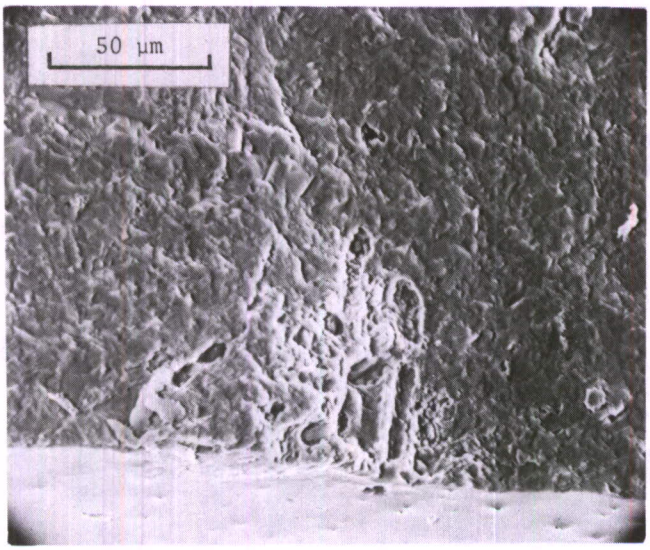

Figure 150. Strength-controlling flaw on a Silcomp CRC STSR survivor. Retained strength was 249 MPa. Sample was loaded to 138 MPa during the STSR test.

appearance, although silicon pockets also contribute to failure. The material is resistant to failure at 1200 C and lower but can creep noticeably at 1200 C. Time-dependent failures occur at temperatures greater than 1250 C and multiple mechanisms are likely involved. Oxidation results in a coherent oxide layer on the surface except where porosity is present. A few pores result in interruptions in the surface, whereas a high pore concentration will result in a mottled appearance.

A slow crack growth process occurs wherein the exposed crack surface had sufficient time to oxidize resulting in a distinct appearance. Accelerated creep cracking can lead to a large zone (around the SCG zone) that is exposed to the oxidizing environment for a much shorter time. All samples exposed to loads at temperatures of 1200 C and above experienced significant permanent deformation. In several cases this led to noticeable lateral creep cracking on the tensile surface.

M. General Electric Silcomp CC Siliconized Silicon Carbide

1. Control Strengths

Fifteen samples were used to obtain room temperature flexural strengths and twenty fractures were obtained. Average strength was 326 MPa with a standard deviation of 52 MPa.* A Weibull plot with a least-squares line of slope 6.5 is an excellent (98% correlation coefficient) fit to the data, Figure 151. Fracture surfaces were quite irregular and had no feature such as a mirror to indicate the failure source. Usually four to eight bands of SiC fibers were observed running from top to bottom on each cross section as shown in Figure 152. The initiation site cannot be identified with certainty in any sample, but it may be the intersection of the SiC bands with the tensile face as shown in Figure 153. In a few fracture surfaces, silicon veins were evident, but none could be correlated with fracture initiation.

2. Stress Rupture, 1200 C

Out of twelve samples tested three failed in a time-dependent manner at 1200 C (Figure 154). The critical stress level is approximately 220 MPa. No markings on the fracture surfaces indicated the time-dependent mechanism or even the initiation site. Three samples survived without failure although one broke during furnace cooldown. The retained strengths of the other two were 289 and 304 MPa. Both had a permanent curvature that translated to a 0.2% maximum tensile strain. A thin coherent and transparent oxide layer developed on the samples. The fiber structure appeared more clearly after oxidation on the exposed surfaces. Some pitting was evident in one of the

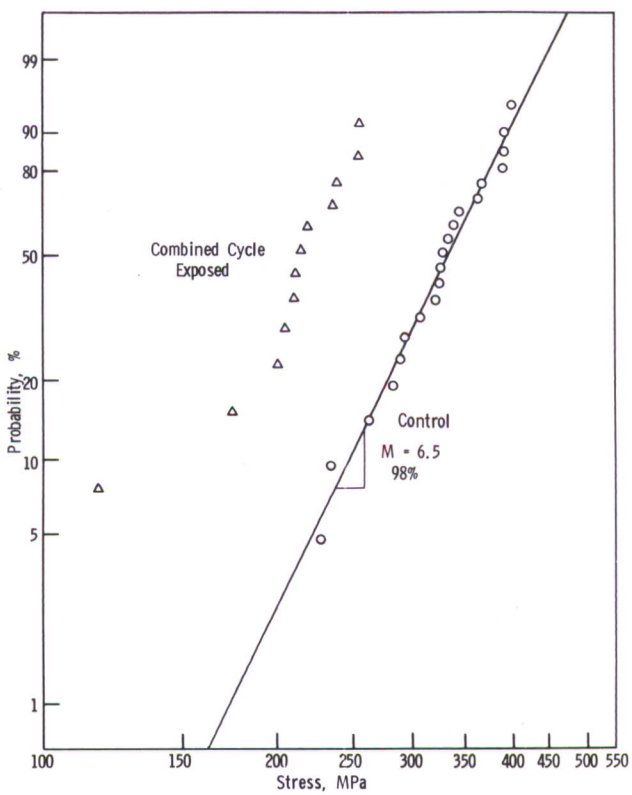

Figure 151. Room temperature control strengths for Silcomp CC silicon carbide.

*The average strength is somewhat higher than the 276 MPa proof test employed but several strength values were below the proof test stress.

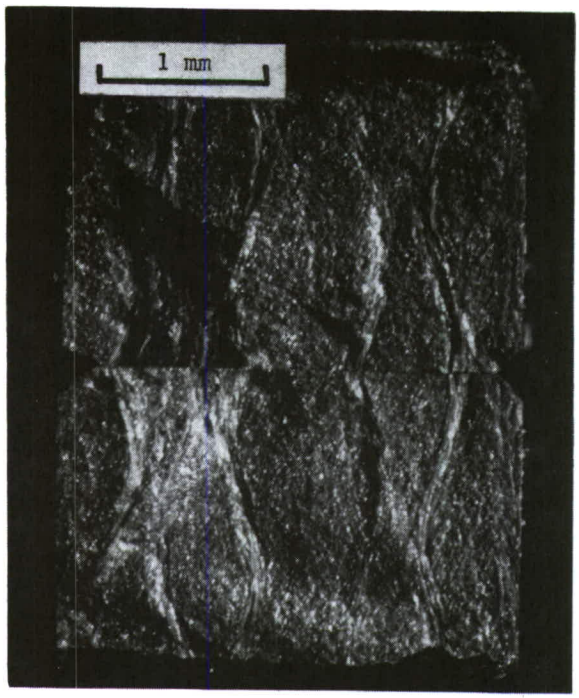

Figure 152. Back-to-back (along tensile edge) matching fracture surfaces of a Silcomp CC sample which failed on loading for a stress rupture trial.

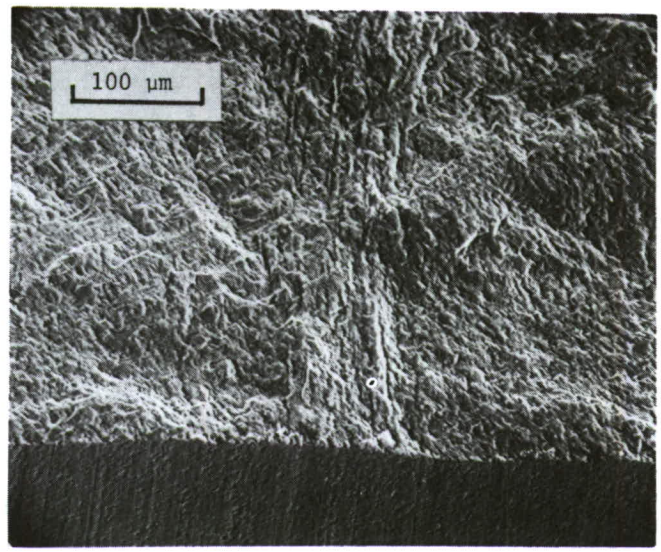

Figure 153. Fracture surface of a control Silcomp CC sample which broke at 292 MPa.

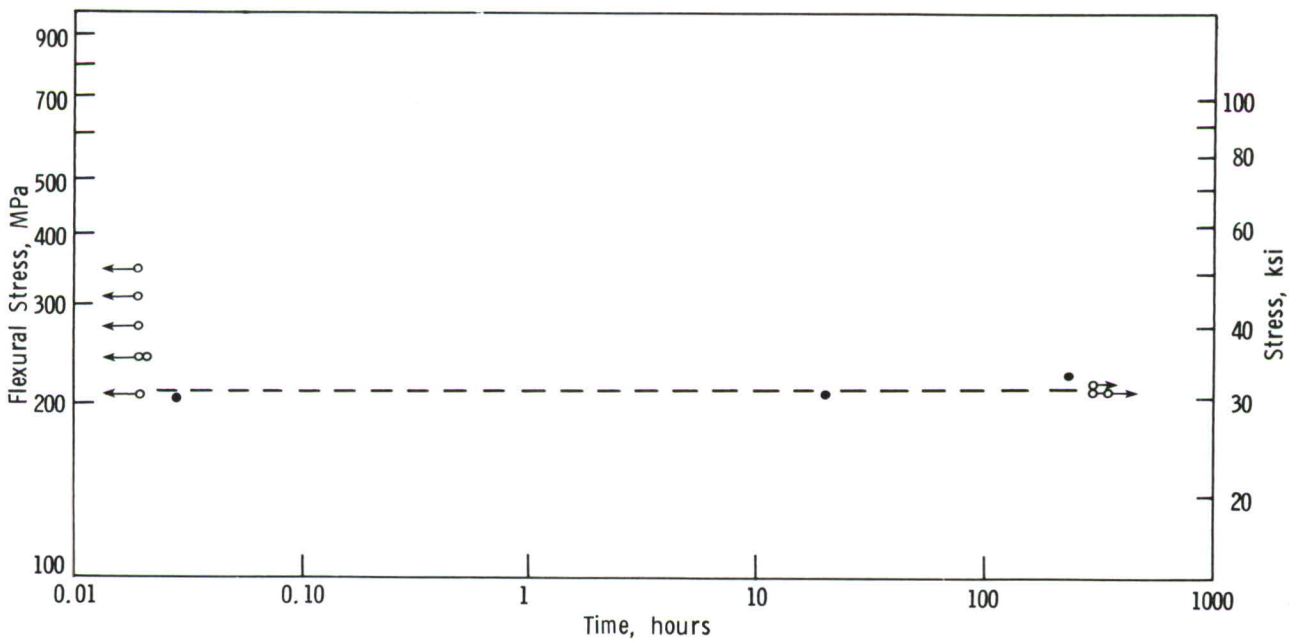

Figure 154. Flexural stress rupture at 1200 C for Silcomp CC.

samples but it was not related to fracture initiation. The oxide was identified as alpha cristobalite. A SEM close-up (Figure 155) shows it is porous and probably interrupted where SiC fibers (or Si or C zones) emerge at the surface.

3. STSR

Time-dependent failures were also obtained in the STSR testing (Figure 156). Failures occurred over the 1000 C to 1300 C range tested. Although a specific origin could not be found in any of the samples that failed, some general observations are of note. Two samples, the 207 MPa at 15 hours at 1000 C and the 207 MPa sample in the 1200 C step, had considerable excess silicon in pockets and veins visible on the fracture surface. Figure 157a shows the fracture surface of the 193 MPa (21 hr at 1300 C) sample and illustrates a silicon vein that intersects the tensile surface. The oxide layer is evident as a smooth, coherent but thin layer (glassy and transparent). The intersection of a fiber pack and the tensile face is shown in Figure 157b. Of interest is the interrupted nature of the oxide layer where the fibers emerge and the high porosity near the fibers compared to the room temperature fracture surfaces (Figure 153). The porosity is evident as elongated pores running parallel with the fibers and also as circular-appearing pores that occur in patches alongside the lengthwise fibers. These latter pores correspond to the emergence of a cross ply in the fracture surface. The porosity, likely the result of oxidation and elimination of residual carbon, was evident in the lower temperature failures as well. The surface oxide was again identified as alpha cristobalite on the high temperature STSR samples.

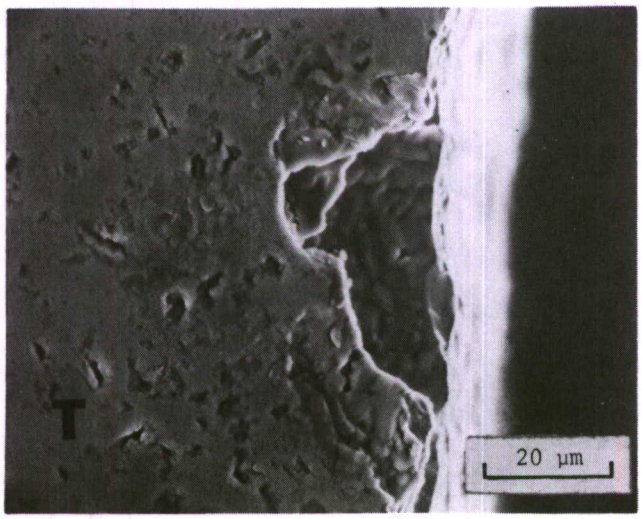

Figure 155. SEM close-up of the tensile face of the sample where it intersects the fracture surface. The oxide layer is porous and interrupted. There is no assurance the large pore was the fracture initiation site for the sample.

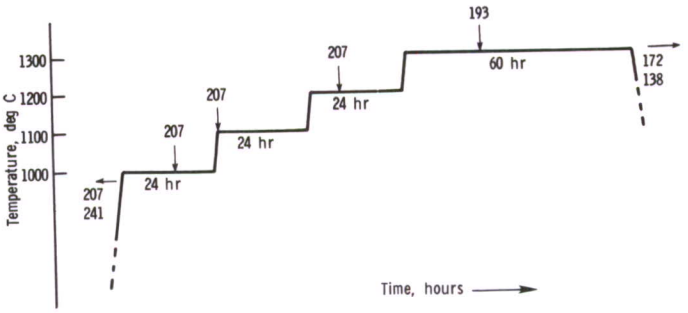

Figure 156. STSR results for Silcomp CC silicon carbide.

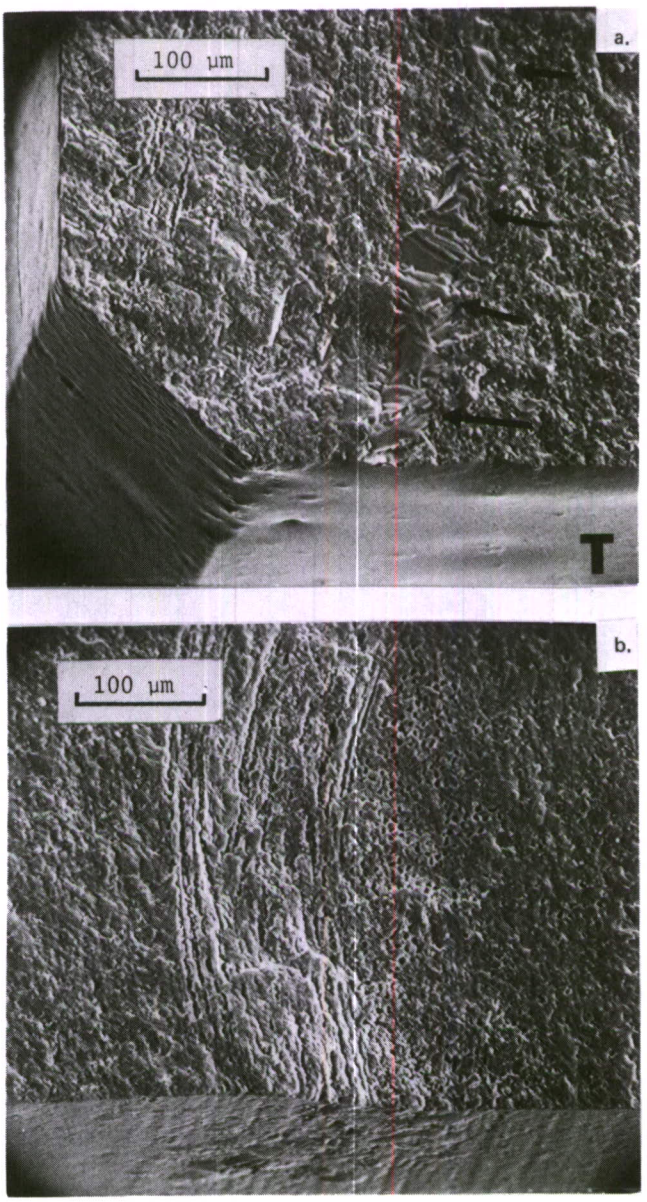

Figure 157. (a) Fracture surface of a Silcomp CC STSR sample that failed at 1300 C and shows a silicon vein running through the sample (arrows). Note the smooth oxide layer on the surface (labeled T); (b) another portion of the sample fracture surface.

Two samples survived intact, but had measurable permanent curvature. The 138 MPa sample had a retained strength of 221 MPa and a maximum strain of 0.2 percent. The 173 MPa sample had a retained strength of 246 MPa and a strain of 0.16 percent.

4. Combined Cycle Procedure

Twelve samples were subjected to the combined cycle durability sequence. Less than 0.002 cm net change in thickness was observed. After the first heat soak cycle, a significant mass loss was observed, 0.0143 gram out of 0.8035 gram, which is due to the elimination of residual carbon in the structure. Thereafter, a slight (0.0005 gram) mass gain per soak cycle was observed with no meaningful mass loss or gain during the thermal fatigue cycling. The surface oxide layer varied in appearance from sample to sample but in general was very irregular and blistered, unlike the stress rupture samples (Figure 158). A close-up examination of the oxide layer (Figure 159) showed the pockmarks or blisters are holes in the oxide layer and that the oxide layer is not smooth but crazed and platelike.

Average retained strength was 211 MPa with a standard deviation of 38 MPa. The Weibull plot of the data indicates one point is uncharacteristically low, but the eleven others can be poorly approximated (85% correlation coefficient) by a line of slope 8.8 (Figure 151). Fracture surface examination again was fruitless with respect to identifying exact failure initiation sites. Close-up examination of the fiber structure reveals the porosity (Figure 160).

5. Discussion

Silcomp CC is a research grade material fabricated from a carbon cloth precursor. As with the CRC grade samples also tested in this study, samples were individually infiltrated after which a screening process was applied by General Electric to discard many samples. Therefore, the samples tested in this study may not accurately reflect larger pieces or the complete flaw distribution to be expected for the material. The Weibull modulus of the samples delivered was a low 6.5, but well described by the two-parameter Weibull line. Failure origins could not be identified. Time-dependent failures occur at temperatures of 1000 C and above and over a range of stresses (unlike the CRC grade). The mechanism of time-dependent failure could not be identified; however, the oxidation of residual carbon and the development of surface-connected porosity that extends throughout the sample may be involved. The critical stress level for survival at 1200 C was similar to that for the CRC grade: 220 MPa, but creep deformations were less for the CC cloth precursor grade. This stress level is well below the room temperature flexural strength (326 MPa).

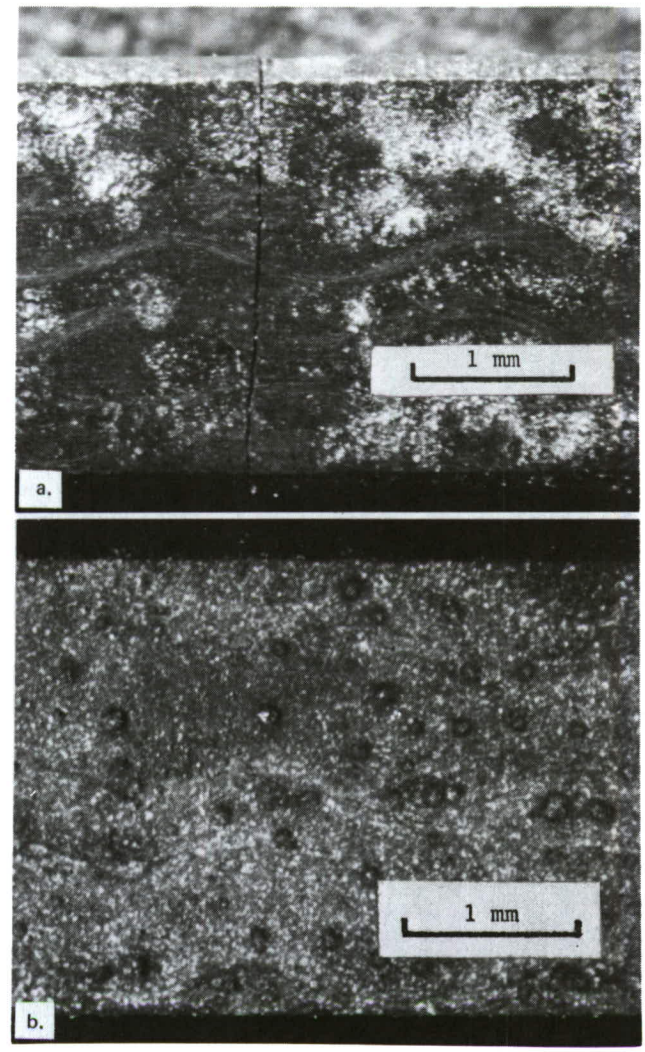

Figure 158. Oxidized surfaces of two combined cycle samples showing the range of surface appearances possible.

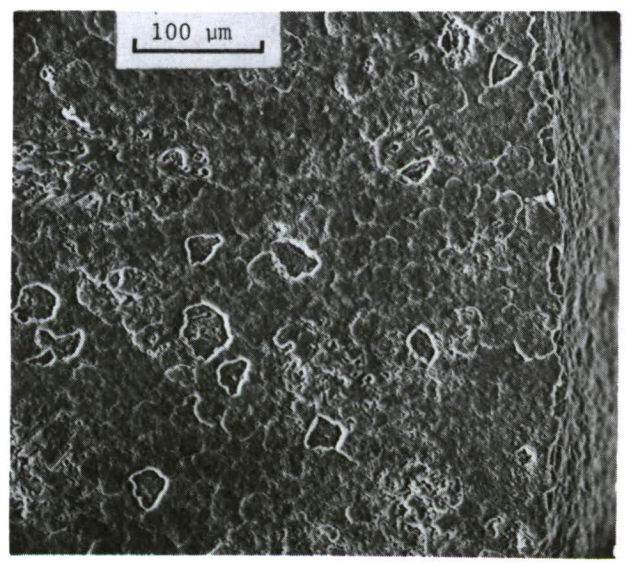

Figure 159. SEM close-up of the oxide at the surface of a combined cycle sample shown in Figure 158a.

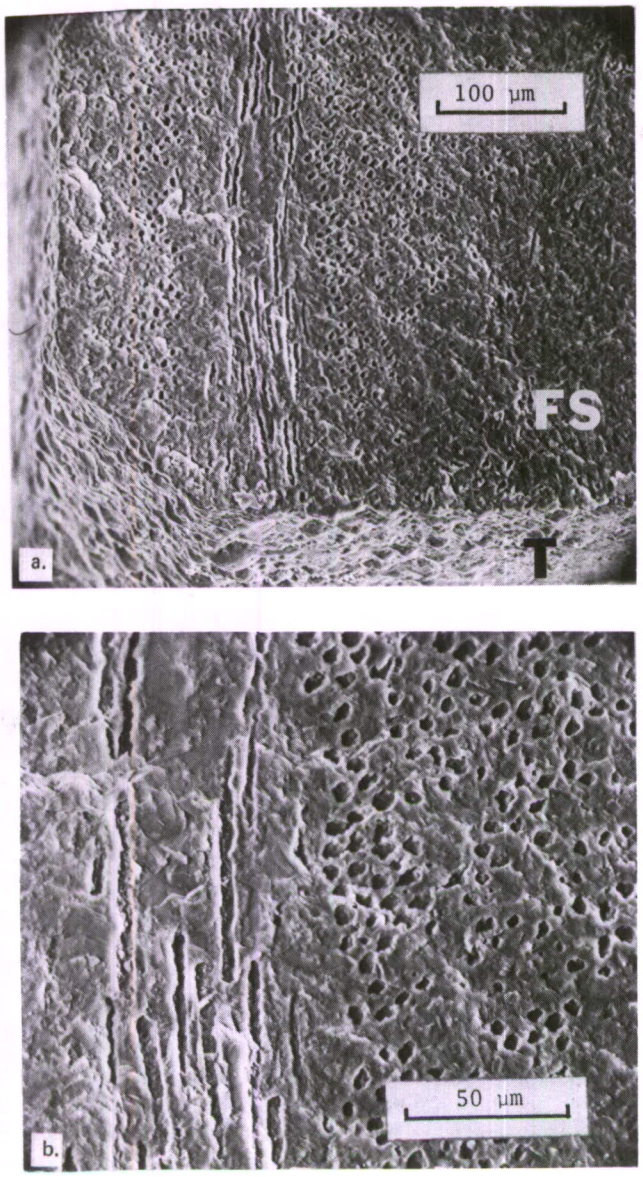

Figure 160. (a) Fracture surface of a Silcomp CC combined cycle sample that was broken for a retained strength measurement. The oxide surface layer is badly blistered and damaged; (b) close-up of the porous fiber structure.

Surface oxide layers were smooth but interrupted at areas where porosity intersected the surface. Permanent deformations of the order of 0.2 percent or less were observed for samples exposed to 1200 C for several hundred hours. No creep cracking was observed in the CC cloth grade, nor was there evidence of slow crack growth. A significant strength loss was observed for samples that were exposed to the combined cycle procedure. The oxide layer was severely affected by that procedure.

V. CONCLUSIONS

The durability-related issues that were directly addressed in this program have been static fatigue in oxidizing environments and combined cycle oxidation-erosion attack. While not truly simulative of any specific service application, the combined cycle procedure did identify problem areas for several materials. The combined cycle procedure clearly highlighted the hazard of extrapolating the oxidation resistance of a material in a static environment to that in a more aggressive situation. For actual applications, there is no substitute for component testing in the service environment, but the combined cycle procedure has merit for quick screening and problem area identification. The ease of experimental testing (laboratory conditions) is an asset. Specific thermal histories can be tailored for the application. Other durability issues considered less exhaustively included creep and static oxidation resistance.

Despite all its limitations (mixed stress state, creep deformation, etc.), the four-point flexural stress rupture test has been shown to be valuable in detecting static fatigue. The ease of testing cannot be understated (although routine good experimental procedure must be applied). The range of crack velocities inherent to the test make it more palatable to use these results for models of life prediction, rather than extrapolating double torsion or variable strain rate strength data. This matter has been addressed in Reference 80. The greatest drawback to the analysis may be the complex stress state due to creep deformation. In addition, the stresses reported in this work have to be considered with respect to the sample size. Larger samples or components will likely fail with lower applied stresses. The use of the STSR procedure quickly identified regimes of time-dependent failure. The imprudence of applying static fatigue resistance at a given temperature to lower temperatures was demonstrated in the case of hot-pressed silicon nitride grade NC 136 and in the reaction-bonded silicon nitrides.

An unexpected result of this program was the number of materials which are sensitive to static fatigue failure at temperatures as low as 1000 C. These include NC 132, NC 136, NCX 34, KBI RBSN, Ford RBSN, NC 203, Carborundum SiC, NC 435, Silcomp CC, and possibly NC 350. Only Silcomp CRC and NC 433 showed definite resistance to failure at low temperature. In some cases, such as the reaction-bonded silicon nitrides, the material seemed more sensitive to failure at 1000 C than at the higher 1200 C temperature. Testing in the future should not neglect *even*

80. WIEDERHORN, S., and RITTER, J., Jr. *Application of Fracture Mechanics Concepts to Structural Ceramics.* Proceedings of the ASTM 11th National Symposium on Fracture Mechanics, Virginia Polytechnic Institute and State University, June 1978.

lower temperatures. Expansion of the STSR testing to include a greater range of temperatures would be reasonable and recommended.

Superficial interpretation of the STSR testing must be avoided, however. For example, the Ford 2.7 RBSN STSR results indicate static fatigue failures occur in the 1000 C to 1100 C range and not in the 1200 C intermediate temperature. The stress rupture testing conducted at 1200 C demonstrates that static fatigue *can* occur. Thus it must be concluded the STSR testing did not include enough samples or, more likely, the low temperature failures mask the 1200 C behavior.

In the materials which did not fail from excessive creep cracking or slow crack growth, it was observed that surface defects, often pores, were the primary origins of failure. This was particularly true in the cases where failure occurred at the lower temperatures such as 1000 C. The materials found to be sensitive to surface-connected porosity were NC 350, KBI RBSN, Ford RBSN, Carborundum 1977 and 1978 SiC, Silcomp CRC, and possibly Silcomp CC. In several of these cases significantly improved retained strengths were measured on samples which survived the stress rupture trials. One is tempted to conclude that the oxide environment is beneficial and promotes flaw healing. There is no assurance that the strength improvement applies at the higher temperatures, however. Furthermore, the indirect evidence suggests the oxidizing environment may *induce* static fatigue failures (surface-connected defects often initiated failure). The oxidation surface heat treating cannot be relied upon for property improvement, even though room temperature strength may be improved. This is particularly true in light of the combined cycle testing, which showed several materials to degrade despite the strength improvement achieved with stress rupture survivors.

The value of the mechanical property data was greatly enhanced by the follow-up fractography. Definite conclusions could not always be made. For example, surface-connected porosity was a common source of time-dependent failure in the materials tested in this study. Close-up examination of many of these pores did not show any difference in their appearance compared to room temperature fractures. It could not be determined whether the pores had grown in size. Very often fracture-initiating defects could not be determined either because the initiation site was not known or no defect could be found in a mirror. Sometimes the specimen would fragment or shatter into many pieces, but reconstruction usually permitted identification of the initial fracture face. In some materials, particularly the composites, it may never be possible to positively determine flaw origins because of the irregular nature of the fracture surface. On the other hand, the success or failure to detect initiation sites can be attributed to the skill of the inspector. During this research program it became apparent that fractographic ability is best acquired by experience. For example, subtle indications of machining damage were often overlooked in the first examinations.

There is a possibility that the mode of viewing may not reveal the defect. In some cases the defect was so small that only the SEM could discern its nature. Alternately, there were numerous instances where the SEM failed to "see" features that were clearly defined by the light microscope and were even visible to the unaided eye. Finally, there were cases where neither the SEM or light microscope readily detected the defect. The best example of this was the very subtle machining damage that can occur with longitudinal grinding (although very careful SEM work did show the markings). Most of the fracture surfaces with suspected surface damage are not as well defined as the cases illustrated in this report.

The matter of the machining damage is serious. The procedure used to prepare these samples was regarded as a sound method and had been reliably used for years. The deleterious effects of transverse machining are well known, but the detrimental effects of longitudinal machining have barely been addressed.[46] The fractographic evidence in this report shows this damage can occur. Sometimes deep striation marks help mark the damage zone. The machining process that produced the striation probably accounted for the subsurface damage as well. Subsequent grinding passes, no doubt, could eliminate most striations, but the subsurface damage would remain because it is much deeper. Even lapped surfaces may have this problem if there was insufficient care in the preliminary slicing and grinding steps. Many of the suspected machining damage flaws in samples broken in this study did not have striations associated with them.

The consequences of this effect are obvious. A machinist may produce two lots of samples cut from the same billet of material, and to all outward appearances (surface finish, sample dimensions, surface markings) the lots would look identical. They may have considerably different strengths, however, depending upon the exact procedure of grinding. Much of the variability in strength data in the literature on otherwise identical materials may be attributed to this effect. Also worth noting is that the chamfer at the corner and the sample sides *must be* longitudinally ground as well as the tensile face or else failure can initiate at these locations. Some of the corner fractures obtained in this program were due to the nonlongitudinal grinding mode used on some chamfers (contrary to specifications).

This matter is of interest to the material scientist who attempts to sample the generic flaws in a material and not artificial defects generated by machining. It may be of academic interest only for the designer who cannot insure longitudinal grinding on components and probably should design on the basis of transverse machining data. For the material scientist the need is evident: a prescribed procedure of ceramic machining of ceramic samples is required to standardize a good procedure (or at least standardize the extent of damage). How to measure quality control may be difficult, other than the outright breaking of the samples.

The value of the mechanical property data was greatly enhanced by the follow-up fractography. For example, the Weibull plots of strength data often indicated a unimodal flaw distribution, that is, a predictable variability in size of a common defect. The fractography nearly always revealed this not to be the case and that, in fact, several different type flaws could be strength controlling. Testing a limited number of samples can hide the bimodal effect. Occasionally one or two "uncharacteristically" low strength samples occurred per group. The temptation is to disregard these data points and consider the "most representative" data. This attitude is wrong and should be discouraged. The single data points may represent a meaningful flaw population that would haunt a manufacturer who scaled up sample size or produced larger quantities. That one or two samples could reflect a genuine flaw population was repeatedly shown in this report. Also of interest is the very broad range of Weibull modulus numbers that are statistically possible as a result of the maximum likelihood estimation analysis (Appendix Tables A-1 and A-4). This further illustrates the undesirability of small sample lots.

Serious consideration was given to estimating K_{Ic} values from flaw size measurements, but this was not done (except in a few instances) for a simple reason. The flaw shapes are usually very irregular (difficult to model analytically) and are subject to wide variability in interpretation. The correlation of fracture mechanics parameters to genuine flaws in ceramics is in its infancy.

This program has demonstrated that all thirteen materials tested have durability-related problems and none can be regarded as the ideal structural ceramic. Most, but not all, have been shown to be susceptible to static fatigue at elevated temperatures. Very often the STSR procedure was successful in identifying unexpected problem temperature regimes (with a minimum amount of effort). The materials resistant to static fatigue, such as NC 350 RBSN or NC 433 SiC, have other limiting factors such as excessive creep deformation or combined cycle damage.

A portent of the difficulty confronting life prediction engineers is indicated by the results of this study. The Carborundum 1978 silicon carbide was shown to fail in static fatigue from two different mechanisms. NC 132 hot-pressed silicon nitride, in addition to immediate overloading, can fail by three modes at high temperature: slow crack growth of preexisting flaws, surface pitting - erosion (stress independent-flaw growth), or alternately by excessive creep deformation. Even if the matter is limited to slow crack growth in NC 132, it has been shown that minor errors in stress or temperature determination can cause major error in life prediction. Couple this with the scatter in initial flaw size and the variability is severe. If the matter is so difficult with a simple laboratory bend test, what will it be like for actual service components? It will be necessary for engineering models to predict temperature to within a few degrees celsius or stress within a few percent. Can this be done accurately for every point in a body with complex temperature and stress distributions? Evidently, generous factors of safety will have to apply, or design codes will be very complex and precise.

The work presented here is the result of experiments on 830 samples. More than 60,000 hours of high temperature exposure were accumulated on 570 of these samples. Most of the stress rupture trials conducted here represent the longest tests reported with these materials while under load. Nevertheless, this data base is extremely small compared to the information required for design purposes. It is encouraging therefore that materials durability work out to 4000 hours exposure is ongoing[81] and component durability work out to 500 hours is underway.[82] Other work of a complementary nature is also underway.[83]

VI. ACKNOWLEDGMENTS

Special thanks are in order to Messrs. Valante Ociepka, Robert Cicerone, and Michael Slavin who performed the bulk of the stress rupture, STSR, and combined cycle testing. These cooperative education students from Northeastern University offered helpful technical evaluation as well and it is hoped this work will spur their studies.

81. BENN, K. W., and CARRUTHERS, W. D. *3500 Hour Durability Testing of Commercial Ceramic Materials.* AiResearch Corporation, NASA Contract DEN 3-27.
82. TRELA, W. *Evaluation of Ceramics for Stator Applications - Gas Turbine Engines.* Ford Motor Company, NASA Contract DEN 3-19.
83. WADE, T. B. *Property Screening and Evaluation of Ceramic Turbine Engine Materials.* IIT Research Institute, AFML Contract F33615-75-C-5196.

Mr. George Gazza, Dr. Donald Messier, and Dr. Edward Lenoe of AMMRC were helpful in discussions regarding the data interpretation. Technical assistance by Messrs. A. Connolly, B. Strauss, and R. Brockelman is appreciated.

Finally, the author extends his appreciation to Dr. R. Nathan Katz of the Ceramic Division, AMMRC, for his guidance and patience through the three years this program has been underway.

APPENDIX. TABULATED SUMMARY OF DATA

Room temperature mechanical property data is summarized in Table A-1 for the silicon nitrides and in Table A-2 for the silicon carbides. A terse summary of static fatigue results is in Table A-3 for silicon nitrides and carbides. Finally, Table A-4 outlines the combined cycle results for the silicon nitrides and silicon carbides.

Bar graph representation of the four-point flexural strength of silicon nitrides and carbides is in Figure A-1. The large arrow marks the mean strength. The coefficient of variation (in percent) is labelled at the end of each bar and the Weibull modulus (two-parameter, maximum likelihood estimator) is labelled underneath each bar.

For some of the materials, a solid triangle marks the mean retained strength after combined cycle exposure. The solid triangle is labelled with a percentage which is the strength loss relative to the reference mean strength.

Table A-1. ROOM TEMPERATURE MECHANICAL PROPERTIES OF SILICON NITRIDES

(1 MPa = 1 MN/m^2 = 0.145 ksi)

	Norton NC 132 Lot A*	Norton NC 132 Lot B†	Norton NC 136	Norton NCX 34	Norton NC 350	KBI RBSN	Ford 2.7 RBSN
Density (g/cm^3)	3.23	3.19	3.37	3.37	2.53	2.58	2.77
Standard deviation	0.015	0.011	0.015	0.008	0.019	0.043	0.014
Room Temperature Flexural Strength (MPa)							
Average	825	714	737	921	294	206	288
Standard deviation	137	60	253	24	41	15	38
High	1010	814	914	947	351	228	339
Low	543	615	253	871	210	176	200
Number of trials	24	16	14	10	16	25	16
Weibull Parameters							
1. Least-squares method							
Modulus	Bimodal	12.4	Multimodal	36.2	7.2	14.8	Bimodal
Correlation coefficient		(97%)		(95%)	(98%)	(98%)	
2. Maximum likelihood estimator							
Modulus	-	12.5	-	47.3	8.4	15.7	-
90% confidence interval		(8.1-16.1)		(26.2-64.1)	(5.5-10.9)	(11.4-19.5)	
Characteristic value (MPa)	-	741	-	932	311	212	-
90% confidence interval		(713-771)		(919-945)	(294-330)	(207-217)	-
Strength-Controlling Defects	Corner Chips; Machining Damage	Corner Chips; Machining Damage	Corners? Machining Damage; Processing Cracks	Corners; Machining Damage	Pores; Machining Damage	Pores; Silicon? Others	Corners; Pores; Others?
Elastic Modulus (x10^5 MPa)‡	3.2	-	3.1	3.1	1.8	2.0	2.1
Poisson's Ratio‡	0.27	-	0.27	0.27	0.22	0.22	0.22

*Stress rupture lot
†Combined cycle lot
‡Determined by measuring the longitudinal and shear velocity of an ultrasonic pulse through a bend bar sample. A minimum of two were tested per material.

Table A-2. ROOM TEMPERATURE MECHANICAL PROPERTIES OF SILICON CARBIDES

(1 MPa = 1 MN/m^2 = 0.145 ksi)

	Norton NC 203 Lot A*	Norton NC 203 Lot B†	Carborundum Alpha 1977	Carborundum Alpha 1978	Norton NC 433	Norton NC 435	G.E. Silcomp CRC	G.E. Silcomp CC
Density (g/cm^3)	3.36	3.36	3.11	3.13	3.06	2.99	2.98	2.95
Standard deviation		0.016	0.020	0.013	0.013	0.020	0.046	0.036
Room Temperature Flexural Strength (MPa)								
Average	683	582	375	363	317	342	389	326
Standard deviation	65	62	52	45	65	53	64	52
High	825	735	431	449	383	419	488	403
Low	645	477	271	224	169	282	266	228
Number of trials	10	24	20	36	37	14	13	20
Weibull Parameters								
1. Least-squares method								
Modulus	9.9‡	10.1‡	Bimodal	10.6**	14.9††	Multimodal	5.9	6.5
Correlation coefficient		(95%)		(96%)	(95%)		(98%)	(98%)
2. Maximum likelihood estimator								
Modulus	9.0‡	9.2		9.6	11.9††		6.8	7.1
90% confidence interval	(5.0-12.2)	(6.6-11.4)		(7.4-11.6)	(9.1-14.4)		(4.2-9.0)	(4.9-9.0)
Characteristic value (MPa)	712‡	610		384	350††		414	348
90% confidence interval	(661-767)	(584-636)		(372-397)	(341-359)		(383-499)	(326-369)
Strength Controlling Defects	Machining Damage	Machining Damage	Pores; Inclusions; other	Pores; Large Grains	Large Grains; Silicon? others?	Silicon Veins; other	Fiber Clumps; Porosity; Sllicon? others?	Unknown
Elastic Modulus†† (x10^5 MPa)	4.6		4.1	4.2	3.9	3.5	3.7	3.2-3.4
Poisson's Ratio††	0.17		0.15	0.16	0.18	0.18	0.17-0.18	0.14-0.17

*Combined cycle lot
†Stress rupture lot
‡Poor fit
**35 point only (see text) probably bimodal
††34 point only (see text) probably bimodal
‡‡Determined by measuring the longitudinal and shear velocity of an ultrasonic pulse through a bend bar. A minimum of two samples per material were tested.

Table A-3. SUMMARY OF STRESS RUPTURE AND STSR RESULTS

Material	1200 C Stress Rupture	STSR	Comments
NC 132 HPSN	TD degradation; A pattern of time to failure inversely related to stress raised to a power; Slow crack growth; Gross creep deformation	TD failures over 1000 C to 1400 C; TD strength degradation; Slow crack growth; Gross creep 1300+ C	Extensive analysis of slow crack growth in text. Combined cycle testing showed an alternate mechanism of degradation: surface pitting.
NC 136 HPSN	Limited TD failures over narrow stress range which is below RT strength; Some creep deformation; Survivors had retained RT strength similar to control strength; Unusual oxidation markings	Severe static fatigue at 1000 C; Irregular fracture surfaces	
NCX 34 HPSN	TD failures over a narrow stress range which is well below RT strength; Some slow crack growth; Moderate creep deformation	TD failures over 1000 C to 1300 C at stresses well below RT strength; Gross creep 1300+ C; Unidentified oxide phase	Nonuniform bands cause excessive creep and failure
NC 350 RBSN	No TD failures; Cut-off stress is over the RT strength; Small creep deformation; Survivors had higher retained RT strengths than the control strength	High resistance to TD failure; Small creep deformation for survivors; Survivors had higher retained RT strengths than the control strength	Flaw healing; Stress rupture trials at 1000 C also showed good resistance to TD failure, but at stress levels only slightly greater than RT strengths; Failures from surface-connected porosity; Combined cycle testing showed strength degradation
KBI RBSN	Failures over a narrow stress range which is slightly less than control RT strength; Small creep deformation; Survivors had retained RT strength same as control strength	Two failure regimes: 1000 C to 1100 C or 1300 C to 1400 C; Failures stresses are somewhat below control RT strength; Small creep deformations for survivors	Pore structure different from NC 350; Stress rupture trials at 1000 C indicate failures over a narrow stress range which is near control RT strengths; Failures are from surface-connected porosity; Combined cycle results show strength degradation
Ford 2.7 RBSN	With exception of one trial, TD failures occur over a narrow stress band, which is about the same as the control strength; Minimal creep deformation; Survivors had higher retained RT strength than control strength	TD failures in the 1000 C to 1100 C range at stresses somewhat below control RT strength; Small creep deformation; Survivors had retained RT strength similar to control strength	Insufficient samples for 1000 C stress rupture trials; Failures from surface defects, usually pores; Combined cycle testing resulted in strength degradation
NC 203 HPSiC	Many TD failures, but confined to a narrow stress band which is well below the control RT strength; Negligible creep deformation; Survivors had higher retained RT strength than control strength	Many TD failures over 1000 C to 1400 C; Stress levels are substantially less than control RT strength; Possible RT strength enhancement for survivors	Additional stress rupture trials at 1200 C recommended; Minor pitting observed; Combined cycle testing resulted in no strength degradation; Static oxidation heals surface damage resulting in major strength improvement at RT
Carborundum Alpha SiC 1977	TD failures over a narrow stress range that is less than the control RT strength; Negligible creep deformation; Minor pitting; Survivors had retained RT strength well above control strength; Unidentified oxide phase	TD failures over 1000 C to 1400 C range, some stresses well below control RT strength; Negligible creep deformation; Retained strength of survivor is higher than control strength; Unidentified different oxide phase	Slow crack growth was observed in some, but not all samples; Failures were often from surface pores
Carborundum Alpha SiC 1978	TD degradation; A pattern of time to failure inversely related to stress raised to a power	TD failures over all temperatures 1000 C to 1400 C at stresses well below RT control strength; Negligible permanent deformation; Retained strength of two survivors are identical and somewhat greater than the control strength	Two mechanisms of TD failure: low temperature failure is from surface-connected defects, usually porosity and possibly from large grains and/or silicon; High temperature failure from slow crack growth
NC 433 SiC	No TD failures; Cut-off stress is same as control RT strength; Moderate creep deformation; Survivors had higher retained RT strengths than control strength	Only one TD failure; Little or no strength loss relative to RT control strength; Moderate creep deformation; Survivor samples had higher retained strengths than control strength	Coarse SiC grains
NC 435 SiC	TD degradation, however, the range of stress is not significantly less than the RT control strength; Moderate creep deformation	TD failures over all temperatures, 1000 C to 1300 C; some stresses below the RT control strength; Considerable creep deformation	Finer SiC grains, but more free Si than NC 433; More creep deformation than NC 433, creep cracking evident; Static fatigue behavior much worse than NC 433; Silicon veins in some samples; Unusual fracture surface markings imply irregular slow crack growth
Silcomp CRC	Only one failure, but critical stress level is substantially less than control strength; Moderate creep deformations; Survivors had lower retained RT strength than control strength	Material resistance to failure for temperatures <1250 C; Failures at 1250 C and higher at stresses substantially less than control RT strength; Samples that were exposed to 1300 C and above had gross permanent deformation; Survivors had lower retained RT strengths than control strength	Surface porosity due to fiber aggregates source of degradation on some samples; Unusual fracture surface markings - slow crack growth?; Excessive creep cracking evident on some samples
Silcomp CC	Limited failures over a narrow stress range which is substantially less than the control RT strength; Some creep deformation; Survivors had lower retained RT strength than control strength	Failures over all temperatures 1000 C to 1300 C at stress levels well below control RT strengths; Some creep deformation; Survivors had lower retained RT strength than control strength	Unknown failure initiation sites; Probably involves oxidation into surface-connected fiber bundles; Combined cycle samples experienced considerable strength degradation

Abbreviations RT = Room Temperature
TD = Time Dependent

Table A-4. SUMMARY OF COMBINED CYCLE TEST RESULTS

Material	Average Strength (MPa)	Standard Deviation (MPa)	LSq* Weibull Modulus	MLE† Weibull Modulus	MLE† Characteristic Strength (MPa)
Silicon Nitrides					
NC 132 HPSN					
Control	714	60	12.4	12.5	741
Exposed	348	36	9.6 (99%)	11.2 (6.7-14.9)	363 (345-382)
Comments:	A 51% strength reduction. Exposed sample failed from surface pits.				
NC 350 RBSN					
Control	294	41	7.2	8.4	311
Exposed	244	37	6.4 (98%)	7.0 (4.0-9.4)	258 (237-283)
Comments:	A 17% strength reduction. Preexisting flaws (pores and machining marks) were enlarged. Cycling was deleterious as opposed to a docile furnace environment.				
KBI RBSN					
Control	206	15	14.8	15.7	212
Exposed	166	12	14.2 (98%)	17.0 (9.8-22.8)	170 (164-177)
Comments:	A 19% strength reduction. Surface-connected porosity was enlarged.				
Ford 2.7 RBSN					
Control	288	38	Bimodal		
Exposed	246	25	Bimodal		
Comments:	A 15% strength reduction. The similarity of Weibull plots and the fractography indicate pore enlargement occurs. Cycling was deleterious as opposed to the static furnace environment.				
Silicon Carbides					
NC 203 HPSiC					
Control	683	65	9.9‡	9.0	712
Exposed	706	85	8.3 (99%)	8.9 (5.3-11.9)	741 (696-792)
Comments:	No degradation! Unknown strength-controlling defects. Shallow pitting was evident and one sample failed from a pit. Alternate data indicates degradation will occur with more cycling.				
Silcomp CC					
Control	326	52	6.6	7.1	348
Exposed	211	38	‡	7.0‡ (4.1-9.3)	225 (207-245)
Comments:	A 35% degradation. Unknown initiation sites. Possibly oxidation into the interior along a fiber bunch.				

*Least squares fitted line through the plots shown in the text. Number in parentheses is the correlation coefficient.
†Maximum likelihood estimator (unbiased). Numbers in parentheses are the 90% confidence interval.
‡Poor fit

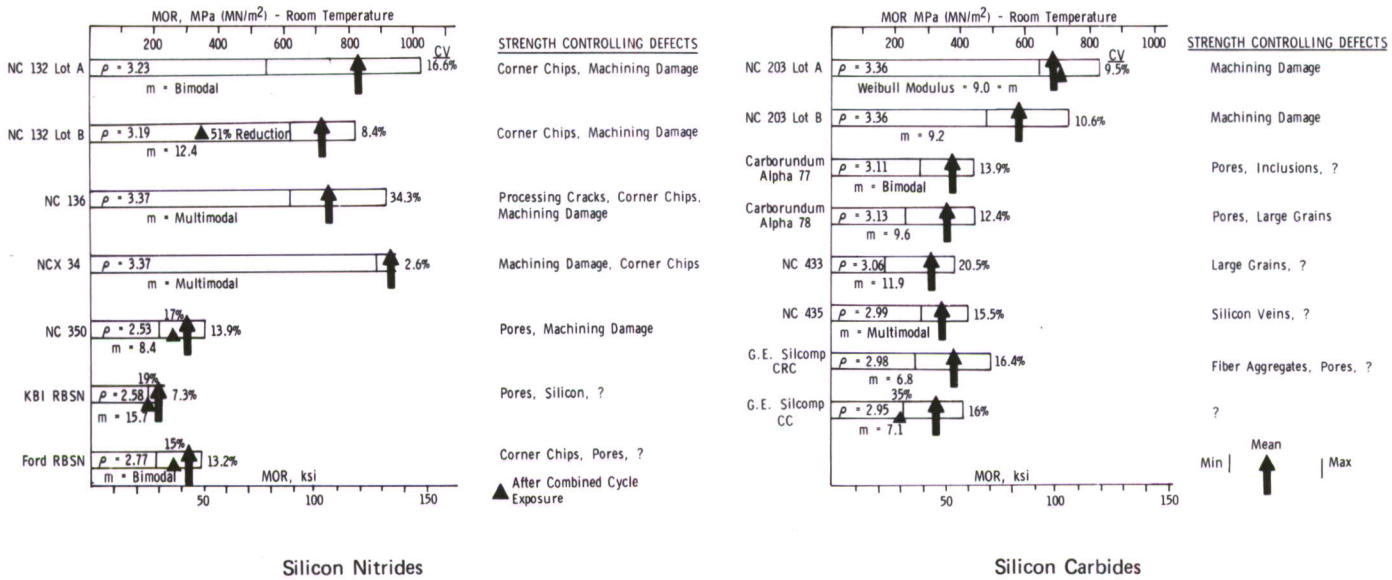

Figure A-1. Varying maturity.

LITERATURE CITED

1. MILLER, D. et al. *Brittle Materials Design, High Temperature Gas Turbine Materials Technology.* Westinghouse Corporation, Contract DAAG46-71-C-0162, Final Report, AMMRC CTR 76-32, Volume IV, December 1976.
2. QUINN, G. D., and KATZ, R. N. *Stepped Temperature Stress-Rupture Testing of Silicon Based Ceramics.* Am. Cer. Soc. Bull., v. 51, no. 11, 1978, p. 1057.
3. QUINN, G. D. *Guide to the Construction of a Simple 1500 C Test Furnace.* Army Materials and Mechanics Research Center, AMMRC TN 77-4, August 1977.
4. SCHENCK, H., Jr. *Theories of Engineering Experimentation.* McGraw Hill Company, New York, 1968.
5. QUINN, G. D., KATZ, R. N., and LENOE, E. M. *Thermal Cycling Effects, Stress Rupture and Tensile Creep in Hot-Pressed Silicon Nitride.* Proceedings of the DARPA/NAVSEA Ceramic Gas Turbine Demonstration Engine Program Review, Castine, Maine, MCIC 78-36, August 1977, p. 715-737.
6. JOHNSON, C. F., and HARTSOCK, D. L. *Thermal Response of Ceramic Turbine Stators* in Ceramics for High Performance Applications, J. J. Burke, A. E. Gorum, and R. N. Katz, ed., Brook Hill Publishing Company, Chestnut Hill, Massachusetts, 1974, p. 549.
7. Instruction Manual 5040 for Pyro 650, Instrument Development Laboratories, Inc., Attleboro, Massachusetts, April 1961.
8. GAZZARA, C. P., and MESSIER, D. R. *Determination of Phase Content of Si_3N_4 by X-ray Diffraction Analysis.* Am. Cer. Soc. Bull., v. 56, no. 9, 1977, p. 777.
9. GAZZA, G. E. *Hot Pressed Si_3N_4* J. Am. Cer. Soc., v. 56, no. 12, 1973, p. 662.
10. McLEAN, A. F., FISHER, E. A., BRATTON, R. J., and MILLER, D. G. *Brittle Materials Design, High Temperature Gas Turbine.* Ford Motor Company, Contract DAAG-46-71-C-0112, Interim Report No. 8, AMMRC CTR 75-28, 1975, p. 138-139.
11. LANGE, F. F., SINGHAL, S. C., and KUZNICKI, R. C. *Phase Relationships and Stability in the Si_3N_4-SiO_2-Y_2O_3 Pseudoternary System.* J. Am. Cer. Soc., v. 60, no. 5-6, 1977, p. 249-252.
12. LANGE, F. F., SINGHAL, S. C., and KUZNICKI, R. C. *Phase Relations and Stability Studies in the Si_3N_4-SiO_2-Y_2O_3 Pseudo-Ternary System.* ARPA-Westinghouse Electric Corporation, Contract N00014-74C-0284, Technical Report No. 6, April 1976.
13. WEAVER, G., and LUCEK, J. *Optimization of Hot Pressed Si_3N_4-Y_2O_3 Materials.* Am. Cer. Soc. Bull., v. 57, no. 12, 1978, p. 1131.
14. WASHBURN, M., FREDRIKSSON, J., and ALLIEGRO, R. *Properties and Applications of Reaction-Bonded Silicon Nitride.* Presented at the 74th Annual Meeting of the American Ceramic Society, Washington, D.C., 6-11 May 1972.
15. WASHBURN, M., and BAUMGARTNER, H. *High Temperature Properties of Reaction-Bonded Silicon Nitride* in Ceramics for High Performance Applications, J. J. Burke, A. E. Gorum, and R. N. Katz, ed., Brook Hill Publishing Company, Chestnut Hill, Massachusetts, 1974, p. 486.
16. HAUCK E., *Future in Ceramic Gas Turbine Design.* Gas Turbine World, September 1974, p. 18.
17. McLEAN, A. F., FISHER, E. A., BRATTON, R. J., and MILLER, D. G. *Brittle Materials Design, High Temperature Gas Turbine.* Ford Motor Company, Contract DAAG46-71-C-0162, Interim Report No. 7, AMMRC CTR 75-8, July to December 1974.
18. McLEAN, A. F., BAKER, R., BRATTON, R. J., and MILLER, D. G. *Brittle Materials Design, High Temperature Gas Turbine.* Ford Motor Company, Contract DAAG46-71-C-0112, Interim Report No. 9, AMMRC CTR 76-12, July to December 1975.
19. McLEAN, A. F., and BAKER, R. *Brittle Materials Design, High Temperature Gas Turbine.* Ford Motor Company, Contract DAAG46-71-C-0142, Interim Report No. 10, AMMRC CTR 76-31, January to June 1976.
20. McLEAN, A. F., and FISHER, E. A. *Brittle Materials Design, High Temperature Gas Turbine.* Ford Motor Company, Contract DAAG46-71-C-0162, Interim Report No. 11, AMMRC CTR 77-20, July to December 1976.
21. MANGELS, J. *Development of Injection-Molded Reaction-Bonded Si_3N_4* in Ceramics for High Performance Applications II, J. J. Burke, E. M. Lenoe, and R. N. Katz, ed., Brook Hill Publishing Company, Chestnut Hill, Massachusetts, 1978, p. 113.
22. KRAFT, E. H., and DOOHER, G. I. *Mechanical Response of High Performance Ceramics.* Presented at Second International Conference of Mechanical Behavior of Materials, Boston, Massachusetts, 16-20 August 1976.
23. KRAFT, E. H., and COPPOLA, J. A. *Thermomechanical Properties of Sintered Alpha Silicon Carbide* in Ceramics for High Performance Applications II, J. J. Burke, E. M. Lenoe, and R. N. Katz, ed., Brook Hill Publishing Company, Chestnut Hill, Massachusetts, 1978, p. 1023.
24. COPPOLA, J. A., SRINIVASAN, M., FABER, K., and SMOAK, R. *High Temperature Properties of Sintered Alpha Silicon Carbide.* Presented at International Symposium on Factors in Densification and Sintering of Oxide and Non-Oxide Ceramics, Hakone, Japan, October 1978.
25. JANOVICZ, M. A. *Ceramic Applications in Turbine Engines.* Detroit Diesel Allison Division, NASA Contract DEN 3-17, Progress Report, June 1978, p. 39.
26. ALLIEGRO, R. A. *Processing and Fabrication of Non-Hot Pressed SiC Ceramics* in Ceramics for High Performance Applications, J. J. Burke, A. E. Gorum, and R. N. Katz, ed., Brook Hill Publishing Company, Chestnut Hill, Massachusetts, 1974, p. 253-264.
27. TORTI, M., LUCEK, J., and WEAVER, G. *Densified Silicon Carbide - An Interesting Material for Diesel Applications.* SAE Technical Paper 780071, presented at SAE Congress and Exposition, Detroit, Michigan, March 1978.
28. TORTI, M. *The Effect of Fabrication Procedures Upon Mechanical Properties of Si_3N_4 and SiC Turbine Components.* Presented at Third Materials Conference Turbine Application, University of Michigan, Ann Arbor, Michigan, November 1974.
29. MEHAN, R. L. *Anistropic Behavior of Si/SiC Ceramic Composites.* Am. Cer. Soc. Bull., v. 56, no. 2, 1977, p. 211.
30. MEHAN, R. L. *Effect of SiC Content and Orientation on the Properties of Si/SiC Ceramic Composites.* J. Mat. Sci., v. 13, 1978, p. 358.
31. HILLIG, W. et al. *Silicon/Silicon Carbide Composites.* Am. Cer. Soc. Bull., v. 54, no. 12, 1975, p. 1054.
32. HILLIG, W. *Tailoring of Si/SiC Composites for Turbine Applications* in Ceramics for High Performance Applications II, J. J. Burke, E. M. Lenoe, and R. N. Katz, ed., Brook Hill Publishing Company, Chestnut Hill, Massachusetts, 1978, p. 989.
33. SMITH, F., EMERY, A., and KOBAYASHI, A. *Stress Intensity Factors for Semicircular Cracks, Part II - Semiinfinite Solid.* J. Appl. Mech., Trans. ASME Series E, v. 34, December 1967, p. 953.
34. HENSHALL, J., ROWCLIFFE, D., and EDINGTON, J. *The Measurement of K_{Ic} and Subcritical Crack Propagation Rates in Hot-Pressed SiC and Si_3N_4* in Fracture, 1977, v. 3, ICF4, Waterloo, Canada, June 1977, p. 875.
35. EVANS, A., and WIEDERHORN, S. *Crack Propagation and Failure Prediction in Silicon Nitride at Elevated Temperatures.* J. Mat. Sci., v. 9, 1974, p. 270.
36. LARSEN, D., and WALTHER, G. *Property Screening and Evaluation of Ceramic Turbine Engine Materials.* IIT Research Institute, AFML Contract F33615-75-C-5196, Interim Report No. 6, July 1978, p. 667.
37. DAVIDGE, R., McLAREN, J., and TAPPIN, G. *Strength Probability Time (SPT) Relationships in Ceramics.* J. Mat. Sci., v. 8, 1973, p. 1699.
38. RITTER, J., Jr. *Engineering Design and Fatigue Failure of Brittle Materials* in Fracture Mechanics of Ceramics IV, R. Bradt, D. Hasselman, and F. Lange, ed., Plenum Press, New York, 1978, p. 667.
39. RITTER, J., Jr,, and JAKUS, K. *Overview of Lifetime Predictions for Silicon Nitride.* Proceedings of 1977 DARPA/NAVSEA Ceramic Gas Turbine Demonstration Engine Program Review, Castine, Maine, MCIC 78-36, August 1977, p. 701.
40. JAKUS, K., COYNE, D., and RITTER, J., Jr. *Analysis of Fatigue Data for Lifetime Predictions for Ceramic Materials.* J. Mat. Sci., v. 13, 1978, p. 2071.
41. JAKUS, K., and RITTER, J., Jr. *Static Fatigue of Si_3N_4.* J. Am. Cer. Soc., v. 61, no. 5-6, May 1978, p. 274.
42. ANNIS, C., and CARGILL, J. *Modified Double Torsion Method for Measuring Crack Velocity in NC 132 (Si_3N_4)* in Fracture Mechanics of Ceramics IV, R. Bradt, D. Hasselman, and F. Lange, ed., Plenum Press, New York, 1978, p. 737.
43. TIGHE, N. *The Structure of Slow Crack Interfaces in Silicon Nitride.* J. Mat. Sci., v. 13, 1978, p. 1455.
44. MENDIRATTA, M. G. *Use of Controlled Surface Flaws in Studying Slow Crack Growth in Ceramics.* Systems Research Laboratories, AFML Contract F33615-75-C-1005, Quarterly Progress Report 3165-10, May 1977.
45. GOVILLA, R., and ELDER, R. *Tensile Stress Rupture Testing of Hot-Pressed Si_3N_4 at 1200°C.* Presented at the 81st Annual Meeting of the American Ceramic Society, Cincinnati, Ohio, 2 May 1979.

46. RICE, R. et al. *Fractography of Si_3N_4 and SiC* in Ceramics for High Performance Applications II, J. J. Burke, E. M. Lenoe, and R. N. Katz, ed., Brook Hill Publishing Company, Chestnut Hill, Massachusetts, 1978, p. 669.
47. RICHERSON, D., and YONUSHONIS, T. *Properties of Silicon Nitride Rotor Blade Materials.* Proceedings of the 1977 DARPA/NAVSEA Ceramic Gas Turbine Demonstration Program Review, Castine, Maine, MCIC 78-36, August 1977, p. 193.
48. MARRS, G., and SMITH, C. *A Study of Local Stresses Near Surface Flaws in Bending Fields* in Stress Analysis and Growth of Cracks, Proceedings of 1971 National Symposium on Fracture Mechanics, Part I, ASTM STP 513, 1972, p. 22.
49. GRANDT, A., and SINCLAIR, G. *Stress Intensity Factors for Surface Cracks in Bending* in Stress Analysis and Growth of Cracks, Proceedings of 1971 National Symposium on Fracture Mechanics, Part I, ASTM STP 513, 1972, p. 37.
50. PARIS, P., and SIH, G. *Stress Analysis of Cracks* in Fracture Toughness Testing and Its Applications, ASTM Special Technical Publication No. 381, 1964, p. 30.
51. PETROVIC, J., JACOBSON, L., TALTY, P., and VASUDEVAN, A. *Controlled Surface Flaws in Hot-Pressed Silicon Nitride.* J. Am. Cer. Soc., v. 58, no. 3, 1975, p. 113.
52. EVANS, A., RUSSEL, L., and RICHERSON, D. *Slow Crack Growth in Ceramic Materials at Elevated Temperatures.* Met. Trans., v. 6A, April 1975, p. 707.
53. FREIMAN, S., MECHOLSKY, J., McDONOUGH, W., and RICE, R. *Effect of Oxidation on the Room Temperature Strength of Hot Pressed Si_3N_4/MgO and Si_3N_4-ZrO_2 Bodies* in Ceramics for High Performance Applications II, J. J. Burke, E. M. Lenoe, and R. N. Katz, ed., Brook Hill Publishing Company, Chestnut Hill, Massachusetts, 1978, p. 1069.
54. RICHERSON, D., and YONUSHONIS, T. *Environmental Effects on the Strength of Silicon Nitride Materials.* Proceedings of the 1977 DARPA/NAVSEA Ceramic Gas Turbine Demonstration Program Review, Castine, Maine, MCIC 78-36, August 1977, p. 247.
55. FREIMAN, S., WILLIAMS, A., MECHOLSKY, J., and RICE, R. *Fracture of Si_3N_4 and SiC.* Proceedings of the Sixth International Materials Symposium, Ceramics Microstructures, 1976, University of California, Berkeley, California, August 1976.
56. WILLIAMS, R., and UY, J. *Ceramic Materials Characterization* in Ceramics for High Performance Applications II, J. J. Burke, E. M. Lenoe, and R. N. Katz, ed., Brook Hill Publishing Company, Chestnut Hill, Massachusetts, 1978, p. 151.
57. WADE, T. *Property Screening and Evaluation of Ceramic Vane Materials.* IIT Research Institute, AFML Contract F33615-75-C-5196, Interim Report No. 2, July 1976.
58. TORTI, M. *The Effect of Fabrication Procedures Upon Mechanical Properties of Si_3N_4 and SiC Turbine Components.* Presented at Third Materials Conference, Turbine Applications, University of Michigan, Ann Arbor, Michigan, October 1974.
59. KNOCH, H., and GAZZA, G. E. *Carbon Impurity Effects on the Thermal Degradation of a Si_3N_4-Y_2O_3 Ceramic.* Submitted to Amercian Ceramic Society.
60. GAZZA, G. E., KNOCH, H., and QUINN, G. D. *Hot Pressed Si_3N_4 with Improved Thermal Stability.* Am. Cer. Soc. Bull., v. 57, no. 11, 1978, p. 1059.
61. BANSAL, G. K. *Effect of Flaw Shape of Ceramics.* J. Am. Cer. Soc., v. 59, no. 1-2, 1976, p. 87.
62. IRWIN, G. *Crack Extension Force for a Part Through Cracking Plate.* Trans. ASME, Series E, 1962, p. 651.
63. ROOKE, D., and CARTWRIGHT, D. *Compendium of Stress Intensity Factors.* Published by Her Majesty's Stationery Office, Ministry of Defense, Hillington Press, Uxbridge, Middlesex, United Kingdom, 1976.
64. LARSEN, D., and WALTHER, G. *Property Screening and Evaluation of Ceramic Turbine Engine Materials.* IIT Research Institute, AFML Contract F33615-75-C-5196, Interim Report No. 5, January 1978.
65. RICHERSON, D., SCHULDIES, J., YONUSHONIS, T., and JOHANSEN, K. *ARPA/NAVY Ceramic Engine Materials and Process Development Summary* in Ceramics for High Performance Applications II, J. J. Burke, E. M. Lenoe, and R. N. Katz, ed., Brook Hill Publishing Company, Chestnut Hill, Massachusetts, 1978, p. 625.
66. BENN, K. W., and CARRUTHERS, W. D. *3500 Hour Durability Testing of Commercial Ceramic Materials.* Third Quarterly Progress Report, September to November 1978, AiResearch Manufacturing Company of Arizona, NASA Contract DEN 3-27, 15 December 1978.
67. LARSEN, D., BORTZ, S., RUH, R., and TALLAN, N. *Evaluation of Four Commercial Si_3N_4 and SiC Materials for Turbine Applications* in Ceramics for High Performance Applications II, J. J. Burke, E. M. Lenoe, and R. N. Katz, ed., Brook Hill Publishing Company, Chestnut Hill, Massachusetts, 1978, p. 651-668.
68. YONUSHONIS, T., and RICHERSON, D. *Strength of Reaction-Bonded Silicon Nitride.* Proceedings of the 1977 DARPA/NAVSEA Ceramic Gas Turbine Demonstration Engine Program Review, Castine, Maine, MCIC 78-36, August 1977, p. 219.
69. LARSEN, D., and WALTHER, G. *Property Screening and Evaluation of Ceramic Vane Materials.* IIT Research Institute, AFML Contract F33615-75-C-5196, Interim Report No. 4, October 1977.
70. McLEAN, A., FISHER, E. A., and BRATTON, R. J. *Brittle Materials Design, High Temperature Gas Turbine.* Ford Motor Company, Contract DAAG46-71-C-0162, Interim Report No. 6, AMMRC CTR 74-59, September 1974.
71. LARSEN, D., and WALTHER, G. *Property Screening and Evaluation of Ceramic Vane Materials.* IIT Research Institute, AFML Contract F33615-75-C-5196, Interim Report No. 5, January 1978.
72. DAVIDGE, R. *Mechanical Properties of Reaction-Bonded Silicon Nitride* in Nitrogen Ceramics, F. Riley, ed., Proceedings of NATO Advanced Study Institute on Nitrogen Ceramics, Canterbury, United Kingdom, August 1976.
73. GRATHWOHL, G., and THUMMLER, F. *Creep of Reaction-Bonded Silicon Nitride.* J. Mat. Sci., v. 13, 1978, p. 1177.
74. GRATHWOHL, G., and THUMMLER, F. *Creep of Reaction-Bonded Silicon Nitride* in Ceramics for High Performance Applications II, J. J. Burke, E. M. Lenoe, and R. N. Katz, ed., Brook Hill Publishing Company, Chestnut Hill, Massachusetts, 1978, p. 573-592.
75. WARBURTON, J., ANTILL, J., and HAWES, R. *Oxidation of Thin Sheet Reaction-Sintered Silicon Nitride.* J. Am. Cer. Soc., v. 61, no. 1, 1978, p. 67.
76. DIN, S. U., and NICHOLSON, P. S. *Creep Deformation of Reaction-Sintered Silicon Nitride.* J. Am. Cer. Soc., v. 58, no. 11-12, 1975, p. 500.
77. MANGELS, J. *Development of a Creep-Resistant Reaction-Sintered Si_3N_4* in Ceramics for High Performance Applications, J. J. Burke, A. E. Gorum, and R. N. Katz, ed., Brook Hill Publishing Company, Chestnut Hill, Massachusetts, 1974, p. 195-206.
78. EVANS, A. G., and LANGE, F. F. *Crack Propagation and Fracture in SiC.* J. Mat. Sci., v. 10, 1975, p. 1659.
79. McHENRY, K. D., and TRESSLER, R. E. *Subcritical Crack Growth in Silicon Carbide.* J. Mat. Sci., v. 12, 1977, p. 1272.
80. WIEDERHORN, S., and RITTER, J., Jr. *Application of Fracture Mechanics Concepts to Structural Ceramics.* Proceedings of the ASTM 11th National Symposium on Fracture Mechanics, Virginia Polytechnic Institute and State University, June 1978.
81. BENN, K. W., and CARRUTHERS, W. D. *3500 Hour Durability Testing of Commercial Ceramic Materials.* AiResearch Corporation, NASA Contract DEN 3-27.
82. TRELA, W. *Evaluation of Ceramics for Stator Applications - Gas Turbine Engines.* Ford Motor Company, NASA Contract DEN 3-19.
83. WADE, T. B. *Property Screening and Evaluation of Ceramic Turbine Engine Materials.* IIT Research Institute, AFML Contract F33615-75-C-5196.

DISTRIBUTION LIST

No. of Copies	To
	Office of the Under Secretary of Defense for Research and Engineering, The Pentagon, Washington, D.C. 20301
1	ATTN: Mr. J. Persh
1	Dr. G. Gamota
12	Commander, Defense Technical Information Center, Cameron Station, Building 5, 5010 Duke Street, Alexandria, Virginia 22314
1	National Technical Information Service, 5285 Port Royal Road, Springfield, Virginia 22161
	Director, Defense Advanced Research Projects Agency, 1400 Wilson Boulevard, Arlington, Virginia 22209
1	ATTN: Dr. A. Bement
1	Dr. Van Reuth
1	MAJ Harry Winsor
	Battelle Columbus Laboratories, Metals and Ceramics Information Center, 505 King Avenue, Columbus, Ohio 43201
1	ATTN: Mr. Winston Duckworth
1	Dr. D. Niesz
1	Dr. R. Wills
	Deputy Chief of Staff, Research, Development, and Acquisition, Headquarters, Department of the Army, Washington, D.C. 20310
1	ATTN: DAMA-ARZ
1	DAMA-CSS, Dr. J. Bryant
1	DAMA-PPP, Mr. R. Vawter
	Commander, U.S. Army Medical Research and Development Command, Fort Detrick, Frederick, Maryland 21701
1	ATTN: SGRD-SI, Mr. Lawrence L. Ware, Jr.
	Commander, Army Research Office, P.O. Box 12211, Research Triangle Park, North Carolina 27709
1	ATTN: Information Processing Office
1	Dr. G. Mayer
1	Dr. J. Hurt
	Commander, U.S. Army Materiel Development and Readiness Command, 5001 Eisenhower Avenue, Alexandria, Virginia 22333
1	ATTN: DRCDMD-ST
1	DRCLDC
	Commander, U.S. Army Electronics Research and Development Command, Fort Monmouth, New Jersey 07703
1	ATTN: DELSD-L
	Commander, U.S. Army Materiel Systems Analysis Activity, Aberdeen Proving Ground, Maryland 21005
1	ATTN: DRXSY-MP, H. Cohen
	Commander, U.S. Army Night Vision Electro-Optics Laboratory, Fort Belvoir, Virginia 22060
1	ATTN: DELNV-S, Mr. P. Travesky
1	DELNV-L-D, Dr. R. Buser
	Commander, Harry Diamond Laboratories, 2800 Powder Mill Road, Adelphi, Maryland 20783
1	ATTN: Mr. A. Benderly
1	Technical Information Office
1	DELHD-RAE
	Commander, U.S. Army Missile Command, Redstone Arsenal, Alabama 35809
1	ATTN: Mr. P. Ormsby
1	Technical Library
1	DRSMI-TB, Redstone Scientific Information Center
	Commander, U.S. Army Aviation Research and Development Command, P.O. Box 209, St. Louis, Missouri 63166
1	ATTN: DRDAV-EXT
1	DRDAV-QE
1	Technical Library
	Commander, U.S. Army Natick Research and Development Command, Natick, Massachusetts 01760
1	ATTN: Technical Library
1	Dr. J. Hanson
	Commander, U.S. Army Satellite Communications Agency, Fort Monmouth, New Jersey 07703
1	ATTN: Technical Document Center
	Commander, U.S. Army Tank-Automotive Research and Development Command, Warren, Michigan 48090
1	ATTN: Dr. W. Bryzik
1	Mr. E. Hamperian
1	D. Rose
1	DRDTA-RKA, Dr. J. Chevalier
1	DRDTA-UL, Technical Library
1	DRDTA-R
	Commander, U.S. Army Armament Research and Development Command, Dover, New Jersey 07801
1	ATTN: Mr. J. Lannon
1	Dr. G. Vezzoli
1	Mr. A. Graf
1	Mr. Harry E. Pebly, Jr., PLASTEC, Director
1	Technical Library
	Commander, U.S. Army Armament Materiel Readiness Command, Rock Island, Illinois 61299
1	ATTN: Technical Library
	Commander, Aberdeen Proving Ground, Maryland 21005
1	ATTN: DRDAR-CLB-PS, Mr. J. Vervier
	Commander, U.S. Army Mobility Equipment Research and Development Command, Fort Belvoir, Virginia 22060
1	ATTN: DRDME-EM, Mr. W. McGovern
1	DRDME-V, Mr. E. York
1	DRDME-X, Mr. H. J. Peters
	Director, U.S. Army Ballistic Research Laboratory, Aberdeen Proving Ground, Maryland 21005
1	ATTN: DRDAR-TSB-S (STINFO)
	Commander, Rock Island Arsenal, Rock Island, Illinois 61299
1	ATTN: SARRI-EN
	Commander, U.S. Army Test and Evaluation Command, Aberdeen Proving Ground, Maryland 21005
1	ATTN: DRSTE-ME
	Commander, U.S. Army Foreign Science and Technology Center, 220 7th Street, N.E., Charlottesville, Virginia 22901
1	ATTN: Military Tech, Mr. W. Marley
	Chief, Benet Weapons Laboratory, LCWSL, USA ARRADCOM, Watervliet, New York 12189
1	ATTN: DRDAR-LCB-TL
	Commander, Watervliet Arsenal, Watervliet, New York 12189
1	ATTN: Dr. T. Davidson
	Director, Eustis Directorate, U.S. Army Mobility Research and Development Laboratory, Fort Eustis, Virginia 23604
1	ATTN: Mr. J. Robinson, SAVDL-E-MOS (AVRADCOM)
1	Mr. C. Walker
	Commander, U.S. Army Engineer Waterways Experiment Station, Vicksburg, Mississippi 39180
1	ATTN: Research Center Library
	U.S. Army Munitions Production Base, Modernization and Expansion, Dover, New Jersey 07801
1	ATTN: SARPM-PBM-P
	Technical Director, Human Engineering Laboratories, Aberdeen Proving Ground, Maryland 21005
1	ATTN: Technical Reports Office
	Chief of Naval Research, Arlington, Virginia 22217
1	ATTN: Code 471
1	Dr. A. Diness
1	Dr. R. Pohanka
	Naval Research Laboratory, Washington, D.C. 20375
1	ATTN: Dr. J. M. Krafft - Code 8430
1	Mr. R. Rice
1	Dr. Jim C. I. Chang
	Headquarters, Naval Air Systems Command, Washington, D.C. 20360
1	ATTN: Code 5203
1	Code MAT-042M
1	Mr. C. F. Bersch
1	Mr. I. Machlin

No. of Copies	To
	Headquarters, Naval Sea Systems Command, 1941 Jefferson Davis Highway, Arlington, Virginia 22376
1	ATTN: Code 035
	Headquarters, Naval Electronics Systems Command, Washington, D.C. 20360
1	ATTN: Code 504
	Commander, Naval Ordnance Station, Louisville, Kentucky 40214
1	ATTN: Code 85
	Commander, Naval Material Industrial Resources Office, Building 537-2, Philadelphia Naval Base, Philadelphia, Pennsylvania 19112
1	ATTN: Technical Director
	Commander, Naval Weapons Center, China Lake, California 93555
1	ATTN: Mr. F. Markarian
1	Mr. E. Teppo
1	Mr. M. Ritchie
	Commander, U.S. Air Force of Scientific Research, Building 410, Bolling Air Force Base, Washington, D.C. 20332
1	ATTN: MAJ W. Simmons
	Commander, U.S. Air Force Materials Laboratory, Wright-Patterson Air Force Base, Ohio 45433
1	ATTN: Dr. N. Tallan
1	Dr. H. Graham
1	Dr. R. Ruh
1	Mr. K. S. Mazdiyasni
1	Aero Propulsion Labs, Mr. R. Marsh
	Commander, Air Force Weapons Laboratory, Kirtland Air Force Base, Albuquerque, New Mexico 87115
1	ATTN: Dr. R. Rudder
	Commander, Air Force Armament Center, Eglin Air Force Base, Florida 32542
1	ATTN: Technical Library
	National Aeronautics and Space Administration, Washington, D.C. 20546
1	ATTN: Mr. G. C. Deutsch - Code RW
1	Mr. J. Gangler
1	AFSS-AD, Office of Scientific and Technical Information
	National Aeronautics and Space Administration, Lewis Research Center, 21000 Brookpark Road, Cleveland, Ohio 44135
1	ATTN: J. Accurio, USAMRDL
1	Dr. H. B. Probst, MS 49-1
1	Dr. R. Ashbrook
1	Dr. S. Dutta
1	Mr. C. Blankenship
	National Aeronautics and Space Administration, Langley Research Center, Hampton, Virginia 23665
1	ATTN: Mr. J. Buckley, Mail Stop 387
	Commander, White Sands Missile Range, Electronic Warfare Laboratory, OMEW, ERADCOM, White Sands, New Mexico 88002
1	ATTN: Mr. Thomas Reader, DRSEL-WLM-ME
	Department of Energy, Division of Transportation, 20 Massachusetts Avenue, N.W., Washington, D.C. 20545
1	ATTN: Mr. George Thur (TEC)
1	Mr. Robert Schulz (TEC)
1	Mr. John Neal (CLNRT)
1	Mr. Steve Wander (Fossil Fuels)
	Department of Transportation, 400 Seventh Street, S.W., Washington, D.C. 20590
1	ATTN: Mr. M. Lauriente
1	Mechanical Properties Data Center, Belfour Stulen Inc., 13917 W. Bay Shore Drive, Traverse City, Michigan 49684
	National Bureau of Standards, Washington, D.C. 20234
1	ATTN: Dr. S. Wiederhorn
1	Dr. J. B. Wachtman
1	Dr. N. Tighe
	National Research Council, National Materials Advisory Board, 2101 Constitution Avenue, Washington, D.C. 20418
1	ATTN: Dr. W. Prindle
1	D. Groves
1	R. M. Spriggs

No. of Copies	To
	National Science Foundation, Washington, D.C. 20550
1	ATTN: B. A. Wilcox
	Admiralty Materials Technology Establishment, Polle, Dorset BH16 6JU, United Kingdom
1	ATTN: Dr. D. Godfrey
1	Dr. M. Lindley
	AiResearch Manufacturing Company, AiResearch Casting Company, 2525 West 190th Street, Torrance, California 90505
1	ATTN: Mr. K. Styhr
1	Dr. D. Kotchick
	AiResearch Manufacturing Company, Materials Engineering Dept., 111 South 34th Street, P.O. Box 5217, Phoenix, Arizona 85010
1	ATTN: Mr. D. W. Richerson, MS 93-393/503-44
1	Dr. W. Carruthers
	AVCO Corporation, Applied Technology Division, Lowell Industrial Park, Lowell, Massachusetts 01887
1	ATTN: Dr. T. Vasilos
	Carborundum Company, Research and Development Division, P.O. Box 1054, Niagara Falls, New York 14302
1	ATTN: Dr. J. A. Coppola
1	Dr. M. Srinivasan
	Case Western Reserve University, Department of Metallurgy, Cleveland, Ohio 44106
1	ATTN: Prof. A. H. Heuer
1	Corning Glass Works, Research Department, Corning, New York 14832
	Cummins Engine Company, Columbus, Indiana 47201
1	ATTN: Mr. R. Kamo
	Defence Research Establishment Pacific, FMO, Victoria, B.C., VOS IBO, Canada
1	ATTN: R. D. Barer
	Deposits and Composites, Inc., 1821 Michael Faraday Drive, Reston, Virginia 22090
1	ATTN: Mr. R. E. Engdahl
	Electric Power Research Institute, P.O. Box 10412, 3412 Hillview Avenue, Palo Alto, California 94304
1	ATTN: Dr. A. Cohn
	European Research Office, 223 Old Maryleborne Road, London, NW1 - 5th, England
1	ATTN: Dr. R. Quattrone
1	LT COL James Kennedy
	Ford Motor Company, Turbine Research Department, 20000 Rotunda Drive, Dearborn, Michigan 48121
1	ATTN: Mr. A. F. McLean
1	Mr. E. A. Fisher
1	Mr. J. A. Mangels
1	Mr. L. Swank
1	Mr. R. Gorvilla
	General Atomic Company, P.O. Box 81608, San Diego, California 92138
1	ATTN: Mr. Jim Holzgraf
	General Electric Company, Research and Development Center, Box 8, Schenectady, New York 12345
1	ATTN: Dr. R. J. Charles
1	Dr. C. D. Greskovich
1	Dr. S. Prochazka
	General Electric Corporation, Mail Stop H-99, Cincinnatti, Ohio 45215
1	ATTN: Mr. Warren Nelson
	General Motors Corporation, AC Spark Plug Division, Flint, Michigan 48556
1	ATTN: Dr. M. Berg
	Georgia Institute of Technology, EES, Atlanta, Georgia 30332
1	ATTN: Mr. J. D. Walton
	GTE Laboratories, Waltham Research Center, 40 Sylvan Road, Waltham, Massachusetts 02154
1	ATTN: Dr. C. Quackenbush
1	Dr. W. H. Rhodes

No. of Copies	To
	IIT Research Institute, 10 West 35th Street, Chicago, Illinois 60616
1	ATTN: Mr. S. Bortz, Director, Ceramics Research
1	Dr. D. Larsen
1	Dr. G. Walther
	Institute fur Werkstoff-Forshung, DFVLR, 505 Porz-Wahn, Linder Hohe, Germany
1	ATTN: Dr. W. Bunk
1	Dr. H. Knoch
	International Harvester, Solar Division, 2200 Pacific Highway, P.O. Box 80966, San Diego, California 92138
1	ATTN: Dr. A. Metcalfe
1	Ms. M. E. Gulden
	Jet Propulsion Laboratory - C.I.T., 4800 Oak Grove Drive, Pasadena, California 91103
1	ATTN: Dr. Richard Smoak
	Kawecki Berylco Industries, Inc., P.O. Box 1462, Reading, Pennsylvania 19603
1	ATTN: Mr. R. J. Longenecker
	Martin Marietta Laboratories, 1450 South Rolling Road, Baltimore, Maryland 21227
1	ATTN: Dr. J. Venables
	Massachusetts Institute of Technology, Department of Metallurgy and Materials Science, Cambridge, Massachusetts 02139
1	ATTN: Prof. R. L. Coble
1	Prof. H. K. Bowen
1	Prof. W. D. Kingery
1	Prof. R. Cannon
	Materials Research Laboratories, P.O. Box 50, Ascot Vale, VIC 3032, Australia
1	ATTN: Dr. C. W. Weaver
	Midwest Research Institute, 425 Volker Boulevard, Kansas City, Missouri 64110
1	ATTN: Mr. Gordon W. Gross, Head, Physics Station
	Norton Company, Worcester, Massachusetts 01606
1	ATTN: Dr. N. Ault
1	Dr. M. L. Torti
	Pennsylvania State University, Materials Research Laboratory, Materials Science Department, University Park, Pennsylvania 16802
1	ATTN: Prof. R. Roy
1	Prof. R. E. Newnham
1	Prof. R. E. Tressler
1	Prof. R. Bradt
1	Prof. V. S. Stubican
	Pratt and Whitney Aircraft, P.O. Box 2691, W. Palm Beach, Florida 33402
1	ATTN: Mr. Mel Mendelson, Mail Stop B-08
	PSC, Box 1044, APO San Francisco 96328
1	ATTN: MAJ A. Anthony Borges
	RIAS, Division of the Martin Company, Baltimore, Maryland
1	ATTN: Dr. A. R. C. Westwood
	Rockwell International Science Center, 1049 Camino Dos Rios, Thousand Oaks, California 91360
1	ATTN: Dr. A. Evans
1	Dr. F. Lange
	Royal Aircraft Establishment, Materials Department, R 178 Building, Farnborough, Hants, England
1	ATTN: Dr. N. Corney
	Shane Associates, Inc., 7821 Carrleigh Parkway, Springfield, Virginia 22152
1	ATTN: Dr. Robert S. Shane, Consultant
	Solar Turbine International, 2200 Pacific Coast Highway, San Diego, California 92138
1	ATTN: Mr. Andrew Russel
	Stanford Research International, 333 Ravenswood Avenue, Menlo Park, California 94025
1	ATTN: Dr. P. Jorgensen
1	Dr. D. Rowcliffe

No. of Copies	To
	State University of New York at Stony Brook, Department of Materials Science, Long Island, New York 11790
1	ATTN: Prof. Franklin F. Y. Wang
	Teledyne CAE, 1330 Laskey Road, Toledo, Ohio 43612
1	ATTN: Dr. Scott Wright, Dept. 602
	United Technologies Research Center, East Hartford, Connecticut 06108
1	ATTN: Dr. J. Brennan
1	Dr. F. Galasso
	University of California, Lawrence Livermore Laboratory, P.O. Box 808, Livermore, California 94550
1	ATTN: Mr. R. Landingham
1	Dr. C. F. Cline
	University of California, Department of Materials Science and Engineering, Hearst Building, Berkeley, California 94720
1	ATTN: Dr. D. Clarke
	University of Florida, Department of Materials Science and Engineering, Gainesville, Florida 32601
1	ATTN: Dr. L. Hench
	University of Massachusetts, Department of Mechanical Engineering, Amherst, Massachusetts 01003
1	ATTN: Prof. K. Jakus
1	Prof. J. Ritter
	University of Newcastle Upon Tyne, Department of Metallurgy and Engineering Materials, Newcastle Upon Tyne, NEI 7 RU, England
1	ATTN: Prof. K. H. Jack
	University of Utah, College of Engineering, Division of Materials Science and Engineering, Salt Lake City, Utah 84112
1	ATTN: Prof. I. B. Cutler
	University of Washington, Ceramic Engineering Division, FB-10, Seattle, Washington 98195
1	ATTN: Prof. James I. Mueller
1	Prof. A. E. Gorum
1	Mr. Francis Gac
	V.P.I., Department of Materials Engineering, Blacksburg, Virginia 24061
1	ATTN: Prof. D. P. H. Hasselman
	Westinghouse Electric Corporation, Research Laboratories, Pittsburgh, Pennsylvania 15235
1	ATTN: Dr. R. J. Bratton
1	Dr. B. Rossing
1	Mr. P. Annese, Bomas Machine Specialties, 114 North Beacon Street, Brighton, Massachusetts 02135
1	Mr. Robert Cicerone, 117 Kimball Road, Dedham, Massachusetts 02026
2	Mr. Robert Keyes, 200 Boring Place, Martinsville, Indiana 46151
1	Dr. D. Munz, DFVLR, Postfach 90 60 58, 5000 Koln 90, West Germany
1	Dr. Bernard North, Springfields Nuclear Power Dev. Lab, United Kingdom Atomic Energy Authority (Northern Division), Springfields, Salick, Preston, PR4 ORR, United Kingdom
	Max Planck Institut fur Metallforschung, Institut fur Werkstoffwissenschaften seestrasse 92, 7000 Stuffgart 1, West Germany
1	ATTN: Dr. Ing. R. F. Pabst
1	C. H. Sump, Combustion Engineering Inc., 911 West Main Street, Chattanooga, Tennessee 37402
1	Prof Dr. F. Thummler, Institut fur Werksloffkunde II der Universitat, Institut fur Material und Festkorperforschung, Postfach 3640, Karlsruhe, West Germany
1	Dr. Richard Tsai, Cornell University, Materials Science and Engineering, Bard Hall, Ithaca, New York 14853
1	Dr. Gunter Ziegler, Institut fur Materials Research, DFVLR, 5000 Cologne 90-FRG, West Germany
	Director, Army Materials and Mechanics Research Center, Watertown, Massachusetts 02172
2	ATTN: DRXMR-PL
1	DRXMR-WD
1	Author

☆U.S. GOVERNMENT PRINTING OFFICE : 1980—600-676/30

Army Materials and Mechanics Research Center,
Watertown, Massachusetts 02172
CHARACTERIZATION OF TURBINE CERAMICS AFTER
LONG-TERM ENVIRONMENTAL EXPOSURE -
George D. Quinn

Technical Report AMMRC TR 80-15, April 1980, 100 pp -
illus-tables, Interagency Agreement EC-76-A-1017

AD_____

UNCLASSIFIED
UNLIMITED DISTRIBUTION

Key Words

Silicon nitride
Silicon carbide
Static fatigue

An experimental program was conducted to investigate the possible degradation in mechanical properties of silicon-based ceramics exposed to high temperature oxidizing environments. Thirteen materials were studied, all with potential for use in energy conversion devices such as the gas turbine. The materials ranged from some of the better known silicon nitrides and carbides to experimental grades. Testing included flexural stress rupture at 1200 C and stepped temperature stress rupture (STSR) experiments. The latter test was devised for this study and is a variation of the stress rupture test in which a range of temperatures is employed. The purpose of the STSR test is to explore the potential stress/temperature regimes of static fatigue failure. In addition, a combined cycle durability sequence was applied to selected materials. This procedure is a simple service simulation involving static heat soaks and rapid thermal cycling on bend bars. In nearly all cases, material degradation and/or time-dependent failure was observed. Extensive fractography was conducted to identify mechanisms of failure.

Army Materials and Mechanics Research Center,
Watertown, Massachusetts 02172
CHARACTERIZATION OF TURBINE CERAMICS AFTER
LONG-TERM ENVIRONMENTAL EXPOSURE -
George D. Quinn

Technical Report AMMRC TR 80-15, April 1980, 100 pp -
illus-tables, Interagency Agreement EC-76-A-1017

AD_____

UNCLASSIFIED
UNLIMITED DISTRIBUTION

Key Words

Silicon nitride
Silicon carbide
Static fatigue

An experimental program was conducted to investigate the possible degradation in mechanical properties of silicon-based ceramics exposed to high temperature oxidizing environments. Thirteen materials were studied, all with potential for use in energy conversion devices such as the gas turbine. The materials ranged from some of the better known silicon nitrides and carbides to experimental grades. Testing included flexural stress rupture at 1200 C and stepped temperature stress rupture (STSR) experiments. The latter test was devised for this study and is a variation of the stress rupture test in which a range of temperatures is employed. The purpose of the STSR test is to explore the potential stress/temperature regimes of static fatigue failure. In addition, a combined cycle durability sequence was applied to selected materials. This procedure is a simple service simulation involving static heat soaks and rapid thermal cycling on bend bars. In nearly all cases, material degradation and/or time-dependent failure was observed. Extensive fractography was conducted to identify mechanisms of failure.

Army Materials and Mechanics Research Center,
Watertown, Massachusetts 02172
CHARACTERIZATION OF TURBINE CERAMICS AFTER
LONG-TERM ENVIRONMENTAL EXPOSURE -
George D. Quinn

Technical Report AMMRC TR 80-15, April 1980, 100 pp -
illus-tables, Interagency Agreement EC-76-A-1017

AD_____

UNCLASSIFIED
UNLIMITED DISTRIBUTION

Key Words

Silicon nitride
Silicon carbide
Static fatigue

An experimental program was conducted to investigate the possible degradation in mechanical properties of silicon-based ceramics exposed to high temperature oxidizing environments. Thirteen materials were studied, all with potential for use in energy conversion devices such as the gas turbine. The materials ranged from some of the better known silicon nitrides and carbides to experimental grades. Testing included flexural stress rupture at 1200 C and stepped temperature stress rupture (STSR) experiments. The latter test was devised for this study and is a variation of the stress rupture test in which a range of temperatures is employed. The purpose of the STSR test is to explore the potential stress/temperature regimes of static fatigue failure. In addition, a combined cycle durability sequence was applied to selected materials. This procedure is a simple service simulation involving static heat soaks and rapid thermal cycling on bend bars. In nearly all cases, material degradation and/or time-dependent failure was observed. Extensive fractography was conducted to identify mechanisms of failure.

Army Materials and Mechanics Research Center,
Watertown, Massachusetts 02172
CHARACTERIZATION OF TURBINE CERAMICS AFTER
LONG-TERM ENVIRONMENTAL EXPOSURE -
George D. Quinn

Technical Report AMMRC TR 80-15, April 1980, 100 pp -
illus-tables, Interagency Agreement EC-76-A-1017

AD_____

UNCLASSIFIED
UNLIMITED DISTRIBUTION

Key Words

Silicon nitride
Silicon carbide
Static fatigue

An experimental program was conducted to investigate the possible degradation in mechanical properties of silicon-based ceramics exposed to high temperature oxidizing environments. Thirteen materials were studied, all with potential for use in energy conversion devices such as the gas turbine. The materials ranged from some of the better known silicon nitrides and carbides to experimental grades. Testing included flexural stress rupture at 1200 C and stepped temperature stress rupture (STSR) experiments. The latter test was devised for this study and is a variation of the stress rupture test in which a range of temperatures is employed. The purpose of the STSR test is to explore the potential stress/temperature regimes of static fatigue failure. In addition, a combined cycle durability sequence was applied to selected materials. This procedure is a simple service simulation involving static heat soaks and rapid thermal cycling on bend bars. In nearly all cases, material degradation and/or time-dependent failure was observed. Extensive fractography was conducted to identify mechanisms of failure.

Army Materials and Mechanics Research Center,
Watertown, Massachusetts 02172
CHARACTERIZATION OF TURBINE CERAMICS AFTER
LONG-TERM ENVIRONMENTAL EXPOSURE -
George D. Quinn

Technical Report AMMRC TR 80-15, April 1980, 100 pp -
illus-tables, Interagency Agreement EC-76-A-1017

AD_____

UNCLASSIFIED
UNLIMITED DISTRIBUTION

Key Words

Silicon nitride
Silicon carbide
Static fatigue

An experimental program was conducted to investigate the possible degradation in mechanical properties of silicon-based ceramics exposed to high temperature oxidizing environments. Thirteen materials were studied, all with potential for use in energy conversion devices such as the gas turbine. The materials ranged from some of the better known silicon nitrides and carbides to experimental grades. Testing included flexural stress rupture at 1200 C and stepped temperature stress rupture (STSR) experiments. The latter test was devised for this study and is a variation of the stress rupture test in which a range of temperatures is employed. The purpose of the STSR test is to explore the potential stress/temperature regimes of static fatigue failure. In addition, a combined cycle durability sequence was applied to selected materials. This procedure is a simple service simulation involving static heat soaks and rapid thermal cycling on bend bars. In nearly all cases, material degradation and/or time-dependent failure was observed. Extensive fractography was conducted to identify mechanisms of failure.

Army Materials and Mechanics Research Center,
Watertown, Massachusetts 02172
CHARACTERIZATION OF TURBINE CERAMICS AFTER
LONG-TERM ENVIRONMENTAL EXPOSURE -
George D. Quinn

Technical Report AMMRC TR 80-15, April 1980, 100 pp -
illus-tables, Interagency Agreement EC-76-A-1017

AD_____

UNCLASSIFIED
UNLIMITED DISTRIBUTION

Key Words

Silicon nitride
Silicon carbide
Static fatigue

An experimental program was conducted to investigate the possible degradation in mechanical properties of silicon-based ceramics exposed to high temperature oxidizing environments. Thirteen materials were studied, all with potential for use in energy conversion devices such as the gas turbine. The materials ranged from some of the better known silicon nitrides and carbides to experimental grades. Testing included flexural stress rupture at 1200 C and stepped temperature stress rupture (STSR) experiments. The latter test was devised for this study and is a variation of the stress rupture test in which a range of temperatures is employed. The purpose of the STSR test is to explore the potential stress/temperature regimes of static fatigue failure. In addition, a combined cycle durability sequence was applied to selected materials. This procedure is a simple service simulation involving static heat soaks and rapid thermal cycling on bend bars. In nearly all cases, material degradation and/or time-dependent failure was observed. Extensive fractography was conducted to identify mechanisms of failure.

Army Materials and Mechanics Research Center,
Watertown, Massachusetts 02172
CHARACTERIZATION OF TURBINE CERAMICS AFTER
LONG-TERM ENVIRONMENTAL EXPOSURE -
George D. Quinn

Technical Report AMMRC TR 80-15, April 1980, 100 pp -
illus-tables, Interagency Agreement EC-76-A-1017

AD_____

UNCLASSIFIED
UNLIMITED DISTRIBUTION

Key Words

Silicon nitride
Silicon carbide
Static fatigue

An experimental program was conducted to investigate the possible degradation in mechanical properties of silicon-based ceramics exposed to high temperature oxidizing environments. Thirteen materials were studied, all with potential for use in energy conversion devices such as the gas turbine. The materials ranged from some of the better known silicon nitrides and carbides to experimental grades. Testing included flexural stress rupture at 1200 C and stepped temperature stress rupture (STSR) experiments. The latter test was devised for this study and is a variation of the stress rupture test in which a range of temperatures is employed. The purpose of the STSR test is to explore the potential stress/temperature regimes of static fatigue failure. In addition, a combined cycle durability sequence was applied to selected materials. This procedure is a simple service simulation involving static heat soaks and rapid thermal cycling on bend bars. In nearly all cases, material degradation and/or time-dependent failure was observed. Extensive fractography was conducted to identify mechanisms of failure.

Army Materials and Mechanics Research Center,
Watertown, Massachusetts 02172
CHARACTERIZATION OF TURBINE CERAMICS AFTER
LONG-TERM ENVIRONMENTAL EXPOSURE -
George D. Quinn

Technical Report AMMRC TR 80-15, April 1980, 100 pp -
illus-tables, Interagency Agreement EC-76-A-1017

AD_____

UNCLASSIFIED
UNLIMITED DISTRIBUTION

Key Words

Silicon nitride
Silicon carbide
Static fatigue

An experimental program was conducted to investigate the possible degradation in mechanical properties of silicon-based ceramics exposed to high temperature oxidizing environments. Thirteen materials were studied, all with potential for use in energy conversion devices such as the gas turbine. The materials ranged from some of the better known silicon nitrides and carbides to experimental grades. Testing included flexural stress rupture at 1200 C and stepped temperature stress rupture (STSR) experiments. The latter test was devised for this study and is a variation of the stress rupture test in which a range of temperatures is employed. The purpose of the STSR test is to explore the potential stress/temperature regimes of static fatigue failure. In addition, a combined cycle durability sequence was applied to selected materials. This procedure is a simple service simulation involving static heat soaks and rapid thermal cycling on bend bars. In nearly all cases, material degradation and/or time-dependent failure was observed. Extensive fractography was conducted to identify mechanisms of failure.